Author:
Dey, Amy

Title:
Investigating the Role of BASP1 Lipidation in WT1/BASP1 Mediated Gene Regulation

Amy E. Dey | University of Bristol | January 2019

Investigating the Role of BASP1 Lipidation in WT1/BASP1 Mediated Gene Regulation

A thesis submitted to the University of Bristol in accordance with the requirements for award of the degree of Doctor of Philosophy in the Faculty of Life Sciences

Table of Contents

I. Abstract

Brain acid soluble protein 1 (BASP1) is a transcriptional corepressor of the Wilms' Tumour 1 (WT1) transcription factor. Previous work from the lab demonstrated that N-terminal myristoylation of BASP1 facilitates an interaction with nuclear lipids such that $PI(4,5)P_2$ is recruited to WT1 target gene promoters. $PI(4,5)P_2$ is required for the assembly of chromatin remodelling complexes to mediate transcriptional repression. BASP1 also interacts with cholesterol through a cholesterol recognition amino acid consensus (CRAC) domain, although the role of cholesterol in BASP1-dependent transcription regulation is unknown.

In this study, the mechanisms of WT1/BASP1 mediated transcriptional regulation employing nuclear lipids were investigated. This work revealed for the first time that BASP1 mediates the removal of multiple activating histone modifications, H3K9Ac, $H3K4me^3$ and $H3K36me^3$ in a myristoyl-dependent manner. BASP1 was also found to mediate the addition of repressive histone modifications, $H3K9me^3$ and $H3K27me^3$, plus recruitment of EZH2 in a myristoyl-independent manner.

The role of cholesterol in transcriptional repression by BASP1 was also investigated. Using click-chemistry and chromatin immunoprecipitation, it was demonstrated that BASP1 can recruit cholesterol to gene promoters. Nuclear cholesterol was found to be an important component of the WT1/BASP1 repression complex, involved in removing $H3K4me^3$ at specific WT1/BASP1 target genes.

The subnuclear localisation of BASP1 was investigated to explore how BASP1 interfaces the inner nuclear membrane (INM) with chromatin modification and gene regulation. For the first time BASP1 was found to interact with Emerin and recruit several INM proteins to WT1 target gene promoters in a myristoyl-dependent manner. The evidence presented supports a model whereby the interaction between BASP1 and INM components is important for mediating transcriptional repression. These findings implicate $PI(4,5)P_2$ as a linker between BASP1 and INM proteins.

Together the findings reveal critical roles for $PI(4,5)P_2$ and cholesterol in mediating changes to the chromatin environment at WT1/BASP1 target gene promoters.

II. Acknowledgements

I would first of my like to express my sincere gratitude to my supervisor Professor Stefan Roberts' for his excellent guidance and knowledge which have been invaluable to my project. His continuous support and steadfast positivity have certainly helped me achieve the best out of my PhD.

I would like to thank the Wellcome Trust for funding my project, and my wonderful Post-Docs, Lindsey Marsh and Samantha Carrera for initiating me into the lab. I would like to acknowledge Paul Verkade and his electron microscopy group for all their help preparing EM samples, and Stephen Cross for help with analysing the microscopy data. I would also like to thank everyone in the G66 lab for their help, stimulating discussions and for providing a great environment to work in. It has been wonderful to do my PhD alongside my fellow Wellcome cohort, Sonam, Lea, Rob and Melanie who have provided great support in and out of the lab.

Outside of my studies, I would also like to thank my amazing Granville girls; Megan, Sara, Lucy and Benita, as well as my lifelong friends Flora, Alice, Nellie, Becki and Becca for emotional support and sometimes much needed weekends away from science. I am ever grateful for the unwavering support and encouragement of my parents, brothers and extended family. We may be spread across the globe, but they have always been enthusiastic about my work and excited to hear the latest developments.

Choosing this PhD was also the best decision because it brought me to Bristol and into the path of my best friend, Jacob. His boundless energy, positivity and his conviction that I can achieve twice what I set my mind to has encouraged me to strive to achieve the very best that I can. Thanks for making the last few years so full of joy. Last but not least, a very special thank you must be given to baby Walter, for giving me a very final deadline to finish my experiments and for making me maximally efficient at thesis writing.

III. Declaration

I declare that the work in this dissertation was carried out in accordance with the requirements of the University's *Regulations and Code of Practice for Research Degree Programmes* and that it has not been submitted for any other academic award. Except where indicated by specific reference in the text, the work is the candidate's own work. Work done in collaboration with, or with the assistance of, others, is indicated as such. Any views expressed in the dissertation are those of the author.

SIGNED: ..... DATE:.....

IV. List of Figures

V. Abbreviations

BASP1	Brain Acid Soluble Protein 1
BSA	Bovine Serum Albumin
ChIP	Chromatin Immunoprecipitation
CRAC	Cholesterol Recognition Amino Acid Consensus
CTD	C-terminal Repeat Domain
$CuBF_4$	Copper(II) Tetrafluoroborate
DAG	Diacylglyceride
DMSO	Dimethyl Sulfoxide
DNA	Deoxyribonucleic Acid
dNTP	Deoxyribonucleotide Triphosphate
DTT	Dithiothreitol
ECL	Enhanced Chemiluminescence
EDTA	Ethylene Diamine Tetraacetic Acid
EGS	Ethylene Glycol Bis(Succinimidyl Succinate)
EGTA	Ethylene Glycol-bis(β-aminoethyl ether) Tetraacetic Acid
ER	Endoplasmic Reticulum
ERα	Oestrogen Receptor
FCS	Foetal Calf Serum
FISH	Fluorescence in Situ Hybridization
FLIP	Fluorescence Loss In Photobleaching
FRAP	Fluorescence Recovery After Photobleaching
FRET	Fluorescence Resonance Energy Transfer
HA	Human Influenza Hemagglutinin
HAT	Histone Acetyl Transferase
HCl	Hydrogen Chloride
HDAC	Histone Deacetylase
HMT	Histone Methyl Transferase
INM	Inner Nuclear Membrane
KCl	Potassium Chloride
kDa	Kilo Dalton
KOH	Potassium Hydroxide
LB	Lysogeny Broth
LC-MS/MS	Liquid Chromatography–mass spectrometry
LiCl	Lithium Chloride
LMP	Low Melting Point
$MgCl_2$	Magnesium Chloride
mRNA	Messenger RNA
NaCl	Sodium Chloride
NEB	New England Biolabs
NH_4Cl	Ammonium Chloride
NLS	Nuclear Localisation Sequence
NP-40	Nonident P40
PAGE	Polyacrylamide Gel Electrophoresis
PBS	Phosphate Buffered Saline
PC	Phosphatidylcholine
PCR	Polymerase Chain Reaction
PE	Phosphatidylethanolamine
PFA	Paraformaldehyde
PI	Phosphoinositide
PI3K	Phosphoinositol-3-kinase

PIP_2	Phosphatidylinositol 4,5-bisphosphate
PIP_3	Phosphatidylinositol 3,4,5-trisphosphate
PKC	Protein Kinase C
PLC	Phospholipase C
PMSF	Phenylmethane Sulfonyl Fluoride
PS	Phosphatidylserine
rDNA	Ribosomal DNA
RNA	Ribonucleic Acid
RNA pol	RNA Polymerase
SDS	Sodium Dodecyl Sulphate
SM	Sphingomyelin
TAE	Tris-Acetate-EDTA
TAF	TBP Associating Factor
TBP	TATA Binding Protein
TMT	Tandem Mass Tag
TSS	Transcription Start Site
VDR	Vitamin D Receptor
WT1	Wilms' Tumour 1

1 Introduction

1.1 Gene Expression

Every cell in the body originates from one fertilised ovum containing one DNA code. In humans this code is spread across 23 pairs of chromosomes, half of maternal and half of paternal origin [13]. As the ovum divides to produce more cells, each and every cell contains an identical copy of DNA code and yet it is clear that brain, heart, skin and every individual type of cell ultimately appears and functions quite uniquely [13]. The finely controlled differences in how each cell type appears and functions is down to its unique gene expression pattern [13]. Of the approximate 20,000 genes encoded in the human genome, a precise combination of genes is expressed in any given cell type, allowing cells to become specialized for their functions [13, 14].

Gene expression is the fundamental process through which a cell's DNA code is translated into functioning RNA and protein molecules which work to fulfil the requirements of the cell. The process of gene expression is used by every known life form, from prokaryotes and eukaryotes to viruses [15]. The multistage process of gene expression begins as double stranded DNA is unwound and separated, and one strand of code forms a template for the synthesis of an RNA transcript (see Figure 1.1) [15]. In the case of protein coding genes, genes are transcribed into 'messenger' RNA (mRNA) which is then edited, translated into protein, and can then be subject to further post translational modifications which control protein function [16].

Both transcription and translation of a gene product are essential for gene expression to result in protein production. Initially, this sequence of events was assumed to be true for all gene products, however insights such as those provided by large scale gene studies including the human genomes project proved that gene transcription occurs at a much higher level than translation, resulting in the production of many more RNA products than ever get translated into protein [14, 17, 18]. There are four main types of RNA product each encoded by its own type of gene; transfer RNA (tRNA), ribosomal RNA (rRNA), small nuclear RNA (snRNA) and messenger RNA (mRNA) [19]. Only mRNA, which accounts for approximately 1-5% of all RNA in the cell is translated into protein, but tRNA, rRNA and snRNA all play vital roles in the splicing, processing and translation of mRNA into protein [19]. MicroRNAs (miRNAs) are a further class of small non coding RNAs, which also contribute to regulating the expression of up to 30% of protein coding genes in

mammals [20]. Additional levels of gene product regulation occur outside of the nucleus, where mRNAs can undergo degradation, and translated products are subject to a range of post-translational modifications to control protein activity [15, 16, 21, 22].

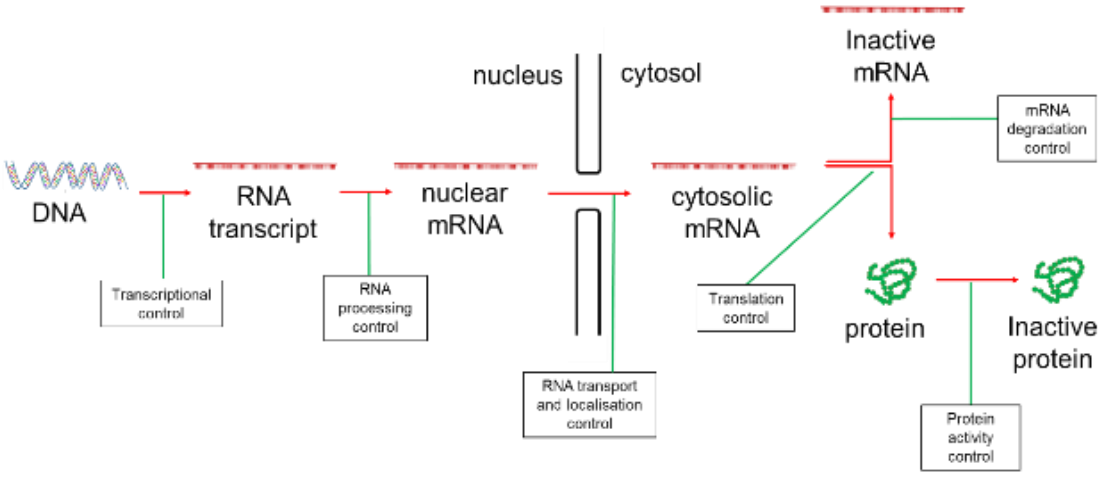

Figure 1.1 The Gene Expression Process. When a gene is expressed a copy of the DNA code is produced in the form of an RNA transcript (transcription). mRNA transcripts go through several stages of editing and processing, and mRNAs are then transported out of the nucleus to undergo translation into an amino acid sequence, which further folds to form the final 3D protein structure. Protein activity can then be altered in a variety of ways including through the addition or removal of protein modifications. Alternatively, cytosolic mRNA transcripts can also undergo degradation as an additional level of regulation of gene products. Control over gene products occurs at all levels from the initial production of an RNA transcript to RNA degradation and protein (in)activation. This multi-layered approach enables cells to precisely regulate gene products, and therefore respond quickly and efficiently to different cellular requirements.

1.2 Gene Regulation

Many diseases can be caused by uncontrolled gene expression whereby the cell experiences aberrant upregulation or downregulation of certain genes which causes abnormal cell function, such as the excessive growth and division that befalls cancer cells [23]. Therefore, it is vital that gene expression is tightly regulated on a number of levels to ensure it is precisely controlled. In both eukaryotes and in bacteria the regulation of transcription initiation is the predominant form of gene regulation for most genes [22]. The regulation of transcription initiation primarily occurs through regulating chromatin structure and regulating the assembly and progression of the transcription machinery. This is intricately controlled through the binding of transcription factors and cofactors to regulatory DNA sequences such as promoters and enhancers [22].

1.2.1 Transcription Machinery

In eukaryotes, transcription itself is carried out by the enzyme RNA polymerase in concert with a number of proteins known as the general transcription factors [24]. The general transcription factors are responsible for the recognition of specific regulatory DNA sequences called gene promoters [22]. The general transcription factors act at the core promoter which is located ~30 base pairs (bp) upstream of the transcription start site (TSS). The general factors are also responsible for responding to additional regulatory factors and mediating the appropriate changes in RNA polymerase protein conformation to allow correct RNA polymerase activity throughout the transcription process [15, 24]. Bacteria and archaea have one RNA polymerase enzyme, however most eukaryotes use three enzymes to synthesise different types of RNA (RNA polymerase I-III) [24]. The RNA polymerase II transcription machinery is the most complex of the eukaryotic transcription machineries, with a total of almost 60 components [24]. It is also RNA polymerase II which is responsible for the synthesis of mRNA [15]. Although there are many more subunits which comprise eukaryotic RNA polymerase II than bacterial RNA polymerase, the catalytic subunits are homologous and display similar structure and mechanism, suggesting functional similarly is conserved [25].

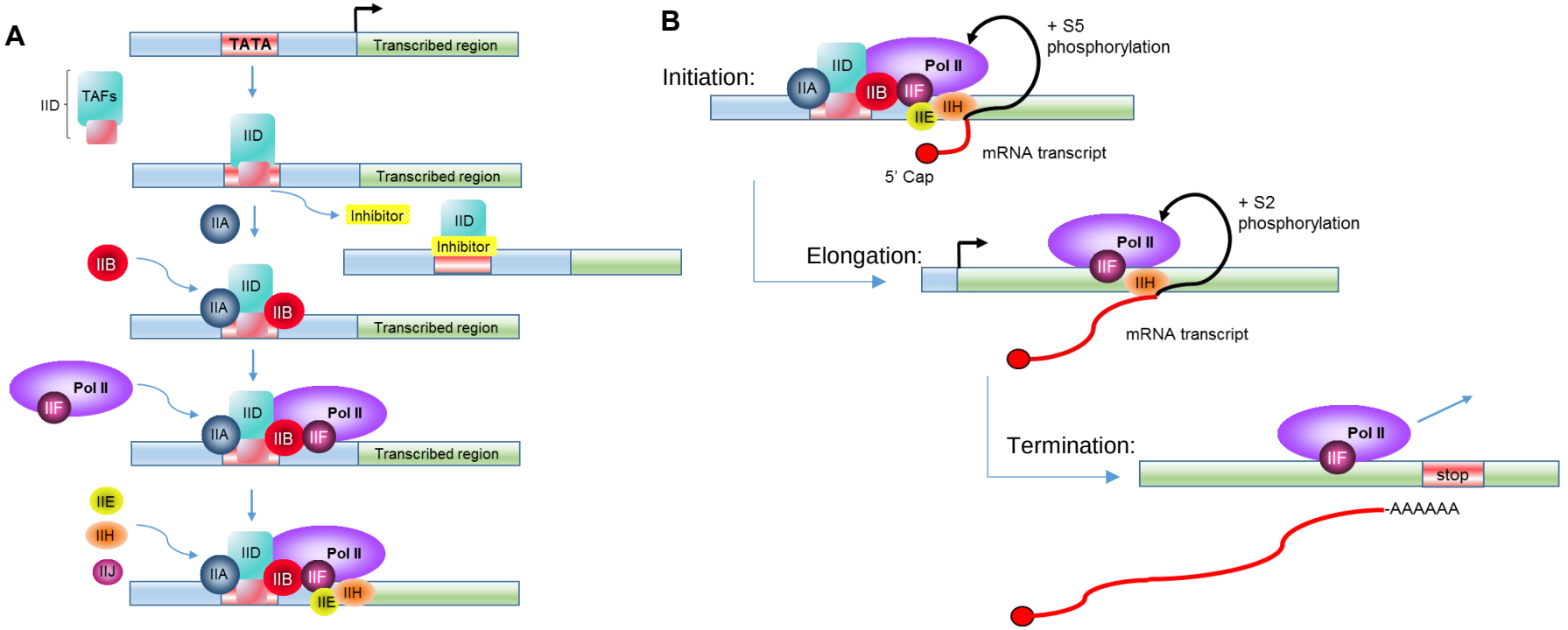

Figure 1.2 The Molecular Basis of Transcription Initiation, Elongation and Termination. A, Assembly begins with the binding of transcription factor TFIID to the TATA box. TFIID comprises the TATA-binding protein (TBP) plus associated factors (TAFs) shown as one large symbol. TFIIA then binds the TFIID promoter complex, followed by TFIIB, followed by binding of a preformed TFIIF/RNA Polymerase II complex. Finally, the other factors TFIIE and TFIIH bind and complete the preinitiation complex. **B**, The DNA helicase activity of TFIIH separates strands of the template DNA and RNA polymerase II (Pol II) begins to transcribe the first 8-9 nucleotides. The protein kinase activity of TFIIH (CDK7 subunit) phosphorylates serine 5 residues (S5) in the C-terminal repeat domain (CTD) of Pol II. This allows Pol II to transcribe beyond the immediate promoter region (promoter clearance). S5 phosphorylation also recruits capping enzymes to cap the 5' end of the nascent transcript. TFIIE is then released from initiation complex. Next, as the pre-mRNA chain grows, the P-TEFb complex (CDK9 subunit) phosphorylates Serine 2 (S2) residues in the Pol II CTD, allowing it to move freely along the DNA template. Then TFIIH dissociates. Finally, Pol II reaches termination signals (stop codons) in the DNA sequence and factors that cleave the transcript from the CTD, and poly-adenylate the 3' end of the transcript. Pol II dissociates from the DNA and the pre-mRNA transcript begins processing and maturation.

The sequence of events that underlies the assembly of the general transcription machinery beginning with the formation of the preinitiation complex followed by transcription initiation, RNA polymerase II pausing, transcription elongation and finally transcription termination are depicted in Figure 1.2 [26-29]. Commonly, the RNA polymerase II mediated transcription process is triggered by the binding of regulatory transcription factors to the gene promoter and enhancer sequences which directly recruit components of the transcription machinery, starting with the TATA binding protein (TBP) [15]. Transcription factors can be repressors or activators of transcription initiation, and in eukaryotes a single gene promoter may be regulated by the simultaneous binding of multiple transcription factors at multiple additional regulatory DNA sequences to provide extra regulatory control [22].

Transcription factors are commonly modular proteins comprising distinct functional domains including a DNA binding domain which can take one of a number of structures; commonly either a homeodomain, basic leucine zipper, helix-loop-helix or a zinc finger structure [30]. Transcription factors also contain one or several activation and/or repression domains which interact with cofactors to stimulate or repress transcription [30]. Some transcription factors also form heterodimers which enables them to bind more DNA sites and interact with more cofactors to control transcription [30]. The transcriptional output following binding of a transcription factor to a target gene promoter depends on the particular cofactors recruited and the influence of other regulatory sequences such as enhancers.

Enhancers help determine spatiotemporal and quantitative gene transcription programmes during development and in response to environmental stimuli [31]. Like promoters, enhancers are also bound by transcription factors and cofactors which results in modulation of the local chromatin environment and alters the accessibility of promoter sequences [32]. Enhancers can be located several thousand base pairs upstream or downstream of target gene promoters but can activate gene expression through DNA looping [32]. More recently enhancer sequences have also been found to be pervasively transcribed into enhancer RNAs (eRNAs) [31]. Whilst further evidence is needed to fully understand the function of eRNAs, early work suggests they may further support transcription activation of target coding genes by modifying chromatin structure to make promoter sequences more accessible, stabilising enhancer-promoter interactions, trapping transcription factors at genomic sites and regulating the pause and release of RNA polymerase II at target promoters [31].

1.2.2 DNA and Chromatin Structure

Gene expression is further regulated through the control of DNA compaction. The billions of base pairs of DNA code that make up eukaryotic genomes is not free inside the nucleus, instead it is tightly associated with an approximately equal mass of protein [21]. Together DNA and the associated proteins form a structure known as chromatin [21]. A dynamic chromatin structure determines the ability of transcription factors and the transcription machinery to interact with DNA sequences [21]. The basic structural component of chromatin is the nucleosome, consisting of 146bp of DNA tightly wrapped around the surface of a core histone octamer, in a left handed superhelix of almost two turns [33, 34]. Nucleosomes are then condensed together into 10nm and then 30nm fibres, and form highly organised coils and loops which are finally packed ever more densely into chromosomes (Figure 1.3) [21, 35]. Chromatin is categorised into euchromatin, a looser structure that permits gene expression, and heterochromatin, a very dense structure that is less accessible to external proteins, including the transcription machinery, and is associated with transcriptional silencing [21].

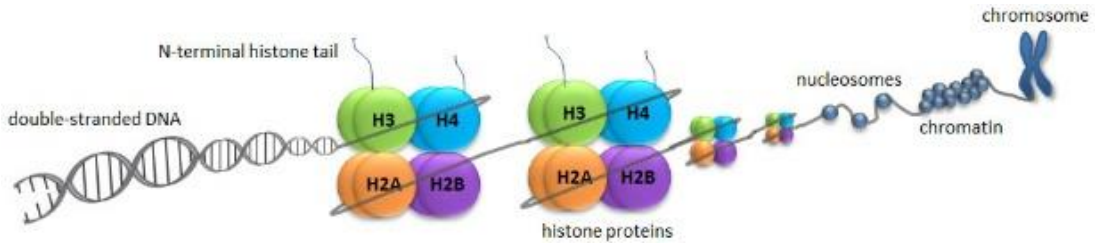

Figure 1.3 Packaging of DNA into Nucleosomes and Chromosomes. Exactly 146bp of double stranded DNA is wrapped around a central histone octamer, consisting of two H3/H4 and two H2A/H2B heterodimers [1]. Additional linker DNA connects to the adjacent nucleosome [9]. Nucleosomes can then progressively form more compact structures; a 10nm fibre, which condenses into a 30nm fibre, which further condenses into 100-200nm fibres, finally forming dense heterochromatin. Image from [12].

A more recent study has argued that chromatin organisation is not quite as simplistic as this text-book model, and that at least some regions of chromatin are comprised of a flexible and disordered granular chain of between 5 and 24nm [36]. The visualisation of chromatin via a DNA labelling method enabled these authors to determine that chromatin structure differs in nuclei in different states, with interphase nuclei displaying more extended chromatin structure, and mitotic nuclei displaying more compact loops [36]. Exactly how changes in chromatin structure are regulated is an ongoing area of research.

1.2.3 Epigenetics

Regulatory factors can modify how tightly DNA binds to its local histone environment, thereby modifying local chromatin structure and controlling access of the transcription machinery to DNA sites [24]. The density of the DNA-histone binding is controlled by the charge of both components [37]. DNA itself can be modified by methylation whilst the lysine rich N-terminus of each histone, which extends out from the surface, is exposed to reversible acetylation, phosphorylation, methylation and ubiquitination (Figure 1.4) [34]. These modifications are placed and removed in a dynamic manner by specific enzymes [38]. Methylation and acetylation of histone tails, and methylation of DNA directly effects the stability of nucleosome particles by altering the charge attracting the two elements together [34, 39]. The more the charges are neutralised the more nucleosomal DNA is unwrapped and the more accessible the DNA becomes [34]. Furthermore, modified histone tails serve as binding sites for proteins that specifically recognise the post-translationally modified histone, including chromatin remodelling proteins, which are crucial for translocating nucleosomes along the DNA sequence to further control accessibility of DNA sequences [34, 40]. Large scale and small scale shifts in the density of different chromatin regions is vital to control gene expression in response to environmental stimuli and through the key regulatory processes of development and differentiation [41].

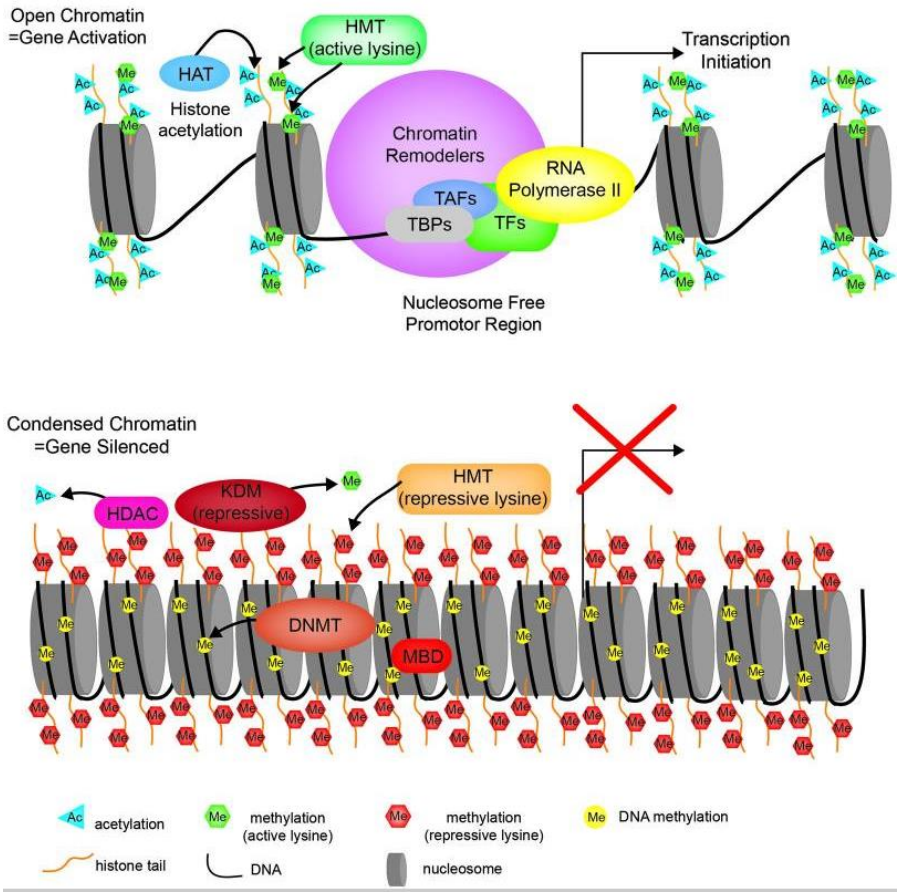

Figure 1.4 Euchromatin and Heterochromatin. Euchromatin (open chromatin) is permissive of gene expression. Histone acetylation by HATs (histone acetyl transferases) and methylation of active lysine residues by HMTs (histone methyl transferases) ensures an open chromatin structure accessible to the transcription machinery (TBP – TATA binding protein, TAFs – TBP associated factors, TFs – transcription factors, RNA polymerase II). Heterochromatin (condensed chromatin) contains silenced genes. Histone deacetylation by HDACs (histone deacetylases), methylation of repressive lysine residues by HMTs, removal of active lysine methylation marks by KDMs (lysine demethylases), and methylation of DNA by DMNT (DNA methyltransferase) ensures close association of DNA and histone proteins, and blocks access of the transcription machinery. Image from [11].

1.3 Wilms' Tumour Suppressor Protein 1 (WT1)

1.3.1 Introduction to WT1

The transcription factor Wilms' tumour protein 1 (WT1) is a major regulator of genes involved in a range of important cellular functions; including tissue development, growth, differentiation, and apoptosis [42]. During mammalian development WT1 is essential for the correct development of a range of tissues and organs including the kidneys, spleen, liver, heart and blood vessels, blood cells, body muscle, nervous system, eye and lungs [42-44]. WT1 is also a major regulator of adult homeostasis, particularly of mesenchymal derived tissues such as bone and fat [45]. The nature of WT1 function has been greatly studied over the last two decades, revealing great complexity and highlighting the importance of WT1 function in regulating the transcription, epigenetic landscape and protein function of its targets for development and adult tissue maintenance.

The importance of WT1 during development is highlighted by the range of developmental disorders that result from mutations affecting WT1 function and expression levels. Intergenic mutations in DNA-binding domains of WT1, often exon 8 or 9, leads to developmental abnormalities such as Denys-Drash syndrome, Meacham syndrome, gonadal dysgenesis, nephropathy and Wilms' tumour predisposition [46]. Further WT1 point mutations which affect splice sites and the balance of WT1 isoforms leads to Frasier syndrome [46]. Mutations leading to loss of WT1 function, or deletion of the *WT1* gene from chromosome 11, leads to aniridia, genitourinary abnormalities and mental retardation (WAGR) syndrome [47]. *WT1* mutations are also associated with lung, prostate, breast, ovarian cancers and leukaemias, plus the formation of tumours including the paediatric nephroblastoma Wilms' tumour (after which it is named) [48-51].

1.3.2 WT1 Protein Isoforms, Structure and Modifications

The human *WT1* gene is located on human chromosome 11 (band p13) and spans approximately 50kb including 10 exons [52]. The region can generate at least 24 different WT1 protein isoforms through a combination of alternative splicing, RNA editing, and use of alternative translation start sites [52]. The two major exons that undergo alternative splicing are exon 5 and exon 9, where the entirety of exon 5 (17 amino acids) and a lysine-threonine-serine (KTS) sequence of exon 9, can be either inserted or excluded [53]. The +KTS and -KTS isoforms perform different functions but are the most conserved, present in all vertebrates, suggesting they comprise the

most important variations [54]. The +KTS form is known to bind RNA more strongly than DNA and is associated with the post-transcriptional regulation functions of WT1 [54, 55]. Mouse models have also demonstrated that the +KTS form is essential for male sex determination and development of the olfactory system [43, 56]. The -KTS form of WT1 preferentially interacts with DNA and is generally considered the main form of WT1 that regulates transcription. Human and rat WT1 transcripts have been identified with either a thymidine or cytosine residue at position 839 in exon 6, proposed to be caused by RNA editing and which leads to the incorporation of leucine or proline at amino acid 280, respectively. The resulting proteins appear to target promoters with differing efficiencies and each play important roles during development [57]. Additionally, an alternative (CTG) translation start site 204bp upstream of the major ATG start site, and another ATG downstream have also been reported and result in the translation of longer and shorter in-frame versions of WT1 [52, 58, 59].

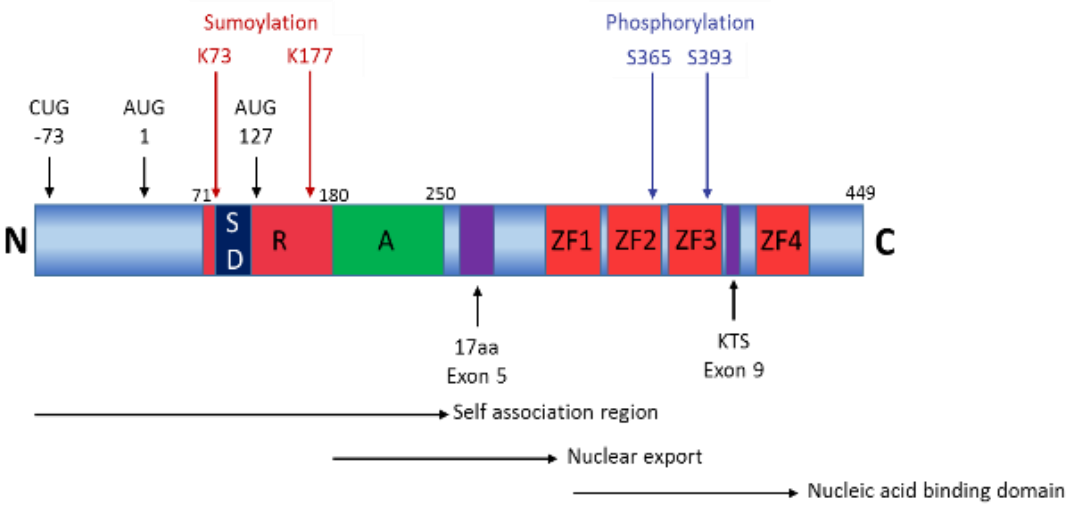

Figure 1.5. Wilms' Tumour 1 Protein Functional Domains and Modifications. A linear schematic of the WT1 protein is shown. Amino acids are numbered, with alternative start sites and sumoylation and phosphorylation sites indicated above. Alternative splice sites are indicated below. Regions involved in self-association, nuclear export and nucleic acid binding are shown. N, N-terminus; SD, suppression domain; R, repression domain; A, activation domain; ZF1-4, zinc fingers 1-4; C, C-terminus.

A schematic depicting the key functional domains and modifications of WT1 is shown in Figure 1.5 The WT1 protein contains functionally independent domains which enable activation and repression of target genes. Residues 71-180 comprise the transcriptional repression domain, and residues 180-250 the transcriptional activation domain [60, 61]. Two domains at amino acids 1-45 and 157-253 permit protein self-association, although a physiological role for this has not been

determined [62]. There are also domains involved in nuclear export, and four zinc fingers at the C terminus involved in DNA binding [61].

The complexity of WT1 function is increased further through post-translational modifications and the binding of an array of cofactors. Phosphorylation of WT1 by protein kinase A (PKA) or protein kinase C (PKC) at serine 365 and serine 393, within the second and third zinc finger domains, blocks DNA (but not RNA binding) [63, 64]. Phosphorylation therefore directly effects transcription and decreases transcriptional repression. Sumoylation of WT1 at Lysine 73 and Lysine 177, within the repression domain, has also been identified although the effect of this modification on the transcriptional regulation function of WT1 remains undetermined [65].

Evidence suggests that mutant forms of WT1 can exert a dominant negative effect on other WT1 isoforms through self-association, highlighting the necessity to better understand the individual functions of WT1 isoforms and their role in disease [66]. Ultimately, despite advances in our knowledge of the importance of different WT1 isoforms, determining the precise roles of individual isoforms for gene regulation, development and disease remains a considerable challenge. Further studies in mouse models are perhaps the best means to provide insight into isoform functions.

1.3.3 WT1 as a Transcriptional Regulator

Transcriptional regulation by WT1 is highly complex largely due to the fact that it can function as both a transcriptional activator or repressor towards its targets depending on its interaction with specific cofactors [67]. Indeed, WT1 can interact with the histone acetyl transferase (HAT) CBP to acetylate histone tails at target gene promoters and promote transcription activation, or it may associate with the co-repressor brain acid soluble protein 1 (BASP1) and recruit histone deacetylases (HDAC), or the CTCF protein to modulate chromatin structure [3, 67-69]. Furthermore, WT1 can recruit DNA methyltransferase 1 (DNMT1) which can modify both histone tails and DNA itself through methylation [70]. Additionally, WT1 can bind DNA directly or it can be recruited to gene promoters by binding to other DNA-binding proteins including p53 [67, 71]. Thus, WT1 has multiple activities which contribute to the state of the local chromatin environment at its target genes. WT1 activity is further complicated by its multiple splice forms which display distinct interactomes and have distinct effects on target gene expression [54, 56].

1.3.4 WT1 and Cancer

Wilms' tumour is the most common paediatric renal tumour, accounting for around 85% of all childhood renal cancers. It affects 1 in 10,000 children, with the median age of children at diagnosis being just over 3 years old [72]. The disease occurs at significantly higher frequencies in individuals with a genetic predisposition such as heritable *WT1* mutations [72].

The tumour driving effect of aberrant WT1 in Wilms' tumour arises from its essential role in kidney development. WT1 is essential for the mesenchymal to epithelial transition (MET) of the developing kidney metanephric mesenchyme into the epithelial nephron [72, 73]. Work with *WT1* mutant mice has highlighted that the timing of *WT1* mutation is critical in determining the effect of the mutation. *WT1* mutations occurring very early or very late in renal development often do not lead to tumour formation, instead often leading to a complete lack of kidney and gonad development (early mutations), or glomerular sclerosis (late mutations) [72]. It is most likely that *WT1* mutation alone is not sufficient to induce tumourigenesis, but when the dysregulation of differentiation is combined with mutations leading to aberrant proliferation, such as *Igf2* overexpression, renal tumour formation can occur [72, 74].

Somatic *WT1* mutations occur in between 5-25% of sporadic Wilms' tumours, making *WT1* one of the most frequently mutated genes in this cancer type [72, 75]. Other common mutations include *WTX* (18%), *TP53* (5%) and *MYCN* (3.8%). All of these are related to WT1, in that *WTX* is associated with *WT1* transcriptional control, p53 interacts directly with WT1 to modulate activation of their both target genes, and WT1 controls *MYCN* expression [71, 76, 77]. These findings highlight that WT1 can affect multiple pathways in tumour development and progression.

WT1 mutations are also associated with several types of leukaemia, affecting both children and adults, and other adult cancers including lung, prostate, breast and ovarian cancers [48, 50, 51]. As WT1 functions to both activate and repress target genes it can act as both an oncogene and a tumour suppressor depending on cellular context, giving it a highly complex role in tumourigenesis [54, 78]. WT1 is expressed at relatively low levels in normal human bone marrow and in leukaemia *WT1* mutations are relatively uncommon, but aberrant overexpression of WT1 protein is common, with 80% of immature leukaemia cells expressing higher levels of WT1 than more mature cells [79]. The effect of excessive *WT1* expression in haematopoietic cells is thought to be related to its role in self-renewal of early

haematopoietic cells, such that when overexpression of *WT1* is combined with other mutations that block differentiation, like the AML-ETO gene fusion, excessive proliferation of immature cells can occur. Therefore, in leukaemia, *WT1* overexpression is associated with poorer prognosis and can be used as an independent prognostic factor for survival in acute myeloid leukaemia (AML), acute promyelocytic leukaemia (APL) and T-lymphoblastic leukaemia patients [72].

In summary, WT1 plays a significant role in a variety of cancers, largely due to its significant and far reaching role in development. *WT1* mutations predominantly affect childhood and adolescent cancers, although WT1's involvement in some adult cancers and solid tumours is also significant. The consequence of WT1 changes is highly dependent upon the tissue, the timing and the effect of the mutation on *WT1* expression levels. The complex interactions and functions of WT1 are continually being better understood, however there remains poor understanding of how cancer associated changes in WT1 drive tumour formation and progression.

1.4 Brain Acid Soluble Protein 1 (BASP1)

1.4.1 Introduction to BASP1

BASP1 was initially identified as an N-terminally myristoylated protein from the cytoplasm of brain cells [80]. At the time it was grouped with three other proteins, BASP2-1, BASP2-2 and BASP3 which shared properties such as a molecular weight of 20-24kDa, abnormally low migration via SDS-polyacrylamide gel electrophoresis (SDS-PAGE), and very acidic isoelectric points (pI 4.3-4.6) [80]. Later BASP2-1 and BASP2-2 were identified as two forms of the neuronal protein GAP-43. BASP1 is now commonly regarded as belonging to a family of growth-associated proteins including GAP-43 and myristoylated alanine rich protein kinase C substrate (MARCKS) [81]. Although these proteins do not share sequence similarity, they do share several properties including high hydrophilicity, N-terminal myristoylation and subsequent linkage to the plasma membrane, preferentially within lipid rafts [81]. BASP1, GAP-43 and MARCKS also all share a highly basic region which facilitates an interaction with acidic phospholipids, including phosphatidylinositol-4,5-bisphosphate (PIP_2), Ca^{2+} bound calmodulin and actin filaments. All these interactions are perturbed by PKC-mediated phosphorylation [81].

In accordance with its expression in neuronal cells, BASP1 has been described as being essential for neuronal development [81]. BASP1 expression levels are particularly high during brain development, and high levels are maintained into adulthood in selected brain regions [81]. During neuronal development BASP1 causes sequestering of PIP_2 in the plasma membrane in a cholesterol dependent manner, producing PIP_2 rich lipid rafts and cholesterol-depleted domains. The formation of these membrane domains and lipid rafts in the plasma membrane are essential for subsequent neurite outgrowth [82, 83]. BASP1 is also often reported to be involved in axonal growth and guidance [81]. Similarly, overexpression of BASP1 in adult neurons also promotes sprouting, and is entirely independent of well-characterised NCAM-mediated neurite outgrowth, which GAP-43 is known to contribute to [81, 84]. These findings lead to the conclusion that the primary function of BASP1 in neuronal tissues is the regulation of cell morphology, through the organisation of lipid rafts prior to neurite outgrowth.

In addition to its described role as a neuronal membrane protein, BASP1 has been identified as a transcriptional regulator. This function of BASP1 was revealed following an *in vitro* transcription assay which provided direct evidence that BASP1

binds to the WT1 suppression domain and mediates WT1 target gene repression [49]. Further investigation of BASP1 expression *in vivo* confirmed it is expressed in multiple tissues throughout the developing embryo including the heart, lungs, thymus, liver, tongue and central nervous system [49]. Importantly, BASP1 is spatially and temporally coexpressed alongside WT1 in many of these tissues, including the kidney, implicating it as an important regulator of WT1 during development [49].

1.4.2 BASP1 Protein Structure and Modifications

BASP1 protein exists in multiple forms due to differences in proteolytic processing and post-translational modifications [3, 49, 85, 86]. Several BASP1 isoforms are commonly present and the ratio of isoforms varies between BASP1 expressing cell types. Myristoylation at the N-terminus of BASP1 is the most notable modification; this occurs co-translationally, mediated by N-myristoyltransferase1, and has been identified in multiple tissues and cell lines [3]. Myristoylation is critical for BASP1's function as it is the sole source of the protein's hydrophobic properties which allow it to effectively interact with cell membranes and function as a transcriptional repressor [3, 80, 81, 86]. After myristoylation, phosphorylation likely has the greatest effect on BASP1 function. Phosphorylation at the N-terminal serine 6 residue, a PKC target site, causes redistribution of BASP1 within the cell through disruption of the positive charge at the N-terminus [3]. This results in unfavourable electrostatic forces near the myristoyl motif and disrupts the interaction with lipids resulting in the release of BASP1 from membranes [3, 80, 87]. The same PKC mediated phosphorylation of the N-terminal region of the MARCKS protein is also known to cause its release from membranes [80].

BASP1 can also undergo sumoylation at lysine residues 78 and 83, causing redistribution of BASP1 from chromatin to the nuclear matrix, including to within PML bodies, and potentially enhancing its WT1 corepressor function [85]. Extensive methylation and/or acetylation of the lysine-rich N-terminus of BASP1 has also recently been identified in the Roberts' lab (unpublished) and most likely also regulates lipid and membrane interactions. The transient nature of most modifications suggests they provide a means of modifying BASP1 activity.

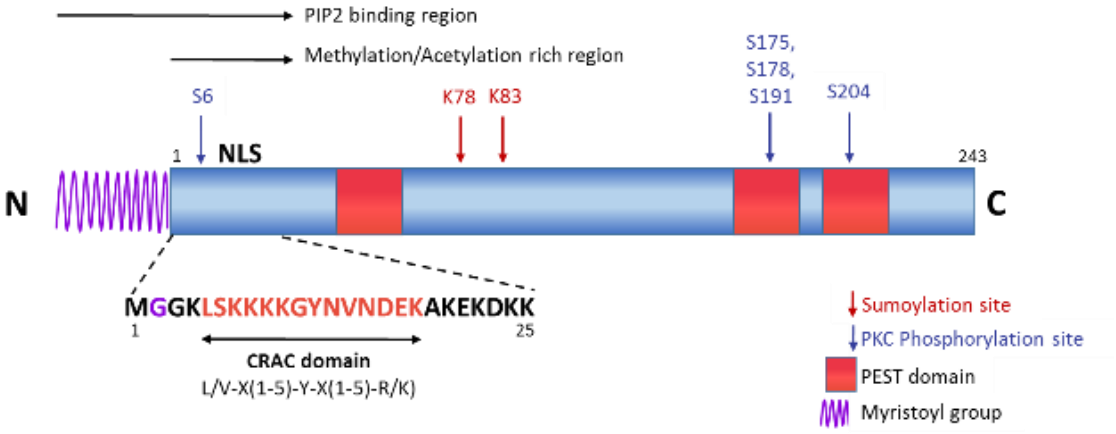

Figure 1.6. Brain Acid Soluble Protein 1 (BASP1) Functional Domains and Modifications. A linear schematic of the BASP1 protein. The N-terminal myristoyl group is shown in purple. Amino acids are numbered 1-243. The highly conserved sequence of the first 25 amino acids is written below. This contains a purple G residue which represents the Glycine to which the myristoyl group is added. The cholesterol recognition amino acid consensus sequence (CRAC) is also indicated in red. PKC targeted phosphorylation sites (purple arrows) and sumoylation targeted residues (red arrows) and indicated. The PIP_2 binding region and the methylation/acetylation rich region are also indicated above (black arrows). The 3 pest domains are shown in red boxes.

The majority of known modifications to BASP1 occur within the N-terminus (see Figure 1.6). This region is also the most highly conserved in amino acid sequence across mammals, birds, amphibians and fish. Overall, the human BASP1 sequence is 80%, 70% and 45% similar to bovine, rat and chicken, respectively, indicating the importance of its function [80]. The N-terminus is also the location of the nuclear localisation sequence and the cholesterol recognition amino acid consensus (CRAC) domain. The CRAC domain, a L/V-X(1-5)-Y-X(1-5)-R/K amino acid sequence, allows an interaction with cholesterol [88]. Additionally, BASP1 contains several PEST sequences, a feature of proteins that undergo high turnover. The conservation of these PEST sequences across species implies their significance for protein function [80]. Many of BASP1's phosphorylation sites fall within these conserved PEST sequences, suggesting the stability of BASP1 could be under the control of a set of kinases which modify the PEST sequences and affect BASP1 degradation. PEST sequences have also been identified in GAP-43 and MARCKS, and transmembrane NCAM which has a role in learning and memory formation [80].

1.4.3 BASP1 as a Transcriptional Regulator

The function of BASP1 as a transcriptional regulator has most often been studied, and is best understood, in the context of it binding the WT1 suppression domain.

The function of BASP1 as a WT1 cofactor will be discussed in section 1.5. It is also important to consider the evidence that BASP1 likely regulates many other proteins. Microarray analysis of K562 cells that ectopically express BASP1 versus control K562 cells revealed that across the genome over 1000 genes were regulated by BASP1 (Figure 1.7) [2]. This indicated that BASP1 function is not limited to the regulation of WT1 targets and therefore that BASP1 has a wider role in transcriptional regulation. Furthermore, BASP1 has also recently been implicated as a cofactor for the oestrogen receptor α (ERα), for which it is also responsible for the repression of ERα target genes [89]. Moreover, a recent report implicated BASP1 as a major regulator of Lin28 and Oestrogen Related Receptor Beta (ESRRB) during the differentiation of pluripotent stem cells, suggesting BASP1 plays a major role in cell fate [90].

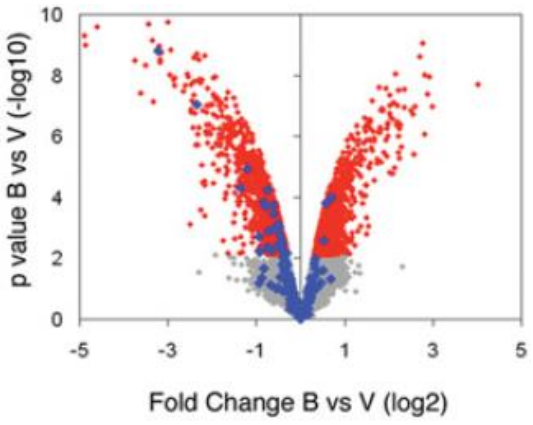

Figure 1.7. BASP1 Regulates the Expression of Over a Thousand Genes in K562 Cells. Microarray analysis was performed with K562 cells that ectopically express BASP1 (B) versus control K562 cells (V) and data were analysed as described in [2]. Red areas show significant changes in gene expression. B cells show an equivalent number of repressed and activated genes. The majority of altered WT1 target genes (blue dots) are repressed. Grey areas indicate small changes below the level of significance. Full details of observed expression changes are shown in [2].

1.4.4 BASP1 and Cancer

BASP1 mediated repression of WT1 target genes, which are involved in cell growth and differentiation, implicates it as a tumour suppressor [1]. Recent establishment of BASP1 as co-repressor of ERα further demonstrates BASP1 functions as a tumour suppressor in breast cancer [89]. A range of other evidence also implicates BASP1 as a tumour suppressor including that the BASP1 gene is silenced via promoter methylation in a broad range of cancer types [91]. Additionally, a genome wide

association study of melanoma identified a polymorphism that results in the suppression of BASP1 expression as a key risk factor for melanoma development [92]. Furthermore, BASP1 is known to inhibit cellular transformation by oncogenic Myc and inhibit the proliferation and migration of thyroid cancer cells [91, 93].

In addition to K562 cells, BASP1 protein has recently been identified as lacking detectable expression in a range of CML cell lines (Figure 1.8). K562, KCL-22, LAMA-84, KU-812, KYO-01, JURL-MK1 cell-lines, all of which are derived from CML in blast crisis, display lack of BASP1 protein expression via western blotting (Jörg Hartkamp, unpublished). WT1 expression is apparent in all lines except KU-812. In contrast, BASP1 is expressed in the analysed AML cell lines (HEL, HL-60, NB-4, U937, MV4-11, MOLM-13) suggesting lack of BASP1 expression is specific to CML. It is possible that BASP1 expression is lost in CML, suggestive of a tumour suppressive function for BASP1 in CML. Alternatively, knowing that clinically AML is the more severe disease with poorer patient prognosis and survival rates, it is possible that BASP1 expression in AML could be contributing to more severe disease and could therefore be suggestive of an oncogenic function for BASP1 [94]. Interestingly, the first evidence that BASP1 acts in an oncogenic manner was recently reported whereby BASP1 is upregulated and promotes the proliferation and tumourigenicity of cervical cancer cells [95]. Further work is required to establish whether BASP1 may function as an oncogene or tumour suppressor in myeloid leukaemias, as well as investigating further the role of BASP1 in other cancers.

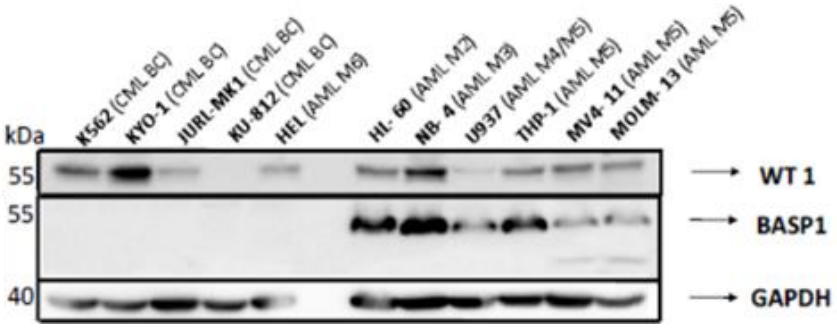

Figure 1.8. BASP1 Protein Expression in CML and AML Cell Lines. A panel of chronic myelogenous leukaemia (CML) and acute myeloid leukaemia (AML) cell lines were assessed for their expression of BASP1 and WT1 protein. GAPDH is shown as a loading control. All CML lines examine are absent of BASP1 expression, whilst WT1 expression is maintained in all AML and CML lines, with the exception of KU-812 (Jörg Hartkamp, unpublished).

1.5 WT1/BASP1 Mediated Gene Regulation

1.5.1 Mechanism of WT1/BASP1 Mediated Gene Repression

The molecular mechanism of BASP1 mediated repression of WT1 target genes has become increasingly clear in recent years (see Figure 1.9). Following the first mechanistic data which showed that BASP1 binds to the WT1 suppression domain at the promoters of WT1 regulated genes, BASP1 was shown to recruit several proteins including prohibitin, BRG1 and HDAC1 to the repression complex, in a myristoyl motif dependent manner [3, 49, 85, 96]. The myristoyl motif allows BASP1 to interact directly with the phosphoinositide $PI(4,5)P_2$ (hereafter referred to only as PIP_2) and this interaction occurs at the target gene promoter, as demonstrated through chromatin immunoprecipitation (ChIP) assays [3]. The presence of PIP_2 at WT1/BASP1 bound target gene promoters is essential in order to recruit further complex components. The recruitment of HDAC1 results in the removal of negatively charged acetyl groups from sites such as histone 3 lysine 9 (H3K9), therefore inducing a stronger DNA-histone association and limiting access for the transcription machinery, leading to gene repression [3]. The WT1/BASP1 repression complex also recruits prohibitin, a well characterised corepressor to the WT1-BASP1 repression complex, in a myristoyl-dependent manner [96]. Furthermore, recruitment of prohibitin is followed by recruitment of BRG1, the catalytic subunit of the chromatin remodelling SWI/SNF complex to mediate transcriptional repression at WT1 target promoters [96].

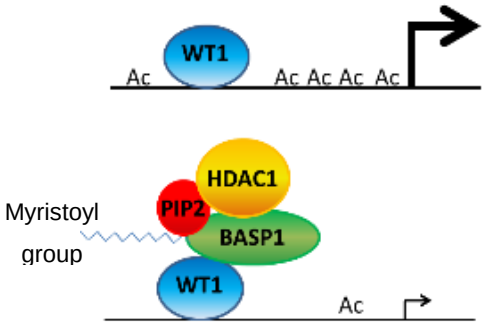

Figure 1.9. Transcriptional Repression by BASP1 Through Interaction with Nuclear Lipids. Myristoylation of the N terminal glycine of BASP1 facilitates an interaction with $PI(4,5)P_2$ at the promoters of WT1 target genes. Subsequent recruitment of chromatin remodelling factors such as HDAC1 mediates target gene repression through the removal of activating H3K9 acetyl groups.

Experiments utilising wild type BASP1 (wtBASP1) expressing K562 cells, and a PIP_2 binding mutant form of BASP1 (G2A-BASP1) expressing cells were used to elucidate the mechanisms described above. The G2A mutant form of BASP1 consists of a glycine-2 to alanine mutation which positions the alanine residue in place of the N-terminal glycine to which the myristoyl motif is cotranslationally

added. This forms a myristoyl null form of BASP1 which is known to be deficient in PIP_2 binding [3]. As well as showing that the myristoyl modification is essential for recruiting components of the repression complex, gene expression analysis confirmed that G2A-BASP1 is defective at repressing WT1 target gene expression [3]. This work implicated PIP_2 as a vital component for WT1/BASP1 mediated gene repression. To date, BASP1 is the only promoter-localised transcriptional regulator known to require a direct interaction with a lipid to carry out its transcription regulation function. BASP1 therefore provides a unique means by which to investigate the role of lipids in transcription.

1.5.2 WT1/BASP1 and Differentiation

WT1 and BASP1 are known to be spatially and temporally coexpressed in multiple tissues in the embryo, including the kidney, spleen, heart, ovary and testis [49]. Their coexpression in a variety of tissues suggests BASP1 may be an important regulator of WT1 through development and differentiation. In cultured cells, expression of BASP1 causes the differentiation of K562 cells to be diverted from a megakaryocyte lineage to a neuron-like lineage following treatment with the phorbol ester PMA [2]. Induction of K562 cell differentiation in culture by various agents had never previously lead to their differentiation to anything other than a blood cell type; yet PMA treatment of BASP1 expressing cells was sufficient to divert towards a neuronal-like state complete with neuron-like morphology, neuronal marker gene expression, and some functional properties of neurons [2, 97]. Further, BASP1 controls WT1 target gene expression through the differentiation of cultured podocytes, altering promoter occupancy and gene repression as differentiation progresses [85]. BASP1 and WT1 have recently been found to be coexpressed at the terminal stages of taste cell differentiation in the mouse. BASP1 is critical to maintain the differentiated cell state of these neuroepithelial cells through repression of WT1 target genes (unpublished). Also, as mentioned previously, BASP1 was recently implicated as a major regulator of pluripotent stem cell fate through its repression of Lin28 and ESRRB target genes in cooperation with WT1 [90]. These studies indicate that BASP1 is a major transcriptional regulator of multiple transcription factors during development, differentiation and maintenance of the differentiated state in adult cells.

1.6 Nuclear Lipids

1.6.1 Introduction to Nuclear Lipids

Lipids are a broad class of largely non-polar organic molecules which play multiple fundamental roles in mammalian cells; they are key structural components of the plasma membrane and cellular compartments such as the endoplasmic reticulum, the golgi apparatus, vesicles, lysosomes and the nuclear membrane [98]. Lipids also provide energy reserves and serve as biologically active molecules in their own right, with fundamental roles in cell signalling [99, 100]. The roles of lipids in the plasma membrane and in the cytoplasm are well documented, however, the role of nuclear lipids remains much less well understood [101]. Decades of biochemical evidence plus more recent studies have established that as well as residing in the nuclear membrane, nuclear lipids are present outside of membranes [102-105]. It is now widely accepted that approximately 70-80% of all nuclear lipids are present in the nuclear membrane, and the remaining 20-30% are known to be associated with the nuclear matrix, chromatin and interchromatin granules [101, 106, 107].

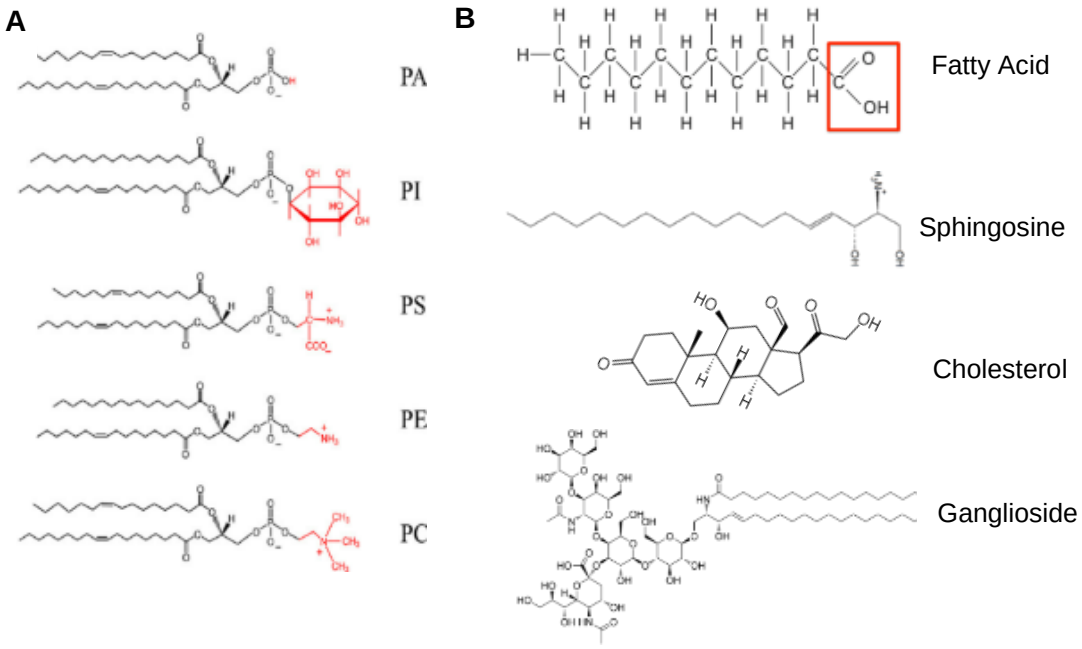

Figure 1.10 Common Nuclear Lipids. The diagrams depict **A**, the structures of the phosphophatidic acid (PA) and the major phospholipid derivatives of PA, phosphatidylinositol (PI), phosphatidylserine (PS), phosphatidylethanolamine (PE) and phosphatidylcholine (PC). The hydrophilic head groups (-H, inositol, serine, ethanolamine and choline) attached to the basic phospholipid structure are shown in red. **B,** the structures of the other most common nuclear lipids. Top; an example of a fatty acid structure, with the characteristic –COOH group (in red box). Fatty acid tails vary in length and in their level of saturation. Also shown is the structure of a basic sphingosine molecule, a cholesterol molecule and a ganglioside molecule. Images adapted from [4-8].

The pool of nuclear lipids consists of phospholipids, sphingolipids, gangliosides, cholesterol and fatty acids [108]. Phospholipids are the most abundant in membranes, where their polar head groups align and allow the hydrophobic hydrocarbon tails to be shielded within the bilayer membrane structure [109]. The most abundant phospholipids in the nucleus are phosphoinositides (PI), phosphatidylethanolamine (PE), phosphatidylcholine (PC) and phosphatidylserine (PS) [108]. The structures of these phospholipids and the other most common lipids in the nucleus are shown in Figure 1.10 [4-8]. The nuclear pool of lipids is further diversified through modifications to these lipids, such as the addition of phosphate groups to the carbons of the inositol ring of PI or the differing length and saturation of fatty acid tails, to create a highly diverse pool of nuclear lipids each with distinct functions [108].

The intranuclear pool of lipids is further regulated through controlled cycles of lipid metabolism by lipid regulating enzymes in the nucleus. The inositide cycle, controlled by phosphoinositol-3-kinase (PI3K) and phospholipase C (PLC) controls levels of differentially phosphorylated forms of PIs as well as the fundamental secondary messengers Ins[3,4,5]P_3 and diacylglyceride (DAG) [108]. Cycles of sphingomyelin (SM) production by sphingomyelin-synthase and degradation by sphingomyelinase into phosphocholine and ceramide regulates nuclear levels of ceramide and DAG [108]. Ceramide is further hydrolysed into free fatty acid and sphingosine, plus sphingosine can undergo conversion to sphingosine phosphate [108]. Such metabolism of intranuclear lipids is distinct from the metabolism of plasma membrane lipids adding to evidence that they form a uniquely functional group of lipids [102, 110]. It is now widely accepted that intranuclear lipids are regulated in accordance with cell behaviour; from cell growth to survival, differentiation and apoptosis [101, 111]. Cross-talk between the activity of enzymes such as sphingomyelinase, sphingomyelin-synthase and PLC also regulates the ratio of different lipids, primarily PC:SM:cholesterol in different subnuclear locations, creating distinct pools of lipids within the nucleus, which carry out distinct functions [112]. The levels of many PI metabolising enzymes are also known to vary in response to a range of stimuli, including DNA damage, oxidative stress, UV irradiation, growth factor stimulation, cell cycle progression and differentiation [113]. This results in different patterns of PIs and second messengers within the nucleus that ultimately regulates cellular response [114]. PI levels are particularly tightly regulated during differentiation and cell cycle progression; indicating their particular importance for gene regulation [114].

1.6.2 Intranuclear Lipids

It is now appreciated that nuclear lipids exist within the nucleoplasm and evidence suggests they are associated with many nuclear structures. Firstly, many PI regulating enzymes have been shown to produce and degrade PIs at the inner nuclear membrane (INM) [115]. This supports evidence that the nucleus does not simply only passively receive lipids from the endoplasmic reticulum and outer nuclear membrane, as once thought, and implicating the INM as a site of dynamic lipid metabolism [115]. In membranes the hydrophobic tails of phospholipids are buried within the bilayer structure and the polar head group is exposed allowing lipids to recruit proteins and function in signalling [116]. In the nucleoplasm however, it is still not well understood how the hydrophobic tail is shielded from the aqueous inner nuclear environment. It is predominantly proposed that inner nuclear lipids must exist as lipid droplets and associate with protein complexes and nuclear bodies. Nuclear lipids have been shown to associate with protein complexes involved in a diverse range of nuclear processes including RNA processing, chromatin remodelling and gene transcription [101, 107, 113, 117, 118]. Still, the molecular detail of how lipid tails are accommodated by such associations and the molecular mechanisms through which lipids are involved in nuclear processes remains largely unknown.

Lipid droplets have been well characterised in the cytoplasm, and have now also been identified in the nucleus, acting as storage repositories and functioning to modulate lipid metabolism, thereby contributing to several physiological processes [119]. In addition to lipid, these droplets contain and interact with numerous proteins [119]. It has been suggested that the interaction of lipids with lipid binding proteins and protein complexes in this way may enable shielding of the lipid tail. Certainly, some nuclear proteins do contain lipid binding domains which can accommodate binding by several phospholipid ligands, such as the transcription factor NR5A1 (Steroidogenic factor 1 receptor) which can engulf the acyl chain of phosphatidylinositol 4,5-bisphosphate (PIP_2) and phosphatidylinositol 3,4,5-trisphosphate (PIP_3) but leave the polar head group exposed [120].

Additionally, since the reporting of BASP1-PIP_2 mediated gene regulation, the myristoylated alanine-rich C-kinase substrate (MARCKS) protein has been implicated in nuclear PIP_2 storage [121]. In the cytoplasm MARCKS is well known to have roles in cell motility, phagocytosis, membrane trafficking, mitogenesis and to act as a PIP_2 store, regulated by reversible cycles of phosphorylation and de-

phosphorylation which releases and re-sequesters PIP_2, respectively [121, 122]. More recent data showing that MARCKS colocalises in nuclear speckles with PIP_2 and is involved in altering nuclear PIP_2 levels has implicated it as a regulator of nuclear PIP_2 [121]. Like BASP1, MARCKS is N-terminally myristoylated, which provides a valid potential biochemical mechanism by which to shield the hydrophobic tail of PIP_2 [3, 85]. As well as myristoylation MARCKS shares several other properties with BASP1, including an identical lysine rich sequence, found within the nuclear localisation sequence of BASP1, and the effector domain of MARCKS, which further mediates PIP_2 binding [121]. The similarity of BASP1 and MARCKS raises the possibility that BASP1 could also have a role in regulating the storage, release and levels of nuclear PIP_2. Furthermore, work from the Roberts' lab has demonstrated that BASP1 colocalises with PIP_2 in nuclear speckles (Figure 1.11) [3]. BASP1 is also known to form oligomers and multimeric structures which could further aid the shielding and sequestering of lipids in the nucleus [123, 124].

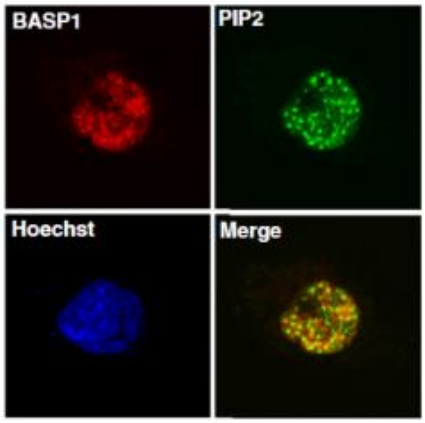

Figure 1.11. BASP1 and PIP_2 Colocalisation in Nuclear Speckles. Confocal microscopy of U2OS cell nuclei subjected to coimmunofluorescence with BASP1 and PIP_2 antibodies shows their colocalisation in nuclear speckles. Comparable results were also seen in MCF7 cells [3].

Other nuclear proteins that are known to interact with lipids include the nuclear receptors, such as Oestrogen Receptor (ERα) and Progesterone Receptor (PR), which are transcription factors activated by steroid hormones and other lipid-soluble signals, such as retinoic acid and oxysterols [102, 125]. Ligands of these receptors remain bound during the receptors trafficking through the cytoplasm and through the nucleus onto target DNA sites, thus these receptors are also able to shield their lipid ligand from the nuclear environment. It has also been shown that, similarly to membrane bound PI function, the binding of $PI(4,5)P_2$ and $PI(3,4,5)P_3$ to NR5A nuclear receptors regulates the interface between NR5A1 (Steroidogenic factor 1 receptor) and its cofactors, resulting in increased coactivator recruitment [126]. This

demonstrates that lipid binding to nuclear receptors permits their movement throughout the cell and regulates receptor activity.

The nuclear structures within which lipids have been visualised can correspond to the nucleolus and a number of nuclear bodies including PML bodies and Cajal bodies. Many of these nuclear structures have been proposed to accommodate lipid tails [127]. Nuclear speckles are predominantly associated with mRNA maturation, are rich in splicing machinery, poly adenylating polymerases and enzymes responsible for post-transcriptional modifications to mRNAs [102, 128]. The association of lipids with such structures implicates a role for them in mRNA maturation.

The bulk of nuclear lipid content is still provided by the lipids of the nuclear membrane [108]. Biochemical isolation of nuclear membranes has demonstrated the existence of lipid microdomains within the membrane which have particular roles in regulating nuclear function [122]. Typically these microdomains are characterised by a PC:SM:cholesterol ratio of 1:1:1 [101]. These microdomains are typically associated with lamin B, signal transducer and activator of transcription-3 (STAT-3) and newly synthesized RNA indicating they are involved in transcription regulation and could serve as a transcription factor resting place and scaffolds for RNA synthesis [122, 129]. It is also hypothesised that these lipid microdomains could act as sites of chromatin anchorage [122]. Such evidence suggests that even within the nuclear membrane distinct clusters of lipids have roles beyond simply providing membrane structure.

There remains much to learn about the function and storage of lipids in the nucleus. Lipids' binding to large protein complexes remains the most commonly proposed mechanism by which they can behave and function in the intranuclear environment. Profiling of all myristoylated proteins in human cells has so far revealed around 100 myristoylated proteins, but the knowledge of nuclear myristoylated proteins and their contribution to nuclear lipid biology is significantly lacking [130]. Further work is much needed to better understand nuclear lipid activity. More debatable is the existence of intranuclear membranes, with some work showing evidence of their formation following overexpression of nuclear lipidated protein [131]. The context of intranuclear membrane formation and their function is another area much in need of greater research.

1.6.3 The Role of Lipids in Gene Regulation

Chromatin bound phospholipids account for 10% of all nuclear lipids and increasing evidence suggests that phospholipids such as PIs, sphingosine-1-phosphate plus inositol phosphates and pyrophosphates are essential for healthy cell function through epigenetic regulation of the genome [101, 119, 132]. The nuclear lipid compartment can also broadly affect chromatin structure through regulating fluidity of the nuclear membrane and nuclear matrix [112]. Chromatin lipids also participate in signal transduction pathways, and many transcriptional regulators and chromatin remodelling factors interact with lipid regulating enzymes, such as PIPkinase, to locally generate lipids in a spatially and temporally controlled manner [113]. The levels of cholesterol-sphingomyelin-protein complexes in chromatin are also changed by altered lipid synthesis and metabolism during key cellular processes such as cell proliferation, indicating their importance for gene expression [133]. Furthermore, nuclear lipids also contribute to the maturation of RNA in intranuclear complexes [112, 114, 134]. It therefore appears that lipids play an important role in many stages of gene regulation.

One of the ways in which lipids contribute to gene regulation is through modulation of transcription factors. For example, cholesterol based molecules such as steroids and oxysterols, fatty acids, and some phospholipids can contribute to transcriptional regulation by serving as hormone-like ligands for the nuclear receptors including PPARs, Liver X Receptor (LXR), Farnesoid X Receptor (FXR) and Oestrogen Receptor (ERα) [135-138]. Many of these receptors control both transcriptional activation and repression of their target genes [102]. Furthermore, the association of SM with the nuclear lamina, a mesh of intermediate filaments that internally supports the nuclear membrane and associates it with chromatin, contributes to the sequestering of transcription factors away from chromatin [99, 101]. Thus, it is clear that many lipids can regulate cell function through binding transcription factors present in the nucleus.

As well as regulating transcription lipids have been heavily implicated in the regulation of chromatin structure. The nuclear matrix, defined as the nuclear component that remains insoluble following extraction with non-ionic detergents, salts and treatment with nuclease, harbours dynamic pools of lipids including PC and PI [101, 108]. The main function of the nuclear matrix is in the organisation of chromatin thus the dynamic regulation of lipids in this compartment indicates that,

as well as serving as parent molecules of lipid second messengers and other phospholipids, PC and PI may have a role in chromatin organisation [101, 108].

Recently, direct binding of cholesterol to chromatin was demonstrated and cholesterol shown to contribute to the formation of mononucleosomes and compaction of chromatin fibres [139]. Cholesterol can bind to six residues in key nucleosome regions, such as the histone 4 (H4) tail, the acidic patch on the nucleosome surface, and the docking domain between the histone 3-histone 4 (H3-H4) and histone 2A-histone 2B (H2A-H2B) clusters [139]. Many of the other small lipid molecules are present in the nucleus are hypothesised to directly bind nucleosomes and modulate chromatin structure [135].

Studying the recruitment of PIP_2 to the promoters of WT1 target genes, via BASP1, provided some of the first mechanistic information regarding the role of PIP_2 in transcriptional regulation at gene promoters [3]. This work revealed a direct role for PIP_2 in recruiting HDAC1 to mediate removal of activating H3K9 acetyl marks at target gene promoters [3]. In a similar way, PIP_2 regulates the interaction of the chromatin remodelling BAF complex and regulates its recruitment to chromatin and the nuclear membrane [118, 140]. Further evidence has also shown that PIP_2 can specifically bind to C terminal histone tails of H1 and H3 and reverse H1 mediated repression of transcription [141]. These findings indicate that PIP_2 influences chromatin structure in a number of ways.

Other PIs have also been shown to bind chromatin remodelling complexes and regulate their nuclear localisation. ING2, a core component of the Sin3a-HDAC1 chromatin remodelling complex, binds multiple PIs, with highest specificity for phosphatidylinositol-5-phosphate (PI5P) [142, 143]. This interaction is thought to help localise ING2 to the nuclear matrix, as downregulation of nuclear PI5P levels by PI4-kinase results in ING2 release from the matrix fraction [143]. Furthermore, production of PI5P, through dephosphorylation of plasma membrane $PI(4,5)P_2$, leads to the specific recruitment of ING2 to the membrane, suggesting that PI5P is also important for membrane localisation of ING2 [144].

PIP_2 is not alone in its ability to the regulate histone acetylation. Inositol phosphates have also been reported to bind HDAC complexes and regulate histone acetylation [145]. HDAC1 and HDAC3 are regulated through the binding of IP4, IP5 or IP6, to the interface between the HDACs and their co-repressors, metastasis-associated protein 1 (MTA1) and SMRT, respectively [119, 146, 147]. Furthermore,

sphingosine has also been found to regulate histone acetylation through inhibiting the activity of HDAC1 and HDAC2, leading to increased acetylation of H3K9, H4K5 and H2BK12 [148, 149]. This activity is promoted through sphingosine kinase 2 activity, which interestingly also inhibits HDAC activity resulting in reduced p53 activation of p21 [102]. These examples demonstrate how multiple lipids can regulate gene transcription through modulation of epigenetic regulators.

Several further examples of lipids contributing to epigenetic gene regulation have been documented. Nuclear $PI(4,5)P_2$ interacts directly with histone lysine demethylase PHD finger protein 8 (PHF8) and represses PHF8 activity through inducing a conformation change in the protein [150]. This $PI(4,5)P_2$ activity caused reduced demethylation of $H3K9me^2$, but not other substrates of PHF8, exemplifying the highly precise nature of this regulation [150]. This work also implicates PIP_2 also as a regulator of rRNA gene transcription at the epigenetic level. $PI(4,5)P_2$ further influences RNA polymerase I transcription and ribosomal RNA processing through its interactions with UBF, RNA polymerase I and fibrillarin [151].

Currently all published data on PIP_2 functions suggest that PIP_2 activity is dependent on the interacting partner; seeing as nuclear PIP_2 has in excess of 250 possible protein-interacting partners it is highly likely that PIP_2 influences the epigenome through other chromatin modifying proteins and subsequently affects many cellular functions [119, 152, 153]. A further study also suggested that PI5P may regulate the interaction of the E3 ubiquitin-protein ligase UHRF1 with H3 and different H3 modifications, primarily $H3K9me^3$ [154]. This suggests that PI5P may also regulate the epigenetic state of chromatin. Furthermore, UHRF1 recognises and binds hemimethylated DNA and recruits the methyltransferase DNMT1, suggesting that PI5P-UHRF1 possibly contributes to the inheritance of genome wide DNA methylation patterns [154]. As a further example of lipids contributing to epigenetic gene regulation, the activity of inositol hexakisphosphate kinase 1 (IP_6K1), responsible for the dynamic metabolism of inositol pyrophosphates, has been shown to be required for the association of Lysine Demethylase 4C (KDM4C) with chromatin [119]. IP_6K1 tightly associates with chromatin and specifically interacts with $H3K9me^3$ and not other KDM4C substrates [119, 155].

Clearly nuclear phospholipids and inositol phosphates contribute to nuclear processes such as transcription, chromatin remodelling, and epigenetics. However, there is still no comprehensive understanding of the molecular

mechanisms underlying the functions of nuclear lipids. Further mechanistic data is much needed to answer crucial questions such as how one lipid can act as both a repressor and an activator, whether lipid function depends strictly on protein binding partners and whether inducing a conformational change in protein binding partners could be a general mechanism by which lipids contribute to transcription control.

1.6.4 Lipids and Cancer

Hanahan and Weinberg outlined “deregulating cellular energetics” as a hallmark of cancer [156]. Lipid metabolism is significantly altered in a range of human diseases including liver disease, insulin resistance, obesity and cancer [157]. The reactivation of lipid biosynthesis is frequently observed in tumour tissue where it causes altered cell signalling, gene expression and enhanced proliferation [158]. Changes in lipid metabolism even contribute to the predisposition of obese patients to developing cancer. 20% of all cancers and 50% of endometrial and oesophageal cancers are attributed to obesity, frequently due to increased insulin and IGF-1 release and the enhancement of cell proliferation and cell survival [159].

The contributions of many lipid metabolising enzymes to cancer initiation and progression have been described. Several deregulated PLC isoforms are known to play important roles in cell proliferation, migration and survival. For example, PLCβ1 increases phosphorylation of retinoblastoma tumour suppressor protein (pRb) and activates expression of the E2F transcription factor, both of which are hallmark events of upregulated progression through the G1 cell cycle phase [160]. Also, PLCβ2 is highly expressed in a large number of breast cancers, where its expression is correlated with tumour size, tumour grade, proliferation index, and poor prognosis [161]. Similarly, upregulation of PLCγ expression is correlated with activation of the oncogenic ERK pathway and rapid proliferation [162].

Additionally, one of the most significant nuclear phospholipid signalling enzymes is the tumour suppressor phosphatase and tensin homolog (PTEN), which dephosphorylates PI substrates and switches off the cell survival, growth and proliferation driving PI3K pathway [102]. PTEN is very commonly mutated in tumours, with more than 60% of primary tumours displaying loss or mutation of at least one PTEN allele [102]. Low expression of another PI regulating enzyme, phosphatidylinositol kinase PIP4Kβ, is correlated with reduced patient survival in breast cancers, largely due to reduced E-cadherin expression [102]. Reduced E-cadherin is a hallmark of the epithelial to mesenchymal transition and part of the

progression to metastasis [102]. PIP4Kβ expression is strongly correlated with histological grade, tumour size and poor prognosis [163].

The composition of the pool of DNA bound lipids in transformed cells is known to significantly differ from that of healthy cells [164]. The quantity of chromatin associated SM in peripheral blood lymphocyte nuclei of patients with chronic lymphocytic leukaemia is significantly reduced compared to healthy lymphocytes [108]. Conversely, the content of SM is higher in the nuclei of hepatoma cells than in normal rat liver [108].

The role of the PI3K/PI(3,4,5)/AKT cascade in tumorigenesis is well documented [165]. Furthermore, PI-PLC and PI3K have been implicated in causing defective control of nucleoskeleton assembly during granulocytic maturation, suggesting they are responsible for dysregulated cell maturation or differentiation in myeloid leukaemia [108]. It is possible that PI-PLC and PI3K may affect the nucleoskeleton assembly of other cell types, meaning that these enzymes not only caused deregulated transcription of their downstream targets but may also more globally affect transcription by causing defective nucleoskeleton assembly and defective chromatin organisation.

Cholesterol is increasingly thought to contribute to the progression and severity of multiple cancer types, with both hypocholesterolaemia and hypercholesterolaemia associated with tumour progression [89, 166-168]. Furthermore, DAG, LPA and prostaglandins can act as promigratory factors, whilst blocking enzymes of the SREBP lipid biogenesis pathway has been shown to block the invasive morphology of breast cancer cells in 3D culture [169]. It is therefore evident that changes in nuclear lipid levels can affect expression of the genome in many ways; including histone modifications, transcription rates, RNA maturation and RNA export, and contribute to disease progression at many stages of cancer [102]. Further study of lipid regulation, and its effects on cell signalling and gene regulation will advance our understanding of gene regulation and will provide insights into how lipids contribute to aberrant gene expression in cancer. Lipid signalling pathways are highly complex, thus regulation is highly specific and could offer new targets for therapeutic intervention and future treatment options.

1.7 Gene Regulation at the Nuclear Periphery

Much evidence suggests that the 3D organisation of the genome and the inner nuclear space plays a role in gene regulation. Early electron microscopy studies of eukaryotic nuclei revealed that heterochromatin is enriched at the nuclear periphery and around nucleoli, whilst euchromatin is predominantly present in the nuclear interior [170]. Similarly, fluorescence in situ hybridization (FISH) experiments have shown that chromosomes are confined to specific nuclear territories [171, 172]. Regions with a high density of active genes are more likely to be located in the centre of the nucleus, and those with a low density of active genes more likely to reside at the nuclear periphery [170, 173]. Cells undergoing division or differentiation experience significant changes to the 3D organisation of chromosomes as genes become activated and repressed, and several associations between gene position and expression level have been demonstrated [174-178]. To understand how genome organisation in the nucleus contributes to gene regulation it is important to first understand nuclear structure.

1.7.1 Introduction to Nuclear Structure

As well as the DNA, packaged into chromosomes, the nucleus is comprised of a number of structures and domains which contribute to key nuclear processes including transcription, RNA processing and ribosome assembly [174]. These include the nuclear membrane, the nuclear lamina, a number of nuclear bodies and the nuclear matrix.

The nuclear membrane is a highly organised double membrane that defines and contains the nuclear compartment and connects it to the surrounding cytoskeleton [170, 179]. The inner and outer nuclear membranes are contiguous with the endoplasmic reticulum (ER), although each leaflet is comprised of a uniquely diverse group of proteins that are typically not enriched in the ER [179, 180]. The nuclear membrane is punctuated with nuclear pore complexes (NPCs), aqueous channels that allow bidirectional transport of proteins, RNA and ribonucleoprotein complexes between the nucleus and the cytoplasm [179, 181]. The outer nuclear membrane includes proteins which contain a KASH domain, allowing them to directly interact with the actin cytoskeleton, such as nuclear envelope spectrin repeat (nesprin) -1 and -2 [182]. This is important for nuclear positioning, particularly during cell polarisation and migration [182]. The INM contains an array of largely uncharacterised transmembrane proteins. Amongst the best characterised are the

LEM-domain containing proteins; emerin, MAN1, LAP2, plus LAP1 and Lamin B receptor (LBR), all of which have been shown to contribute to nuclear functions such as chromatin organisation, gene expression and DNA metabolism [129, 170, 179].

The nuclear lamina is a meshwork system of intermediate filaments and proteins that underpins the INM and stabilises the whole nuclear structure [183]. It is predominantly formed of the two types of lamin filaments; A-type lamins and B-type lamins, encoded by the LMNA, LMNB1 and LMNB2 genes [183]. There are two B-type lamins, B1 and B2, and two splice variants of A-type lamins named lamin A and C [184]. In most mammalian cell types all the lamins reside at the nuclear lamina, but A-type lamins are also present in the nucleoplasm [184]. The lamin proteins bind many proteins of the INM including emerin, LAP1, LAP2, MAN1, barrier-to-autointegration (BAF) and LBR, as well as nuclear pore complexes, making the lamina contiguous with the nuclear membrane [185].

A catalogue of interactions between proteins of the INM and lamin filaments helps to form a stabilising structure which connects the INM with chromatin [183]. BAF is one protein of the INM which interacts with a plethora of nuclear lamina proteins including the LEM domain containing proteins, A- and B-type lamins and Nemp1. BAF also directly binds DNA and therefore acts as a bridging factor to link chromatin to the nuclear membrane [184, 186-188]. As well as serving as an anchoring point for chromatin, the nuclear lamina is bound by transcription factors and plays an important role in signal transduction [170, 189-191].

Mutations in genes encoding components of the nuclear lamina and lamina interacting proteins which affect protein localisation or function lead to a huge variety of clinical problems; including neuropathies, muscle dystrophies, and lipodystrophies, collectively termed laminopathies [170, 185, 192]. Classic laminopathy patients have mutations in the LMNA gene leading to loss of function of the Lamin A/C protein, mostly famously in Hutchinson-Gilford Progeria syndrome, where the unstable nuclear envelope causes progressive nuclear damage and premature cell ageing [185]. This has generated considerable interest in nuclear lamina biology in order to understand the disease biology and attempt to develop treatments.

The existence of a filamentous backbone inside the nuclear space which provides a structural scaffold for chromosomes and nuclear bodies, much like that of the

cytoskeleton, has been considerably debated but it is now largely accepted that such a structure in fact does not exist [193, 194]. Instead, it has now been proposed that the chromatin fibres of interphase chromosomes themselves define the inner nuclear domains, such that the inner nucleus can simply be divided into the intrachromatin domain and the interchromatin domain [193].

Although the existence of a defined filamentous nuclear matrix has been denied, undoubtedly a protein network of sorts does exist in the interchromatin domain. Furthermore there is evidence that various noncoding RNAs have skeletal functions during the assembly of different nuclear compartments [193]. Plus sphingomyelin is also reported to play a role in the organisation of the intranuclear space, highlighting that the structural organisation of the nucleus is likely achieved through the cooperation of a wide variety of nuclear compounds [193, 195]. The nuclear matrix can instead be thought of as a tightly packed body of protein, RNA and lipid that together act as a scaffold for the attachment of both heterochromatin and euchromatin [196]. Specific chromosome regions, termed scaffold/matrix attachment regions (S/MARs), bind to proteins of the nuclear matrix which stabilises the organisation of interphase chromosomes within the nucleus, aids the regulation of transcription, RNA processing and DNA replication [196-199]. Therefore, the attachment of chromosomes to the nuclear matrix impacts on nuclear organisation and function.

Found abundantly in the nuclear matrix are the lamin proteins, A, B and C, nucleophosmin and components of core heterogeneous nuclear ribonucleoproteins (hnRNPs) [196, 200]. Also abundantly present are the Matrins, a group of 8 proteins ubiquitously present within the nucleoplasm but excluded from nucleoli [183, 200]. Of all the matrin proteins (matrin 3, matrin 4, matrins D-G, matrin 12, matrin 13) matrin 3 is the most studied, and appears to play an important role in connecting the nuclear matrix with the nuclear periphery, primarily through an interaction with lamin A [183, 201]. Interestingly, mutations in the MATR3 gene, which encodes matrin 3, disrupt matrin 3 interactions and lead to distal myopathies, amyotrophic sclerosis, skeletal muscle degeneration and neurodegenerative disorders, similarly to mutations in *LMNA* and lamina interacting proteins [202-204]. Interestingly, another abundant nuclear matrix protein is nuclear mitotic apparatus protein 1 (NuMa), a protein which *in vitro* forms 3D space filling structures, leading to speculation that it may contribute to a space-filling scaffold throughout the interchromatin space [205].

This is supported by evidence that altered NuMa expression leads to changes in nuclear shape and chromatin organisation [206].

Also in the nuclear matrix resides a number of membrane-less subnuclear organelles that dynamically respond to basic physiological processes, stress, metabolic state and cell signalling, known as nuclear bodies (Figure 1.12) [10]. Nuclear bodies include nucleoli, Cajal bodies, histone locus bodies, nuclear speckles, Polycomb bodies, and paraspeckles [10, 207]. Each nuclear body contains its own subset of proteins, has its own morphology and can often be biochemically isolated from other nuclear compartments [208-210]. Nuclear bodies coordinate with noncoding RNAs, chromatin modifying proteins and other nuclear machinery to carry out a range of functions including sequestering and modifying proteins, processing RNAs, assembling ribonucleoprotein complexes and epigenetic regulation of gene expression [10].

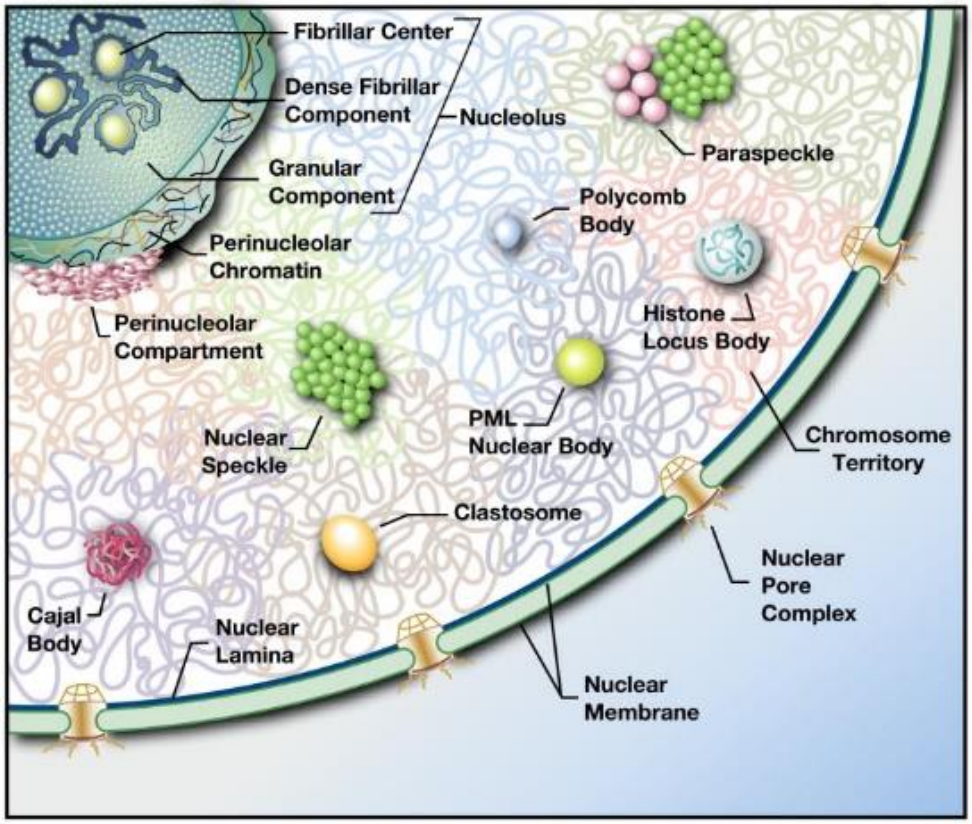

Figure 1.12. Nuclear Bodies. Schematic representation of nuclear bodies in an interphase mammalian nucleus. The interchromatin space harbours multiple nuclear bodies, Cajal bodies, clastosomes, histone locus bodies, nuclear speckles, nucleoli, paraspeckles, perinuclear compartments, PML bodies and Polycomb bodies. The nucleolus consists of three main compartments; the fibrillar centre, a dense fibrillar component and a granular component. The nucleolus is bordered by perinucleolar heterochromatin. Image obtained from [10].

The nucleolus is the largest nuclear body and is the site of ribosomal RNA (rRNA) transcription, rRNA processing and of ribosome assembly [211]. Morphologically, nucleoli consist of three distinct subregions; the fibrillar centre, a dense fibrillary component, and a granular component [211]. The nucleolus is centred around clusters of ribosomal DNA (rDNA) on human chromosomes 13, 14, 15, 21 and 22, which contain the genes for rRNAs 5.8S, 18S and 28S [208]. Transcription of a single 45S rRNA precursor from these genes by RNA polymerase I occurs primarily at the fibrillar centre boundary [211]. The 45S precursor is processed to form the 5.8S, 18S and 28S ribosomal subunits, which are assembled with ribosomal proteins to form almost complete preribosomal subunits, ready for export to the cytoplasm [211].

Another nuclear body, Cajal bodies are small spherical structures, typically appearing as a mesh of coiled fibrillar strands of 40-60nm diameter [212]. There are commonly 1-5 Cajal bodies per nucleus, and each contains multiple components including spliceosomal small nuclear ribonucleic particles (snRNPs), U3, U7, U8, U14 small nucleolar RNAs (snoRNAs), TFIIF, TFIIH, cleavage-stimulation factor, cleavage and polyadenylation specificity factor, as well as nucleolar components fibrillarin, protein B23 and Nopp140 [213]. The precise role of Cajal bodies is still unclear, although they have been implicated in multiple processes including snRNP and snoRNA processing, assembly, modification and maturation, as well as processing of pre-mRNAs, recycling of spliceosome components and telomerase biogenesis [214-216]. It is also thought that Cajal bodies and the nucleolus are functionally connected [215]. Cajal bodies have almost always been seen within the nuclear matrix, but they have also been reported within the nucleolus of human breast carcinoma cells, brown adipocytes and hepatocytes in hibernating mice [208, 217, 218]. Within the nuclear matrix Cajal bodies are predominantly associated with the periphery of chromosome territories at the interface of multiple chromosomes [215]. Cajal bodies are also known to interact with loci enriched with highly expressed histone genes and snRNP and snoRNA loci [215].

PML bodies are small spherical structures of 0.1-1.0μm diameter found scattered throughout the interchromatin space in most cell types, with approximately 10-30 PML bodies per nuclei [219]. PML bodies are characterised by the presence of the PML protein, a member of the TRIM/RBCC protein family, which largely contains ubiquitin ligases which generate subcellular structures through autoassembly [220, 221]. PML is the key organiser of PML bodies and it recruits a huge variety of proteins, many of which are seemingly unrelated, to create a diverse range of PML

domains in response to different cell stresses [220]. PML bodies often recruit sumoylated proteins, including BASP1 [85]. Although a wide range of proteins are known to be recruited to PML bodies, allowing these proteins to be sequestered, modified and degraded, the precise function of these nuclear bodies remains largely unknown [220].

Nuclear speckles, otherwise known as splicing factor compartments or interchromatin granule clusters, consist of fibres known as perichromatin fibrils [208]. These differing size fibres are strands of nascent transcripts together with snRNPs, spliceosome components and other pre-mRNA splicing machinery [222]. Nuclear speckles range in size from one to several μm in diameter, with often 20-50 present per nuclei [222]. Nuclear speckles are thought to function primarily to store and assemble the spliceosomal components, rather than being the primary sites of pre-mRNA splicing as most active genes are found at the periphery of nuclear speckles, not within them [208, 223].

The final nuclear domain to be mentioned here are the discrete sites at which transcription occurs, named transcription factories. Transcription factories are composed of approximately 4-30 RNA polymerase molecules plus a host of other proteins including transcription factors, coactivators, chromatin remodellers, histone modification enzymes, RNPs, splicing and processing factors and RNA helicase [224, 225]. Transcription factory size varies from around 40nm to 200nm, likely according to the genes within the factory and their level of transcription activity [224]. Transcription factories consist of a protein rich core, with DNA templates and nascent RNA transcripts laying on the surface [224]. The number of transcription factories per cell varies widely depending on cell type and species, but usually ranges from a few hundred to a thousand per nucleus [224].

1.7.2 Nuclear Compartments and Gene Regulation

Chromatin structure, organisation, and interaction with nuclear structures all contribute to regulation of the genome. Several studies have now demonstrated that gene position is related to gene expression, with thousands of genes known to reposition during differentiation, correlated with changes in transcription and replication timing [175-178]. It is not always clear whether changes in gene expression are a cause or consequence of gene repositioning and vice versa. Most often, tethering of reporter genes or endogenous genes to the INM has been sufficient to induce gene repression, whilst detachment from the nuclear lamina has frequently been followed by gene activation [175-178].

A specific range of large genomic regions, approximately ~10kb to ~10Mb, directly interact with proteins of the nuclear lamina [184]. These regions, termed lamina associated domains (LADs), together comprise approximately 40% of the genome [184]. Approximately 50% of LADs are consistent between mammalian cell types, named constitutive LADs (cLADs), whilst others are cell type specific, named facultative LADs (fLADs) [174, 226]. cLADs are often AT-rich in sequence, rich in long interspersed nuclear elements, poor in short interspersed nuclear elements, and are less gene dense than fLADs [226]. cLADs genomic positions and sizes are strongly conserved between the human and mouse genomes, although the precise DNA sequences are not [226]. It is hypothesised that cLADs form the structural backbone of chromosomes tethering to the nuclear lamina at defined positions and therefore help guide the overall folding of interphase chromosomes [186]. fLADs on the other hand are generally the more gene dense and their positions are less conserved between species [226].

All LADs are commonly enriched in the heterochromatic histone modifications in H3K9me^2, H3K9me^3 and H3K27me^3 marks and exhibit low levels of transcriptional activity [186, 227, 228]. The methylation of H3K9 is particularly critical for the anchoring of chromatin to the nuclear periphery. It has been shown to be involved in targeted specific loci, such as the β-globin locus to the nuclear lamina [229]. Plus knockdown of H3K9 methyltransferases, such as G9a, reduces the interaction between LADs and the nuclear lamina, and lower levels of H3K9me^2 are observed when LADs are located in the nuclear space [174, 184, 227, 228, 230, 231]. Such evidence suggests that H3K9 methylation does at least partly drive contact with the nuclear lamina. Similarly, knockdown of the Polycomb group (PcG) protein EZH2, the methyltransferase that deposits H3K27me^3 marks, was shown to reduce nuclear lamina interactions of an ectopically integrated LAD fragment [232]. Additionally, following artificial tethering of the DNA-binding factor Ying-Yang 1 (YY1) to a reporter locus, H3K27me^3 marks accumulated and the locus was relocated to the nuclear periphery [232]. The nuclear lamina therefore contributes to the spatial organisation of the genome and appears to have an important role in gene repression.

Several proteins of the nuclear lamina, including the lamin proteins, emerin, BAF and LBR, are important contact points for LADs and also interact with transcription factors and chromatin modifying enzymes [186, 226, 233]. The nuclear periphery is thereby cohabited by chromatin and its regulatory factors making it a major site of genome regulation. LBR can interact with heterochromatin components such as

HP1 and the repressive histone mark H4K20me^3 [234]. Knockout of LBR and Lamin A/C has been found to result in heterochromatin amassing in the nuclear interior, similarly to what is seen in retinal rod cells which express neither Lamin A/C nor LBR [186, 235]. Similarly, ectopic expression of LBR in rod cells results in the relocation of heterochromatin to the nuclear periphery [186]. Loss of Lamin A/C expression causes mislocalisation of PcG proteins, including EZH2, preventing their repressive action and causing chromatin detachment from the nuclear periphery [170, 191]. This has been shown to lead to accelerated differentiation of myoblasts into myotubes [191]. Lamin A/C is also particularly important for maintaining the peripheral location of nuclear factors; for example, together with emerin, it regulates the nuclear translocation and downstream signalling of the mechanosensitive transcription factor megakaryoblastic leukaemia 1 (MKL1) [236].

Emerin also tethers chromatin to the nuclear lamina through its interaction with chromatin binding proteins including BAF [237]. The mislocalisation or knockdown of emerin results in changes in chromosome positioning and partial replacement of histone marks H3K9me^2, H3K9me^3 with H3K27me^3, indicating that emerin is important for chromosome positioning and maintenance of a repressive state [186]. This is further evidenced by the binding of emerin to LAP2β and the histone deacetylase HDAC3, which enhances HDAC3 enzymatic activity, leading to increased gene repression [190, 238]. Other less well characterised NET proteins of the INM including NET5, NET29, NET39, NET45 and NET47 have also been associated with the relocation of specific loci to the nuclear periphery [239]. It is therefore evident that the nuclear lamina tethers chromatin to the INM through a wide variety of components, regulating the localisation of chromatin, and its interaction with a host of chromatin modifying enzymes. All of these components can be individually regulated giving huge complexity and flexibility to gene regulation at the nuclear periphery. The implications of this potential complexity on transcription or cell behaviour are only just beginning to be understood.

There is also evidence that a number of nuclear bodies can also contribute to gene regulation. Cajal bodies, for example, have been associated with gene positioning events observed for chromosome 1 [215]. Disruption of Cajal body assembly by RNA interference also disrupts gene clusters targeting Cajal bodies resulting in the repression of snRNA, snoRNA and histone genes [215]. Such evidence implicates Cajal bodies in genome organisation, with global effects on gene expression and RNA splicing. The nucleolus also binds specific genomic regions including rDNA loci, and often it is bound by sequences that overlap considerably

with LADs [240, 241]. It has been shown that loci located at the nuclear periphery in mother cells can locate either to the nuclear periphery or the nucleolar periphery in daughter cells following mitosis [172, 227]. Therefore, it is possible that both the nuclear lamina and the nucleolus are sites at which repressed genomic domains locate.

Furthermore, both nuclear speckles and transcription factories have been suggested to contribute to the formation of chromatin loops and clustering of coregulated genes that may be located megabases apart on the same or different chromosomes [224, 242-245]. FISH studies have suggested that active genomic regions are often located on the borders of chromosome territories, as loops of DNA making contact with the nuclear matrix and are associated with transcription factories [171, 172, 243, 244]. “Looping out” of DNA is seen in only a proportion of alleles and it is unclear whether this occurs due to the dynamic movement of DNA in and out of the chromatin territory but live cell analysis has suggested that looping out occurs in order for genes to interact with transcription factories and nuclear speckles and aids transcription activation [171]. Therefore, nuclear speckles and transcription factories may have roles in genome organisation and gene regulation, although their exact contribution requires further investigation.

Proteins within the nuclear matrix have also been shown to have roles in gene regulation through their interaction with S/MARs. Matrin 3 has been reported to contribute to gene regulation through a number of means; firstly, it appears to play an important role in connecting the nuclear matrix with the nuclear periphery, primarily through an interaction with lamin A [183, 201]. Matrin 3 also has a reported role in localising transcriptional regulators, such as the Pit1 transcription factor, to their target genes [246]. Pit1 requires this matrix interaction to recruit further transcription factors β-catenin and SATB1 to specific enhancer loci in order to activate transcription [196]. Further evidence suggests matrin 3 may also function in alternative splicing and RNA stability [196].

Interestingly, it has been noted that many membrane-less nuclear compartments share similar properties to liquid droplets [247-250]. The structure of the nucleus has subsequently been thought of as an emulsion of many phase separated droplets of DNA and protein [247]. It has been argued that phase separation could aid the compartmentalisation of chromosomes into discrete nuclear territories, and that liquid-liquid phase separation drives the assembly of liquid-like nuclear bodies around their binding sites on chromatin [250]. Phase separation could offer a

physical means to control gene expression throughout the nucleus by controlling the interplay between different liquid-like components [251]. Several nuclear proteins, including many proteins of the eukaryotic transcription machinery such as the Mediator transcriptional coactivator and RNA polymerase II have been shown to behave as biomolecular condensates [251, 252]. HP1α also condenses DNA into liquid-like droplets which has been suggested to be a robust mechanism of heterochromatin formation and gene silencing [249, 253]. Such evidence supports the possibility that the organisation and expression of the genome may be regulated through phase separation. These mechanisms could explain how chromatin bodies can act as dynamic spherical structures which coalesce and constantly and rapidly exchange components with the surrounding nucleoplasm. Work to understand how these properties contribute to gene organisation and expression remains in its infancy.

1.8 Project Aims

The study of BASP1, as a transcriptional regulator that interacts with PIP_2 and cholesterol, provides a unique opportunity to investigate the contribution of nuclear lipids to the regulation of WT1/BASP1 target genes. Very little is currently known about the role of nuclear lipids in gene regulation and molecular data is particularly lacking. How BASP1 uses cholesterol in its mechanism of gene regulation is currently unknown. Furthermore, BASP1 is an established cofactor of other transcriptional regulators, including ERα, and is known to regulate over a thousand genes in K562 cells, so it possible that mechanisms of gene regulation employed by BASP1 at WT1 target genes could extend to a multitude of regulated genes [2, 89]. Moreover, nuclear myristoylated proteins are very poorly understood and so study of BASP1 will enhance our understanding of the function and behaviour of these proteins. It is important to understand more about how BASP1-lipid complexes regulate chromatin remodelling in transcriptional regulation.

The study of BASP1 also provides an opportunity to examine the importance of the WT1/BASP1 repression complex localisation on its function. BASP1 is a transcriptional corepressor with the capacity to interact with membranes, but that is also found localised together with PIP_2 in nuclear speckles [3]. Examination of the localisation of the WT1/BASP1/PIP_2 repression complex could give insight into potential mechanisms of gene repression at the nuclear periphery and improve understanding of how lipids interact with proteins within the nucleoplasm. As the only known transcription regulator that requires lipidation for its transcription function, BASP1 provides a means to explore and better understand the mechanisms through which lipids contribute to transcriptional regulation and chromatin organisation.

Moreover, BASP1, WT1 and many lipids have all been implicated in a variety of cancers. Improved understanding of the behaviour of the WT1/BASP1/PIP_2 complex will in turn improve the wider understanding of the mechanisms gene regulation and could even lead to the identification of therapeutic targets.

2 Materials and Methods

2.1 General Chemicals

The following chemicals were purchased from Sigma-Aldrich (Dorset, UK):
Phosphate Buffered Saline (PBS), Triton X-100, phorbol 12-myristate 13-acetate (PMA), Lovastatin (Mevinolin), Lithium Chloride, Sodium Deoxycholate, Ammonium Acetate, Trizma, Acetonitrile, Azide-PEG3-biotin, Tetrakis(acetonitrile)copper(I) tetrafluoroborate ($CuBF_4$), Paraformaldehyde (PFA).

The following chemicals were purchased from Thermo Fisher Scientific (Loughborough, UK): Methanol, Ethanol, Agarose, Glycerol, Glycine, Tris, Ammonium Persulphate, sodium dodecyl sulfate (SDS), 4-(2-hydroxyethyl)-1-piperazineethanesulfonic acid (HEPES), Tween, Bromophenol Blue, Ethylenediaminetetraacetic acid (EDTA), Sodium Pyruvate, Sodium Bicarbonate.

Sodium Chloride, Potassium Chloride and Magnesium Chloride were purchased from VWR Chemicals (Leicestershire, UK). Urea and NP-40 were purchased from Millipore (Watford, UK). Potassium Hydroxide and Dithiothreitol (DTT) was purchased from Santa Cruz Biotechnology. TEMED was purchased from Flowgen Bioscience. Trypan Blue was purchased from Invitrogen. DMSO was purchased from Corning.

2.2 Tissue culture

K562 cells were maintained in RPMI 1640 (Life Technologies, Inc.) supplemented with 10% (v/v) FCS, 1% (v/v) Pen-Strep and 1% (v/v) L-glutamine (all from Life Technologies, Inc.). MCF7 cells were maintained in DMEM (Life Technologies, Inc.) supplemented with 10% (v/v) FCS and 1% (v/v) Pen-Strep. shN (shNegative control) and shB (shBASP1) stable MCF7 lines were additionally supplemented with 1mg/ml G418 (Melford Laboratories). All cells were kept at 37°C in humidified 95% air and 5% CO_2 atmosphere.

2.3 Vectors and transfection of stable cell lines

Stable K562 cell lines were prepared as described previously [2]. Essentially, K562 cells were stably transfected using Effectene (Qiagen) transfection reagent and positive cells selected with 2mg/ml G418 (Melford Laboratories). Transfected

vectors were; pc-DNA3 vector only (V-cell lines), pc-DNA3 vector containing wild type BASP1 sequence (B-cell lines), pc-DNA3 vector containing Y12L-BASP1 sequence (Y-cell lines) or pc-DNA3 containing G2A-BASP1 sequence (G-cell lines). All BASP1 sequences were followed by a hemagglutinin (HA) tag sequence to tag BASP1 protein with HA at the C terminus. pc-DNA3, pc-DNA3-BASP1 and pc-DNA3-Y12L-BASP1 vectors were obtained from previous laboratory members. Mutant derivative G2A-BASP1 was generated via cloning of the mutant G2A-BASP1 sequence into digested pc-DNA3 vector as described below.

2.4 Transfection of siRNA

Mission(R) esiRNA against emerin (Sigma Aldrich) or Mission(R) esiRNA control siRNA (#SIC003, Sigma Aldrich) was transfected into shN (shNegative control) and shB (shBASP1) stable MCF7 cell lines using Hiperfect transfection reagent (Qiagen). Transfected cells were analysed 48 hours post transfection for western blotting and RNA analysis.

2.5 Cloning

2.5.1 PCR Reaction

A PCR reaction of the following components was assembled:
1µl 10mM dNTPs
4µM G2A-BASP1 primers [Fwd:5'-CTCGGATCCATGGCAGGCAAGCTCAGC-3']
[Rev: 5'-GCTGAGCTTGCCTGCCATGGATCCGAG-3']
5µl NEB standard 10x buffer
2ng pc-DNA3-BASP1 template
1.5µl DMSO
ddH_2O up to 50µl

0.25µl (1.25 units) Taq polymerase (NEB) was then added immediately prior to PCR reaction. A negative control containing ddH_2O in place of pc-DNA3-BASP1 template was also set up and run on a Techne TC3000 thermocycler.

The following cycling parameters were set up:
95°C for 30s, followed by 40 cycles of 95°C for 30s, 45°C for 30s, 68°C for 1min, followed by a final extension at 68°C for 5mins and samples then held at 10°C.

2.5.2 Agarose Gels

DNA products or fragments were resolved on a 1.5% (w/v) agarose gel dissolved in TAE buffer (Thermo Fisher Scientific) (40mM Tris, 20mM acetic acid, 1mM EDTA) and containing 0.5 µg/ml ethidium bromide (VWR). DNA loading dye (Thermo Fisher Scientific) was added to each sample prior to loading. Samples were loaded and electrophoreised at 100V in TAE buffer for ~45mins alongside an appropriate DNA ladder (GeneRuler Low Range DNA ladder – Thermo Fisher Scientific, or 1kb DNA ladder – Sigma Aldrich). Bands were visualised under UV light.

2.5.3 Product digestion

A small sample of PCR product was resolved on a 1.5% (w/v) agarose gel to validate successful production of ~700bp product. Following this, PCR product and pc-DNA3 were each digested for 2 hours at 37°C via addition of 1µl (10 units) BamHI, 1µl (10 units) EcoRI, 1µl 10x Buffer R (Thermo Fisher Scientific #ER0051, #ER0271, #BR5) 1µg DNA. Digested products were then resolved on a 1.5% (w/v) agarose gel and DNA extracted using a Qiaquick gel extraction kit (Qiagen).

2.5.4 Gel Extraction

Digested G2A-BASP1 PCR product, and digested pc-DNA3 were extracted from agarose gels using the Qiaquick gel extraction kit (Qiagen) according to manufacturer's instructions. This involved excising the region of agarose gel containing the relevant DNA product from the gel using a scalpel blade and freezing in a clear bag for 20 mins at -80°C. Slices were squeezed by hand to release DNA, which was collected by pipetting.

2.5.5 Ligation

Enzyme-cleaved G2A-BASP1 PCR product and linearised pc-DNA3 were then ligated together using the following conditions:

100ng pc-DNA3 vector, 170ng G2A-BASP1 PCR product, 1µl T4 DNA Ligase buffer (Promega #C126B), 1µl T4 DNA Ligase (1 unit) (Promega #M180A) up to 10µl with nuclease free water. Samples were incubated overnight at 15°C in a thermocycler (Techne TC3000).

2.5.6 Bacterial Transformation

Thawed OneShot TOP10 (Thermo Fisher Scientific) competent cells were transformed with ligated PCR product. This was achieved via incubation of 1.5µl ligated DNA product with 45µl of competent cells on ice for 30 mins. Competent cells were heat shocked at 42°C for 30s, cooled on ice, and plated onto 100µg/ml ampicillin/LB plates. Water controls containing competent cells incubated with water only were also heat shocked and plated. Agar plates were incubated at 37°C overnight.

The next day, individual colonies of ampicillin resistant transformed bacteria were picked and grown again in 3ml LB broth containing 100µg/ml ampicillin overnight, shaking at 37°C.

2.5.7 Qiagen Mini Preps

DNA from a 3ml overnight culture was extracted using a QiaPrep Miniprep kit (Qiagen) according to manufacturer's instructions. This involved collecting bacteria via centrifugation for 5 mins at 3000 x g followed by step by step completion of the QiaPrep Miniprep protocol. DNA was eluted and the concentration measured on a NanoDrop Lite spectrophotometer (Thermo Fisher Scientific).

2.5.8 DNA Sequencing

All plasmids were sequenced using the Source Bioscience Sanger sequencing service (1 Orchard Place, Nottingham Business Park, Nottingham)

2.6 Colony Formation Assay

V-K562, B-K562 and G-K562 cells were seeded onto agar bases (0.7% (w/v) LMP Agarose, 10% (v/v) FBS, 1% (v/v) Pen Strep, 1% (v/v) L-glutamine in DMEM media supplemented with 0.15% (v/v) $NaHCO_3$, 200µM sodium pyruvate and 800µM NaOH at a density of $2x10^5$ cells per ml of agar. Agar dishes were fed with additional agar (2ml) on days 7 and 14 post seeding. The colony formation efficiency (%CFE) was calculated 7, 14 and 21 days post seeding via counting colonies consisting of greater than 50 cells, in a minimum of ten 15.89mm^2 fields of view per 60mm^2 dish. Average colony area was measured using ImageJ software. All experiments were performed in triplicate.

2.7 Gene Expression Analysis

RNA samples were isolated from pellets of cells using an RNeasy Mini Kit (Qiagen) according to manufacturer's instructions. RNA samples were quantified using a NanoDrop™ Lite spectrophotometer (Thermo Fisher Scientific) and diluted to 0.5µg/µl to complete cDNA reaction using iScript cDNA synthesis kit (Bio-Rad) according to manufacturer's instructions. cDNA was then prepared for q-PCR reactions with appropriate gene primers using iTaq Universal SYBR Green Supermix (Bio-Rad).

Components for each q-PCR reaction consisted of:
2µl cDNA
10µl SYBR Green Supermix
1µl forward primer (10µM stock)
1µl reverse primer (10µM stock)
6µl H_2O

The following cycling parameters were set up:
95°C for 3 mins, followed by 40 cycles of 95°C for 20s, 60°C for 30s, 72°C for 30s, plate read.

A melt curve was then initiated using the following parameters:
95°C for 10s, followed by 65.0°C for 5s, then temperature of increases 0.5°C every 0.5s, plus plate read, up to 95°C.

2.7.1 Primers for Gene Expression Analysis

Gene	Forward Primer 5'-3'	Reverse Primer 5'-3'
AREG	TGGATTGGACCTCAATGACA	ACTGTGGTCCCCAGAAAATG
ETS-1	AAACTTGCTACCATCCCGTACGT	ATGGTGAGAGTCGGCTTGAGAT
REN	GAAAGCCTGAAGGAACGA	GTACTGGGTGTCCATGTAGTT
GAPDH	ACAGTCAGCCGCATCTTCTT	ACGACCAAATCCGTTGACTC

2.8 Subnuclear Fractionation

V-K562, B-K562 and G-K562 cells were collected and washed once in PBS. Nuclei were isolated using the Nuclei EZ Prep kit (Sigma) according to manufacturer's instructions (15ml of cell suspension per 4ml Nuclei EZ lysis buffer). Briefly, cells were incubated in lysis buffer on ice for 5 mins, then centrifuged at 500 x g for 5 mins. Lysis and centrifugation were repeated twice. To fractionate, the nuclei pellet was resuspended in 100µl CSK buffer (10 mM Pipes pH 6.8, 100mM NaCl, 300mM sucrose, 3mM $MgCl_2$, 1mM EGTA, 1mM DTT, 0.5% (v/v) Triton X-100) plus protease inhibitors (Calbiochem). After extraction for 5 mins on ice, soluble proteins were recovered following separation from the insoluble fraction by centrifugation at 5000 x g for 3 mins. The pellet was resuspended in CSK buffer with 30 units DNAse1 (RNase-free) (Thermo Fisher Scientific) and incubated at 37°C for 30 mins. The chromatin fraction was extracted by 5 mins incubation on ice following addition of 0.25M ammonium sulphate (final concentration) and then centrifuging at 500 x g for 5 mins. The resulting pellet was treated with 2M NaCl in CSK buffer on ice for 5 mins, and this matrix fraction solubilised in 8M Urea. Protein concentrations were estimated via incubation with Bradford protein assay reagent (Bio-Rad) and measurement of absorption at 595nm on a spectrophotometer. Protein samples were then heated at 95°C in SDS-loading buffer (50mM Tris-Cl pH 6.8, 100mM DTT, 2% (w/v) SDS, 0.1% (w/v), Bromophenol Blue, 10% Glycerol) and analysed by western blot.

2.9 Western Blotting

Prepared western samples were loaded into wells of prepared denaturing polyacrylamide gels (37.5mM Tris pH 8.8, 0.1% (w/v) SDS, 7.5-12.5% (w/v) Acrylamide/Bis gel mix). Proteins were separated by resolving gels in SDS-PAGE buffer (25mM Tris, 192mM Glycine, 0.1% (w/v) SDS) at ~200 V until the bromophenol dye front reached the bottom of the gel. Separated proteins were then transferred onto methanol activated Immobilon-FL polyvinylidene difluoride membranes (Millipore) in transfer buffer (25mM Tris, 192mM Glycine, 20% (v/v) Methanol) using semi-dry blotting apparatus (Bio-Rad). Transfer was usually conducted for 45mins at 25V depending on the molecular weight of proteins being analysed. Following transfer, membranes were blocked in 5% (v/v) dried Milk (Marvel) in PBST (1 x PBS containing 0.1% (v/v) Tween), followed by overnight incubation at 4°C with the appropriate primary antibody diluted in the same buffer.

After washing four times for 5 mins each in PBST/5%(v/v) dried milk, membranes were incubated with horseradish peroxidase-conjugated secondary antibody diluted in 5% (v/v) milk in PBST for 1 hour at room temperature. Washes were repeated as before. Detection was carried out using a chemiluminescence system (Thermo Fisher Scientific) and CL-X Posure™ films (Thermo Fisher Scientific) developed using a Konica Minolta™ SRX-101A Film Processor.

2.9.1 Western Blotting Antibodies

Antibody	Species	Source	Dilution
BASP1	Rabbit	Pacific Immunology, California	1:1000
WT1	Rabbit	Pacific Immunology, California	1:1000
β-actin	Mouse	Sigma, #A5316	1:10000
Emerin	Mouse	Santa Cruz Biotech, #sc-25284	1:1000
Lamin A/C	Mouse	Santa Cruz Biotech, #sc-20681	1:1000
Prohibitin	Rabbit	Santa Cruz Biotech, #sc-28259	1:1000
EZH2	Rabbit	Abcam #ab186006	1:1000
BAF	Mouse	Abcam #ab88464	1:1000
LAP2α	Rabbit	Abcam #ab5162	1:1000
MARCKS	Goat	Santa Cruz #sc-6455	1:500
HDAC1	Mouse	Cell Signalling, #5356	1:1000
TGN46	Sheep	GeneTex #GTX74290	1:1000
Anti-Rabbit HRP	Goat	Jackson ImmunoResearch Laboratories	1:5000
Anti-Mouse HRP	Goat	Jackson ImmunoResearch Laboratories	1:5000
Anti-Sheep HRP	Goat	Jackson ImmunoResearch Laboratories	1:5000

2.10 Chromatin Immunoprecipitation (ChIP)

K562 cells were collected and resuspended to a density of $1x10^6$ cells/ml in PBS. Crosslinking was achieved by adding formaldehyde into the PBS to a final concentration of 1.42% (v/v), and incubating, rocking, at room temperature for 15 mins. When ethylene glycol bis(succinimidyl succinate) (EGS) (#E3257, Sigma) was also used to aid crosslinking, EGS at 1mM, 2mM or 3mM (final concentration) was added to samples following this 15mins incubation in 1.42% PFA and left for a further 15 mins rocking, at room temperature. Formaldehyde was quenched with ice-cold 125mM glycine for 5 mins at room temperature. Cells were collected by centrifugation at 2000 x g for 5 mins at 4°C and washed with ice cold PBS. Cells were resuspended to a concentration of $1x10^7$ cells/ml, and lysed in 1ml IP buffer (150mM NaCl, 50mM Tris-HCl (pH 7.5), 5mM EDTA, 0.5% (v/v) NP-40 and 1% (v/v) Triton X 100) plus protease inhibitors (Calbiochem), for 15 mins on ice. Lysed samples were centrifuged at 2000 x g for 5 mins at 4°C, supernatant removed and the pellet resuspended in 1ml IP buffer plus protease inhibitors for sonication.

Chromatin was sheared via sonication using a QSonica Q500 at 60% amplitude. Successful sonication giving fragments 200-500bps in length was confirmed by resolving a small (decrosslinked) sample on a 1.5% (w/v) agarose gel. Following sonication the lysate was cleared by centrifugation at 12000 x g for 10 mins at 4°C. Samples were precleared by incubating with 10µl Mag-G beads (Life Technologies) for 1 hour, rotating at 4°C. 5µl Mag-G beads, 600µl IP buffer, 1µl 10mg/ml acetylated BSA (Sigma) and appropriate antibody were also incubated together in one microtube per desired chromatin immunoprecipitation for a minimum of 4 hours, rotating at 4°C. 200µl of pre-cleared chromatin was then added to the incubated microtube of antibody and beads and rotated at 4°C overnight. A 2% input sample was also stored for later decrosslinking and processing.

Immunoprecipitated samples were then magnetised, supernatant discarded and beads sequentially washed once in IP buffer, high salt IP buffer (500mM NaCl, 50mM Tris-HCl (pH 8.0), 5mM EDTA, 0.5% (v/v) NP-40, 1% (v/v) Triton X 100), LiCl buffer (10mM Tris-HCl (pH 8.0), 250mM LiCl, 1mM EDTA, 1% (v/v) NP-40, 1% (w/v) Sodium Deoxycholate), and TE buffer (10mM Tris-HCl (pH 8.0), 1mM EDTA). After the final wash beads and 2% input samples were resuspended in 100µl of PK buffer (125mM Tris-HCl (pH 8.0), 10mM EDTA, 150mM NaCl, 1% (w/v) SDS) and placed at 65°C overnight. Samples were then incubated with 1µl of 20mg/ml Proteinase K (Ambion #AM2546) for 3-4 hours at 55°C. Finally, samples were

purified using Qiaquick PCR purification kit (Qiagen) according to manufacturer's instructions. Eluted DNA was placed at 95°C for 10 mins and prepared for qPCR.

Components for each q-PCR reaction consisted of:
2µl DNA sample
10µl SYBR Green Supermix
1µl forward primer (10µM stock)
1µl reverse primer (10µM stock)
6µl H_2O

The following cycling parameters were set up:
95°C for 3 mins, followed by 40 cycles of 95°C for 10s, 60°C for 10s, 72°C for 30s, plate read.

A melt curve was then initiated using the following parameters:
95°C for 10s, followed by 65.0°C for 5s, then temperature of increases 0.5°C every 0.5s, plus plate read, up to 95°C.

2.10.1 ChIP Antibodies

Antibody	Species	Source	Volume per IP
BASP1	Rabbit	Pacific Immunology, California	50µl
WT1	Rabbit	Pacific Immunology, California	50µl
$H3K4me^3$	Rabbit	Millipore #07-473	4µl
$H3K36me^3$	Rabbit	Abcam, #ab9050	4µl
$H3K27me^3$	Mouse	Abcam, #ab6002	4µl
H3K9Ac	Rabbit	Abcam, #ab10812	4µl
H3K9me3	Rabbit	Abcam #ab8898	4µl
RNA polymerase II	Rabbit	Abcam #ab817	4µl
RNA polymerase II S5	Rabbit	Abcam #ab5408	4µl
$PI(4,5)P_2$	Mouse	Abcam, #ab11039	3µl
HDAC1	Mouse	Cell Signalling #5356	2µl
Emerin	Mouse	Santa Cruz Biotech, #sc-25284	10µl

BAF	Mouse	Abcam #ab88464	4µl
CDK7	Mouse	Santa Cruz Biotech	4µl
Lap2α	Rabbit	Abcam #ab5162	4µl
EZH2	Rabbit	Abcam #ab186006	4µl
Normal IgG	Rabbit	Cell Signalling #2729	1µl
Normal IgG	Mouse	Millipore #12-371	1µl

2.10.2 ChIP Primers

Gene	**Forward Primer 5'-3'**	**Reverse Primer 5'-3'**
AREG	TTTAAGTTCCACTTCCTCTCA	GGTGTGCGAACGTCTGTA
ETS-1	CCTAAAGAGGAGGGGAGAGC	AGGGGAAGTTGGCACTTTG
REN	GCTTAACCTCCTAGGTCTTG	GTGGAGGAAGTCTGTAAATC
JUNB	GGTCCTGGTATTTGTCCCAG	CTCGCGTCACTGTCAGGAAG
VDR	CACCTGGCTCAGGCGTCC	GCCAGGAGCTCCGTTGGC
18S	GTAACCCGTTGAACCCCATT	CCATCCAATCGGTAGTAGCG
BAX internal	CTGACGGCAACTTCAAC	GGTGCACAGGGCCTT
Control	CAGCTCAGTGCTGTTGGTGG	ACCATCCAACCCTGGAGATC

*Control primers recognise an uncharacterized ncRNA gene, LOC10537228, found at 19p13.13

2.11 Protein Immunoprecipitation (IP)

All protein immunoprecipitation was carried out using nuclear extracts. To prepare nuclear extracts K562 cell lines were collected via centrifugation for 3 mins at 1400 x g. The packed cell volume (PCV) was estimated, and the pellet incubated with 2/3 PCV of NE1 buffer (10mM HEPES pH 8.0, 1.5mM $MgCl_2$, 10mM KCL, 1mM DTT) for 15 mins on ice, with protease inhibitors. Cells were then passed through a 23 gauge needle 4-5 times, and microfuged at full speed for 30 secs to isolate nuclei. The supernatant was discarded and remaining pellet resuspended in one PCV of NE2 buffer (20mM HEPES pH 8.0, 1.5mM $MgCl_2$, 25% (v/v) Glycerol, 420mM NaCl, 0.2mM EDTA, 1mM DTT and 0.5mM PMSF) on ice for with regular stirring for 30 mins, with protease inhibitor cocktail. Nuclear debris was pelleted by 5 mins microfuge at full speed. The supernatant (nuclear extract) was dialysed against Buffer D (20mM HEPES pH 8.0, 100mM KCl, 0.2mM EDTA, 20% (v/v) Glycerol and 0.5mM DTT) for 2 hours at 4°C. Dialysed samples were cleared by centrifugation at 13,000 x g for 5 mins at 4°C and precleared by incubation with 10µl Protein-G beads and appropriate IgG antibody for 1-2 hours at 4°C. Following the preclear, samples were divided as necessary onto fresh Protein G beads, IP buffer (20mM HEPES pH 8.0, 100mM KCl, 0.2mM EDTA, 20% (v/v) Glycerol, 0.5mM DTT and 0.05% (v/v) NP-40) and the appropriate antibody. Samples were rotated at 4°C overnight. Lastly, magnetic beads were collected and washed 3 times in 1ml IP buffer. To western blot, beads were resuspended in 10µl 1 x SDS loading buffer per gel and boiled at 95°C for 3 mins before loading SDS-PAGE gels and performing western blotting as previously described.

2.11.1 IP Antibodies

Antibody	Species	Source	Volume per IP
BASP1	Rabbit	Pacific Immunology, California	50µl
HA	Rabbit	Cell Signalling #3724S	4µl
Emerin	Mouse	Santa Cruz #sc25284	10µl
Normal IgG	Rabbit	Millipore #12-370	1µl
Normal IgG	Mouse	Millipore #12-371	1µl

2.12 TMT Mass Spectrometry

To carry out Tandem Mass Tag (TMT) mass spectrometry of K562 cell lines, protein immunoprecipitation samples were collected as described above. The washed protein-bound magnetic beads were processed by the Faculty of Life Science Proteomics Facility, University of Bristol. Samples were differentially labelled with TMT reagents such that V-K562, B-K562 and G-K562 samples were distinguishable. Samples were mixed, fractionated and analysed by high resolution Orbitrap LC-MS/MS to identify present peptides. Only proteins with a minimum of 95% confidence that all peptides were present in the sample (<5% false discovery rate) were assumed to be genuine interactors based on a human-specific protein database. The abundance of peptides from each sample is then calculated according to relative abundance of reporter ions.

2.13 Immunofluorescence and Confocal Imaging

K562 cells grown in suspension culture were collected via centrifugation at 1400 x g for 3 mins. Nuclei were isolated using the Nuclei EZ Prep nuclei isolation kit (Sigma) according to manufacturer's instructions. Nuclei were collected via centrifugation at 500 x g for 5 mins. Nuclei were fixed in 4% (v/v) PFA and rotated at room temperature for 15 mins. Nuclei were incubated with 50mM NH_4Cl for 15 mins, rotating, then washed three times in PBS, and blocked in blocking buffer (2% (w/v) BSA, 0.25% (w/v) Gelatin, 0.2% (w/v) Glycine, 0.2% (v/v) Triton X-100 in PBS) for 1 hour, rotating at room temperature. Primary antibody was diluted in PBS with 1% (w/v) BSA, 0.25% (w/v) gelatin and 0.2% (v/v) Triton X-100 and incubated for 1 hour, rotating at room temperature. Nuclei were washed three times with washing buffer (0.2% (w/v) Gelatin in PBS). Fluorescent secondary antibody was then applied for 45 mins in the same buffer as the primary antibody, and samples were rotated in the dark. Nuclei were washed three times in washing buffer before 10 mins incubation with DAPI (Thermo Fisher Scientific) solution. Nuclei were resuspended in a minimum volume of DABCO (Sigma) mounting media to mount onto poly-lysine coated slides. Samples were viewed using a Leica SP5-II AOBS confocal laser scanning microscope attached to a Leica DM I6000 inverted epifluorescence microscope with oil 63x lens. Images were processed using ImageJ or Volocity 6.3 software.

2.13.1 Immunofluorescence Antibodies

Antibody	Species	Source	Dilution
BASP1	Rabbit	Pacific Immunology, California	1:300
BASP1	Sheep	SAPU, Edinburgh, Scotland	1:100
HA-tag	Rabbit	Cell Signalling #3724S	1:500
$PI(4,5)P_2$	Mouse	Abcam, #ab11039	1:200
Prohibitin	Rabbit	Santa Cruz Biotech, #sc-28259	1:500
HDAC1	Mouse	Cell Signalling #5356	1:250
Emerin	Mouse	Santa Cruz Biotech, #sc-25284	1:500
Lamin A/C	Mouse	Santa Cruz Biotech, #sc-20681	1:500
AlexaFluor Anti-rabbit secondary (488)	Goat	Thermo Fisher Scientific, Rockford #a21206	1:300
AlexaFluor Anti-mouse secondary (594)	Goat	Thermo Fisher Scientific, Rockford #35510	1:500
AlexaFluor Anti-Sheep secondary (594)	Donkey	Thermo Fisher Scientific, Rockford #35510	1:100

2.14 Click Chemistry

K-562 and MCF7 cells were incubated in lipid free media (RPMI and DMEM, respectively) containing 10µg/ml of alkyne-Myristic Acid (Caymen Chemical #13267) or alkyne-Cholesterol (Avanti #700143) for 16 hrs. Samples were washed once in PBS, and either whole cells or nuclei (obtained using EZ Prep nuclei kit according to manufacturer's instructions) were fixed in 3.7% (v/v) formaldehyde in Buffer A [0.1M HEPES/KOH (pH 7.4)] for at least 16 hrs. Samples were washed once in 155mM ammonium acetate, and twice in Buffer A. For detection, 50µM Azide-PEG3-biotin conjugate (Aldrich #762024) was dissolved in prewarmed Buffer A and added to samples. The click reaction was initiated via addition of 2mM $CuBF_4$ in 2% (v/v) acetonitrile, and the reaction was left to proceed at 43ºC for 30 mins with gentle agitation. Samples were then extensively washed in Buffer A.

2.14.1 Click Chemistry Immunofluorescence:

If samples were being costained for BASP1, they were next incubated in IF blocking buffer (2% (w/v) BSA, 0.25% (w/v) Gelatin, 0.2% (w/v) Glycine, 0.2% (v/v) Triton X-100 in PBS) for 60 mins, rotating at room temperature. Primary BASP1 antibody was then diluted 1:300 in PBS with 1% (w/v) BSA, 0.25% (w/v) gelatin and 0.2% (v/v) Triton X-100 and incubated for 1 hour, rotating at room temperature. Nuclei were washed three times with washing buffer (0.2% (w/v) Gelatin in PBS). Samples were next incubated with fluorescent secondary antibody (Thermo Fisher Scientific, #a21206) (1:500 dilution in Buffer A) and fluorescent streptavidin antibody (AlexaFluor #S32356) (1:400 dilution in Buffer A) and rotated for 45 mins at room temperature in the dark. Samples were then washed in Buffer A before 10 mins incubation with DAPI solution. Nuclei were resuspended in minimum volume of DABCO (Sigma) mounting media to mount onto poly-lysine coated slides for visualisation.

If samples were not being costained, they were simply incubated with fluorescent streptavidin antibody (as described above) immediately following completion of the click reaction. Samples were then washed in Buffer A, incubated for 10 mins with DAPI solution and mounted using DABCO (Sigma) mounting media (as above).

All samples were viewed using a Leica SP5-II AOBS confocal laser scanning microscope attached to a Leica DM I6000 inverted epifluorescence microscope with oil 63x lens. Images were processed using ImageJ or Volocity 6.3 software.

2.14.2 Click Chemistry Immunoprecipitation:

Following completion of the click chemistry reaction at 43ºC for 30 mins (described above), nuclear extracts were prepared by resuspending samples in one PCV of NE2 buffer (20mM HEPES pH 8.0, 1.5mM $MgCl_2$, 25% (v/v) Glycerol, 420mM NaCl, 0.2mM EDTA, 1mM DTT and 0.5mM PMSF) and incubating on ice with regular stirring for 30 mins. Nuclear debris was pelleted by 5 mins microfuge at full speed. The subsequent nuclear extracts were then subjected to immunoprecipitation using streptavidin magnetic beads (Invitrogen) and IP buffer (20mM HEPES pH 8.0, 100mM KCl, 0.2mM EDTA, 20% (v/v) Glycerol, 0.5mM DTT and 0.05% (v/v) NP-40) overnight at 4°C. Magnetic beads were collected and washed 3 times in IP buffer, and prepared for western blotting by resuspending in 10µl SDS loading buffer per gel and heating to 95°C for 5 mins before loading SDS-PAGE gels and performing western blotting as previously described.

2.14.3 Click Chemistry Chromatin Immunoprecipitation:

$5x10^6$ K-562 cells were incubated in lipid free media containing 10µg/ml of alkyne-Myristic Acid (Caymen Chemical #13267) or alkyne-Cholesterol (Avanti #700143) for 16 hrs. Samples were washed once in PBS and crosslinked in 3.7% (v/v) formaldehyde in PBS for 15 mins (Myristic Acid) or 4 hours (Cholesterol). Cells were collected by centrifugation at 2000 x g for 5 mins and washed once in 155mM ammonium acetate and twice in Buffer A. The click reaction was performed by resuspending the cell pellet in 50µM Azide-Reporter in prewarmed Buffer A, followed by the addition of 2mM $CuBF_4$ in 2% (v/v) acetonitrile. The reaction was left to proceed at 43°C for 30 mins with gentle agitation. Samples were then extensively washed in Buffer A. Next, samples were fixed again in 3.7% (v/v) formaldehyde in PBS for 15 mins, and formaldehyde quenched with ice-cold 125mM glycine for 5 mins at room temperature and cells collected by centrifugation at 2000 x g for 5 mins.

Cell pellets were resuspended to a concentration of $5x10^6$ cells/ml, and lysed in IP buffer (150mM NaCl, 50mM Tris-HCl (pH 7.5), 5mM EDTA, 0.5% (v/v) NP-40 and 1% (v/v) Triton X 100) plus protease inhibitors (Calbiochem), for 15 mins on ice. Chromatin was sheared via sonication of $5x10^6$ cells in 1ml IP buffer, using a QSonica Q500 at 60% Amplitude. Successful sonication giving fragments 200-500bps in length was confirmed by resolving a small (decrosslinked) sample on a 1.5% (w/v) agarose gel. Following sonication the lysate was cleared by centrifugation at 12000 x g for 10 mins at 4°C.

500µl of cleared lysates were incubated with 10µl streptavidin beads (Invitrogen) with 100µl IP buffer, rotating at 4°C overnight. Samples were then magnetised, supernatant discarded and beads sequentially washed once in IP buffer, high salt IP buffer (500mM NaCl, 50mM Tris-HCl (pH 8.0), 5mM EDTA, 0.5% (v/v) NP-40, 1% (v/v) Triton X 100), LiCl buffer (10mM Tris-HCl (pH 8.0), 250mM LiCl, 1mM EDTA, 1% (v/v) NP-40, 1% (w/v) Sodium Deoxycholate), and TE buffer (10mM Tris-HCl (pH 8.0), 1mM EDTA). After the final wash beads were resuspended in 100µl of PK buffer (125mM Tris-HCl (pH 8.0), 10mM EDTA, 150mM NaCl, 1% (w/v) SDS) and placed at 65°C overnight. Samples were then incubated with 1µl of 20mg/ml Proteinase K for 3-4 hours at 55°C. Finally, samples were purified using Qiaquick PCR purification kit (Qiagen). Eluted DNA was placed at 95°C for 10 mins and prepared for qPCR.

Components for each q-PCR reaction consisted of:
2µl DNA sample
10µl SYBR Green Supermix
1µl forward primer (10µM stock)
1µl reverse primer (10µM stock)
6µl H_2O

The following cycling parameters were set up:
95°C for 3 mins, followed by 40 cycles of 95°C for 10s, 60°C for 10s, 72°C for 30s, plate read.

A melt curve was then initiated using the following parameters:
95°C for 10s, followed by 65.0°C for 5s, then temperature of increases 0.5°C every 0.5s, plus plate read, up to 95°C.

2.15 Transmission Electron Microscopy

B-K562 and G-K562 cells were frozen onto TEM gold grids using a Leica EM PACT2 high pressure freezing system. Grids were then placed into a Leica EM ASF2 freeze substitution processor for automated low temperature embedding and resin (lowicryl) polymerisation. Once embedded in lowicryl resin, samples were sectioned at thickness of 70nm and subjected to immunogold labelling. Labelling was achieved by incubating grids in blocking solution (0.1% (w/v) BSA in PBS) for 15 mins, followed by 1 hour incubation with primary antibody in blocking solution. Grids were then washed three times in blocking solution before a 30 min incubation with secondary antibody in blocking solution. Finally, grids were washed three times in blocking solution, and six times in distilled H_2O. Images were obtained using an FEI Tecnai T12 TEM microscope.

2.15.1 Antibodies for Immunogold Labelling

Antibody	Source	Dilution
HA (mouse)	Kind gift from Paul Verkade	1:5
Emerin (rabbit)	Millipore #06-1052	1:5
Anti-mouse Gold 6nm	Kind gift from Paul Verkade	1:50
Anti-rabbit Gold 10nm	Kind gift from Paul Verkade	1:50

3 Results Chapter 1: Molecular Mechanism of Gene Repression by the WT1/BASP1/PIP_2 Complex

3.1 Introduction

Previous work from our laboratory established a PIP_2 dependent mechanism of transcriptional repression mediated by the WT1/BASP1 complex [3]. This work provided the first evidence for the recruitment of PIP_2 directly to gene promoters, and implicated PIP_2 as an essential factor for the recruitment of the chromatin modifying protein HDAC1, and subsequent gene repression. Very little is known about the role of lipids in gene regulation, and currently the WT1/BASP1 repression complex is the only transcription regulating complex known to require PIP_2 binding for its repression mechanism. Recently the N-terminally myristoylated MARCKS protein has also been shown to bind nuclear PIP_2, suggesting protein lipidation could be a more widespread requirement for transcription regulation [121]. The experiments presented in this chapter were conducted to gain further insights into the BASP1 mechanism of action and the roles of lipid interaction in transcription. Here the effect of BASP1-PIP_2 on the local chromatin environment at WT1 target gene promoters was examined. The aim was to build upon previous findings by studying the effects of PIP_2 binding on additional active chromatin marks. It has also previously been suggested that BASP1 could also have a role in generating an increase in the repressive H3K27me^3 mark at WT1 target gene promoters [69]. Thus, here it was also aimed to examine a role for BASP1 in mediating an increase in repressive chromatin marks and establish whether this activity was lipid dependent. These experiments serve to provide better understanding of how the WT1/BASP1/PIP_2 complex mediates the alterations in the local chromatin environment that ultimately lead to transcriptional repression.

In order to achieve this aim, generation of stable BASP1 expressing K562 cell lines and optimisation of the chromatin immunoprecipitation (ChIP) method was first necessary. The ChIP method was optimised through examination of BASP1 and WT1 recruitment to WT1 target gene promoters in the K562 cell lines. The levels of active and repressive chromatin marks at bound promoters was subsequently studied. Additionally, the effects of BASP1-PIP_2 on transcriptional activation events downstream of chromatin changes were also studied to gain new insights into how the WT1/BASP1/PIP_2 complex regulates the general transcription machinery.

3.2 Generation of Stable K562 Cell Lines

K562 cells endogenously express WT1 but do not endogenously express BASP1, so stable K562 cell lines were generated that express either wild type BASP1 protein (hereafter referred to as wtBASP1), a glycine-2 to alanine (G2A) mutant BASP1 protein, or control vector for use throughout this study. A pcDNA3 vector as shown in Figure 3.1A was used. The BASP1 sequence was inserted in the pcDNA3 vector between the BamHI and EcoRI restriction sites, under the control of the CMV promoter (Figure 3.1A). A pcDNA3-BASP1 vector was previously generated in the laboratory. The G2A-BASP1 derivative was generated using G2A-BASP1 primers and the pcDNA3-BASP1 plasmid. The glycine residue mutated in the G2A mutant BASP1 is highlighted in the schematic in Figure 3.1B. The previously characterised G2A mutation removes the glycine residue to which the myristoyl motif is added by N-myristoyltransferase 1, completely abrogating myristoylation and disrupting the BASP1-PIP_2 interaction [3, 81, 254, 255]. G2A-BASP1 PCR product was most efficiently produced following the addition of 3% DMSO to the PCR reaction (Figure 3.1C). The PCR product and pcDNA3 vector were digested with BamHI and EcoRI enzymes and ligated together before being transformed into E. coli. Diagnostic digestion of plasmid DNA isolated from E. coli colonies with BamHI/EcoRI confirmed the insertion of a 700bp fragment in the pcDNA3 vector (Figure 3.1D). Presence of the G2A mutation was confirmed by sequencing.

K562 cells were transfected with either unmodified pcDNA3 vector (V-K562 control cell line), pcDNA3-BASP1 sequence (B-K562 cell line), or pcDNA3-G2A-BASP1 sequence (G-K562 cell line). Positively transfected cells were selected with 2µg/ml G418. Three sets of V-K562, three sets of B-K562 and two sets of G-K562 derivative cell lines were generated via stable transfection and selection of G418 resistant cells. The expression of BASP1 and mutant derivatives in these cell lines was confirmed by western blotting (Figure 3.1E).

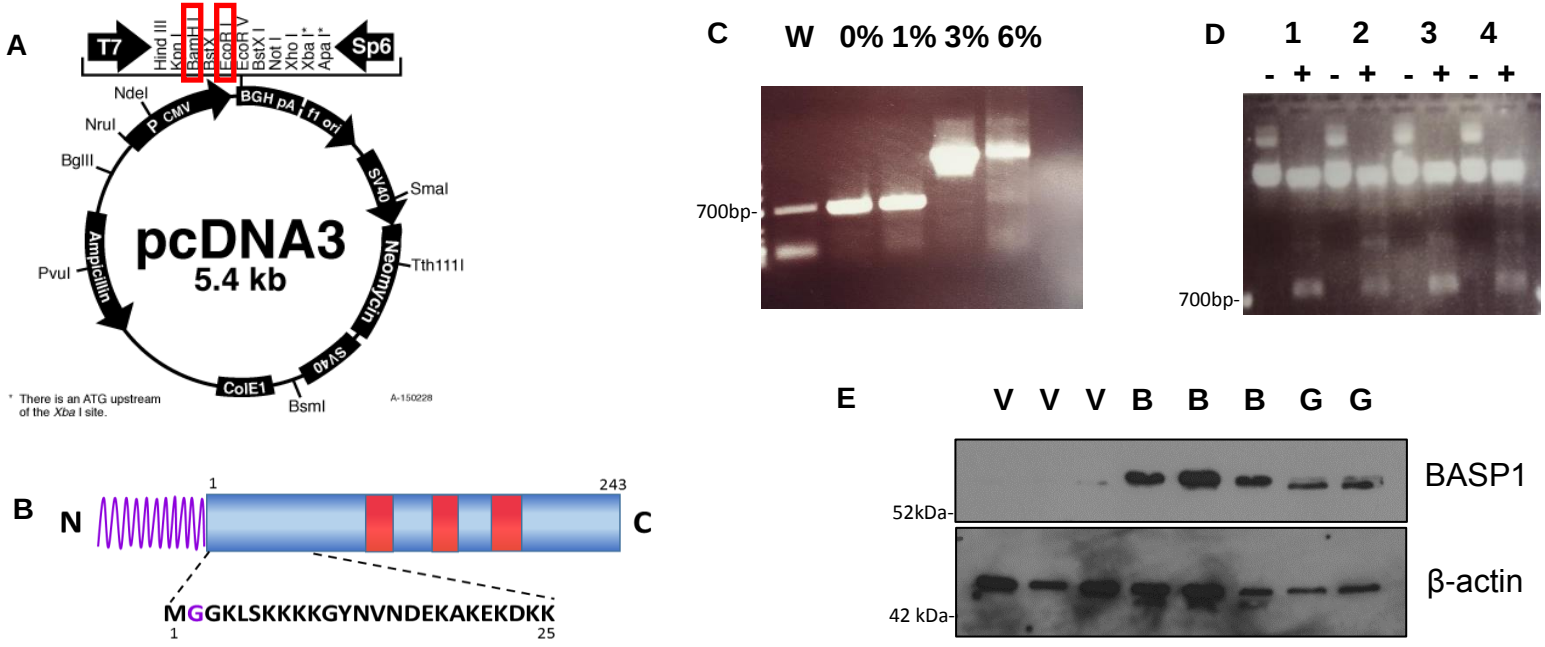

Figure 3.1. Generation of Stable BASP1 Expressing K562 Cell Lines. A, Map of the pcDNA3 mammalian expression vector. The BASP1 coding sequence is inserted between the BamHI and EcoRI sites (highlighted in red boxes), under the control of the CMV promoter. **B**, Schematic of BASP1 protein and the N-terminal amino acid sequence. Glycine-2 is highlighted in purple; this amino acid is mutated to alanine in this study. The attachment of the myristoyl group is shown via the zig-zag purple line. **C**, Agarose gel of G2A-BASP1 product from PCR amplification. %DMSO added to PCR reaction mix is shown above, or W for water control. Base pair markers (bp) are shown at left. **D**, Agarose gel of undigested and digested (-/+) DNA from picked colonies of E. coli transformed with pcDNA3-G2A-BASP1. DNA was digested with BamHI and EcoR1 enzymes. **E**, V-K562 (V), B-K562 (B) and G-K562 (G) cells were generated by stably transfecting K562 cells with the appropriate pcDNA3-based vector, selected with 2µg/ml G418 and tested for BASP1 expression via western blotting. Molecular weight markers (kDa) are shown at left. β -actin was probed as a loading control

3.3 Gene Expression Analysis of WT1 Target Genes in V-K562, B-K562 and G-K562

The stable K562 cell lines were tested for their expression levels of a selection of WT1 target genes. Total RNA and then cDNA were prepared from V-K562, B-K562 and G-K562 cells and expression quantified using real time quantitative PCR. Multiple WT1 target genes that have previously been identified as repressed by BASP1 were examined including AREG (Amphiregulin), ETS-1 and REN (Renin) (Figure 3.2) [2, 3, 96]. In agreement with these previous reports wtBASP1 repressed these target genes. Transcriptional repression was not observed in G-K562 cells; indeed the ETS-1 gene was even upregulated in the G-K562 cells compared to V-K562 cells. These results recapitulate previous findings from our laboratory and support a role for BASP1 in mediating repression of WT1 target genes in a myristoyl-dependent manner. Since myristoylation is required for the BASP1-PIP_2 interaction this implicates PIP_2 as being important for the repression mechanism at these target genes.

3.4 PMA Treatment of V-K562, B-K562 and G-K562 Cells

It is well established that PMA treatment induces the differentiation of K562 cells towards a megakaryocyte lineage [2, 256, 257]. Our lab has previously shown that this PMA induced differentiation pathway is entirely diverted in K562 cell line derivatives that express wtBASP1, whereby cells instead differentiate into neuron-like cells [2]. The stable K562 cell lines generated for this project were similarly tested (Figure 3.3). Upon PMA treatment the V-K562 cells adhere to the culture dish and retain a round morphology. B-K562 cells also adhere to the culture dish, and some arborisation was observed indicative of neuron-like differentiation. Furthermore, also in accordance with previous reports, G-K562 cells adhere to the culture dish but remain round in morphology, reminiscent of the V-K562 cells [3]. No arborisation of G-K562 cells was evident. These observations confirm that the K562 cells used in this study differentiate in the presence of PMA similarly to previous reports and again demonstrate that myristoylation of BASP1 is essential for the BASP1 mediated differentiation of K562 cells into neuron-like cells. This in turn implicates the PIP_2 interaction as being important for the BASP1 mediated effect on K562 cell differentiation.

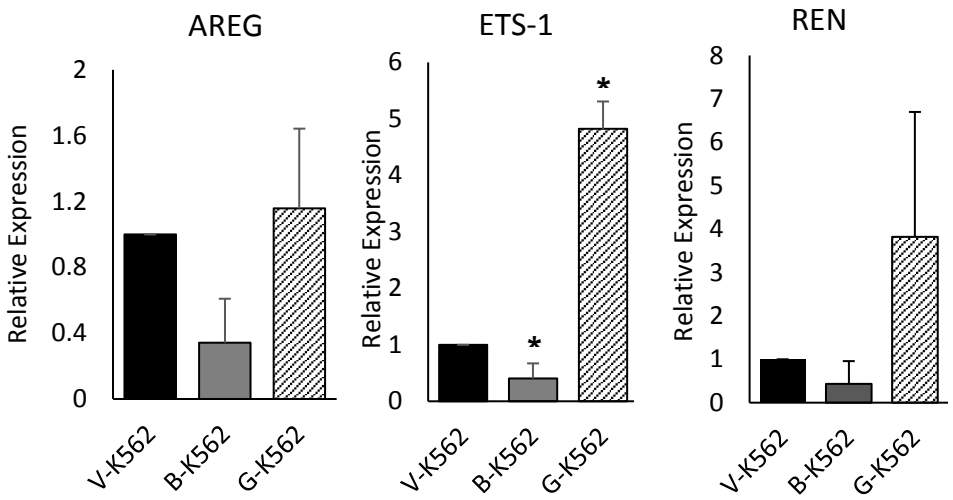

Figure 3.2. WT1 Target Genes are Repressed in Wild Type BASP1 Expressing K562 Cells. Relative expression of WT1 target genes in V-K562, B-K562 and G-K562 cell lines was analysed, compared to control gene GAPDH. The expression levels of three target genes; AREG, ETS-1 and REN are shown. Error bars representative of the standard deviation of the mean, n=3. *p<0.05, by Student's t test comparing B-K562 or G-K562 with V-K562 cells.

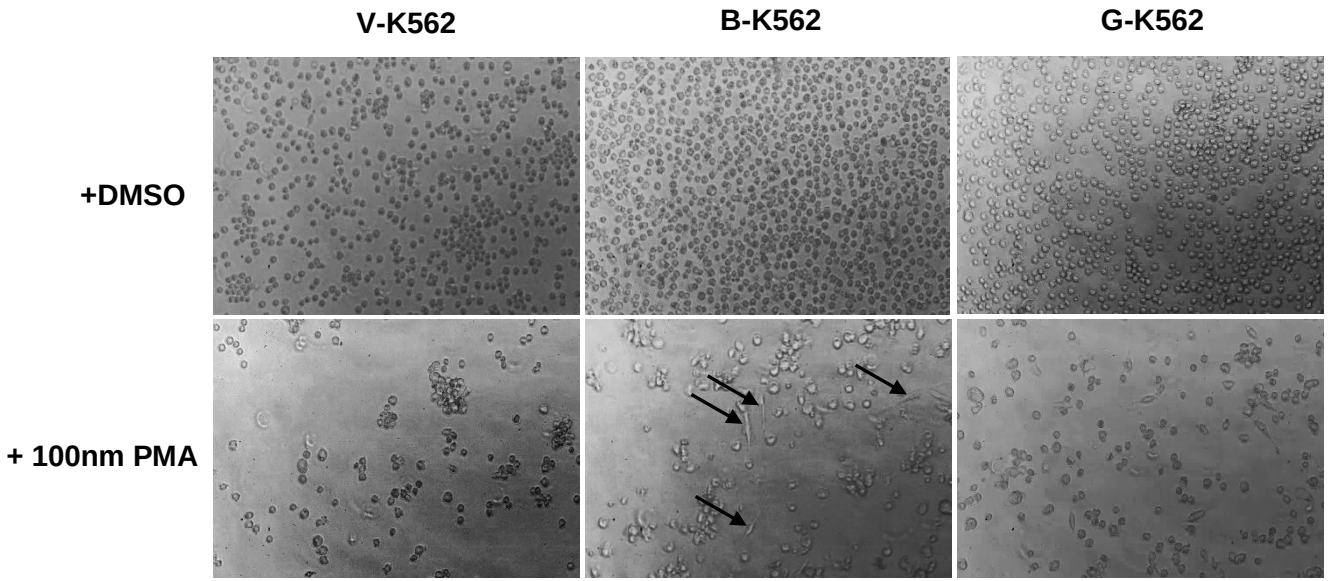

Figure 3.3. PMA Treatment Causes Neuronal-like Differentiation in B-K562 Cells. V-K562, B-K562 and G-K562 cells were treated with DMSO (control) or 100nm PMA for 72 hours in 6 well plates and examined for the presence of differentiating cells. All DMSO treated cells remained in suspension. Black arrows highlight adherent cells with neuron-like protrusions. Images representative of cells from across three independent experiments.

3.5 Soft Agar Colony Formation Efficiency of Stable K562 Cell Lines

Our laboratory has previously demonstrated that expression of wtBASP1 leads to growth suppression of K562 cells in culture [2]. Given that the G2A mutation of BASP1 is sufficient to abolish transcriptional repression by BASP1, it was hypothesised that G2A-BASP1 expression in K562 cells may lead to loss of growth suppression. K562 cells can be used in soft agar assays as a measure of tumorigenicity [258, 259]. The K562 cell line derivatives generated here were therefore tested in soft agar assays to establish their ability to form anchorage independent colonies.

The number of V-K562, B-K562 and G-K562 colonies greater than 50 cells in size were counted over a three-week period (Figure 3.4). Expression of wtBASP1 lead to a significant decrease in the colony forming ability of K562 cells (Figure 3.4B). Images taken to qualitatively assess differences in colonies, and subsequent measurement of the average area of colonies revealed that as well as forming fewer colonies, B-K562 cells form significantly smaller colonies (Figure 3.4C). Expression of G2A-BASP1 also lead to a significant decrease in the colony forming ability of K562 cells (Figure 3.4B). However, the average area of G-K562 colonies did not significantly differ to that of V-K562 colonies. This result suggests that BASP1 reduces anchorage independent colony formation of K562 cells. This result also suggests that myristoylation, and subsequently interaction of BASP1 with PIP_2, is not required to suppress formation of anchorage independent colonies but does contribute to the growth of established colonies.

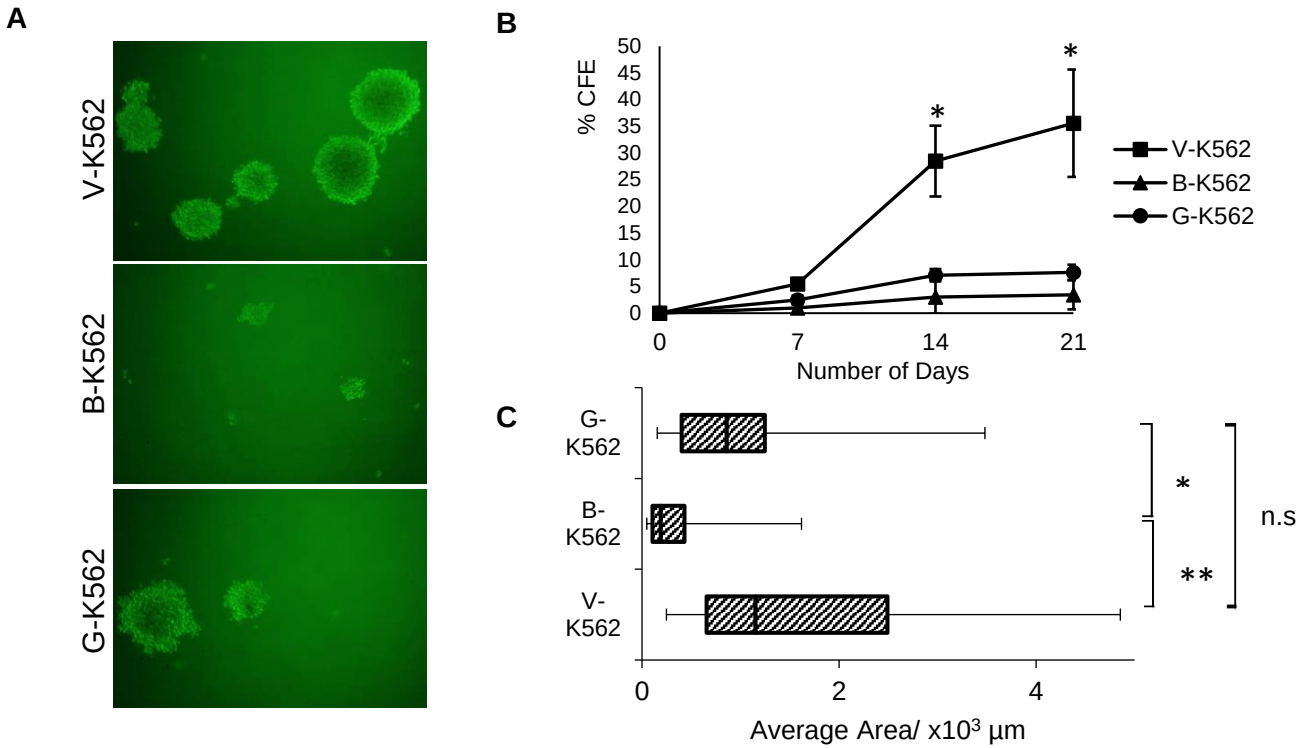

Figure 3.4. BASP1 Expression Leads to Reduced Colony Formation in K562s. V-K562, B-K562 and G-K562 cells were seeded into agar dishes and colony formation efficiency was assessed at days 7,14 and 21. **A**, Representative images of V-K562, B-K562 and G-K562 cells after 21 days growth in soft agar. **B**, Colony formation efficiencies (CFE) for both BASP1 expressing cell lines are significantly lower at all time points compared to V-K562 control. There is no significant difference between B-K562 and G-K562 colony formation efficiency. Error bars representative of the standard deviation of the mean across 3 independent experiments. **C**, Box and Whisker plot of average colony area after 21 days growth of V-K562, B-K562 and G-K562 cells in agar. *p<0.05, **p<0.005, n.s. (no significant difference) by Student's t test comparing V-K562, B-K562 and G-K562 colony areas across 3 independent experiments.

3.6 Development and Optimisation of the Chromatin Immunoprecipitation Method for K562 Cells

As previously described our laboratory has demonstrated a BASP1-PIP_2 dependent mechanism of transcriptional repression of WT1 target genes [3]. PIP_2 is an essential component of the repression complex which recruits histone deacetylase 1 (HDAC1) to target gene promoters [3]. HDAC1 subsequently mediates the removal of acetyl groups from histone 3 lysine 9 (H3K9Ac) and thus produces a more repressive chromatin environment. To further explore how BASP1-PIP_2 mediates changes in chromatin dynamics at WT1 target gene promoters chromatin immunoprecipitation (ChIP) experiments were conducted to examine the levels of other activating histone marks, as well as repressive histone marks at WT1- and WT1/BASP1-bound promoters.

Previous studies using ChIP experiments in our laboratory have found that considerable optimisation of the crosslinking and fragmentation steps in particular are required for K562 cells. Firstly, several methods were tested to establish the most efficient and reproducible method to produce high quality DNA fragments (Figure 3.5). Prior to fragmentation, cells were crosslinked in 1.42% PFA, lysed and nuclear extracts collected via centrifugation. The first method of DNA fragmentation tested was via digestion by the micrococcal nuclease (Mnase) enzyme. Mnase enzyme digestion of the collected DNA reliably produced a dense band of DNA fragments of approximately 300bp, and a smaller band of approximately 150bp (Figure 3.5A). This indicated digestion of DNA into di and mono nucleosomes, respectively. Additionally, partially digested DNA was detected as a diffuse smear above these bands on agarose gels. Longer mnase digestion times (10, 15, 20, 30 mins) and changes in initial crosslinking times (15, 20, 25 mins) did not greatly affect the production of dinucleosomes, mononucleosomes or significantly reduce the proportion of partially digested DNA. Optimal DNA fragmentation using the Mnase digestion method was achieved when samples were digested for 30 mins.

Secondly, identically prepared DNA samples placed in a bioruptor to fragment DNA resulted in poor DNA fragmentation (Figure 3.5B). Despite identifying a band of DNA fragments of approximately 400-500bp when samples were resolved on agarose gels, all biorupted samples contained a large proportion of unfragmented DNA that did not migrate out of the loading wells. Increasing the number of bioruptor pulses did not improve DNA fragmentation.

Thirdly, DNA fragmentation via sonication was also examined. 16 pulses of sonication for 30 seconds (s), followed by 30s on ice was recommended by previous lab members as a starting protocol. Sonication using this method produced DNA fragments of approximately 300bp, however a large proportion of sample remained several thousands of base pairs in length as seen on agarose gels (Figure 3.5C). It was predicted that a larger number of shorter sonication pulses would more efficiently fragment the DNA and give higher quality fragments. To this end, shorter sonication pulses of 3x3s at 60% amplitude, with 2s on ice between each pulse was trialled. This shorter sonication protocol reliably produced fragments of approximately 400bp, even at the lowest number of pulses (16) (Figure 3.5D). This method was also most effective at fragmenting the whole DNA sample, with minimal DNA detected above 400bp on agarose gels. To ensure maximum optimisation of the sonication protocol different amplitudes were also tested (Figure 3.5E). Using 50% or 60% amplitude for sonication had no determinable effect on the size of fragments produced.

From these results it was concluded that the optimal method of DNA fragmentation was sonication, and that the best DNA fragmentation was achieved using 16 pulses of 3x3s sonication, with 2s on ice between each. Therefore, using this method the enrichment of BASP1 and WT1 protein at the AREG promoter in V-K562 and B-K562 cells was then examined (Figure 3.5F). No enrichment of BASP1 or WT1 could be detected in the B-K562 cell line regardless of the number of sonication pulses. Both BASP1 and WT1 signal was enriched at the AREG promoter in the V-K562 cells. Given that BASP1 is not expressed in these cells it is reasonable to conclude that the signal obtained in this experiment was not specific and that further optimisation of the ChIP method was required.

Simultaneously to experiments exploring the optimal DNA fragmentation method for ChIP, experiments examining a variety of crosslinking times and methods were also conducted in order to improve the reliability of protein enrichment. Direct comparison of ChIP signal from V-K562 and B-K562 cells crosslinked in 1.42% paraformaldehyde (PFA) for different lengths of times was examined. Having already found 20 mins of crosslinking to result in high levels of background signal, crosslinking for 10 and 15 mins with 1.42% PFA was tested (Figure 3.6A and 3.6B). Detection of both BASP1 and WT1 signal above that of IgG control was limited in both crosslinking conditions. Whilst the fold enrichment for BASP1 was greater in B-K562 than V-K562 cells after 10 mins of crosslinking, this is also true for WT1. WT1 is expressed in both cell types and therefore capture of WT1 via this ChIP method

was successful only in one of the two cell lines. After 15 mins crosslinking both BASP1 and WT1 were detected at similarly low levels in both cell lines. Following these results it was concluded that neither ChIP experiment had resulted in successful pull down of BASP1 and WT1 and therefore that further optimisation was required.

V-K562, B-K562 and G-K562 cells were next crosslinked using either 1.42% PFA alone, or in combination with 1mM, 2mM or 3mM ethylene glycol bis(succinimidyl succinate) (EGS) (Figure 3.6C-G). EGS has previously been used to enhance the crosslinking of proteins not directly bound to DNA but bound as part of protein complexes [260, 261]**.** Fragmentation of DNA via sonication was unaffected by addition of EGS as a crosslinker (Figure 3.6C). Detection of BASP1 protein at the REN promoter was unimproved by the addition of EGS at any concentration. Conversely, in this experiment BASP1 was more reliably detected in the absence of EGS (Figure 3.6D). It was therefore concluded that samples for further ChIP experiments would be crosslinked using only 1.42% PFA. It was also found that crosslinking with PFA in phosphate buffered saline (PBS) gave more efficient crosslinking than adding PFA directly to the culture medium.

Based on the unimproved ChIP signal following any of the crosslinking conditions tested it was determined that optimisation of other stages of the ChIP protocol was necessary in order to gain reliable ChIP signal. To proceed it was decided that a 15 min crosslinking was the most appropriate to use whilst further optimising the ChIP protocol in order to ensure the best capture of target proteins. Only upon combining the optimally devised sonication protocol with the 15 mins 1.42% PFA crosslinking method was reliable and convincing detection of BASP1 and WT1 bound to target gene promoters achieved. It proved essential that both high quality crosslinking and sonication were achieved in order to gain successful protein capture and DNA detection. This detection was further improved through additional protocol adaptations which included the use of acetylated bovine serum albumin (BSA) during pre-blocking of dynabeads, lengthening the immunoprecipitation stage to approximately 20 hours, decrosslinking in the presence of Ambion Proteinase K (#AM2548), testing multiple aliquots of BASP1 and WT1 antibodies, and using always freshly made IP and washing buffers throughout. Once optimisation of all these aspects of the protocol were combined successful detection of BASP1 and WT1 at target gene promoters could be attained.

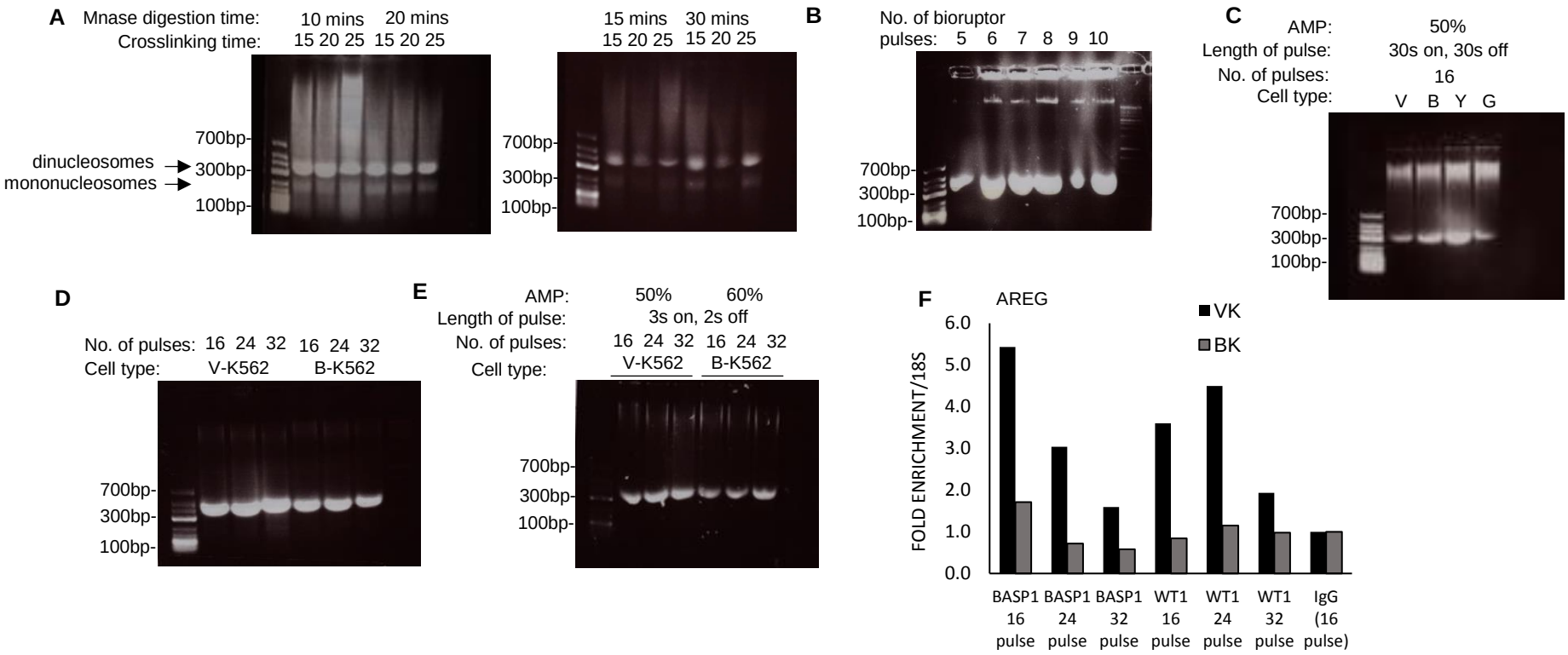

Figure 3.5. Testing Methods of DNA Fragmentation for ChIP. Gel electrophoresis showing sizes of DNA fragments following different DNA fragmentation protocols. Base pair markers are shown at left. **A,** size of fragments following varying times of Mnase enzyme digestion of crosslinked B-K562 for 15, 20 or 25 mins. **B,** size of fragments achieved following 5-10 pulses of 30s in a bioruptor after 15 mins crosslinking (B-K562). **C,** Crosslinked K562 cells (V-, B-, Y- and G-) were sonicated using an amplitude of 50%, for 16 pulses of 30s sonication, 30s on ice. **D,** size of fragments following pulses of sonication for 3s, followed by 2s on ice for increasing number of rounds (16-32) in V-K562 and B-K562 crosslinked for 15 mins. **E,** V-K562 and B-K562 cells were sonicated at 50% or 60% amplitude, respectively, for either 16, 24 or 32 pulses of 3s sonication, 2s on ice. **F,** BASP1 and WT1 fold enrichment compared to control region (18S) from V-K562 and B-K562 cells after 16, 24 or 32 sonication pulses at 60% amplitude

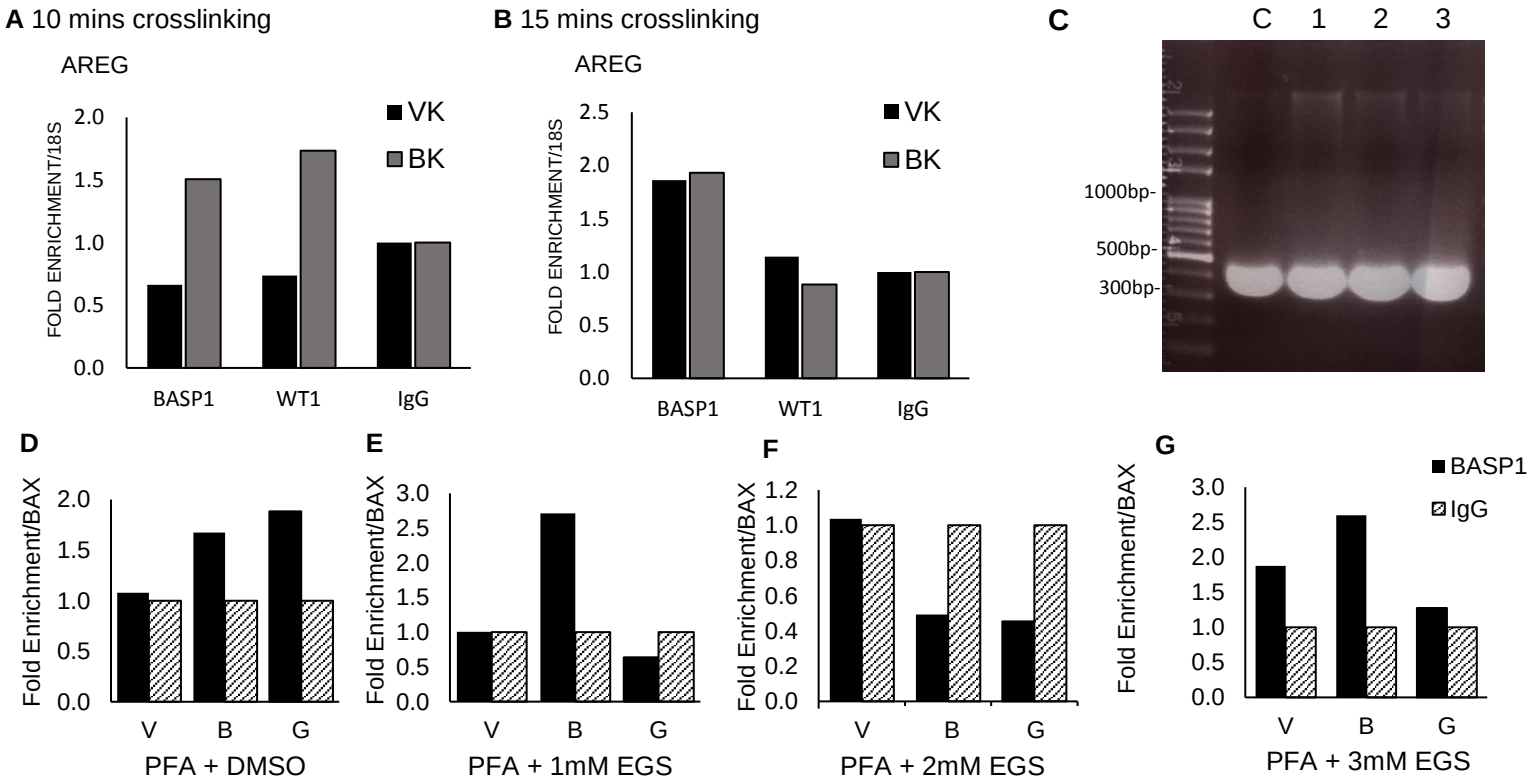

Figure 3.6. Optimising PFA + EGS Crosslinking for ChIP. ChIP was performed on V-K562 and B-K562 cells following crosslinking with PFA for either **A**, 10 mins or **B**, 15 mins. BASP1 and WT1 immunoprecipitates were analysed for signal above IgG control at the AREG gene compared to negative control region. B-K562 cells were crosslinked with either PFA plus DMSO (control), PFA plus 1mM EGS, PFA plus 2mM EGS, or PFA plus 3mM EGS (C,1,2,3 in **C**). **C**, Gel electrophoresis showing size of DNA fragments following PFA + EGS crosslinking and sonication. Base pair markers (bp) are shown at left. **D-G**, ChIP signal obtained at the REN promoter, after crosslinking V-K562, B-K562 and G-K562 cells with PFA plus DMSO (control), PFA plus 1mM EGS, PFA plus 2mM EGS, or PFA plus 3mM EGS, sonication, and incubation with BASP1 antibody overnight. Graphs show detected fold enrichment of BASP1 compared to control region (BAX gene).

3.7 Chromatin Immunoprecipitation of BASP1 and Repression Complex Components to the Promoters of WT1 Target Genes

Having optimised the protocol for ChIP in K562 cells, detection of BASP1 and WT1 at the promoters of WT1 target genes was performed. V-K562, B-K562 and G-K562 cells were subjected to ChIP using antibodies against BASP1, WT1 or IgG control (Figure 3.7). Both wtBASP1 and G2A-BASP1 were bound at the AREG, ETS-1, REN, VDR and JUNB promoters. As would be predicted, BASP1 enrichment was statistically significantly greater in B-K562 and G-K562 cells than in V-K562 cells as determined using a Student's t test (Figure 3.7A). Further, the enrichment of BASP1 at these sites was also statistically significantly greater than the enrichment of IgG. Therefore, both wtBASP1 and G2A-BASP1 were detected at these WT1 target gene promoters above the level of background signal. Similarly, WT1 was detected above the level of background signal in all three cell line derivatives, indicating that WT1 was bound to its target gene promoters regardless of BASP1 expression (Figure 3.7B). There was no statistically significant difference in the binding of WT1 at these sites between V-K562, B-K562 and G-K562 cells as determined using a Student's t test. These findings indicate that WT1 was successfully detected bound to WT1 target gene promoters in V-K562, B-K562 and G-K562 cells, whilst wtBASP1 and G2A-BASP1 were successfully detected bound to WT1 target gene promoters in the B-K562 and G-K562 cell lines, respectively.

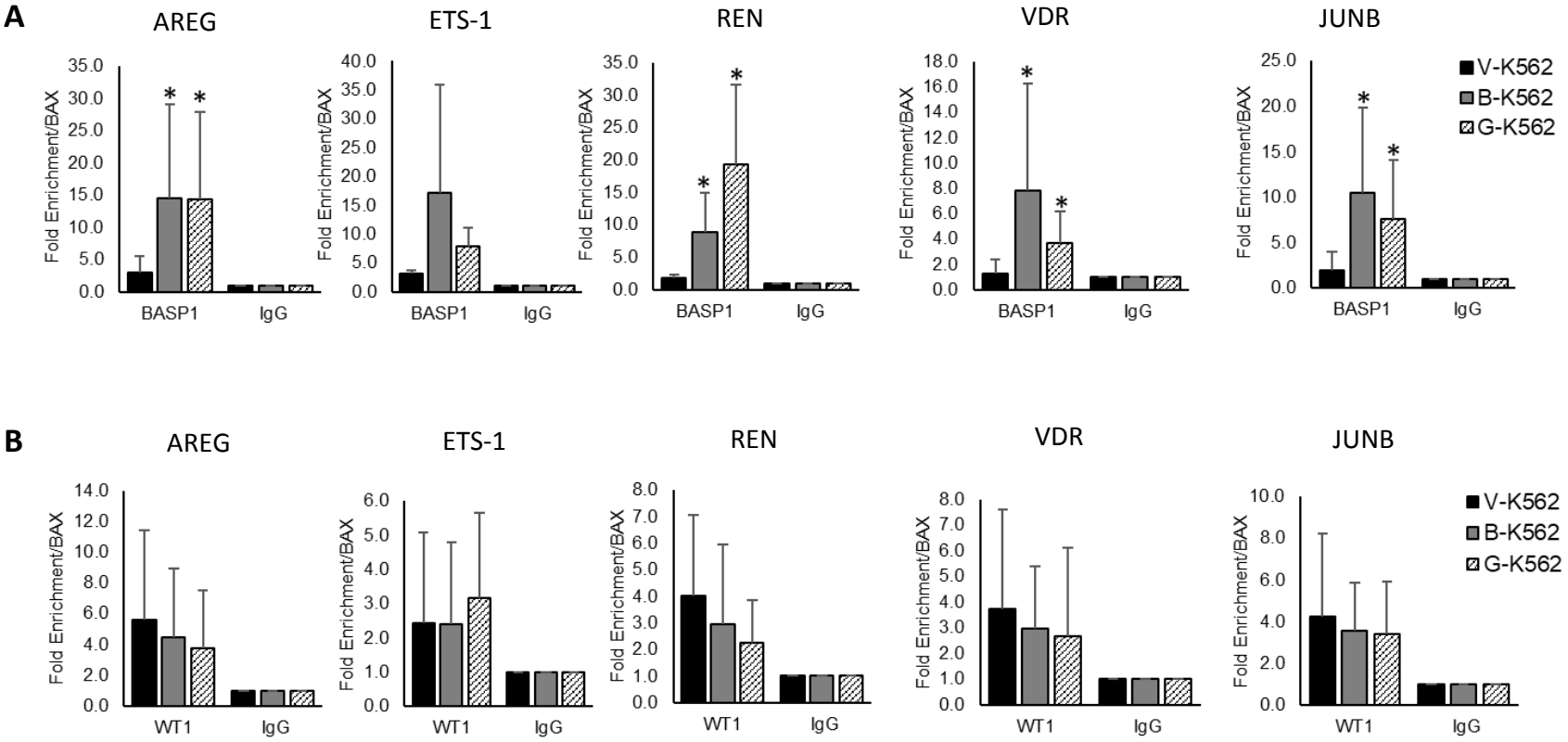

Figure 3.7. Recruitment of BASP1 and WT1 to AREG, ETS-1, REN, VDR and JUNB Promoters in K562 Cells. The presence of (**A**) BASP1 and (**B**) WT1 at the promoters of AREG, ETS-1, REN, VDR and JUNB was examined using chromatin immunoprecipitation in V-K562, B-K562 and G-K562 cells. Error bars representative of the standard deviation of the mean, A) n=6, B) n=10 *p<0.05 by Student's t test comparing B-K562 or G-K562 with control line V-K562.

3.8 Chromatin Immunoprecipitation of Active and Repressive Chromatin Marks at WT1 Target Gene Promoters in V-K562, B-K562 and G-K562 Cells

Following successful detection of BASP1 and WT1 bound to target gene promoters in the K562 cell lines via ChIP, examination of BASP1-dependent changes in histone modifications at these sites was next conducted. As described, our lab has previously demonstrated a decrease in histone H3 lysine 9 (H3K9) acetylation at BASP1 bound sites in a PIP_2-dependent manner [3]. Therefore, ChIP was conducted in V-K562, B-K562 and G-K562 cells to verify that changes in H3K9Ac levels could be detected using the optimised ChIP protocol (Figure 3.8). In agreement with previous findings H3K9Ac marks were significantly reduced at promoters bound by wtBASP1 at all five target genes examined (AREG, ETS-1, REN, VDR and JUNB). At G2A-BASP1 bound sites there is no decrease in H3K9Ac marks at any of the gene promoters. In fact, at the AREG and JUNB promoters levels of H3K9Ac are higher in the G-K562 than V-K562 cells. This result further validates that the implemented ChIP protocol can be used to reproduce previous observations.

To further explore how BASP1-PIP_2 mediate changes in chromatin dynamics at WT1 target gene promoters, the abundance of other activating histone modifications at these sites was examined. The relative fold enrichment of two additional active histone marks, H3K36me^3 and H3K4me^3, at the AREG, ETS-1, REN, VDR and JUNB promoters in V-K562, B-K562 and G-K562 cells are shown in Figure 3.9. Similarly to H3K9Ac, a significant reduction in H3K36me^3 was observed at the REN, VDR and JUNB promoters in B-K562 but not G-K562 cells. This was not the same for the ETS-1 promoter where there was no significant difference in the abundance of H3K36me^3 marks in V-K562, B-K562 or G-K562 cells. The AREG promoter also showed no significant difference in H3K36me^3 marks in V-K562 and B-K562 cells. Additionally, like H3K9Ac, at several gene promoters there was in fact an increase in H3K36me^3 marks in G-K562 compared to V-K562 cells. Furthermore, H3K4me^3 marks were significantly reduced at all target gene promoters only in the B-K562 compared to V-K562 cells. No reduction in H3K4me^3 was observed at any of the promoters bound by G2A-BASP1. These data provide evidence that BASP1 recruitment to WT1 target gene promoters affects multiple activating histone modifications, and that myristoylation of BASP1 is required for the WT1/BASP1 complex to mediate the observed reduction in active histone modifications. The

requirement for BASP1 myristoylation to induce the observed changes in histone modifications implicates PIP_2 in being an essential BASP1 interactor for this process.

In addition to examining activating histone marks, levels of the repressive histone marks H3K27me^3 and H3K9me^3 were also studied. BASP1 has previously been connected to the placement of H3K27me^3 marks at the WT1 regulated Wnt4 locus during differentiation of epicardial cells [69]. It was suggested that loss of BASP1 resulted in the switching of WT1 genes from a repressed to an active state, and thus we hypothesised BASP1 to have a dual role in driving removal of active chromatin marks and placement of repressive marks to induce a repressive chromatin state. Here it was tested whether BASP1 induces a repressive state at WT1 target genes in the K562 cell lines and if this is dependent on the myristoylation of BASP1. V-K562, B-K562 and G-K562 cells were subjected to ChIP using antibodies against H3K27me^3 and H3K9me^3 (Figure 3.10). A significant increase in the enrichment of H3K27me^3 marks was detected at the AREG and ETS-1 promoters in B-K562 cells. H3K27me^3 marks were also significantly increased at the AREG promoter in G-K562 cells (Figure 3.10A). As a trend, levels of H3K27me^3 marks at the REN, VDR and JUNB promoters were greater in B-K562 and G-K562 cells than V-K562 cells, although not to a statistically significant level. Similarly, increases in H3K9me^3 marks were detected at selected gene promoters (AREG, JUNB) in B-K562 and G-K562 cells, although only to a statistically significant level in the latter. These results suggest that BASP1 could indeed have a role in increasing repressive histone modifications at WT1 target gene promoters. It appears that this activity is independent of BASP1 myristoylation and therefore independent of the BASP1-PIP_2 interaction.

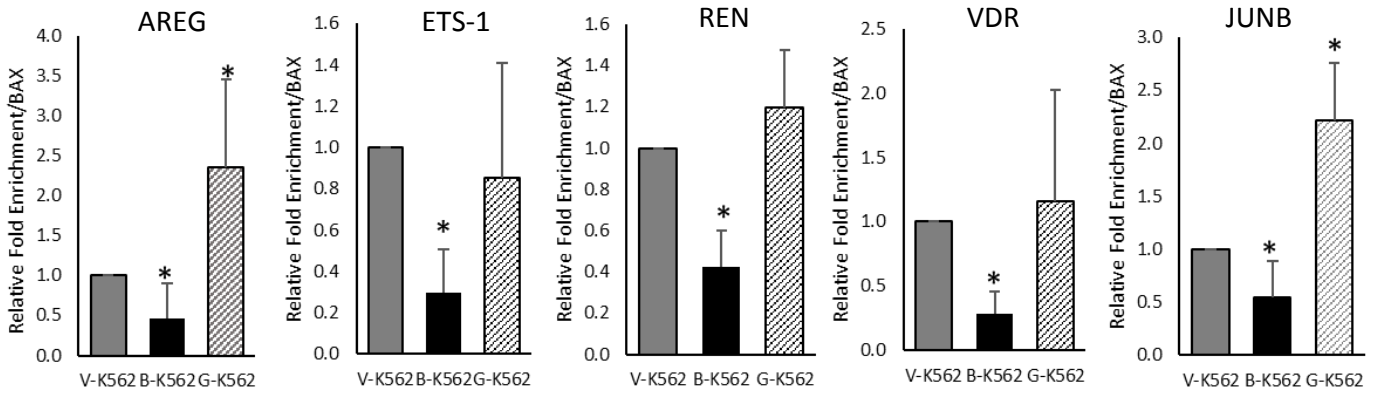

Figure 3.8. H3K9Ac Marks are Decreased at WT1 Target Genes in Wild Type BASP1 Expressing K562s. The presence of H3K9Ac marks at the promoters of the WT1 target genes AREG, ETS-1, REN, VDR and JUNB was examined using chromatin immunoprecipitation in V-K562, B-K562 and G-K562 cells. Error bars representative of the standard deviation of the mean, n=5. *p<0.05 by Student's t test comparing B-K562 or G-K562 with control line V-K562.

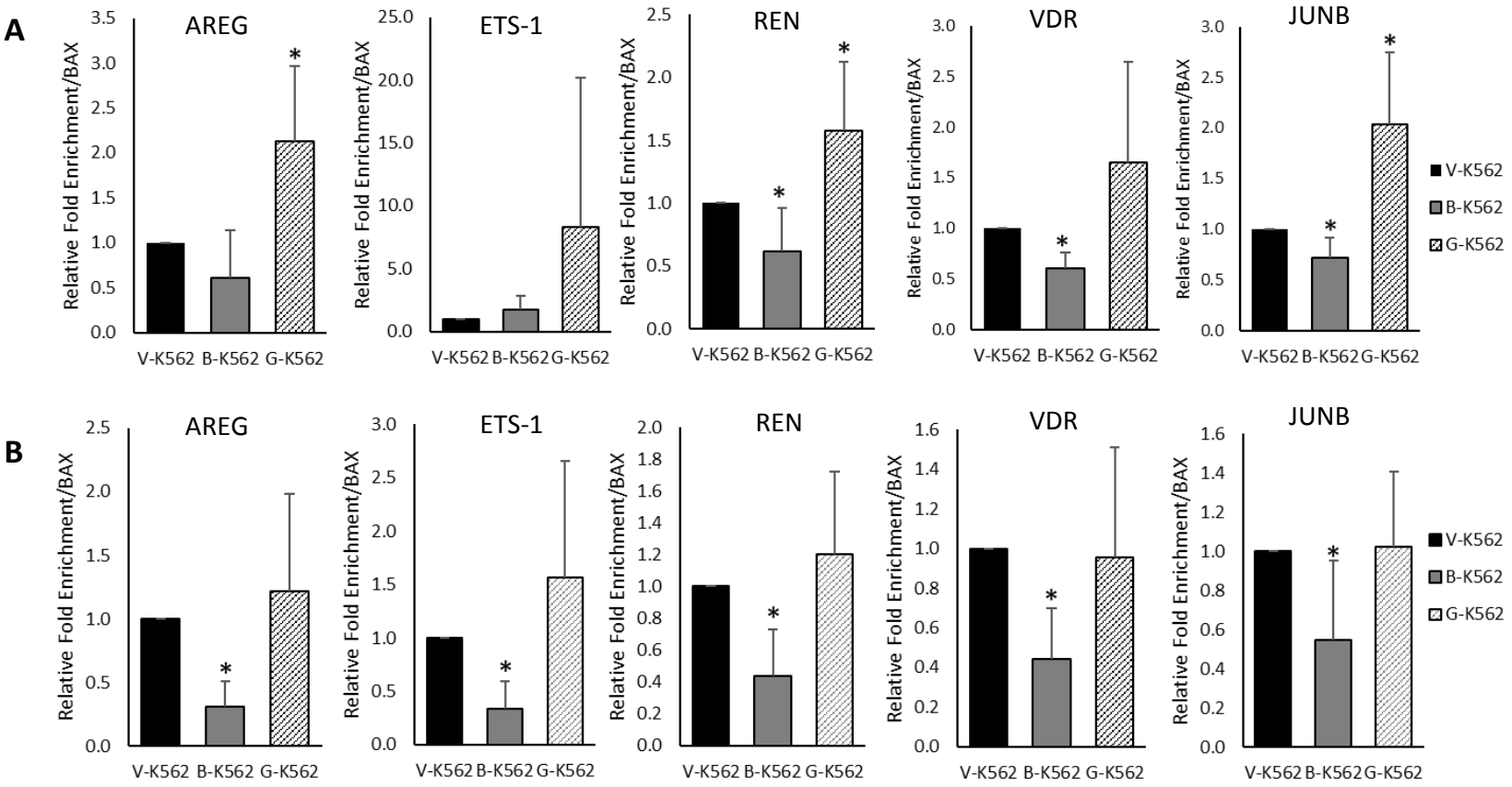

Figure 3.9. Active Histone Marks H3K36me^3 and H3K4me^3 are Decreased at WT1 Target Genes in Wild Type BASP1 Expressing K562s. The presence of (**A**) H3K36me^3 marks and (**B**) H3K4me^3 marks at the promoters of AREG, ETS-1, REN, VDR and JUNB was examined using chromatin immunoprecipitation in V-K562, B-K562 and G-K562 cells. Error bars representative of the standard deviation of the mean, A) n=6, B) n=5. *p<0.05 by Student's t test comparing B-K562 or G-K562 with control line V-K562.

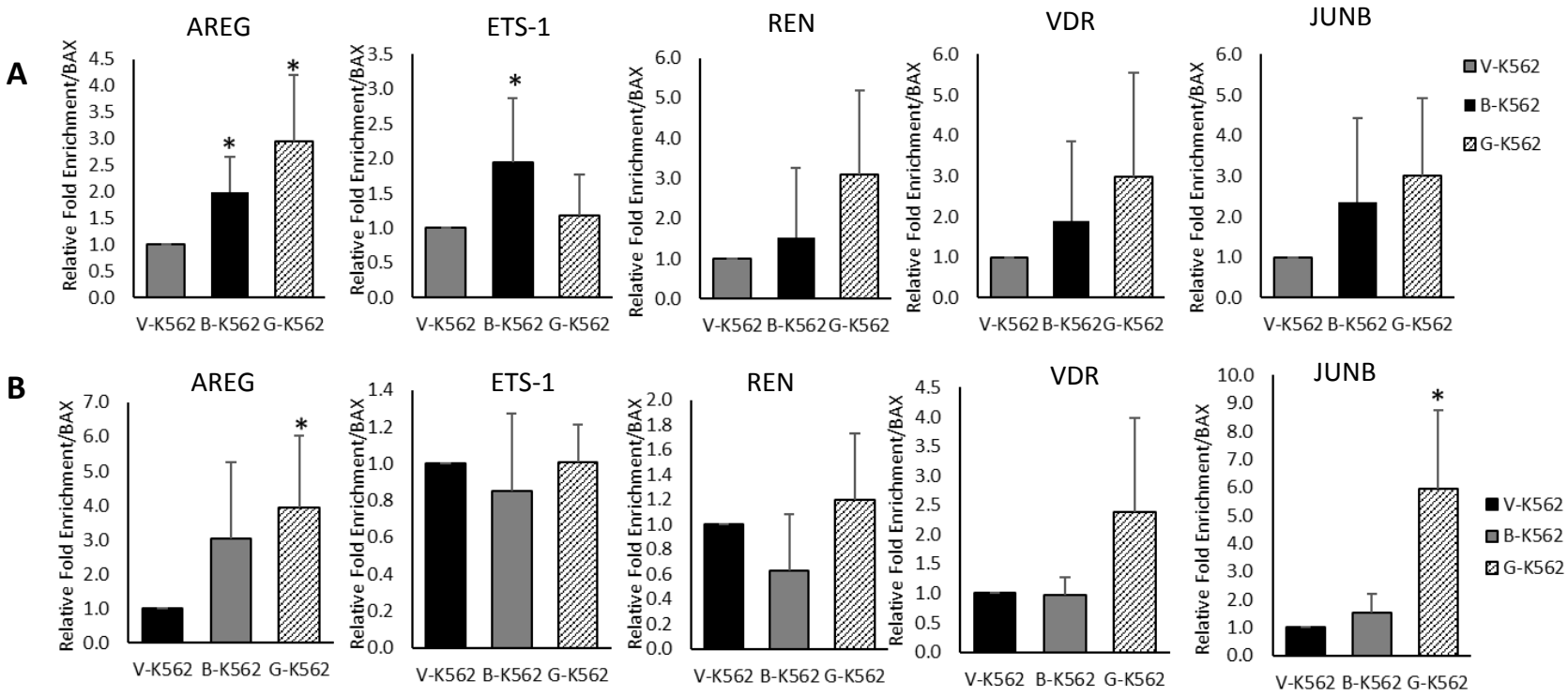

Figure 3.10. Repressive Histone Marks H3K27me^3 and H3K9me^3 are Increased at WT1 Target Genes in Wild Type and G2A-BASP1 Expressing K562s. The presence of (**A**) H3K27me^3 marks and (**B**) H3K9me^3 marks at the promoters of AREG, ETS-1, REN, VDR and JUNB was examined using chromatin immunoprecipitation in V-K562, B-K562 and G-K562 cells. Error bars representative of the standard deviation of the mean, A) n=7, B) n=6. *p<0.05 by Student's t test comparing B-K562 or G-K562 with control line V-K562.

3.9 BASP1-Dependent Chromatin Immunoprecipitation of EZH2 at WT1 Target Gene Promoters

The molecular mechanism behind the observed increase in abundance of repressive histone marks H3K27me^3 and H3K9me^3 at WT1 target gene promoters in B-K562 and G-K562 cells was investigated further. Mining of BASP1 interactome data obtained via a combination of Tandem Mass Tag (TMT) mass spectrometry and standard interactome LC-MS mass spectrometry of BASP1 immunoprecipitates identified a number of chromatin modifying enzymes including histone methyltransferases and histone demethylases (refer to results chapter 2, Figure 4.2). Amongst the candidate histone methyltransferases that were found to interact with BASP1 in the mass spectrometry data sets was enhancer of zeste 2 polycomb repressive complex 2 subunit (EZH2). EZH2 is the enzymatic N-methyltransferase component of the Polycomb Repressive Complex 2 (PRC2), a complex well known to initiate silencing of genomic regions primarily through methylation of H3K27, but also of H3K9 [262-264]. Reports that EZH2 predominantly targets H3K27 methylation, resulting in H3K27me^3 marks, as well as having weaker methyltransferase activity towards H3K9me^2, forming H3K9me^3 marks is consistent with ChIP data presented here [265-269]. This data shows an increase in H3K27me^3 marks, with a more modest increase in H3K9me^3 marks at BASP1 bound promoters and so it was hypothesised that EZH2 could be responsible for mediating the increase in these marks in BASP1 expressing cells. To test this, ChIP experiments were conducted to examine the recruitment of EZH2 at WT1 target gene promoters and assess whether this enzyme could be responsible for the observed increase in methylation of H3K27 and H3K9.

Indeed, upon examination of EZH2 recruitment to WT1 target genes via ChIP, at three genes (AREG, REN and JUNB) EZH2 was significantly enriched in B-K562 and G-K562 with respect to V-K562 cells (Figure 3.11A). At the other two genes (ETS-1 and VDR) EZH2 was significantly enriched in G-K562 cells and was also elevated in B-K562 cells, although not to a statistically significant level. This result indicates that EZH2 is indeed recruited to WT1 target gene promoters in a BASP1-dependent manner that correlates with the observed increase in BASP1-dependent H3K27 and H3K9 trimethylation. Just as the increase in H3K27me^3 and H3K9me^3 is not dependent upon myristoylation (and PIP_2 interaction) of BASP1, recruitment of EZH2 is also not dependent upon myristoylation of BASP1. These data support the

hypothesis that BASP1 induces a repressive chromatin environment via the recruitment EZH2 to WT1 target gene promoters.

Next, to validate the BASP1-EZH2 interaction nuclear extracts of V-K562, B-K562 and G-K562 cells were immunoprecipitated with BASP1 antibodies, western blotted and probed for EZH2 (Figure 3.11B). A direct interaction between wtBASP1 or G2A-BASP1 and EZH2 was not detected. The western blotting technique is not as sensitive as mass spectrometry and so it is possible that the affinity of EZH2 for BASP1 is below the detection level for western blotting. Probing of the western blot membranes with other EZH2 antibodies could be performed to determine whether antibody specificity could be at fault. It is also possible that the BASP1-dependent recruitment of EZH2 as seen in the ChIP data is the result of wider BASP1 mediated effects on the local chromatin environment rather than BASP1 directly interacting with EZH2 to recruit it to target sites. It is possible that BASP1 has effects on additional histone marks which act as a signal for EZH2 recruitment. The BASP1 mediated effects that result in EZH2 recruitment are clearly independent of myristoylation.

3.10 Chromatin Immunoprecipitation of RNA Polymerase II and CDK7 at WT1 Target Genes Promoters

So far, the data has shown the BASP1 repression complex mediates its effect on gene transcription through changes to the chromatin environment at WT1 target gene promoters. Whether BASP1 mediates effects downstream of chromatin alterations had yet to be explored. Here, the recruitment and activation of the transcription machinery was analysed through further ChIP experiments. To this end, the recruitment of RNA polymerase II to WT1 target gene promoters in V-K562, B-K562 and G-K562 cells was examined (Figure 3.12A). Since mRNA expression data showed wtBASP1 causes gene repression, whilst G2A-BASP1 does not, it was hypothesised that RNA polymerase II recruitment may be reduced by wtBASP1 and not by G2A-BASP1.

No statistically significant differences were identified in the level of recruitment of total RNA polymerase II in V-K562, B-K562 and G-K562 cells at three of the five examined target gene promoters (ETS-1, REN, JUNB) (Figure 3.12A). At the VDR promoter, significantly greater recruitment of RNA polymerase II was identified only in the G-K562 with respect to the V-K562 cells. Only at the AREG promoter was the

recruitment of RNA polymerase II significantly reduced in the B-K562 cell line compared to V-K562. These results suggested instead that for most target genes BASP1 has no effect on the overall recruitment of RNA polymerase II.

Following this finding, the phosphorylation status of RNA polymerase II at serine 5 was also examined via ChIP. Serine 5 within the C terminal domain of the large subunit of RNA polymerase II is phosphorylated by the CDK7 kinase subunit of TFIIH [270]. This phosphorylation event transforms RNA polymerase II from its pre-initiation state to a transcription initiating state where it is released from the promoter and begins to transcribe approximately 30bp of DNA to RNA [271]. Further phosphorylation of RNA polymerase II serine 2 by the Ctk1 subunit of the CTDK-1 complex leads to transcription elongation [272]. As RNA polymerase II recruitment to the promoter is unchanged by the presence of BASP1, it was hypothesised that perhaps the initiation of transcription via RNA polymerase II serine 5 phosphorylation is perturbed by the BASP1 repression complex. Indeed, at multiple target gene promoters (AREG, REN and ETS-1) phosphorylation of RNA polymerase II at serine 5 was reduced specifically in the B-K562 cells, with no difference seen between G-K562 and V-K562 cells. At two promoters this trend was not observed, there was no significant changes in RNA polymerase II serine 5 phosphorylation at the JUNB promoter and at the VDR promoter RNA polymerase II serine 5 phosphorylation was significantly increased only in the B-K562 cells compared to V-K562 cells.

Next, having seen that at the majority of target gene promoters there was significantly less phosphorylation of RNA polymerase II serine 5 the recruitment of CDK7, the kinase subunit of TFIIH responsible for RNA polymerase II phosphorylation, was examined. In line with the RNA polymerase II serine 5 phosphorylation data, recruitment of CDK7 was significantly reduced specifically in B-K562 cells at the AREG, ETS-1 and REN promoters. No significant change was observed at the VDR or JUNB promoters (Figure 3.12C).

Figure 3.11. BASP1 Recruits EZH2 to the Promoters of WT1 Target Genes. A, The presence of EZH2 at the promoters of AREG, ETS-1, REN, VDR and JUNB was examined using chromatin immunoprecipitation in V-K562, B-K562 and G-K562 cells. Error bars representative of the standard deviation of the mean, n=10. *p<0.05 by Student's t test comparing B-K562 or G-K562 with V-K562. **B,** Nuclear extracts of V-K562 (V), B-K562 (B) and G-K562 (G) were immunoprecipitated with BASP1 antibodies, western blotted and probed for EZH2**.**

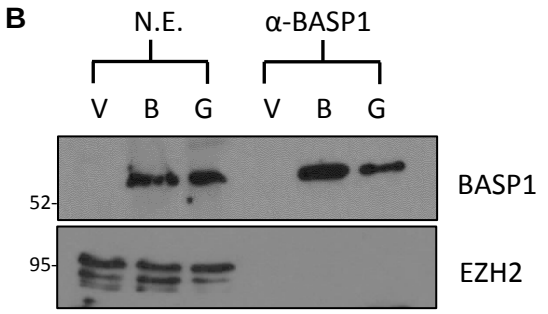

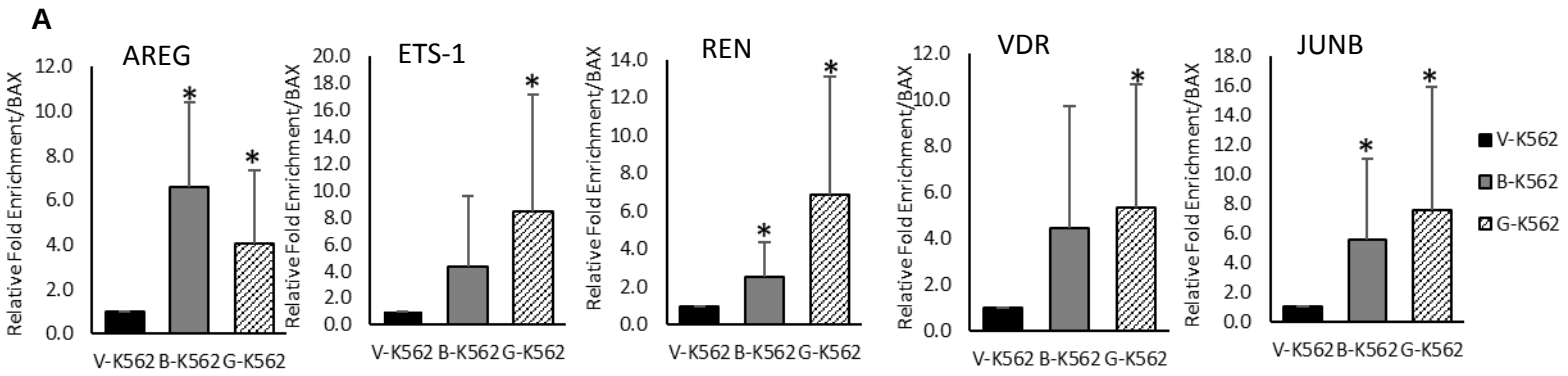

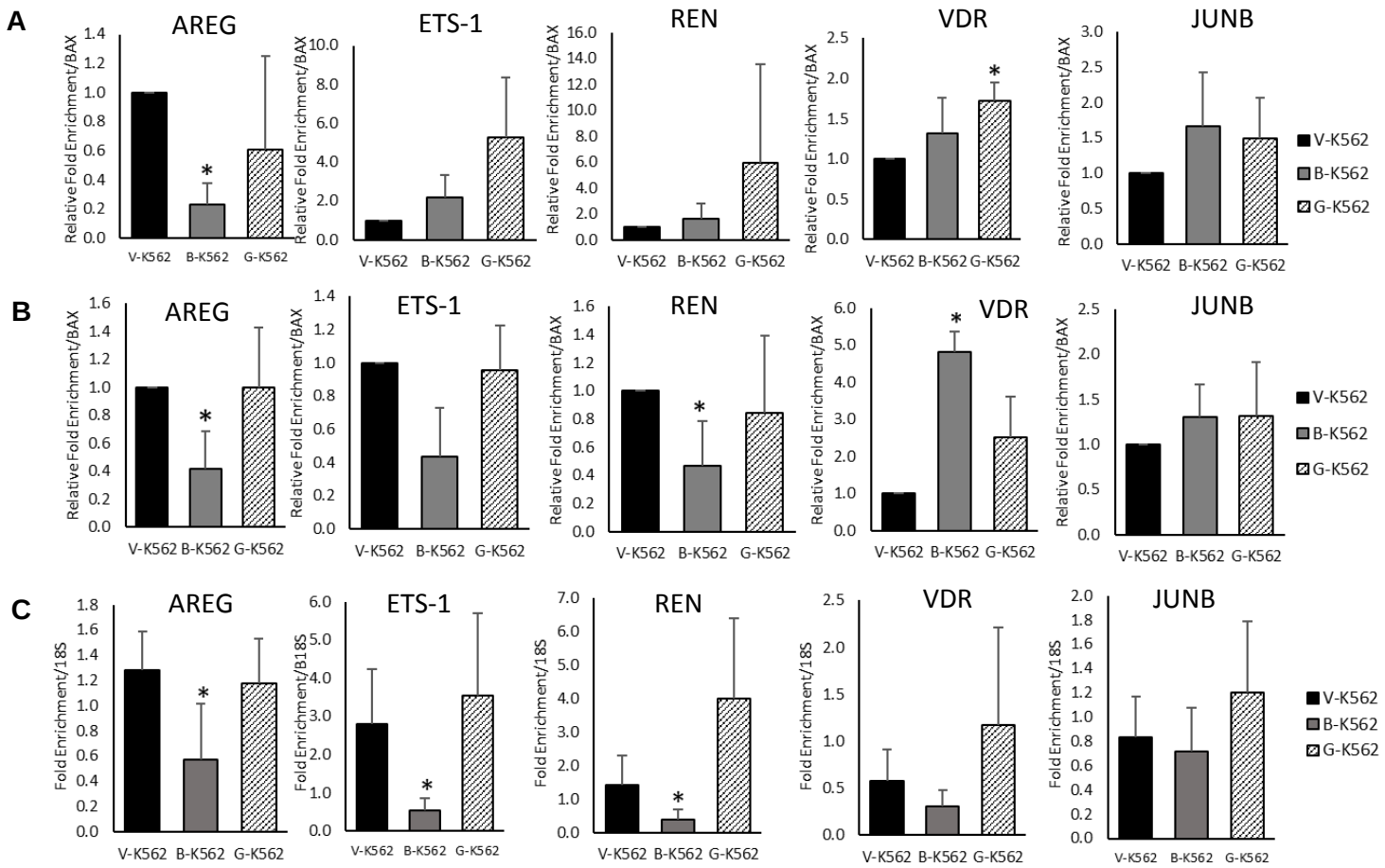

Figure 3.12. BASP1 Reduces RNA Pol II S5 Phosphorylation and CDK7 Recruitment to WT1 Target Gene Promoters. The presence of total RNA polymerase II (**A**) phospho S5 RNA polymerase II (**B**) and CDK7 (**C**) at the promoters of AREG, ETS-1, REN, VDR and JUNB was examined using chromatin immunoprecipitation in V-K562, B-K562 and G-K562 cells. Error bars representative of the standard deviation of the mean, A) n=5, B) n=5, C) n=6. *p<0.05 by Student's t test comparing B-K562 or G-K562 with control line V-K562.

3.11 Discussion of Results Chapter 1

3.11.1 Validation of Cell Lines

The work presented at the beginning of this chapter showed the generation of stable K562 cell lines for use throughout this investigation. This was followed by gene expression analysis to demonstrate myristoyl-BASP1 mediated repression of WT1 target genes in these lines, and PMA treatment to demonstrate BASP1 driven differentiation towards a neuron-like lineage. Following previous reported effects of BASP1 on the differentiation and growth of K562 cells, soft agar assays were conducted to assess the effect of BASP1 on tumourigenicity [2]. Cells expressing wtBASP1 showed both reduced colony formation and limited colony growth compared to control K562 cells, but it was shown here for the first time that expression of G2A-BASP1 results in an intermediate cellular phenotype of K562 cells grown in 3D agar. G-K562 cells had a reduced capacity to form colonies but significantly greater colony growth compared to B-K562 cells. This suggests a myristoyl-independent function for BASP1 in inhibiting colony formation and a myristoyl-dependent role for BASP1 in inhibiting colony growth. The necessity of myristoylation for BASP1 function in transcription control has only previously been studied by our group and this forms our first evidence of a myristoyl-independent function of BASP1 in reducing colony formation.

3.11.2 BASP1 Regulates Active and Repressive Chromatin Modifications at WT1 Target Genes

Further work presented in this chapter details the careful optimisation of the ChIP method. The lab has consistently found that K562 cells need particular finetuning of the crosslinking and sonication steps so optimisation was focused in these areas. The final method was used to explore the mechanisms of BASP1 mediated transcriptional repression at WT1 target genes. Together, the ChIP data suggest the BASP1 complex likely mediates gene repression via different molecular mechanisms at different genes. As hypothesised, BASP1 mediates a reduction in multiple active chromatin marks (Figure 3.9). In addition to the previously reported removal of H3K9Ac, BASP1 also decreased H3K4me^3 at all target gene promoters and H3K36me^3 at the majority of target genes in a myristoyl-dependent manner. These findings demonstrate that BASP1 modulates the chromatin environment by affecting multiple modifications. This activity is largely myristoyl-dependent and

therefore implicates PIP_2 as an important regulator of the chromatin environment at BASP1 regulated genes.

Additionally, in agreement with previous work and our hypothesis, the BASP1 repression complex mediates an increase in repressive H3K27me^3 marks (Figure 3.10) [69]. It has been shown here for the first time that repressive H3K9me^3 marks are also increased at many wtBASP1 and G2A-BASP1 bound target gene promoters (Figure 3.10). G2A-BASP1 doesn't recruit HDAC1 to remove acetyl groups from H3K9 therefore it must be assumed from this data that H3K9me^3 marks accumulate at non-acetylated H3K9 residues as these modifications cannot both be present on the same histone residue. This work implicates BASP1 as a regulator of chromatin dynamics that induces compaction of chromatin via the removal of activation marks and addition of repressive marks (refer to Figure 3.13 for proposed model of BASP1 activity). Here BASP1's role in placing repressive chromatin marks was shown to be independent of myristoylation, and therefore independent of PIP_2 interaction. This work shows for the first time that BASP1 has additional myristoyl-independent repression inducing function. This provides new insight into BASP1 mediated transcriptional repression as a multi-step process with both myristoyl-dependent and myristoyl-independent steps. This further implicates PIP_2 as an important cofactor specifically for the removal of activation marks.

Later work showed that the methyltransferase EZH2 is recruited to BASP1 bound promoters and is therefore a candidate for executing the methylation of both H3K27 and H3K9. EZH2 is the enzymatic component of the Polycomb Repressive Complex 2 (PRC2), a complex associated with inducing silencing of genomic regions primarily through methylation of H3K27, but also of H3K9 [262-264]. EZH2 has been identified via mass-spec within BASP1 immunoprecipitates, which further implies a BASP1-EZH2 interaction (refer to Figure 4.2). Moreover, EZH2 is known to be critical for WT1-dependent regulation of the Wnt4 gene during nephrogenesis [70]. Recruitment of EZH2 and subsequent upregulation of repressive chromatin marks is therefore a potential mechanism through which wtBASP1 may exert its down-regulation of WT1 target genes. Recruitment of EZH2 by G2A-BASP1 and subsequent placement of repressive chromatin marks does not offer explanation as to the mechanism by which these sites remain actively transcribed.

The occurrence of only the myristoyl-BASP1 independent changes to the chromatin environment around G2A-BASP1 bound sites results in promoters exhibiting both active and repressive marks. A number of bivalent sequences have been described

by others, where both activating H3K4me^3 and repressive H3K27me^3 are present [273]. Bivalent domains are usually associated with embryonic stem cells and commonly occur at transcription start sites of genes encoding transcription factors and developmentally significant genes that establish cell identity. It is thought that bivalent modification patterns pause genes in a bipotential state, and an active or a repressive state is selected as cells differentiate depending on cell lineage. WT1 is an important regulator of development in multiple tissues. Its function is highly context specific, acting to both activate and repress transcription of its targets depending on the binding of particular cofactors [274, 275]. A recent report demonstrated that BASP1 mediated regulation of WT1 blocks pluripotency and is a major driver of differentiation [90]. Thus, the WT1/BASP1 complex plays a major role in controlling cell fate and it is perhaps unsurprising that WT1/BASP1 regulated sites are among those known to be bivalent. Perhaps a lipid regulated switch could control the fate of bivalent promoters, whereby the WT1/BASP1 complex is paused on bivalent promoters and upon lipid binding the displacement of activation marks is triggered, prompting a more repressive chromatin environment.

H3K9Ac and other active histone marks including H3K14Ac have also previously been shown to cluster at sites displaying H3K27me^3 marks [276]. It is generally accepted that the biological effect of histone marks is additive rather than defined, thus it is often the abundance of a range of active and repressive marks that tips the balance towards active transcription or repression. Bivalent promoters are usually associated with low levels of transcription; however, our work demonstrates that bivalent G2A-BASP1 bound promoters do not undergo gene repression [273, 277]. Other exceptions have previously been identified where loci in mouse embryonic stem cells containing H3K4me^3, H3K9Ac and H3K27me^3 do undergo active transcription [276]. Equally, it appears that a general phenomenon of cancer cells is the upregulation of bivalent genes [273, 277]. Therefore, in the context of a K562 cell, the addition of H3K27me^3 and H3K9me^3 marks by BASP1/EZH2 without removal of any active marks may not be sufficient to ensure gene repression. Additionally, many bivalent PRC2 targeted loci marked with both H3K4me^3 and H3K27me^3 have now been identified [278, 279]. This suggests PRC2 could indeed be recruited to WT1/BASP1 target genes despite the presence of active marks.

3.11.3 BASP1 Regulates Transcription Initiation

The effects of BASP1 binding on transcriptional events downstream of chromatin changes were also examined in this chapter for the first time. It was discovered that

BASP1 reduces the initiation of transcription through different means at different promoters. BASP1 can reduce total RNA polymerase II binding (AREG) or inhibit CDK7 recruitment thereby limiting RNA polymerase II S5 phosphorylation (ETS-1, REN) (Figure 3.12). These data provide the first evidence of BASP1-mediated effects on transcription downstream of RNA polymerase II recruitment. The data also provide the first evidence that myristoylation of BASP1 is important for this function. The myristoyl-dependent nature of this activity implicates PIP_2 as an important binding partner in BASP1 mediated regulation of transcription initiation. Examples of PIP_2 involvement in RNA polymerase I driven transcription are already known; PIP_2 forms a complex with the RNA polymerase I transcription factor UBF, interacts with a subset of the Pol I transcription machinery to promote transcription, and plays a structural role as an anchor for the RNA polymerase I pre-initiation complex [151, 280]. PIP_2 has also been shown to aid epigenetic repression of rRNA gene transcription [150]. Recent evidence also proposes the formation of PIP_2 and RNA rich nuclear lipid islets is important to provide a structural platform for RNA polymerase II driven transcription [281]. Data here therefore contributes to emerging evidence that PIP_2 is an important player in RNA polymerase II function.

3.11.4 Summary of Results Chapter 1

A summary of the data presented in this chapter is shown in Figure 3.13 in the form of a schematic illustrating chromatin modifications and proteins present at unbound, wtBASP1 bound and G2A-BASP1 bound WT1 target gene promoters. A WT1 target gene unbound by BASP1 is shown to have H3K4me^3, H3K9Ac and H3K36me^3 active chromatin marks, is bound by WT1, and bound by RNA polymerase II which is subsequently phosphorylated by CDK7 to initiate transcription. A WT1 target gene bound by wtBASP1 is instead shown to have H3K27me^3 and H3K9me^3 repressive chromatin marks, is bound by WT1 and the BASP1 repression complex (including established components such as prohibitin and BRG1). H3K4me^3 and H3K36me^3 marks are shown as being removed by KDM2B. Removal of these marks by KDM2B has not been tested in this study, thus at this stage it is only hypothesised as having a role in this process. This prediction is based upon the presence of KDM2B in BASP1 immunoprecipitates (discussed in results chapters 2 and 3). The wtBASP1 bound gene promoter is either not bound by RNA polymerase II, or the bound RNA polymerase II is yet to be phosphorylated by CDK7 and thus transcription initiation is prevented. A WT1 target gene promoter bound by WT1 and G2A-BASP1 is shown to have both active and repressive chromatin marks present. Binding of some repression complex components, such as HDAC1, is known to be PIP_2-dependent and therefore these factors are not present. G2A-BASP1 bound sites recruit RNA polymerase II which can subsequently be phosphorylated by CDK7 and thus transcription initiated. Ultimately, despite the presence of repressive histone marks, G2A-BASP1 bound sites retain activation marks and retain RNA polymerase II binding and S5 phosphorylation and therefore the initiation of transcription cannot be prevented. This highlights the necessity for both the removal of activation marks and the increase in repressive marks in order to fully induce a repressive chromatin environment and effectively prevent gene transcription.

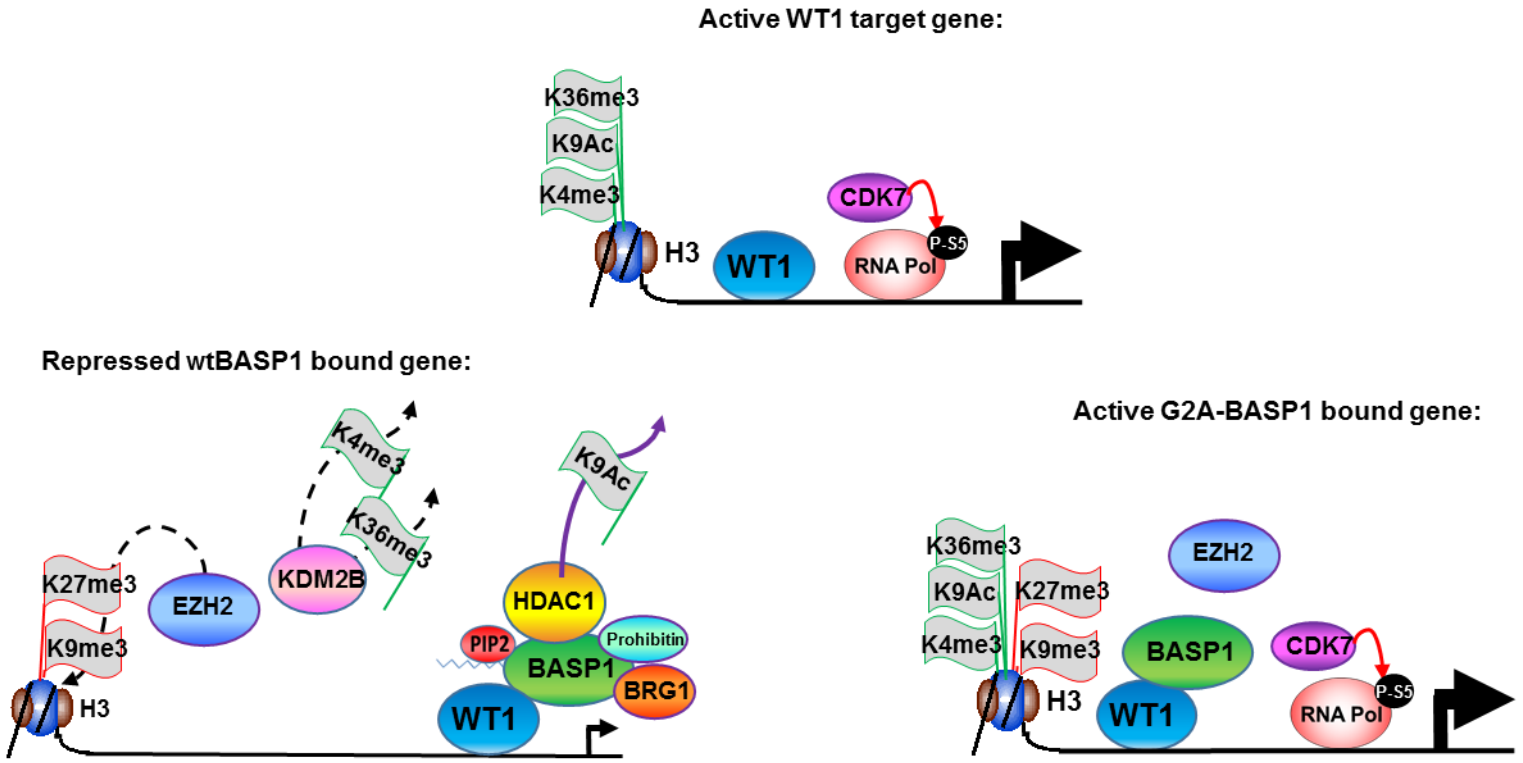

Figure 3.13. Chapter 1 Summary: Mechanism of BASP1-PIP$_2$ Mediated Gene Repression.

Representation of WT1 target gene promoters. Top promoter; bound by WT1 only. Bottom left promoter; bound by WT1 and wtBASP1. Bottom right promoter bound by WT1 and G2A-BASP1. Known present active chromatin marks shown in green flags (H3K36me^3, H3K9Ac, H3K4me^3), known present repressive chromatin marks shown in red flags (H3K27me^3, H3K9me^3). Red arrow indicates phosphorylation of serine 5 of RNA polymerase II by CDK7. Large black arrow represents active transcription. Smaller black arrow represents reduced levels of transcription. Dashed arrows represent hypothesised activity of EZH2 and KDM2B in increasing H3K27me^3 and H3K9me^3 marks and removing H3K36me^3 and H3K4me^3 marks. Purple arrow represents previously reported removal of H3K9Ac by HDAC1. Some known components of the BASP1-PIP$_2$ repression complex are shown (HDAC1, prohibitin, BRG1).

4 Results Chapter 2: Localisation of the WT1/BASP1/PIP_2 Repression Complex

4.1 Introduction

It has been known for several decades that lipids and the enzymes that regulate lipid metabolism are present in the nucleus. Nuclear lipids have been shown to associate with protein complexes involved in a diverse range of nuclear processes including RNA processing, chromatin remodelling and gene transcription, but the mechanisms through which lipids are involved in such processes remain unclear [101, 107, 113, 117, 118]. Very little is known about the role of lipids in gene regulation and how they affect transcriptional and cellular responses. Nuclear lipids are present within the nuclear membrane where their hydrophobic tail is buried within the bilayer structure, but lipids are also extensively present within the nuclear space [101, 113]. How hydrophobic lipid tails can exist in the nucleoplasm remains poorly understood. It has been hypothesised that they could be housed within nuclear speckles such as PML bodies, although the structure of such speckles, the protein complexes present within them and how they accommodate hydrophobic lipid tails is not yet known [127].

BASP1 interacts directly with phospholipids and cholesterol through the myristoyl motif and a cholesterol recognition consensus sequence (CRAC domain) [80, 82, 83, 282]. As BASP1 is the only myristoylated protein with a confirmed role for the myristoyl motif in transcription regulation, it provides a rare opportunity to examine the role of nuclear lipids in gene regulation. Although it is known that N-terminal myristoylation of BASP1 enables it to associate with membranes it is not yet known whether BASP1 mediated repression occurs at the nuclear membrane or within the nucleoplasm [3]. The subnuclear localisation of genes and their recruitment to the nuclear periphery and incorporation into heterochromatin is now known to play a vital role in gene expression [174-177]. Thus, here it was examined whether the myristoyl-dependent nature of BASP1 gene repression activity could be due to a necessity for interaction with the nuclear membrane and the repressive environment of the nuclear periphery.

In addition to potential roles at the nuclear membrane BASP1 is also found localised throughout the cytoplasm and nucleus [3, 282]. Here it was hypothesised that non-membrane nuclear lipids could be stabilised within the nucleoplasm by lipidated proteins such as BASP1. The study of BASP1 in this chapter provides insight into the nuclear localisation of lipids and the importance of lipid interaction for BASP1

mediated gene regulation. Experiments presented in this chapter aimed to explore the localisation of nuclear myristoylated BASP1. This includes the use of biochemical and immunofluorescence techniques examining BASP1 and lipids throughout the nucleus and the nuclear membrane. Association of the WT1/BASP1/PIP_2 repression complex with protein components of the nuclear periphery was examined through imaging, interaction studies and ChIP. These experiments were completed with the aim of understanding if interaction with inner nuclear membrane (INM) components is important for WT1/BASP1/PIP_2 driven gene repression.

4.2 Subnuclear Fractionation of V-K562, B-K562 and G-K562 Nuclei

First, to explore the importance of BASP1 myristoylation for the subnuclear localisation of the WT1/BASP1/PIP_2 repression complex biochemical fractionation of nuclei isolated from V-K562, B-K562 and G-K562 cells was performed. Nuclei were purified using the Nuclei EZ Prep Kit (Sigma) which involved two cycles of incubating whole cells in lysis buffer, on ice, and collecting nuclei via centrifugation. Initially, validation of this nuclei purification method was conducted (Figure 4.1A). Successful isolation of pure nuclei was confirmed via western blotting of whole cells and the purified nuclei, followed by probing with antibodies against a marker of the golgi apparatus, TGN46. Control protein TGN46 was detected in whole cells of V-K562, B-K562 and G-K562, but not in purified nuclei. BASP1 expression was confirmed in the whole cells and nuclei from B-K562 and G-K562. Secondly, purified nuclei were then subjected to biochemical fractionation. The fractionation procedure results in the isolation of the soluble, chromatin and matrix fractions. The soluble fraction consists of all soluble nuclear proteins, the chromatin fraction consists of chromatin itself plus chromatin bound proteins, and the matrix fraction consists of nuclear structures including the nuclear membrane, nucleolus, pml bodies, cajal bodies as well as the nuclear actin-matrix network itself. Upon isolation of the three nuclear fractions samples were western blotted and probed for the presence of repression complex components (BASP1, WT1, HDAC1, prohibitin) as well as characterised nuclear membrane components (emerin, lamin A/C), negative control TGN46 and positive control β-actin (Figure 4.1B).

Negative control TGN46 was not detected in any of the nuclear fractions, whilst positive control β-actin was detected throughout. WT1 was found most abundantly in the matrix fraction; a finding consistent with previous experiments from our laboratory. The presence of WT1 in a range of nuclear bodies associated with the

nuclear matrix, including paraspeckles and nucleoli where it is involved in RNA processing and splicing, has been well documented [283-287]. A low level of WT1 protein was also detected in the soluble and chromatin fractions of V-K562 nuclei, although WT1 could not be detected in these fractions for B-K562 or G-K562 nuclei. This could be due to the lower expression level of WT1 in these cell lines and/or poor antibody detection. HDAC1 was evenly distributed through all nuclear fractions and Prohibitin was detected in the soluble and chromatin fractions for all cell lines [288, 289]. Predictably for a nuclear membrane protein, Lamin A/C was exclusively isolated from the nuclear matrix fraction in all cell lines. Emerin was detected predominantly in the nuclear matrix, although emerin protein was also present in both the soluble and chromatin fractions. This result reflects the evidence that emerin is predominantly found in the inner nuclear membrane and supports the body of evidence for emerin's role in chromatin organisation and gene regulation. There is very little evidence of soluble emerin being present within the cytoplasm or nucleus (only reported for mutant derivatives), thus it is most likely that emerin detected here in the soluble fraction is an artificial product of the fractionation procedure [290]. Also notable is the doublet of emerin apparent within the nuclear matrix. This extra protein band was not pursued here but approximately 40 different residues of the emerin protein have been reported to be phosphorylated, many of which occur in a cell cycle dependent manner and regulate emerin binding partners [237, 291]. The doublet of emerin seen here is speculated to be caused by alternatively phosphorylated forms in the matrix.

The most interesting result from the subnuclear fractionation experiment is the discovery that wtBASP1 and G2A-BASP1 distribute differently through the nuclear fractions (Figure 4.1B). Both forms of BASP1 protein localise to the soluble and chromatin fractions, however only wtBASP1 localised to the nuclear matrix fraction. Thus, myristoylation appears essential for BASP1 localisation to the nuclear matrix. Myristoylation also appears to affect the level of BASP1 localised to chromatin, as G2A-BASP1 is reduced by approximately 66% in comparison to wtBASP1 in this fraction. This data suggests that myristoylation is required for BASP1 to localise to the matrix, and subsequently that PIP_2 interaction could be critical for the association of BASP1 with the nuclear matrix. It suggests that the interaction with PIP_2 is important not only for the WT1/BASP1 repression complex to interact with components such as HDAC1, but also to localise the complex to subnuclear regions.

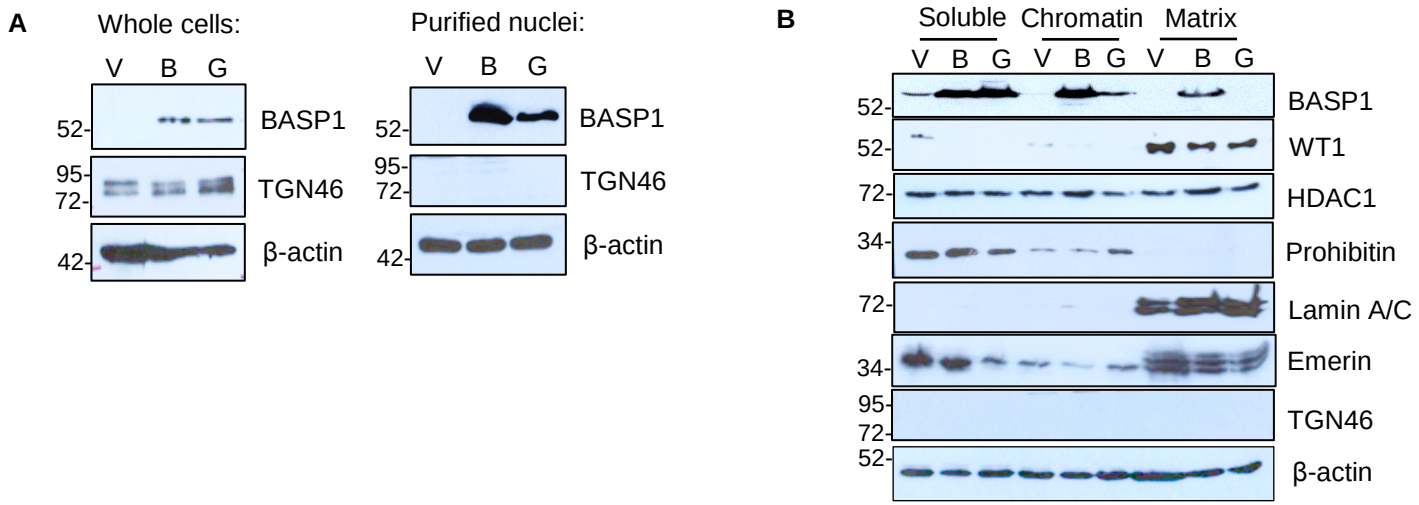

Figure 4.1. Myristoylation is Required for BASP1 to Localise into the Matrix. A, Whole cells and nuclei purified from V-K562 (V), B-K562 (B) and G-K562 (G) cell lines were western blotted and probed with antibodies against BASP1, TGN46 and β-actin. **B**, Purified nuclei from V-K562, B-K562 and G-K562 cells were biochemically fractionated into soluble, chromatin and matrix subnuclear fractions and western blotted for BASP1 repression complex components, nuclear membrane protein emerin, nuclear matrix protein lamin A/C and further negative and positive controls, TGN46 and β-actin, respectively. Molecular weight in kDa shown to left of each blot.

4.3 Investigation of BASP1 Interactions with Nuclear Membrane Proteins

4.3.1 Mining of BASP1 Interactome Proteomic Data Sets

Previous work in our laboratory included the generation of several proteomic data sets of BASP1 interactors. These data sets included BASP1 interactome studies achieved through BASP1 immunoprecipitation from V-K562, B-K562, and G-K562 followed by LC-MS mass spectrometry of immunoprecipitates. In this investigation, further tandem mass tag (TMT) mass spectrometry was completed in triplicate on BASP1 immunoprecipitates from V-K562, B-K562 and G-K562 cells (see Table 1, appendix). Together, these interaction studies reliably and repeatedly predicted a number of potential BASP1 interactors. Some interactors that are of particular interest to our laboratory have been repeatedly identified across proteomic datasets, including within the TMT mass spectrometry dataset gained in this study. Such repeatedly identified proteins are summarised in Figure 4.2, divided into four main categories; chromatin remodelling proteins, basal transcription proteins, inner nuclear membrane (INM) proteins and nuclear actin complexes. Some of these BASP1 interactors identified by the proteomics have previously been validated (HDAC1, BRG1, Prohibitin) and are known to bind BASP1 in a myristoyl dependent manner [3, 96]. Many other interactions have been directly tested and confirmed via western blotting [89]. The remaining proteins listed require direct testing to validate a specific interaction with BASP1, and whether they could be myristoyl-dependent or independent interactions. These proteomic data sets have provided a list of candidate interactors that will be explored during further investigation into the mechanisms of BASP1-dependent transcriptional regulation.

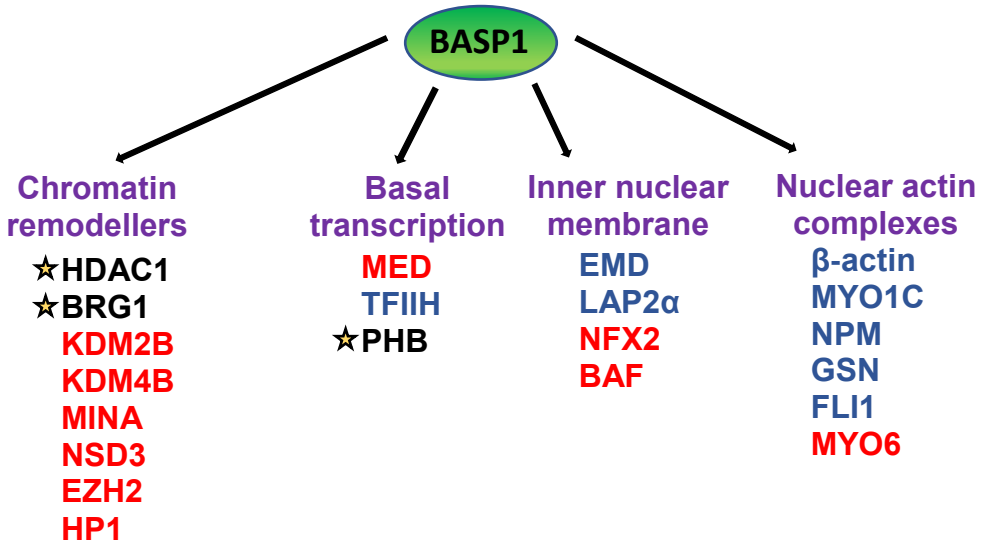

Figure 4.2. BASP1 Interacting Proteins. Using a combination of direct testing and comparative TMT/Orbitrap Mass Spectrometry several BASP1 binding proteins have been repeatedly identified. Categorized interactors are shown (under purple headings). Through analysis of BASP1 mutant derivatives defective in myristoylation and PIP_2-binding (G2A-BASP1) the dependency of this protein interaction on the presence of PIP_2 has been predicted (yellow star indicates known PIP_2 dependent BASP1 interactor). BASP1 interactions with HDAC1, BRG1, PHB1 are published (black text). Interactions with TFIIH, EMD, LAP2, actin, MYO1C, NPM, GSN, FLI1 have previously been confirmed by western blotting with specific antibodies (blue text). Remaining proteins are predicted interactors based on at least two TMT/Mass spec repeats (red text).

4.3.2 Immunoprecipitation of BASP1 and Nuclear Membrane Proteins

The proteomic datasets summarised above indicate that BASP1 may interact with a number of nuclear membrane and nuclear lamina proteins including emerin, lap2α, nesprin, HP1 and barrier-to-autointegration (BAF). Direct testing of an interaction between BASP1 and candidate interactors was conducted in order to validate the interactions and assess their dependence on BASP1 myristoylation. This was achieved via immunoprecipitation of nuclear extracts prepared from V-K562, B-K562 and G-K562 cells with BASP1 antibody followed by western blotting and probing for nuclear membrane proteins. BASP1 protein was successfully harvested using the immunoprecipitation method in both B-K562 and G-K562 nuclei (Figure 4.3Ai). Emerin protein was present in wtBASP1 immunoprecipitates but was absent from G2A-BASP1 immunoprecipitates. Additionally, emerin protein was successfully immunoprecipitated from V-K562, B-K562 and G-K562 nuclear extracts, but BASP1 was present only in B-K562 immunoprecipitates (Figure 3.3Aii). This data provides evidence of a myristoyl dependent BASP1 and emerin interaction.

It is not possible to determine the nuclear localisation of the BASP1-emerin interaction from this immunoprecipitation data, thus it cannot be concluded that the interaction occurs at the nuclear membrane, or within the nucleoplasm. However, validation of the emerin interaction does serve to support the hypothesis that myristoylation of BASP1 could be a prerequisite for localising the BASP1 repression complex to the nuclear periphery.

BASP1 immunoprecipitates from V-K562, B-K562 and G-K562 cell nuclear extracts were also tested for the presence of other nuclear membrane and nuclear lamina proteins (Figure 4.3 B). Whilst Lamin A/C, BAF and Lap2α could all be detected in K562 nuclear extracts, none could be reliably identified in BASP1 immunoprecipitates from any of the K562 cell derivatives. A weak protein band in B-K562 BASP1 immunoprecipitates western blotted and probed for BAF was detected, however the molecular weight of this band (approximately 25kDa) is significantly larger than the reported molecular weight of the BAF protein (10kDa) and therefore was not assumed to be specific. Similarly, weak bands of protein around 45kDa were irregularly detected in V-K562, B-K562 and G-K562 BASP1 immunoprecipitates western blotted and probed for lap2α but were not considered to be specific. Positive control β-actin however, an established BASP1 interactor, was detected in all nuclear extracts and was present in B-K562 BASP1 immunoprecipitates. We have previously shown that BASP1 interacts with multiple

components of the nuclear actin network including β-actin, FLI1, NPM, MYO1C [89]. Here, this result confirms our previous finding that β-actin interacts with BASP1 and indicates for the first time that the BASP1-β-actin interaction is dependent upon myristoylation. It suggests that the interaction of BASP1 and the other established nuclear actin complex components could also be myristoyl dependent, although direct testing is needed to confirm this. If so, the myristoyl-dependence of these interactions could also explain the loss of G2A-BASP1 protein from the nuclear matrix.

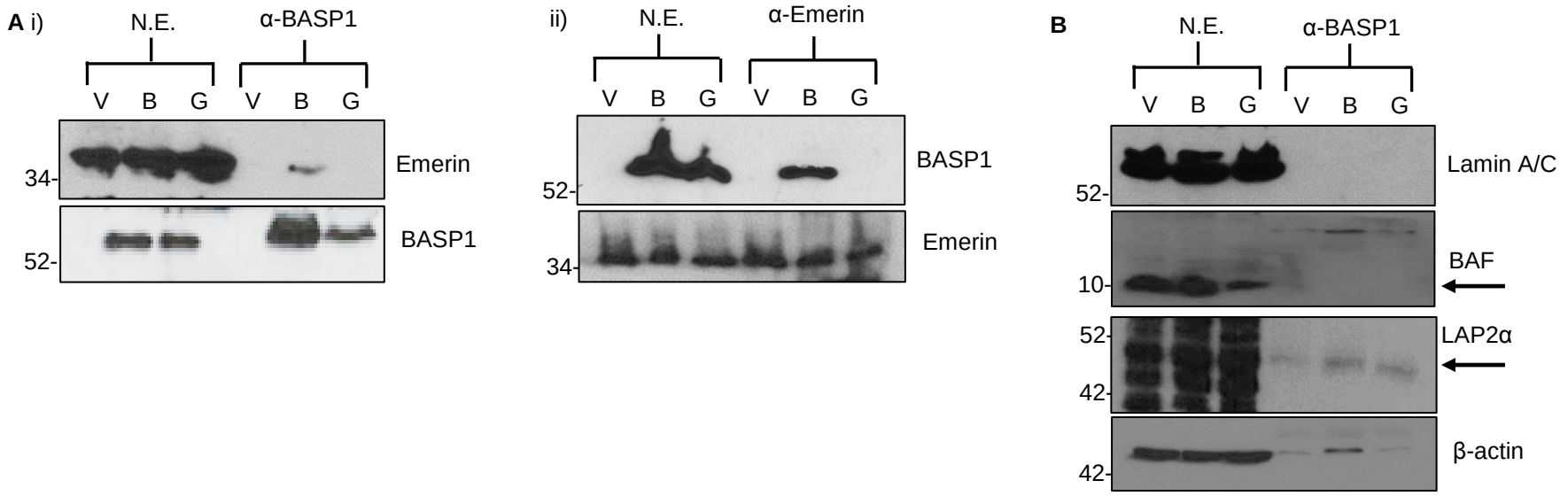

Figure 4.3. Immunoprecipitation of BASP1 and Nuclear Membrane Proteins. A, (i) Nuclear extracts from V-K562 (V), B-K562 (B) and G-K562 (G) nuclei were subjected to immunoprecipitation with BASP1 antibodies, and western blotted for BASP1 and emerin. **A,** (ii) Nuclear extracts from V-K562, B-K562 and G-K562 nuclei were subjected to immunoprecipitation with emerin antibodies, and western blotted for BASP1 and emerin. **B**, Nuclear extracts from V-K562, B-K562 and G-K562 nuclei were subjected to immunoprecipitation with BASP1 antibodies and western blotted for other nuclear membrane proteins (Lamin A/C, BAF and Lap2α) as well as previously reported interactors of the nuclear actin complex (β-actin). Black arrows point to predicted specific protein bands for BAF and Lap2α.

4.4 Confocal Microscopy of BASP1 in the K562 Cell Derivatives

Having determined from the biochemical analysis that BASP1 myristoylation is essential for localisation to the nuclear matrix fraction and interaction with emerin and β-actin, visual methods of examining BASP1 localisation were explored. The first approach adopted was confocal microscopy of B-K562 and G-K562 nuclei.

4.4.1 Immunofluorescence of BASP1 and Repression Complex Components

Initially validation of the immunofluorescence protocol was conducted to ensure that images obtained reliably represented BASP1 nuclear localisation. Whole B-K562 cells or purified nuclei were subjected to immunostaining in suspension with antibodies against BASP1 and TGN46, plus DAPI staining (Figure 4.4A). Cells or nuclei were then centrifuged into a pellet, resuspended in a minimum volume of mounting media (DABCO, Sigma), pipetted onto slides and mounted with coverslips. TGN46 signal was seen in whole cells only, indicating that nuclei purification was again successful and able to produce high quality nuclei for imaging. Next, BASP1 antibody dilutions of 1:200, 1:300 and 1:500 were tested in V-K562 and B-K562 nuclei (Figure 4.4B). Concentrations of both 1:200 and 1:300 reliably gave BASP1 signal in B-K562, and not in V-K562. The weaker dilution of 1:500 gave no signal above background levels and thus it was concluded a 1:300 dilution of BASP1 antibody should be used throughout this study. Finally, a secondary antibody only control was performed to ensure the secondary antibody used for BASP1 staining (anti Rabbit-488) was specific (Figure 4.4C). No signal was detected in this secondary antibody only control in either V-K562 or B-K562 nuclei.

Having optimised the immunofluorescence protocol for confocal imaging of purified nuclei, it was then sought to image BASP1 and other repression complex components in B-K562 and G-K562 nuclei. Confocal imaging of B-K562 and G-K562 nuclei stained for BASP1, Prohibitin, PIP_2 and HDAC1 is shown in Figure 4.5. All proteins were detected within B-K562 and G-K562 nuclei. Both wtBASP1 and G2A-BASP1 appear abundantly throughout the nuclear space. The difference in BASP1 staining pattern between Figure 4.5A, and Figure 4.5B and 4.5C is the result of the use of two different BASP1 antibodies. The sheep derived BASP1 antibody utilised in Figure 4.5A has consistently shown a broader nuclear staining pattern in multiple cell types analysed in our laboratory compared to the routinely used rabbit BASP1 antibody. This difference is likely caused by recognition of different BASP1 epitopes by antibodies raised in different species. Nevertheless, both antibodies

detect BASP1 throughout the nucleoplasm and at the nuclear periphery in both B-K562 and G-K562 nuclei. Similarly to BASP1, prohibitin and HDAC1 are also highly abundant throughout the nuclei. No substantial difference in their localisation could be determined between B-K562 and G-K562 nuclei. PIP_2 was also successfully detected within the nuclei of both cell types, appearing at the nuclear periphery and within intranuclear speckles, consistent with previous reports by us and others [3, 107, 151, 292]. Whilst all proteins and PIP_2 were successfully visualised in B-K562 and G-K562 nuclei using this immunofluorescence technique, no determinable differences in their localisation between the B-K562 and G-K562 derivatives could be identified. It was concluded that due to the abundance of these proteins and PIP_2 throughout the nucleus higher resolution imaging techniques combined with colocalisation analysis must be pursued to definitively assess whether differences in localisation occur.

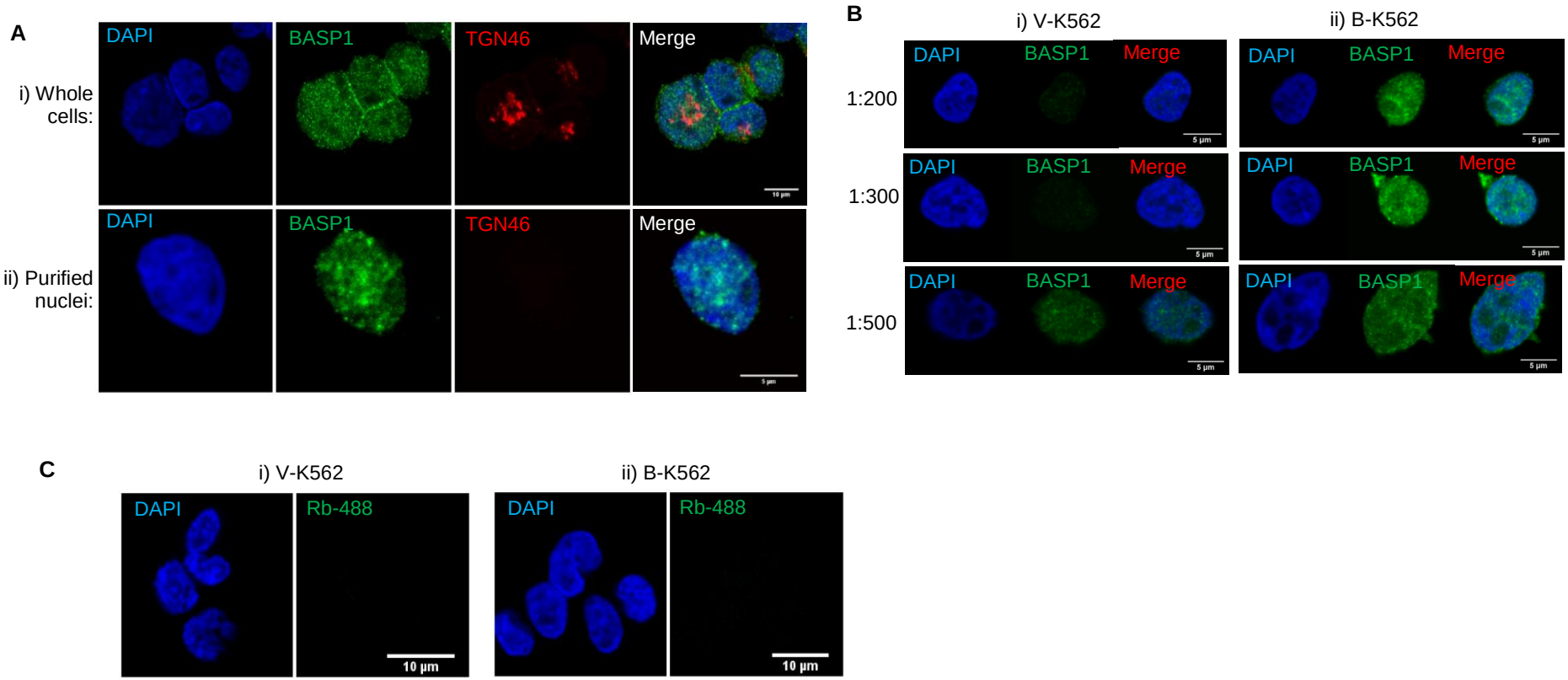

Figure 4.4. Optimisation of BASP1 Staining and Nuclei Purification Technique for Immunofluorescence. A, Confocal images of i) whole cells and ii) purified nuclei, showing validation of nuclei purification technique. B-K562 cells were immunostained for BASP1 and TGN46, plus DAPI. Scale bar 10µm in whole cells (i) and 5µm in purified nuclei (ii). **B**, Confocal images of V-K562 nuclei (i) and B-K562 nuclei (ii) immunostained with BASP1 antibody at dilutions of 1:200, 1:300 and 1:500, and stained with DAPI. Scale bar 5µm. **C**, Confocal images of V-K562 cells (i) and B-K562 cells (ii) immunostained with only Rb-488 secondary antibody at a dilution of 1:500. Scale bar 10µm.

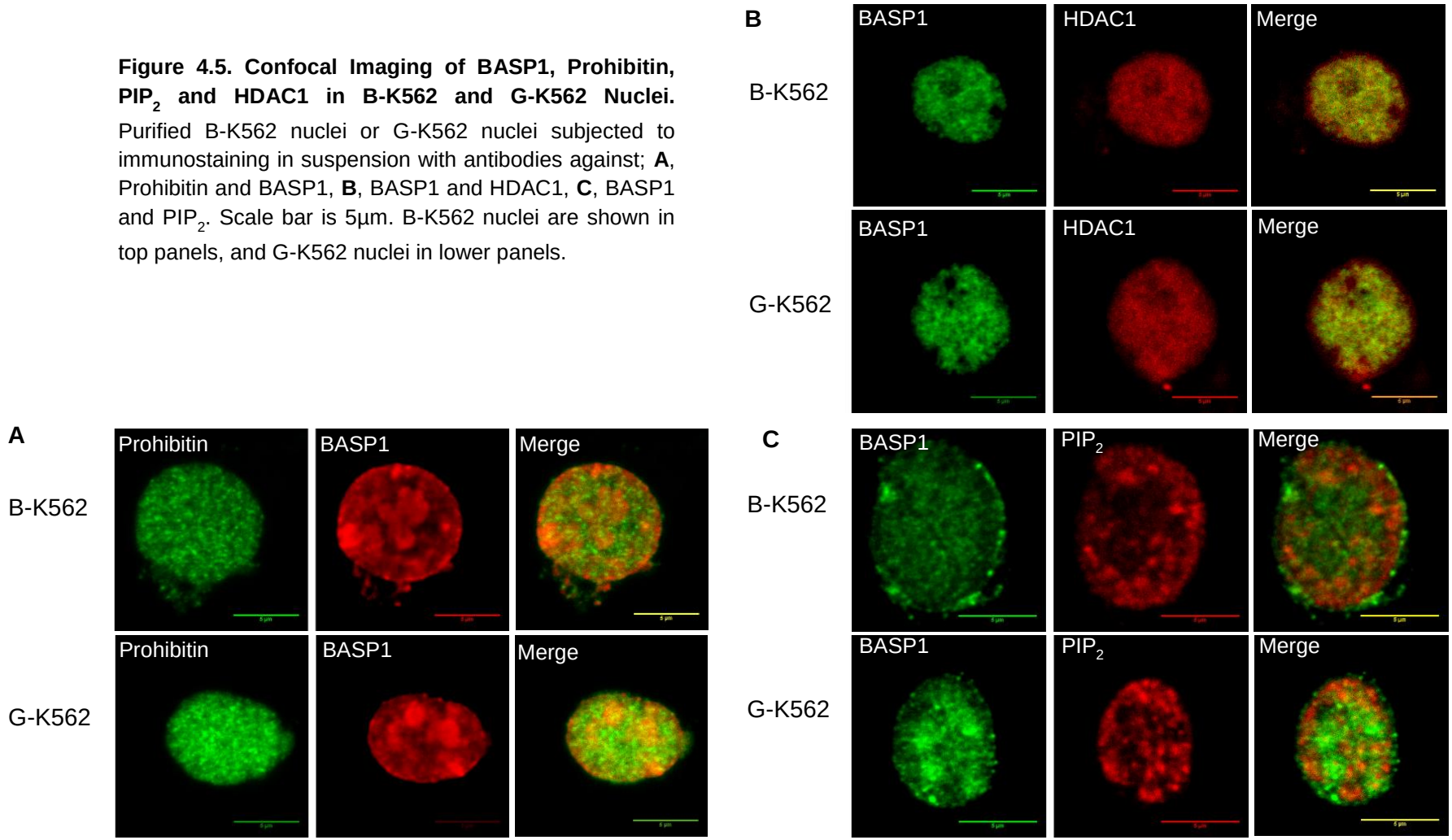

Figure 4.5. Confocal Imaging of BASP1, Prohibitin, PIP_2 and HDAC1 in B-K562 and G-K562 Nuclei. Purified B-K562 nuclei or G-K562 nuclei subjected to immunostaining in suspension with antibodies against; **A**, Prohibitin and BASP1, **B**, BASP1 and HDAC1, **C**, BASP1 and PIP_2. Scale bar is 5µm. B-K562 nuclei are shown in top panels, and G-K562 nuclei in lower panels.

4.4.2 Immunofluorescence of BASP1 and Nuclear Membrane Proteins

Simultaneously to examining the localisation of BASP1 repression complex components in B-K562 and G-K562 nuclei, it was sought to examine whether wtBASP1 and G2A-BASP1 could be visualised alongside markers of the nuclear membrane and nuclear periphery via immunofluorescence. Due to the biochemical data previously presented (Figure 4.1, Figure 4.3) it was hypothesised that wtBASP1 might be present at the inner nuclear membrane alongside emerin. Based on the immunoprecipitation results (Figure 4.3) it was also hypothesised that G2A-BASP1 would lack membrane association. To examine this, B-K562 and G-K562 nuclei were subjected to immunostaining in suspension with antibodies against BASP1, emerin and lamin A/C, as well as a DAPI stain (Figure 4.6). Points of colocalisation between BASP1 and both Lamin A/C and emerin were observed in B-K562 nuclei, but this was comparable to that observed G-K562 nuclei. As may be expected from the biochemical data, greater colocalisation was apparent between BASP1 and emerin compared to BASP1 and lamin A/C, evidenced by the greater overlap of fluorescent signal in these images. The images provide initial evidence to support the presence of both wtBASP1 and G2A-BASP1 at the nuclear periphery. This is in contrast to the biochemical data which suggested that G2A-BASP1 could no longer localise to the nuclear matrix.

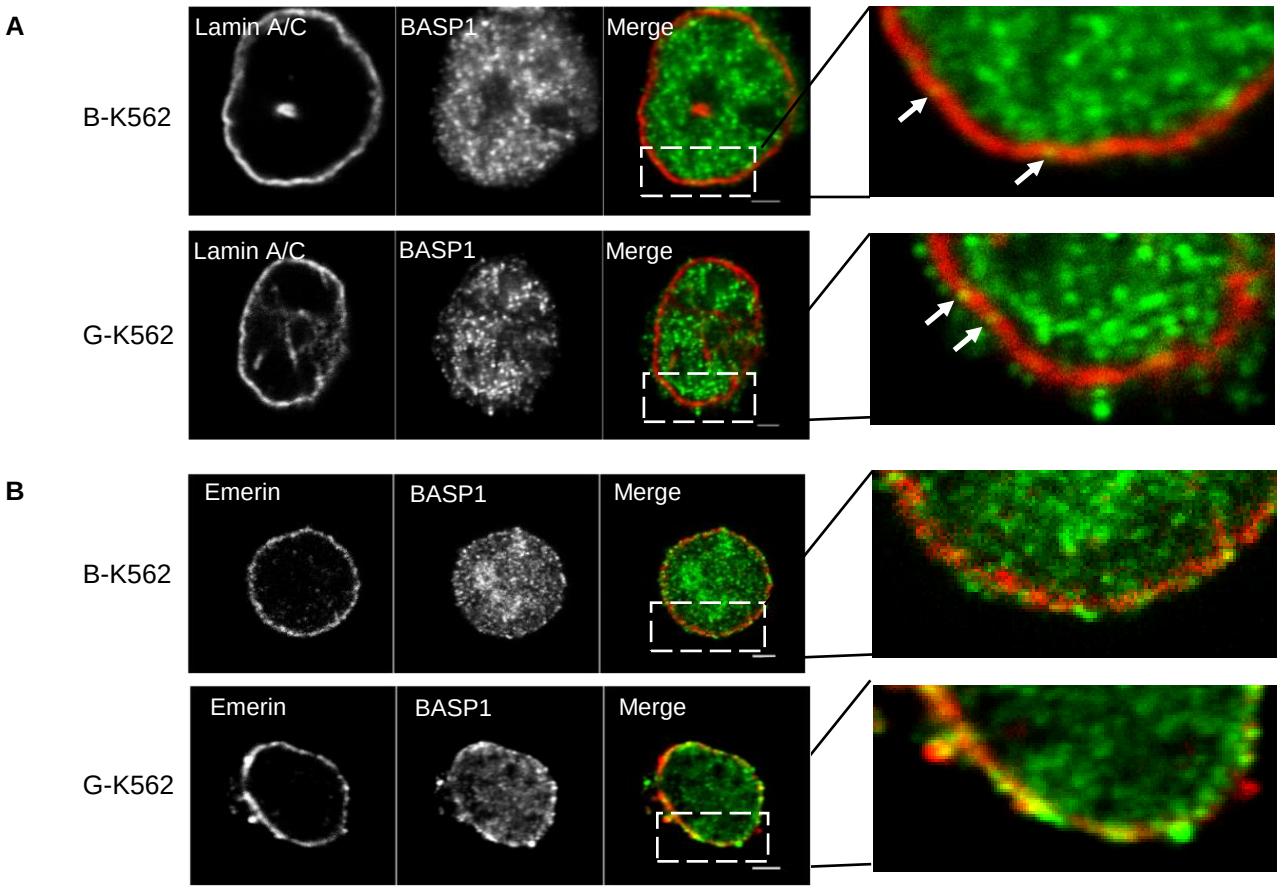

Figure 4.6. Confocal Imaging of BASP1 and Emerin or Lamin A/C in B-K562 and G-K562 Nuclei. Purified B-K562 nuclei and G-K562 nuclei were subjected to immunostaining in suspension with; **A**, BASP1 and lamin A/C antibodies, **B**, BASP1 and emerin antibodies. Scale bar 2µm. Right-hand panel shows zoom of boxed portion from merged image.

4.5 Click Chemistry Analysis of BASP1 and Alkyne-Myristic Acid

Experiments presented so far have used the G2A-BASP1 mutant to infer the importance of the myristoyl motif in BASP1 subnuclear localisation and function. There are currently no antibodies available that can detect the myristoyl motif directly, so it is not possible to employ standard immunoprecipitation or immunofluorescence techniques to detect myristoyl. As an alternative method to examine the BASP1 myristoyl motif a click chemistry technique was utilised. This technique involves incubating cells with an alkyne conjugated myristic acid, which is readily incorporated into myristoylated proteins. A cycloaddition reaction of the alkyne to an azide molecule is then performed, followed by detection of the azide molecule in an assay dependent manner. Two protocols incorporating click chemistry were devised; a click chemistry immunoprecipitation method, and a click chemistry immunofluorescence method.

4.5.1 Immunoprecipitation of wtBASP1 via Alkyne-Myristic Acid Pull Down

A summary of the click chemistry immunoprecipitation process is shown in the below diagram. Briefly, V-K562, B-K562 and G-K562 cells pre-incubated with alkyne myristic acid were subject to click chemistry reaction with an azide-PEG3-biotin conjugate. Nuclear extracts were then incubated with streptavidin conjugated magnetic beads to pull down myristoylated proteins (refer to Materials and Methods for full protocol).

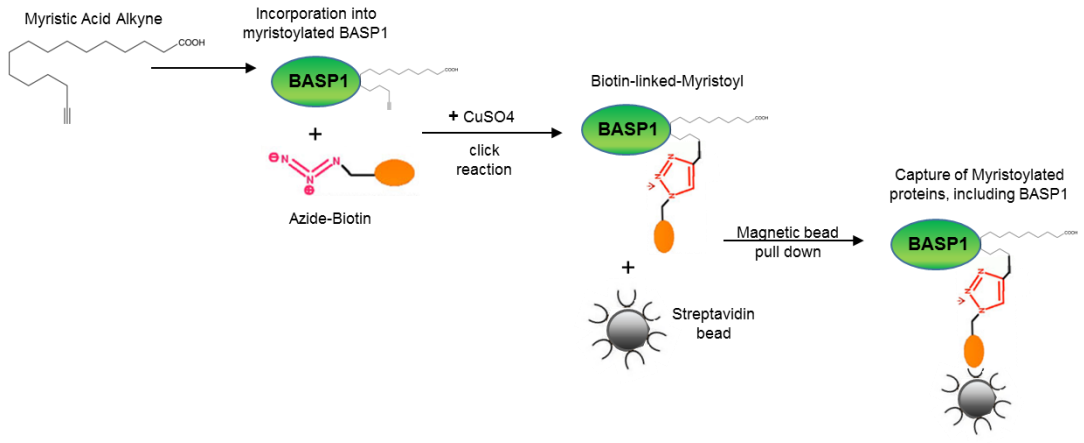

Western blotting confirmed successful immunoprecipitation of wtBASP1 but not G2A-BASP1 (Figure 4.7). Negative control β-actin confirmed specific pull down of myristoylated protein from this sample. A further alkyne-free negative control with V-K562, B-K562 and G-K562 incubated with vehicle (ethanol) alone confirmed that the

click chemistry reaction itself does not lead to protein immunoprecipitation. This result provides additional evidence to validate the G2A-BASP1 mutant protein as lacking the myristoyl modification, i.e. BASP1 is not myristoylated at any other residues. This also validates the myristoyl click chemistry protocol as a means of examining wtBASP1.

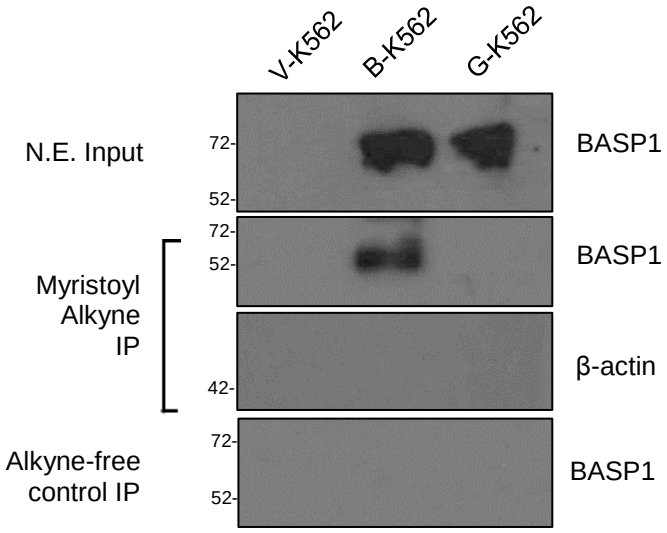

Figure 4.7. Pull Down of wtBASP1 via Click Chemistry of Alkyne-Myristic Acid Immunoprecipitation. V-K562, B-K562 and G-K562 cells incubated with ethanol (alkyne-free control) or 10µg/ml alkyne-Myristic acid and subjected to a click chemistry reaction. Pull downs using streptavidin beads were then performed on nuclear extracts, and western blots used to detect the presence of BASP1, or negative control β-actin. Molecular weight marker in kDa shown to left of each blot

4.5.2 Confocal Imaging of BASP1 and Alkyne-Myristic Acid

Next, to image the myristoyl motif whole MCF7 cells pre-incubated with alkyne myristic acid were subject to click chemistry reaction followed by immunostaining in suspension. A summary of the click chemistry immunofluorescence process is shown in the below diagram. For this method, following the click reaction whole cells were incubated with streptavidin conjugated antibody (refer to Materials and Methods for full protocol).

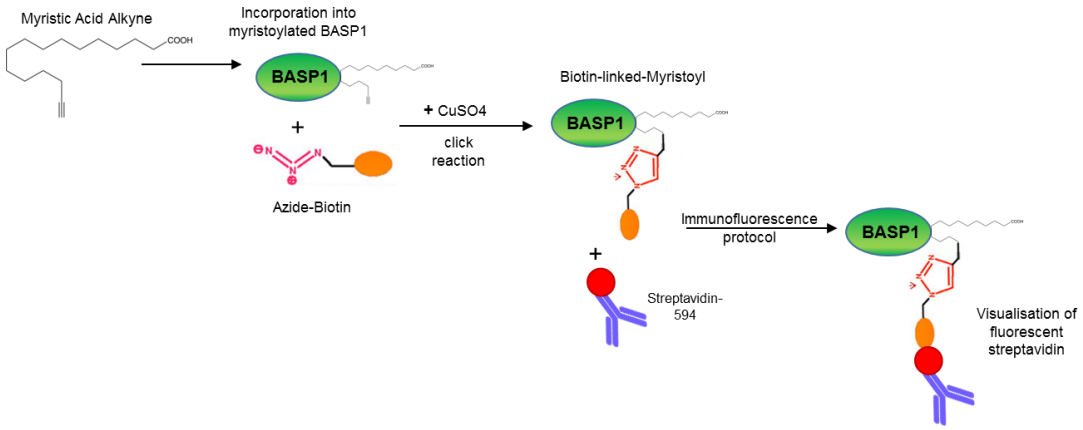

Two stable MCF7 cell lines were used; shN MCF7 (negative control knockdown line) and shB MCF7 (stable BASP1 knockdown line). BASP1 protein was calculated to be 63% knocked-down in shB MCF7 compared to shN MCF7 via quantification using ImageJ (Figure 4.8Ai). Both negative controls (alkyne-free is cells incubated with vehicle only, and azide-free is cells without azide-PEG3-biotin added) revealed no streptavidin-594 signal via confocal microscopy (Figure 4.8Aii). BASP1 was successfully detected throughout the cytoplasm of the shN MCF7 cells, and only low level BASP1 signal was detected in the shB MCF7 cells, as expected in this knockdown cell line (Figure 4.8Bi). Like BASP1, in whole cells, the myristoyl signal observed is predominantly within the cytoplasm and the cell membrane.

To more closely examine nuclear BASP1 and myristoyl signal and avoid interference from cytoplasmic immunofluorescence signal the click chemistry imaging technique was applied to purified nuclei. Therefore, shN MCF7 and shB MCF7 cells were incubated with alkyne-myristic acid, then the nuclei were purified and the nuclei only were subjected to the click chemistry reaction followed by immunostaining in suspension (Figure 4.8Bii). Here, without interference from cytoplasmic signal, nuclear BASP1 and myristoyl were successfully visualised in shN MCF7 nuclei. Interestingly, in both the whole cell images and the purified nuclei images a lower level of myristoyl signal was seen in the shB MCF7 cells than in shN MCF7 cells (Figure 4.8Bi and 4.8Bii). It is surprising that knockdown of BASP1 alone would account for such a loss in observed myristoyl signal. It is possible that either BASP1 alone accounts for a considerable proportion of the myristoylated protein is these cells or that BASP1 forms complexes with other myristoylated nuclear proteins which are disrupted following BASP1 depletion leading to diminished myristoyl signal.

Close study of the nuclear myristoyl signal in MCF7 nuclei suggests that not only is myristoyl present at the nuclear periphery, most probably within the nuclear membrane, but is also present as speckles within the nuclear space. A proportion of intranuclear signal coincides with BASP1 signal, but additional nuclear myristoyl signal, including within the nucleolus, is apparent. This imaging therefore contributes to evidence that nuclear myristoylated proteins can also be present in the nucleoplasm and are not restricted to the nuclear membrane.

Nuclear BASP1 and myristoyl signal in the K562 cell lines was next explored. Nuclei were purified from V-K562, B-K562 and G-K562 cells following incubation with alkyne-myristic acid. Purified nuclei were subjected to the click reaction and immunostaining in suspension with BASP1 antibodies as previously described. Once again both negative controls (alkyne-free and azide-free control) revealed no streptavidin-594 signal via confocal microscopy (Figure 4.8C). BASP1 protein was present as speckles throughout B-K562 and G-K562 nuclei, and not detected in V-K562 nuclei (Figure 4.8D). Similar to MCF7 nuclei, myristoyl is localised most abundantly around the nuclear membrane of K562 nuclei, however myristoyl is also convincingly present throughout the inner nuclear space, including within the nucleolus. In K562 cells BASP1 is excluded from the nucleolus, therefore this myristoyl signal must be produced by other myristoylated proteins within the nucleolus. Once again diminished myristoyl signal is apparent in V-K562 nuclei compared to B-K562 nuclei much like that observed in the MCF7 cell lines. This again suggests that BASP1 could account for a large proportion of nuclear myristoylated protein, or that BASP1 may contribute to the stabilisation of nuclear myristoylated protein complexes.

As well as gaining qualitative imaging data exploring nuclear myristoyl signal, it was anticipated that the click chemistry imaging conducted here could provide quantitative analysis of colocalisation between wtBASP1 and G2A-BASP1 with myristoyl within the nucleus. Colocalisation analysis was performed using both the Pearson's correlation coefficient (PCC) and Manders colocalisation analysis methods. Both these approaches are widely accepted as valid approaches to analyse complex colocalisation data [293]. The PCC method revealed an average correlation coefficient of 0.17 for BASP1 and myristoyl in B-K562 nuclei, and 0.066 in G-K562 nuclei (Figure 4.8E). This analysis suggests a weak positive correlation between wtBASP1 and myristoyl signal, with a statistically significant reduction in correlation between G2A-BASP1 and myristoyl, as hypothesised. The low PCC

values obtained here for wtBASP1 and myristoyl is most likely representative of fact that there is a large proportion of myristoylated protein in addition to BASP1. This finding suggests it is more likely that the diminished myristoyl signal apparent in non-BASP1 expressing cells is caused at least in part by BASP1 acting to stabilise nuclear myristoylated protein complexes.

Manders colocalisation analysis examining the overlap of BASP1 and myristoyl signals in B-K562 and G-K562 nuclei is also shown in Figure 4.8E. Here, M1 values represent the proportion of BASP1 signal that colocalises with myristoyl signal. For wtBASP1 this was determined as 20.9%, and for G2A-BASP1 it was 17.9%. M2 values represent the proportion of myristoyl signal that colocalises with BASP1. For wtBASP1 this was 32.1%, and for G2A-BASP1 it was 25.8%. Whilst there is no significant difference in the proportion of wtBASP1 and G2A-BASP1 associated with myristoyl (M1 values), this analysis suggests significantly less myristoyl associates with G2A-BASP1 than with wtBASP1 (M2 values). Once again, these values indicate that a significant proportion of nuclear myristoyl signal is accounted for by proteins other than BASP1. The apparent similarity between M1 values from B-K562 and G-K562 could perhaps be indicative that both wtBASP1 and G2A-BASP1 have some capacity to associate with other myristoylated proteins in the nucleus.

Figure 4.8. Click Chemistry Confocal Imaging of Myristoyl in MCF7 Whole Cells, MCF7 Nuclei and K562 Nuclei.
Click chemistry of shNegative (shN) and shBASP1 (shB) MCF7 cells, and V-K562, B-K562, G-K562 nuclei incubated with 10µg/ml alkyne-Myristic acid. Click chemistry reaction was followed by immunofluorescence with BASP1 and streptavidin antibodies, and confocal microscopy. **A**i) Expression level of BASP1 in shN and shB MCF7s, **A**ii) MCF7 (shN) Azide-free and alkyne-free controls. **B**i) BASP1 and Myristoyl in whole MCF7 cells, **B**ii), BASP1 and Myristoyl in MCF7 nuclei. Scale bar 10µm.

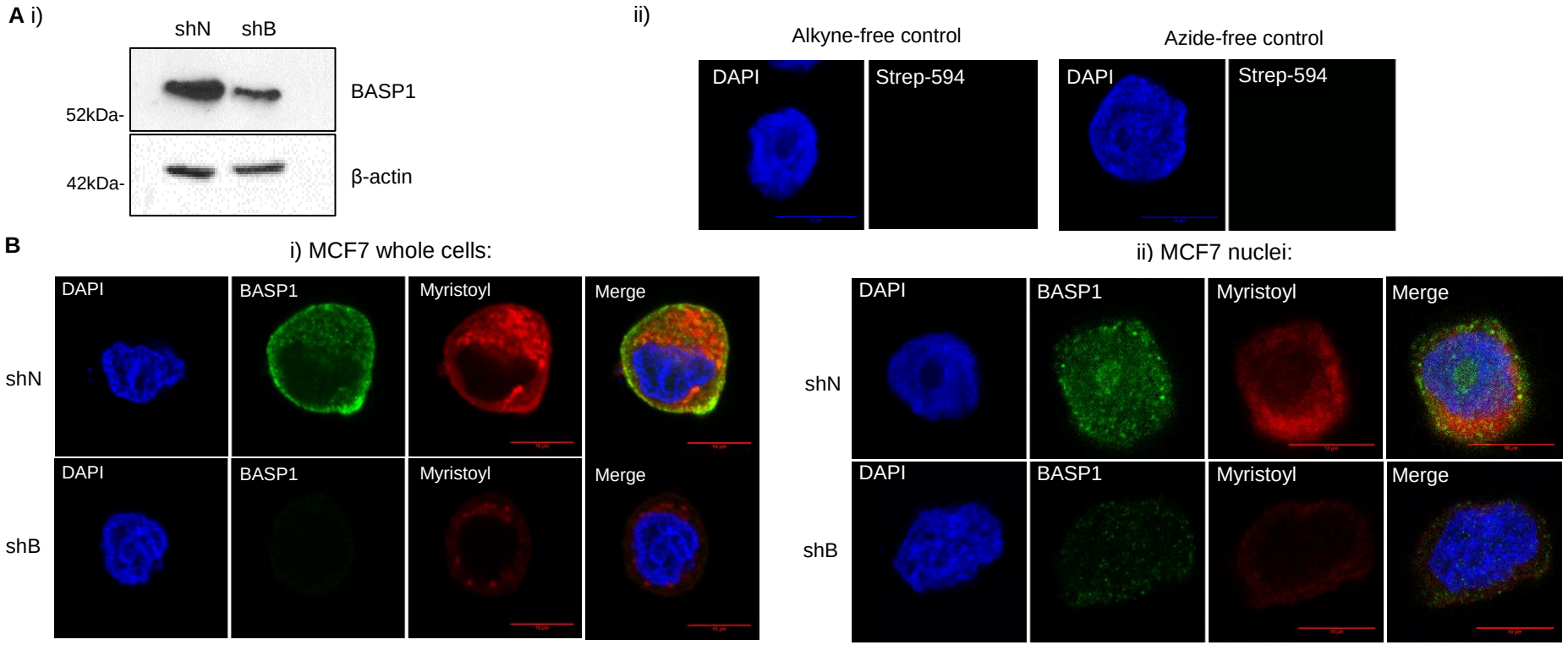

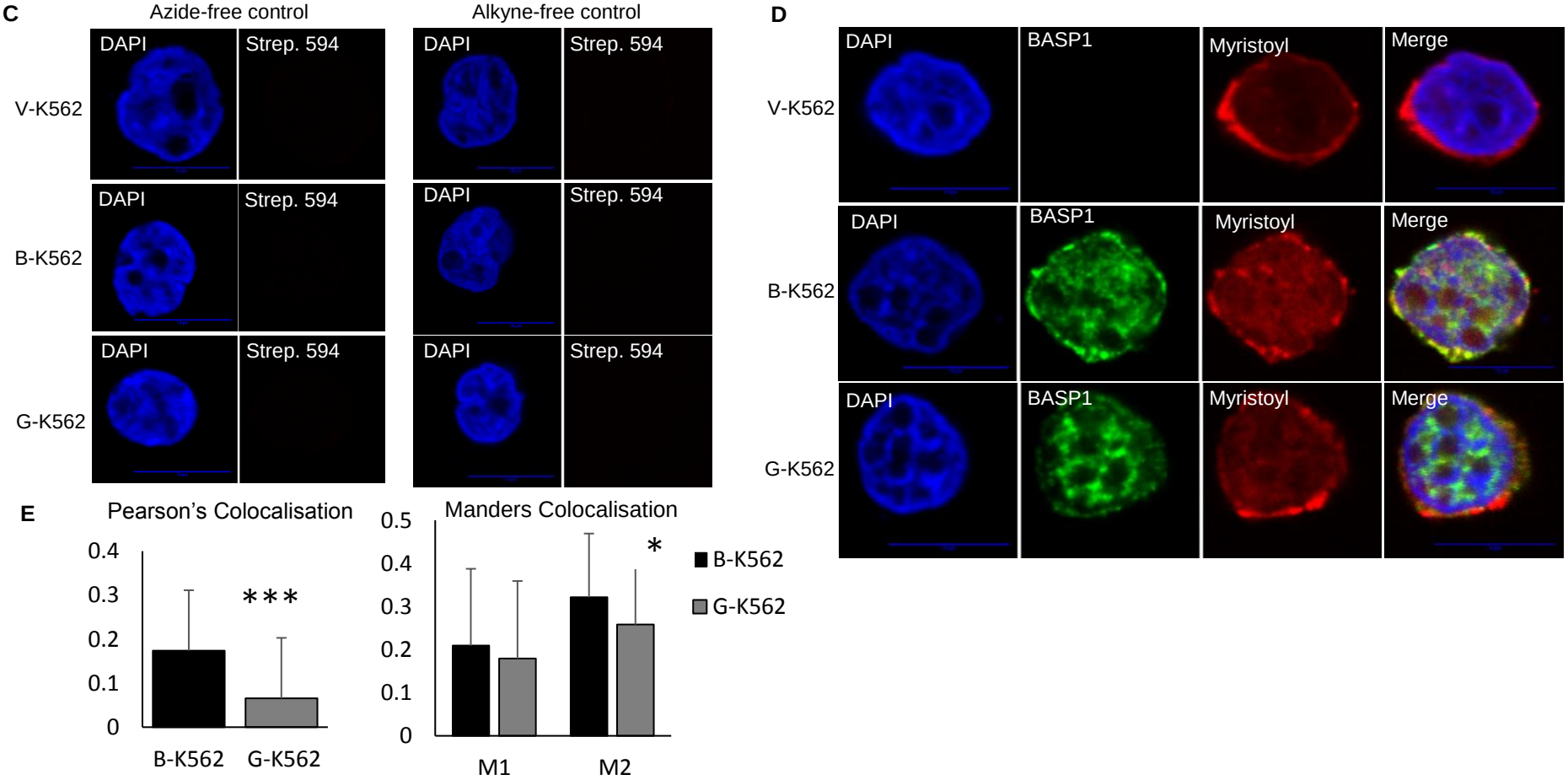

Figure 4.8. Continued: C, Azide-free controls and alkyne-free controls in V-K562, B-K562 and G-K562 nuclei. **D**, BASP1 and Myristoyl in V-K562, B-K562 and G-K562 nuclei. Scale bar 10µm. **E**, Quantification of the colocalisation of BASP1 and Myristoyl in B-K562 and G-K562 nuclei as analysed using the Pearson's correlation coefficient and the Manders' colocalisation technique. *p<0.05 following students t test comparing M1 values from BK and GK nuclei, and M2 values from BK and GK values over 3 independent experiments, n=67.

4.6 Electron Microscopy of BASP1 and Emerin in B-K562 Cells

Completion of the click chemistry imaging of intranuclear BASP1 and myristoyl provided quantitative data of the difference in myristoyl association of wtBASP1 and G2A-BASP1. It also enabled visualisation of intranuclear myristoyl motifs and gave insight into the nuclear localisation of myristoylated proteins. Next, high resolution imaging was explored in order to examine the localisation of BASP1 to the nuclear periphery. To achieve this B-K562 cells were high pressure frozen, embedded in lowicryl resin, sectioned and subjected to immunogold labelling to detect BASP1 (via HA tag) and emerin. Sections were then imaged via transmission electron microscopy to examine BASP1 and emerin localisation in the nucleus (Figure 4.9).

A significant challenge to the production of high quality immunogold labelled sections is the simultaneous preservation of cellular structures and attainment of high contrast for TEM imaging. Use of the Leica EM PACT2 high pressure freezing system facilitated good preservation of cellular structures although this is accompanied with relatively low contrast across the sections (Figure 4.9A and 4.9B). Antibody penetrance through the embedding resin is an additional technical challenge. Immunogold labelling using HA rather than BASP1 antibodies was recommended by the Electron Microscopy facility in order to achieve specific binding and reliable signal for BASP1. Following optimisation of antibody concentrations for the immunogold labelling a concentration of 1:5 HA antibody provided the best protein labelling. Using this protocol immunogold labelled particles were localised throughout the B-K562 cell and nucleus, indicative of good antibody penetration of the lowicryl resin (Figure 4.9B). Examination of HA-BASP1 in the nucleus and at the nuclear periphery enabled identification of 6nm gold labels, labelling HA-BASP1, throughout the nucleus including at the inner nuclear membrane (Figure 4.9C). The labelling of emerin functions as a positive control in this assay. Examination of emerin, labelled by 10nm gold particles, identified emerin at the nuclear membrane however this labelling was accompanied by emerin labelling throughout the cell. It was concluded that the emerin labelling likely included some non-specific particles. Subsequently, firm conclusions regarding the localisation of HA-BASP1 could not be made from these images. However, the images obtained here do support previous evidence to suggest that wtBASP1 is present within the nucleoplasm and provide initial evidence that wtBASP1 is also localised at the inner nuclear membrane. Further TEM study of wtBASP1 and G2A-BASP1 localisation is required, accompanied by thorough image analysis, to determine and quantify differences in wtBASP1 and G2A-BASP1 localisation.

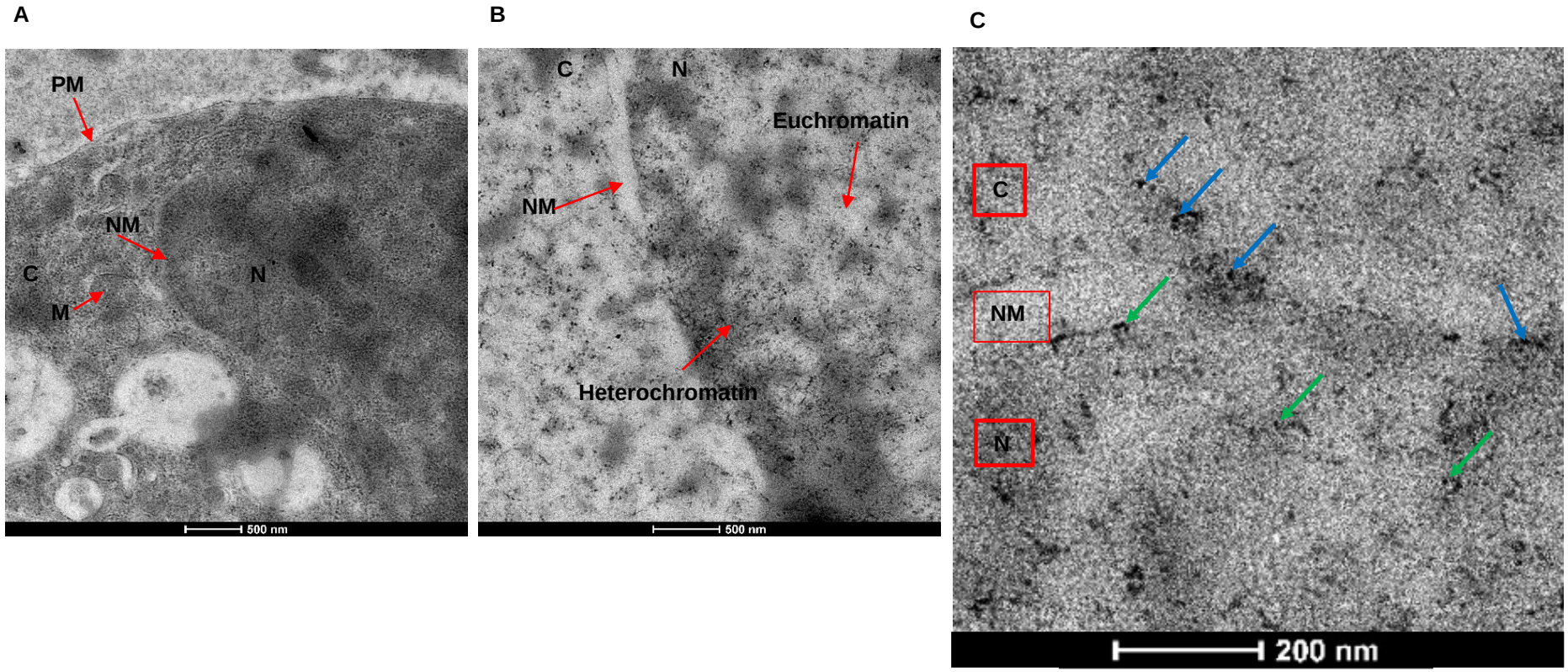

Figure 4.9. Electron Microscopy of Gold-Labelled HA-BASP1 and Emerin in B-K562 Cells. B-K562 cells were high pressure frozen, lowicryl embedded, sectioned and subjected to antibody and gold labelling. **A**, TEM image of B-K562 cell showing preservation of cellular structures. PM, plasma membrane, NM, nuclear membrane, N, nucleus, C, cytoplasm, M, mitochondria. **B**, TEM image of B-K562 cell showing distribution of heterochromatin and euchromatin in the nucleus and gold labelling throughout the cell. **C**, TEM image of B-K562 cell showing nuclear periphery with HA-BASP1 (6nm) and emerin (10nm) gold labelling indicated by green and blue arrows, respectively. Scale bar shown below each image.

4.7 Click Chemistry Chromatin Immunoprecipitation of Myristoyl at WT1 Target Gene Promoters

Previous work from our laboratory demonstrated for the first time that BASP1 induces gene repression of WT1 target genes in a myristoyl-dependent manner [3]. It was shown that PIP_2 and HDAC1 were only recruited to gene promoters by wtBASP1, and not the G2A-BASP1 myristoyl mutant. At the time, it was not directly demonstrated that the BASP1 present at the promoter was myristoylated. Here, the click chemistry approach has proven useful in detecting myristoyl for visualisation and for protein capture via magnetic beads. Therefore, it was predicted that with further optimisation the click chemistry approach could be employed in combination with the optimised ChIP protocol to directly test myristoyl-BASP1 recruitment to WT1 target genes.

Indeed, development of a click chemistry combined with chromatin immunoprecipitation technique (click-ChIP) identified recruitment of myristoyl to the promoter of all examined WT1 target genes (AREG, ETS-1, REN, VDR and JUNB), which coincided with the recruitment of wtBASP1 and not G2A-BASP1 (Figure 4.10). For this method, following incubation with alkyne-myristic acid cells were fixed in 4% formaldehyde for 15 mins, subjected to click reaction, then fixed again in 4% formaldehyde for 15 mins before cell pellets were lysed, chromatin sheared via sonication and lysates incubated with streptavidin beads to capture myristoyl (refer to Materials and Methods for full protocol). A summary of the click-ChIP process is shown in the below diagram:

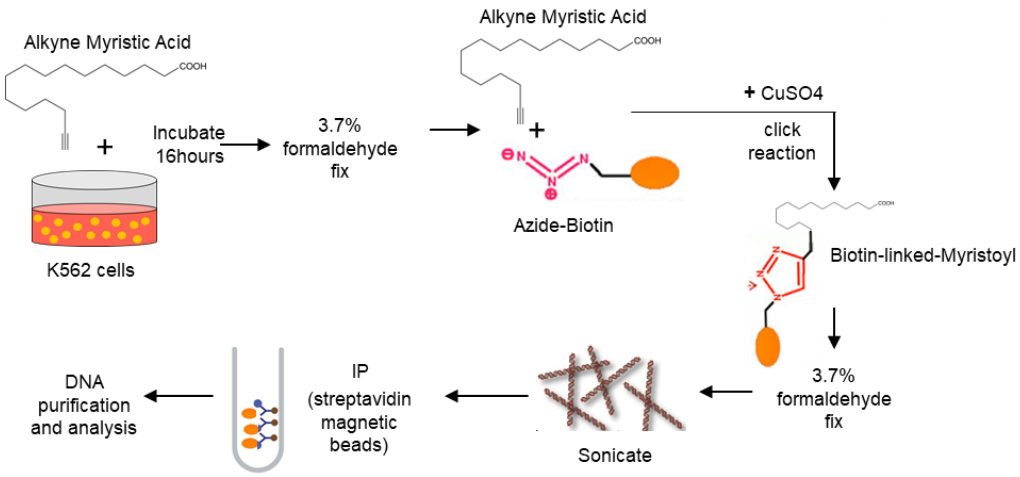

Fold enrichment was calculated as enrichment of myristoyl above signal from the negative control; an alkyne-free control ChIP from each cell line. Fold enrichment of

myristoyl was then compared to a control gene region (18S). Myristoyl was significantly enriched only in B-K562 cells compared to V-K562 cells. The G-K562 line acted as a negative control in this experiment since G2A-BASP1 lacks the vital N-terminal glycine acceptor for the myristoyl modification. This result confirms that the detected myristoyl signal is indeed dependent on myristoylated BASP1. It confirms that the nuclear pool of BASP1 includes an N-terminally myristoylated form and that it is recruited to WT1 target genes.

Figure 4.10. Myristoyl is Present at the Promoters of WT1 Target Genes in wtBASP1 Expressing K562 Cells. A, DNA gel electrophoresis shows DNA fragment sizes following the incubation of V-K562, B-K562 and G-K562 cells with either ethanol (alkyne-free control) or 10ug/ml alkyne-Myristic acid, followed by a click chemistry reaction and sonication of the DNA. ChIP experiments were performed using a streptavidin-biotin pull down of azide-alkyne-Myristoyl bound DNA regions. Base pair markers (bp) are shown at left. **B**, Fold enrichment of Myristoyl at the AREG, ETS-1, REN, JUNB and VDR promoters in V-K562, B-K562 and G-K562 cells compared to the alkyne-free control pull down, and control region 18S. Error bars representative of the standard deviation of the mean, n=10. *p<0.05, by Student's t test comparing B-K562 or G-K562 with control cell line V-K562.

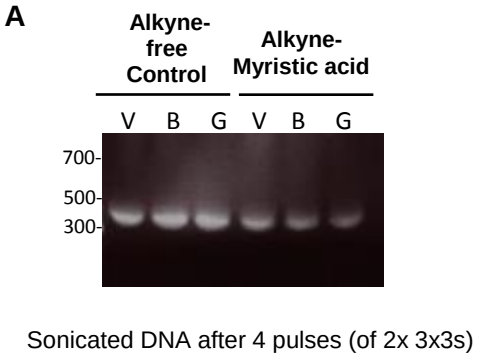

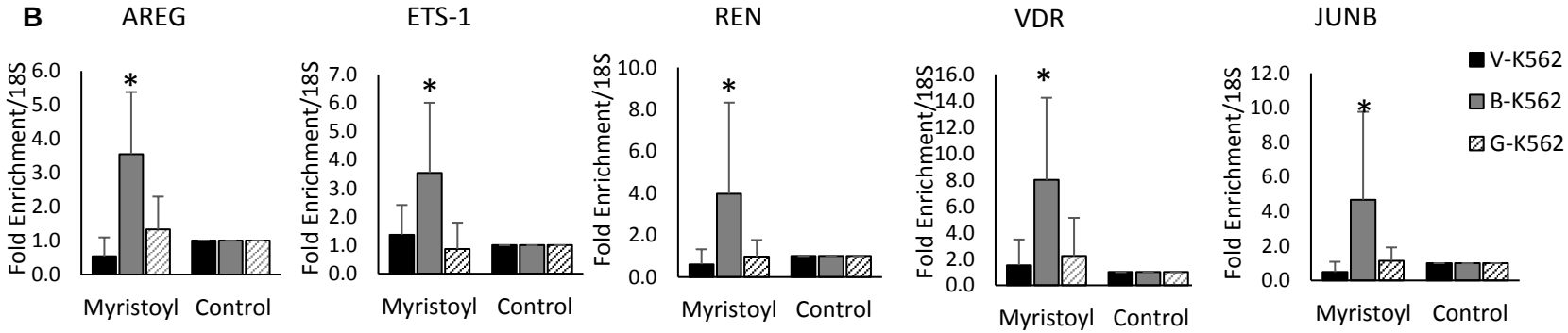

4.8 Role of Inner Nuclear Membrane Components in WT1/BASP1/PIP_2 Mediated Gene Repression

Work from our laboratory and data presented in the first chapter of this study have shown that G2A-BASP1 is defective at gene repression [3]. In this chapter subnuclear fractionation revealed that unlike wtBASP1, G2A-BASP1 does not localise to the nuclear matrix. It has also been shown that wtBASP1 interacts with the INM protein emerin in a myristoyl dependent manner. Therefore, it was next sought to investigate whether interaction with INM proteins is important for BASP1 gene repressor function. Here it was reasoned that if BASP1 interacts with INM proteins to repress transcription, then the INM components should be recruited to the promoters of wtBASP1, but not G2A-BASP1 bound WT1 target genes. It was further reasoned that depletion of INM components would relieve BASP1-mediated transcriptional repression.

4.8.1 Chromatin Immunoprecipitation of Nuclear Membrane Proteins at WT1 Target Gene Promoters

To examine whether nuclear membrane proteins are recruited to BASP1 repressed genes a series of ChIP experiments was conducted with V-K562, B-K562 and G-K562 cells. Sonicated chromatin samples were subjected to immunoprecipitation with emerin, BAF or lap2α antibodies. Strikingly, enrichment of all three proteins was apparent at WT1 target gene promoters specifically in wtBASP1 expressing cells (Figure 4.11). Emerin and BAF protein were both significantly enriched at the promoters of the AREG, ETS-1, VDR and JUNB promoters in B-K562 compared to V-K562 control, and not enriched in G-K562 cells. Similarly, lap2α was statistically significantly enriched at the promoters of the ETS-1, REN, VDR and JUNB promoters in B-K562 compared to V-K562 control, and not enriched in G-K562 cells. These results indicate that the expression of wtBASP1, and it's binding to WT1 target gene promoters, coincides with the recruitment of multiple INM proteins. The binding of these INM components does not occur in G2A-BASP1 expressing cells, and therefore appears to be dependent on BASP1 myristoylation.

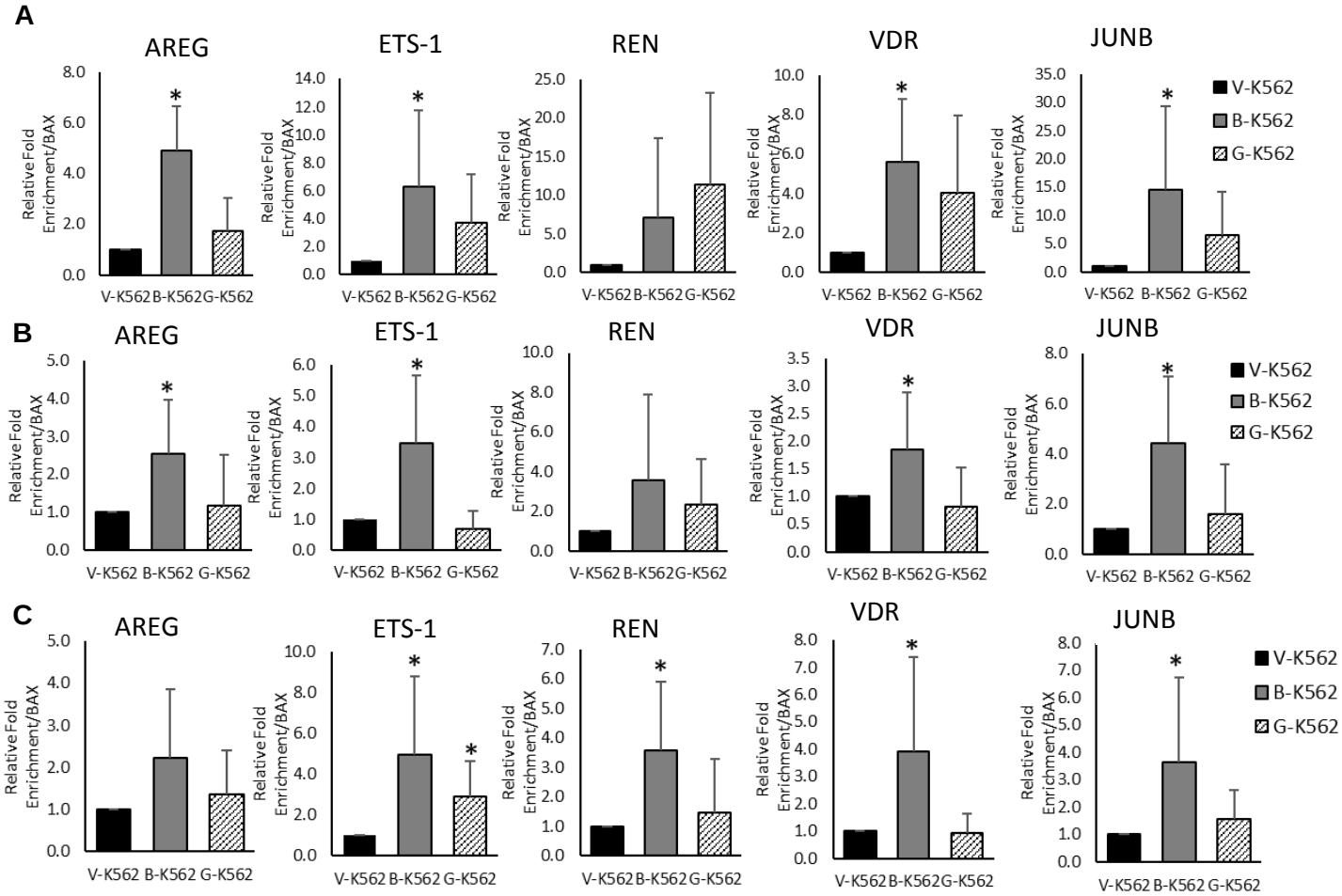

Figure 4.11. Nuclear Membrane Proteins Emerin, BAF and LAP2α are Bound to WT1 Target Gene Promoters in B-K562 cells. The binding of Emerin (**A**), BAF (**B**) and LAP2α (**C**) at the promoters of AREG, ETS-1, REN, VDR and JUNB was examined using chromatin immunoprecipitation in V-K562, B-K562 and G-K562 cells. Fold enrichment above IgG and compared to control region BAX. Error bars representative of the standard deviation of the mean, A) n=8, B) n=8, C) n=8. *p<0.05, by Student's t test comparing B-K562 or G-K562 with control cell line V-K562.

4.8.2 Gene Expression Analysis Following Knockdown of Emerin via siRNA

The results so far have demonstrated that BASP1 interacts with emerin and that it recruits several INM proteins to the promoter region of WT1 target genes. These activities of BASP1 are abolished by the G2A mutation suggesting that they are dependent on BASP1 myristoylation. To investigate whether INM proteins are involved in the mechanism of BASP1 mediated gene repression an siRNA knockdown experiment was conducted targeting emerin. The stable shN MCF7 and shB MCF7 cell lines were transfected with either a control siRNA sequence or an siRNA sequence targeting emerin. Expression levels of WT1 target genes were analysed via quantitative PCR 48 hours post transfection (Figure 4.12A). Western blots were conducted to confirm emerin protein knockdown (Figure 4.12B). ImageJ analysis indicates emerin protein was reduced by ~50%. As expected, in the control condition the expression level of all three WT1 target genes examined (AREG, ETS-1 and VDR) was increased in shB MCF7 cells compared to shN MCF7 cells, indicating that loss of BASP1 expression leads to loss of repression of these genes. Upon emerin knockdown two effects are seen. Firstly, for AREG and ETS-1 in the presence of BASP1 the knockdown of emerin leads to an increase in gene expression, but when both BASP1 and emerin are depleted no loss of repression is apparent. Secondly, for VDR, in the presence of BASP1 the knockdown of emerin leads to a small increase in gene expression, but when both BASP1 and emerin are depleted loss of repression is maintained. The fact that emerin depletion has different effects in shN and shB MCF7 cells suggests a relationship between BASP1 and emerin that is important for gene repression. However, it is also clear that simultaneous knockdown of Emerin and BASP1 inhibits expression of AREG and ETS-1 rather than leading to de-repression.

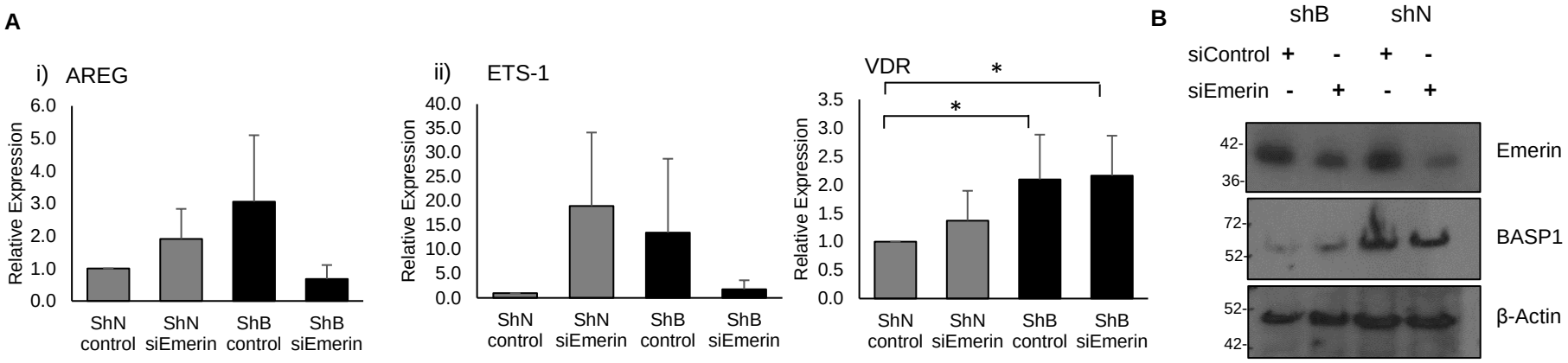

Figure 4.12. Knockdown of Emerin via siRNA Reduces BASP1 Mediated Gene Repression. A, Relative expression of (i) AREG, (ii) ETS-1 and (iii) VDR in MCF7 shN (shNegative control stable MCF7 cells) and shB (shBASP1 stable MCF7 cells) following transfection of either siControl or siEmerin. Relative expression normalised to GAPDH. Error bars represent standard deviation across 3 independent experiments for AREG and ETS-1 and 5 independent experiments for VDR. *$p<0.05$ following students t test compared to ShN control sample. **B**, samples of transfected shB and shN MCF7 were western blotted and probed for emerin, BASP1 and β-Actin. Molecular weight markers in kDa shown to left of each blot.

4.9 Discussion of Chapter 2 Results

4.9.1 Myristoylation Affects BASP1 Localisation

The work presented in this chapter has further explored the importance of myristoylation for the transcriptional repression function of BASP1. This included examination of the localisation of the BASP1 repression complex, identification of myristoyl dependent interaction partners, and investigation into the role of INM proteins in BASP1 mediated repression. Biochemical fractionation of the nucleus provided the first evidence that the subnuclear localisation of BASP1 is affected by the myristoyl modification, whereby lack of myristoylation results in loss of BASP1 from the nuclear matrix fraction. Furthermore, immunoprecipitation data revealed that myristoylation is essential for BASP1 to interact with proteins largely associated with the nuclear membrane and nuclear matrix, namely emerin and β-actin. The myristoyl dependent nature of these interactions is likely to contribute to loss of G2A-BASP1 from the nuclear matrix fraction. The myristoyl dependent nature of these interactions also posed the question of whether they play a role in BASP1 mediated gene repression.

Having discovered that BASP1 nuclear localisation is affected by the myristoyl modification, microscopy approaches were then adopted with the aim of visualising wtBASP1 and G2A-BASP1 in the nucleus. Following confocal microscopy of BASP1 alongside repression complex components prohibitin, HDAC1 and PIP_2 it was concluded that the abundance of these nuclear components called for higher resolution imaging techniques in order to gain meaningful localisation data. Preliminary TEM observation of immunogold labelled HA-BASP1 in B-K562 cells suggested that wtBASP1 may indeed localise at the inner nuclear membrane, as well as throughout the inner nuclear space. Further TEM observation and analysis of wtBASP1 and G2A-BASP1 is now required to confirm BASP1 presence at the nuclear membrane and examine any differences in the localisation of wtBASP1 and G2A-BASP1.

4.9.2 Nuclear Localisation of BASP1 and Myristoyl

Next, the development of click chemistry techniques enabled visualisation of the nuclear colocalisation of BASP1 and the myristoyl modification. Following validation of the click chemistry technique and pull down of wtBASP1 using streptavidin beads, confocal images were obtained which provided evidence for the presence of myristoyl modification, not only at the nuclear membrane, but also within the inner

nuclear space, including the nucleolus (Figure 4.7 and Figure 4.8). A handful of other myristoylated proteins have previously been found in the nucleoplasm and the nucleolus and include the tyrosine kinase c-ABL, MARCKS and ARL4 [130, 294-297]. Myristoyl was observed in the nucleolus of both cell types examined in this study, whilst BASP1 was only apparent in the nucleolus of MCF7 cells, suggesting that BASP1 contributes to the pool of myristoylated proteins in the nucleolus in some cell types. It is possible this difference may be due to the ectopic expression of BASP1 protein in K562 cells compared to endogenous MCF7 BASP1 protein.

The click chemistry imaging of BASP1 and myristoyl has also provided quantitative data to show reduced association of G2A-BASP1 with myristoyl. This agrees with the click chemistry immunoprecipitation data (Figure 4.7) and is further supported by the click-ChIP data which is consistent with myristoylation occurring only at the G2 residue of BASP1. The presence of the myristoyl modification was detected at all wtBASP1 bound sites, confirming that BASP1 is recruited to WT1 target genes in an N-terminally myristoylated form. BASP1 remains the only protein known to have a function in gene regulation that is dependent upon myristoylation and the click-ChIP data presented here directly demonstrates recruitment of myristoylated BASP1 to gene promoters for the first time.

4.9.3 Myristoyl Dependent Interaction of BASP1 and the INM

Work presented later in this chapter demonstrated that BASP1 interacts with the inner nuclear membrane protein, emerin, in a myristoyl dependent manner. BASP1 immunoprecipitation followed by mass spectrometry also revealed that BASP1 interacts with a range of other nuclear periphery components. The data collected from a series of ChIP experiments described here demonstrate recruitment of multiple inner nuclear membrane components (emerin, BAF and lap2α) to BASP1 bound promoters in a myristoyl dependent manner. This is the first evidence that membrane components are recruited to BASP1 bound promoters. Given that myristoylation of BASP1 is essential for transcriptional repression, interaction with emerin, and recruitment of INM proteins to gene promoters, it was reasoned that interaction with INM components may be important for BASP1 gene repressor activity.

The subnuclear localisation of these promoter bound INM components cannot be confirmed from the ChIP data, however a role for these factors in inducing gene repression at the nuclear periphery has previously been described. Emerin has

been associated with gene repression through a number of means; firstly through the anchoring of transcriptional regulators to the nuclear membrane, such as β-catenin to downregulate Wnt signalling, the Notch intracellular domain to downregulate Notch signalling and Lmo7 which regulates heart and muscle relevant genes [298-301]. Secondly, emerin has been implicated in promoting a repressive chromatin environment at the nuclear periphery through its association with chromatin modifying complexes like the nuclear corepressor (NCoR) complex [189]. Emerin directly binds HDAC3, the catalytic subunit of the NCoR complex, resulting in its recruitment to the nuclear periphery and enhanced deacetylation of H4K5 and adjacent acetyl lysines, leading to gene repression [189]. Similarly, emerin activation of HDAC3 activity causes relocalisation of *Myf5, MyoD* and *Pax7* genes to the nuclear membrane where they undergo repression during differentiation of myogenic progenitors [238]. These findings support a role for emerin in repositioning DNA at the nuclear periphery.

BAF also has functions associated with chromatin reorganisation and gene repression at the nuclear periphery, partly in association with emerin. BAF binds to the LEM domain of emerin and anchors it in the nuclear membrane [302]. This anchoring is essential for emerin function, evidenced by BAF downregulation leading to the release of emerin into the cytosol and subsequent upregulation of Notch signalling [301]. BAF can also directly bind transcription factors, such as the homeodomain transcription factor Crx and related transcription factors and repress their transactivation activity [303]. Many groups have demonstrated that BAF also dynamically binds other LEM domain containing proteins, including the Lap2 family and lamins, which assemble together to govern chromatin organisation and capture segregated chromosomes at the nuclear envelope [304, 305]. Furthermore, BAF is also associated with heterochromatin formation through epigenetic mechanisms including binding to the methyltransferase SETD1A which mediates repression through H3K4 methylation [306-308].

The binding of both BAF and emerin to LAP2 proteins further serves to bridge chromosomes to the nuclear lamina [302, 309]. Alongside the other lap2 isoforms (β, δ, ε, ɣ, ξ), lap2α forms an integral structural component of the nuclear lamina where it complexes with chromatin, DNA and Lamin A/C [310]. Unlike the other Lap2 isoforms, as well as localising in the nuclear lamina and interacting with the nuclear membrane, Lap2α also localises throughout the nucleoplasm as part of the structural make-up of the nuclear matrix [311]. Lap2α can directly bind

chromosomes via its chromatin interaction domain, which has been shown to be important during dynamic structural organisation of the nucleus in processes such as spermiogenesis and post mitotic nuclear reassembly [311-313]. Lap2α is therefore a vital collaborative component for chromatin reorganisation.

Here, emerin knockdown leads to a reduction in BASP1 mediated gene repression of multiple targets, supporting the hypothesis that the BASP1-emerin interaction is important for the gene repression. One limitation of this experiment is the adverse effect of emerin knockdown on cellular health. Loss of emerin is associated with severe motor and cardiac defects, as documented in the emerin knockout mouse, and mutations in emerin lead to X-linked recessive Emery–Dreifuss muscular dystrophy and cardiac abnormalities including cardiomyopathy [314-317]. *In vitro*, emerin knockdown has been shown to cause nuclear shape instability, induce changes in gene expression patterns including the MAPK pathway, impair the differentiation potential of cells and even to promote metastasis [318-320]. It is comprehendible that depleting emerin levels by even 50%, as achieved in our emerin knockdown experiment, is sufficient to cause severe loss of cellular fitness leading to general adverse effects on the transcription of some gene products. Despite this caveat, these data still provide the first suggestion that emerin could be important for BASP1 mediated repression of WT1 target genes. Further investigation is required before more firm conclusions can be made about the requirement for emerin and the other INM proteins in the mechanism of BASP1 mediated repression. However, given this preliminary transcription data and the finding that emerin, BAF and lap2α localise with BASP1 at WT1 target genes, it is reasonable to speculate that the interaction of the BASP1 repression complex with these components might facilitate recruitment to the nuclear periphery, resulting in relocalisation of target genes and subsequent gene repression.

As discussed following findings from results chapter 1, BASP1 assembly at a gene promoter coincides with recruitment of EZH2 and an increase in repressive H3K27me^3 and H3K9me^3 chromatin marks. It is therefore speculated that BASP1 recruits EZH2 and the PRC2 complex to gene promoters which contributes to the induction of a repressive chromatin environment around these genes. The PRC2 complex also already has a well-defined role in mediating the repression of specific targets at the nuclear periphery through laying down of H3K27me^3 marks and heterochromatin formation. PRC2 recruitment to the nuclear periphery is essential for downregulation of Msx1 target genes during myoblast differentiation [321]. High

levels of H3K27me^3 are also found on target chromatin following PRC2 recruitment to the INM by the YY1 transcription factor [232]. Such PRC2 activity is vital for development and differentiation. The recruitment of PRC2 by BASP1 provides another mechanism through which gene repression could be mediated at the nuclear periphery.

4.9.4 Myristoyl Dependent Interaction of BASP1 and β-actin

In addition to the myristoyl-dependent interaction of BASP1 with emerin, it was also demonstrated in this chapter that the BASP1-β-actin interaction is myristoyl dependent (Figure 4.3). As well as being a crucial architectural component of the nucleus, β-actin is a vital component of many chromatin remodelling complexes including members of the SWI/SNF family and the BAF complex [322]. β-actin binds directly to the BRG1 ATPase subunit, stabilises the complex and facilitates the binding of the BAF complex to chromatin and the nuclear matrix [118, 322]. We have previously shown that BRG1 is recruited to WT1 target gene promoters in a BASP1 and prohibitin-dependent manner [96]. The importance of β-actin interaction for BASP1 repression function was not pursued here, but it would be interesting to establish whether a BASP1-β-actin interaction is important for recruiting BRG1 to BASP1 bound promoters and whether it could have a role in linking the BASP1 repression complex to chromatin and/or the nuclear matrix. Furthermore, PIP_2 has also been shown to be important in enhancing the association of the BAF complex with the nuclear matrix and with chromatin [118]. It would be interesting to examine whether the myristoyl-dependent BASP1-β-actin interaction is due to a requirement for PIP_2 to link the BASP1 complex with chromatin and the nuclear matrix.

Nuclear actin is increasingly thought to be important for transcription initiation and elongation and has been copurified from preinitiation complexes at RNA polymerase I and II transcribed genes [323-325]. Two models of actin's contribution to transcription elongation have been proposed; firstly through an actomyosin motor which helps the transcription machinery move along DNA, and secondly through recruitment of histone modifiers including HATs to RNA polymerase II transcribed genes [323]. These functions of actin are of direct interest to this study as it was shown here for the first time that BASP1 regulates RNA polymerase II recruitment in a myristoyl-dependent manner. Although not pursued here, it would be interesting to establish whether β-actin plays a role in recruiting histone modifiers to BASP1 regulated genes, and in Ser5 phosphorylation of RNA polymerase II by CDK7 at BASP1 regulated genes.

Nuclear actin is also known to play a vital role in the reorganisation of gene positioning as they undergo expression changes. Expression of mutant actin or nuclear myosin IC with actin binding and polymerisation defects inhibits intranuclear repositioning of genes upon transcriptional activation [326, 327]. These results highlight the importance of actin dynamics for gene repositioning and large-scale chromatin rearrangement. Given the working hypothesis that BASP1 mediates transcriptional repression through interaction with the nuclear membrane and relocalisation of WT1 target genes to the nuclear periphery, it would be interesting to investigate whether the lack of gene repression function of G2A-BASP1 could be related to deregulated gene positioning due to lack of actin binding capacity.

Furthermore, it is interesting that myosin IC has been implicated in gene repositioning, as we have also previously identified a BASP1-Myosin IC interaction [89, 326]. An emerin-myosin IC interaction has also been shown to anchor myosin IC at the nuclear membrane [300]. Proteomic examination of emerin complexes has led to the proposal that emerin forms architectural complexes with nuclear actin, myosin IC and lamin proteins that are entirely distinct from its gene regulatory complexes with binding partners such as histone 1, histone 3, BAF, HDAC1, HDAC3 and actin [300]. Although it remains unclear, it has been suggested that these architectural complexes function to facilitate actin motor activity [300]. This highlights the need for further investigation to establish how the presence of emerin at WT1/BASP1 target genes contributes to repression; it may be through contributing to an architectural complex to anchor BASP1 to the membrane or repositioning WT1 target genes, or perhaps through contributing to a chromatin modifying complex.

4.9.5 Summary of Chapter 2

A summary of the data presented in this chapter is shown in Figure 3.13 in the form of a schematic depicting the hypothesis that BASP1 recruits WT1 target genes to the nuclear periphery to mediate gene repression. The figure demonstrates a WT1 target gene unbound by BASP1, with active histone marks present at the gene promoter and transcription initiated by the phosphorylation of RNA polymerase II Serine 5 by CDK7. In line with the hypothesis this gene is shown in a central euchromatic region. Conversely a wtBASP1 bound gene is shown with repressive histone marks present at the gene promoter, and repression complex components including HDAC1 present. The complex is depicted interacting with INM proteins and is hypothesised to be located at the nuclear periphery within a heterochromatic region.

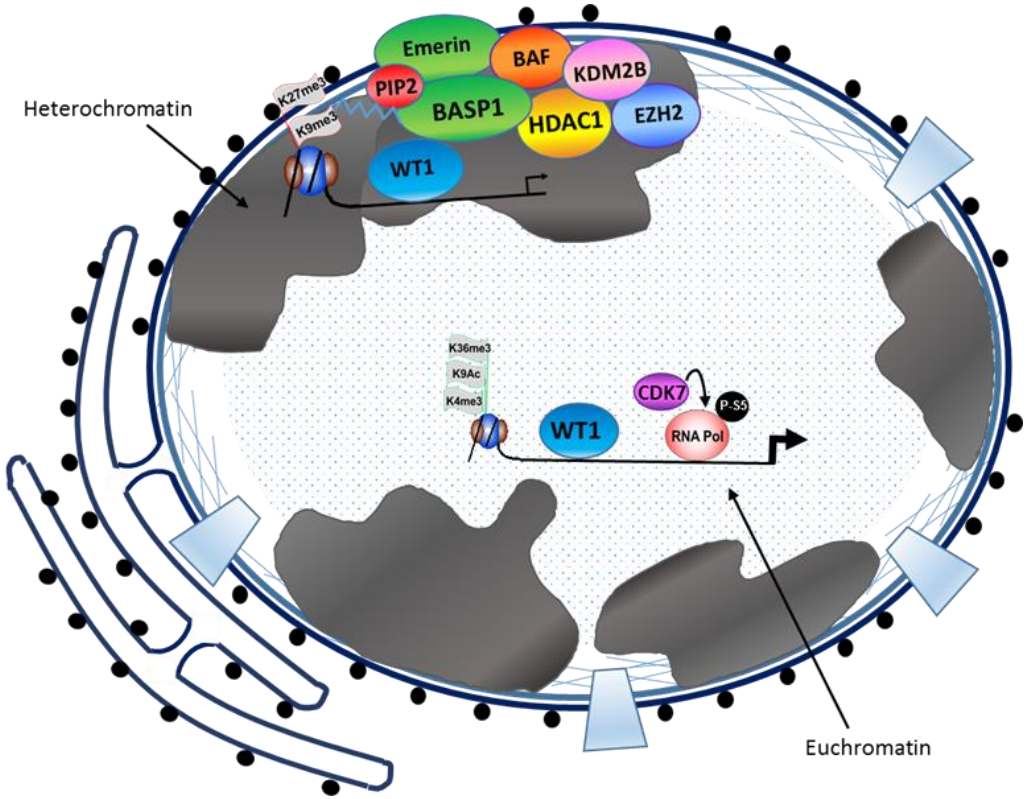

Figure 4.13. Chapter 2 Summary: Membrane Localisation of BASP1-PIP$_2$ Complex Plays a Role in WT1 Target Gene Repression.

Representation of hypothesised localisation of WT1 target genes. A promoter bound only by WT1 is located within euchromatin in the centre of the nucleus with known present active chromatin marks shown in green flags (H3K36me^3, H3K9Ac, H3K4me^3). Black arrow indicates phosphorylation of serine 5 of RNA polymerase II by CDK7. Large black arrow represents active transcription. A promoter bound by wtBASP1 is located within heterochromatin at the nuclear periphery. Known present repressive chromatin marks shown in red flags (H3K27me^3, H3K9me^3). Small black arrow represents reduced levels of transcription. HDAC1 is shown to represent previously established components of the repression complex. Emerin and candidate BASP1 interactors KDM2B, EZH2 and BAF are depicted as part of the repression complex at the nuclear periphery.

5 Results Chapter 3: The Role of Cholesterol in WT1/BASP1 Mediated Gene Repression

5.1 Introduction

BASP1 is a unique transcriptional regulator which is known to require an interaction with lipids, specifically PI(4,5)P_2 (PIP_2), to mediate gene repression. Our laboratory showed for first time that BASP1 recruits PIP_2 to target gene promoters, where the lipid subsequently recruits additional repression complex components and chromatin modifiers (HDAC1, BRG1, prohibitin) to mediate gene repression [2, 3, 96]. The work presented in the previous chapters of this study has provided further insight into the mechanism of WT1/BASP1/PIP_2 mediated gene repression and how lipidation of BASP1 contributes to the intranuclear localisation of the repression complex. In addition to PIP_2, BASP1 also has the capacity to interact with cholesterol through a cholesterol recognition amino acid consensus (CRAC) motif [82, 83, 328]. As a role for PIP_2 in WT1/BASP1 mediated gene regulation is becoming increasingly clear, here an investigation into a potential role for cholesterol in WT1/BASP1 mediated gene regulation was initiated. Current knowledge of cholesterol's role in gene regulation is limited, thus examination of the BASP1-cholesterol interaction provides an excellent means by which to explore this poorly understood topic.

The aim in this chapter was to examine the effect of expressing a cholesterol binding mutant BASP1 protein on the expression of WT1 target genes in K562 cells. The contribution of cholesterol to BASP1 gene repression activity was assessed through a variety of assays including gene expression analysis, differentiation assays and confocal imaging of intranuclear BASP1 and cholesterol. ChIP of BASP1 and cholesterol at target gene promoters was utilised to examine recruitment of the cholesterol binding mutant BASP1 protein and of cholesterol itself to WT1 target genes. Further ChIP assessed the contribution of the BASP1-cholesterol complex to levels of active histone modifications and RNA polymerase II recruitment at WT1 target genes.

5.2 Validation of Y12L-BASP1 Mutant

5.2.1 Generation of Stable Y12L-BASP1 K562 Cell Line

A stable K562 cell line expressing a tyrosine-12 to leucine (Y12L) mutant BASP1 protein (hereafter referred to as Y12L-BASP1) was generated in the same way as previously described in chapter 1 for G-K562 cells (results chapter 1, Figure 3.2). The Y12 residue is the critical tyrosine of the CRAC motif, its substitution for leucine removes the sole aromatic amino acid, eliminating cholesterol binding [88]. Transfection into K562 cells was followed by selection with 2µg/ml G418. Western blotting confirmed expression of BASP1 in this Y-K562 cell line at a similar level to that of the B-K562 stable line (Figure 5.1A). Further, visualisation of BASP1 expression in B-K562 and Y-K562 cells via immunofluorescence and confocal microscopy confirmed similar expression levels and nuclear localisation of wtBASP1 and Y12L-BASP1 in the K562 cells (Figure 5.1B).

To confirm that the Y12L mutation of BASP1 results in the loss of cholesterol binding, recombinant wtBASP1 or Y12L-BASP1 was incubated with a membrane dot blotted with increasing concentrations of cholesterol, followed by detection with BASP1 antibodies (Figure 5.1C). Recombinant wtBASP1 and the mutant derivative Y12L were generated using E. coli engineered to express N-myristoyl transferase. Quantification of wtBASP1 and Y12L-BASP1 binding to cholesterol confirmed a statistically significant decrease in cholesterol binding by the Y12L-BASP1 mutant protein. This work and the data presented in Figure 5.1 was generated by Samantha Carrera.

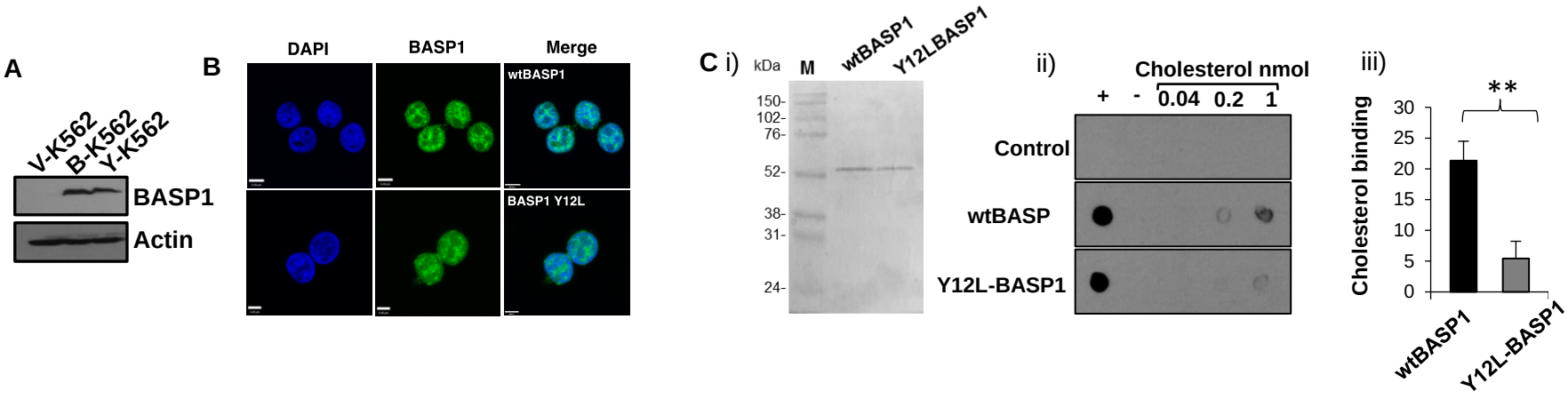

Figure 5.1. Generation and Validation of Stable Y12L-BASP1 Expressing K562 Cell Line. A, K562 cells were stably transfected with pcDNA3-Y12L-BASP1 vector, selected with 2µg/ml G418 and tested for BASP1 expression via western blotting. **B**, Confocal microscopy images of wtBASP1 and Y12L-BASP1 expression in K562 nuclei. **C**, recombinant wtBASP1 and Y12L-BASP1 were generated (i) and incubated with increasing concentrations of cholesterol via dot blot assay (ii). +, positive control sheep BASP1 antibody and -, negative control vehicle (ethanol) only. Cholesterol binding by wtBASP1 and Y12L-BASP1 is quantified in **C** (iii). **represents $p<0.005$, following students t test comparing wtBASP1 and Y12L-BASP1 binding. Error bars representative of the standard deviation across 3 independent experiments. ***Work carried out by Samantha Carrera.***

5.2.2 Immunoprecipitation of wtBASP1 via Alkyne-Cholesterol Pull Down

A click chemistry immunoprecipitation technique was previously developed in this study to pull down the myristoyl motif (refer to Chapter 2, Figure 4.7). As secondary validation that the Y12L-BASP1 protein is defective at cholesterol binding the click chemistry immunoprecipitation technique was applied using alkyne-cholesterol. Briefly, V-K562, B-K562 and Y-K562 cells pre-incubated with alkyne-cholesterol were subject to click chemistry reaction with an azide-PEG3-biotin conjugate. Nuclear extracts were then incubated with streptavidin conjugated magnetic beads to pull down cholesterol and cholesterol interacting proteins (refer to Materials and Methods for full protocol).

Western blotting confirmed successful pull down of wtBASP1 but not Y12L-BASP1 using this technique (Figure 5.2). β-actin served as a negative control. A further alkyne-free negative control with V-K562, B-K562 and Y-K562 cells incubated with vehicle (ethanol) alone confirmed that the click chemistry reaction itself does not lead to BASP1 protein pull down. These results provide additional evidence to validate that the Y12L-BASP1 protein lacks cholesterol binding activity, and that the Y12 residue is critical for this interaction.

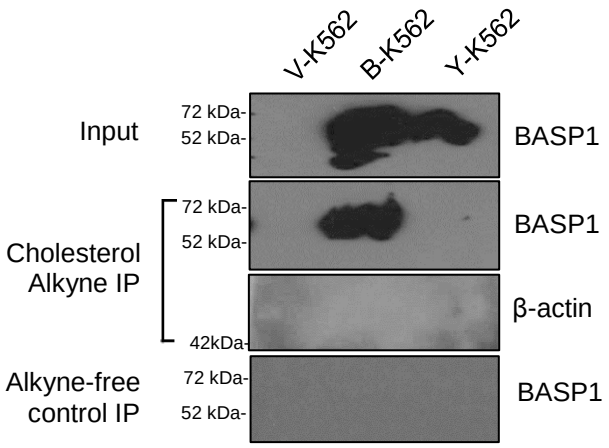

Figure 5.2. Pull Down of wtBASP1 via Click Chemistry of Alkyne-Cholesterol Immunoprecipitation. V-K562, B-K562 and Y-K562 cells incubated with either vehicle (alkyne-free control) or 10µg/ml alkyne-Cholesterol and subjected to a click chemistry reaction. Pull downs using streptavidin beads were then performed on nuclear extracts, and western blots used to detect the presence of BASP1, or negative control β-actin.

5.3 Confocal Imaging of BASP1 and Alkyne-Cholesterol

Earlier work presented in this study involved the imaging of alkyne-myristoyl in K562 nuclei via click chemistry immunofluorescence. Using the same technique, following the incubation of K562 cells with alkyne-cholesterol, confocal imaging of nuclear cholesterol was performed. Briefly, V-K562, B-K562 and Y-K562 cells with incubated with alkyne-cholesterol and subjected to the click chemistry reaction followed by immunostaining in suspension. For this method, following the click reaction either whole cells or intact purified nuclei were incubated with streptavidin conjugated antibody (refer to Materials and Methods for full protocol).

The alkyne-cholesterol imaging was initially conducted in whole MCF7 derivative cells and nuclei as described earlier (Figure 5.3A). Azide-free and alkyne-free negative controls are shown in Figure 5.3C and demonstrate that no fluorescence signal is obtained without incubation with alkyne-cholesterol and completion of the click reaction. In whole cells, the cholesterol signal observed is most abundant within the cytoplasm, most likely the golgi body, and in the cell membrane. Nuclear BASP1 was also successfully visualised in purified nuclei from shN MCF7 and shB MCF7 cells, where BASP1 signal was markedly diminished in shB MCF7 nuclei as expected. In the nuclei, cholesterol is present not only around the nuclear periphery, presumably within the nuclear membrane, but also speckled throughout the nuclear space. Interestingly, similar to the observations with alkyne-myristoyl, the level of cholesterol signal was lower in the shB MC7 cell line compared to the shN MC7 line in both whole cells and in nuclei. This suggests that downregulation of BASP1 expression coincides with a decrease in total cellular cholesterol levels. This suggests BASP1 could contribute to the stabilisation of cholesterol and/or cholesterol containing complexes in the cell.

To further examine a potential relationship between nuclear cholesterol and BASP1, imaging of alkyne-cholesterol was next conducted in nuclei from the K562 cell lines. V-K562, B-K562 and Y-K562 cells were incubated with alkyne-cholesterol, then purified nuclei from these cell lines were subjected to the click reaction and immunostaining in suspension with BASP1 and streptavidin antibodies. BASP1 protein was present throughout B-K562 and Y-K562 nuclei, and not detected in the negative control V-K562 nuclei (Figure 5.3B). Like in MCF7 nuclei, expression of BASP1 coincided with greater nuclear cholesterol signal. Cells expressing both wtBASP1 and Y12L-BASP1 appear to have a greater abundance of cholesterol in the nucleus, again suggesting BASP1 could have a role in controlling cholesterol

levels or stabilising cholesterol complexes. In the nuclei of all cell types cholesterol can be seen localised to the nuclear membrane, but also speckled throughout the intranuclear space, often in large distinct puncta. These images suggest that cholesterol is present throughout the nucleoplasm.

Mander's colocalisation analysis examining the overlap of BASP1 and cholesterol signals in B-K562 and Y-K562 nuclei is shown in Figure 5.3D. Here, M1 values represent the proportion of BASP1 signal that colocalises with cholesterol signal. The proportion of wtBASP1 colocalising with cholesterol was determined as 37.0%, and the proportion of Y12L-BASP1 colocalising with cholesterol was determined as 16.9%. This difference reveals a statistically significant decrease in the proportion of Y12L-BASP1 associated with cholesterol compared to wtBASP1. This provides further quantitative data to support the lack of cholesterol binding activity by Y12L-BASP1. These results also suggest that only a proportion of BASP1 in the cell is interacting with cholesterol at any one time, or that the alkyne-cholesterol visualised here does not necessarily represent the entire pool of nuclear cholesterol. M2 values generated from the Mander's colocalisation analysis represent the proportion of nuclear cholesterol signal that colocalises with BASP1. This was determined as 3.15% for wtBASP1 11.2% for Y12L-BASP1. These M2 values suggest that there is a large amount of nuclear cholesterol which is not associated with BASP1. Surprisingly, the values also indicate a statistically significant increase in the proportion of cholesterol coinciding with Y12L-BASP1 signal than wtBASP1 signal. Although this result could suggest that Y12L-BASP1 associates with cholesterol to a greater extent than wtBASP1 through other cholesterol binding proteins, an alternative is that the lower abundance of cholesterol in the Y-K562 cells causes the association between Y12L-BASP1 and cholesterol to appear artificially raised. Like all colocalisation data, the values from the Mander's colocalisation analysis should be carefully interpreted. False positive and false negative associations can easily be gained depending on the exact analysis parameters. Although the colocalisation analysis cannot provide clear quantitative evidence regarding the association of nuclear BASP1 and cholesterol, it has suggested a difference between wtBASP1 and Y12L-BASP1 cholesterol interaction and importantly has provided evidence to support the presence of cholesterol within the nuclear space.

Figure 5.3. Click Chemistry Confocal Imaging of Alkyne-Cholesterol in MCF7 Whole Cells, MCF7 Nuclei and K562 Nuclei. Click chemistry of shNegative (shN) and shBASP1 (shB) MCF7 or V-K562/B-K562/Y-K562 cells incubated with 10µg/ml alkyne-Myristoyl. Click chemistry reaction was followed by immunofluorescence with BASP1 and streptavidin antibodies. **A i)**, Cholesterol in whole MCF7 cells, **A ii)**, Cholesterol in purified MCF7 nuclei. Scale bar 10µm. **B**, BASP1 and Cholesterol in V-K562, B-K562 and Y-K562 nuclei. Scale bar 5µm. **C,** Azide-free control MCF7 (shN) and alkyne-free controls MCF7 (shN), V-K562, B-K562 and Y-K562. Scale bar 10µm. **D**, Quantification of the colocalisation of BASP1 and alkyne-cholesterol in B-K562 and Y-K562 nuclei as analysed using the Mander's colocalisation technique. **represents p<0.005, ***represents p<0.0005 following Students t test comparing M1 values from B-K562 and Y-K562 nuclei, and M2 values from B-K562 and Y-K562 nuclei over two independent experiments, n=35.

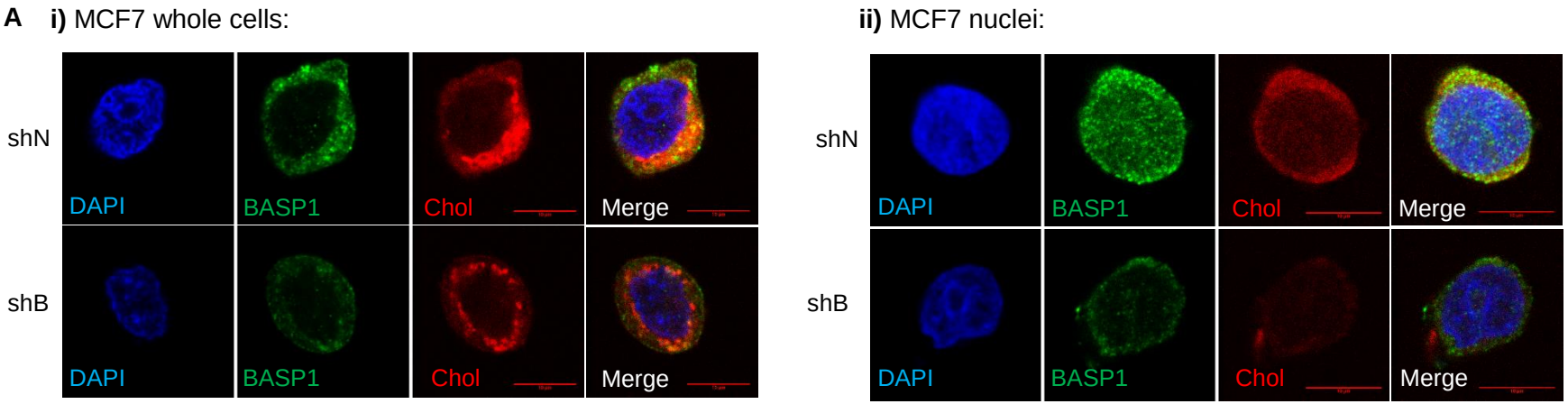

B K562 nuclei:

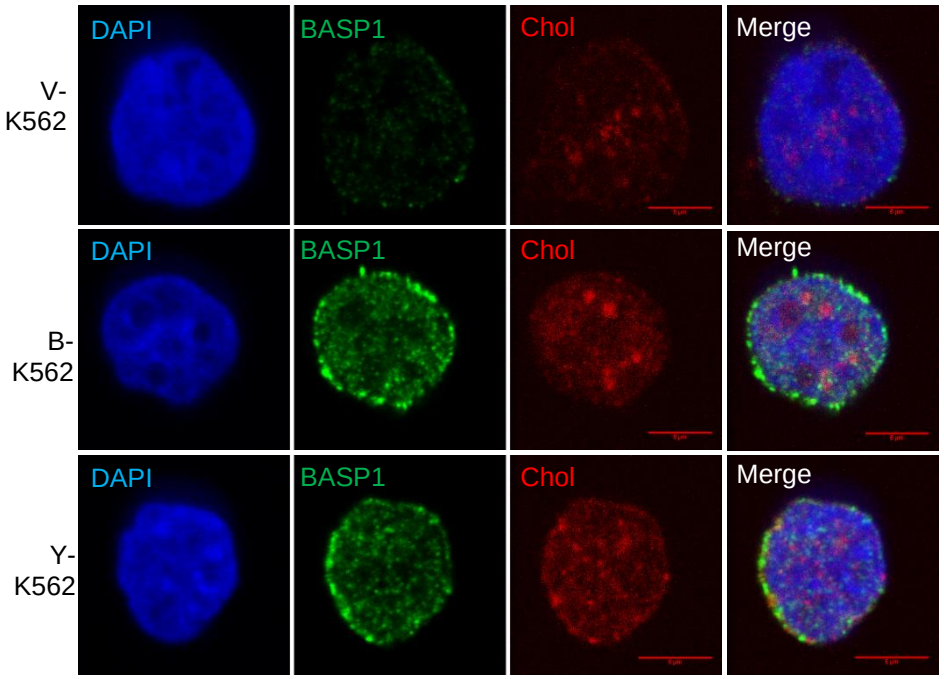

D

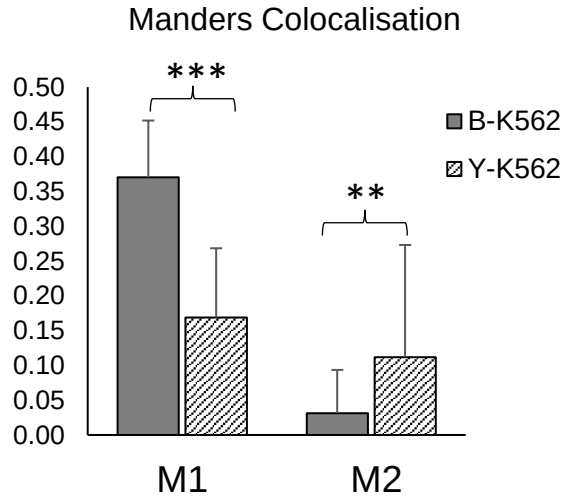

C

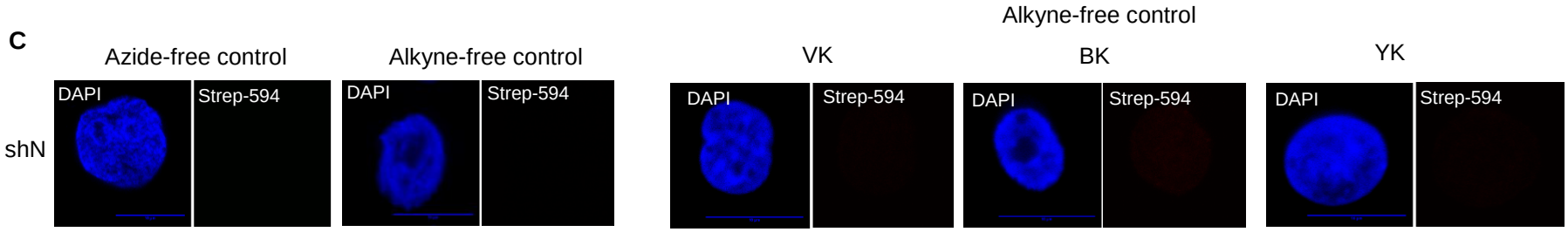

5.4 Gene Expression Analysis of WT1 Target Genes in V-K562, B-K562 and Y-K562

The V-K562, B-K562 and Y-K562 cell lines were next tested for their expression levels of a selection of WT1 target genes. Total RNA was extracted, cDNA samples were prepared and RNA expression levels determined using real time quantitative PCR. Three WT1 target genes AREG, ETS-1 and REN, were examined and confirmed to be repressed by BASP1 (Figure 5.4) [2, 3, 96]. Transcriptional repression of AREG and ETS-1 was not observed in Y-K562 cells but was still observed for REN. This result indicates that Y12L-BASP1 lacks gene repression activity towards select WT1 target genes and implicates cholesterol as an important BASP1 binding partner. Data presented in Figure 5.4 was generated by Samantha Carrera.

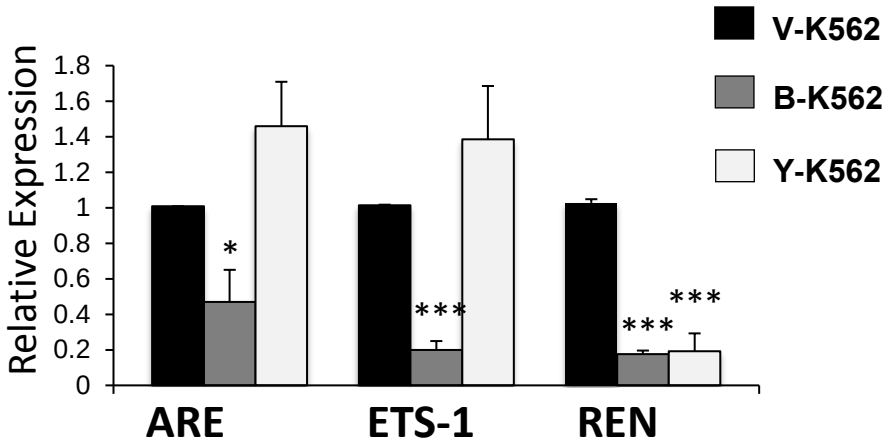

Figure 5.4. WT1 Target Genes are Selectively Repressed in Y12L-BASP1 Expressing K562 Cells. The relative expression of WT1 target genes in V-K562, B-K562 and Y-K562 cell lines was analysed, compared to control gene GAPDH. The expression levels of three target genes; AREG (amphiregulin), ETS-1 and REN are shown. Error bars representative of the standard deviation across 3 independent experiments. *p<0.05, ***p<0.0005 by Student's t test comparing B-K562 or Y-K562 with V-K562. ***Work carried out by Samantha Carrera.***

5.5 Investigating the Differentiation of V-K562, B-K562 and Y-K562 Cells

In order to further investigate the importance of the BASP1-cholesterol interaction, V-K562, B-K562 and Y-K562 cells were subjected to PMA treatment to induce their differentiation. As seen in previous reports treatment of V-K562 cells with PMA leads to their differentiation towards a megakaryocyte lineage [2, 256, 257]. V-K562 cells adhered to the culture dish and retained a round morphology (Figure 5.5). PMA-treated V-K562 cells upregulated expression of megakaryocyte markers DAB2 and ITGA2 (Figure 5.6). PMA treated B-K562 cells differentiated into neuron-like cells, as previously reported (Figure 5.5), and upregulated expression of neuronal markers MAO-A and ENC1 instead of the megakaryocyte markers (Figure 5.6) [2]. PMA treated Y-K562 cells also adhered to the culture dish, however arborisation was limited (Figure 5.5B). The gene expression profile of PMA treated Y-K562 cells shows that limited arborisation of these cells is likely due to the upregulation of both the megakaryocyte and neuronal markers (Figure 5.6). DAB2 was upregulated in Y-K562 cells to a level similar to that observed in V-K562 cells, and ITGA2 was upregulated in Y-K562 cells to approximately 50% the level seen in V-K562 cells. Neuronal marker MAO-A was not upregulated in Y-K562 cells, but ENC1 was upregulated to a similar level observed in differentiating B-K562 cells. These observations suggest that mutation of the cholesterol binding domain of BASP1 results in partial BASP1 function in both gene regulation and differentiation.

To further examine whether cholesterol interaction is important for BASP1 mediated differentiation of K562 cells to a neuronal phenotype, V-K562, B-K562 and Y-K562 cells were pre-treated for 12 hours with mevinolin and then subjected to PMA treatment for 72 hours. Mevinolin is a statin that inhibits the HMG-CoA reductase enzyme which is required for cholesterol biosynthesis [329]. The depletion of cholesterol by mevinolin caused a reduction in arborisation of B-K562 cells upon PMA treatment. Mevinolin treatment also lead to increased clumping of V-K562 and Y-K562 cells in suspension, and limited adherence of these cell lines to the culture dish. This suggests that cholesterol is broadly required for differentiation, and depletion of total cholesterol levels leads to diminished differentiation for all cell lines. It cannot therefore be reliably concluded from this data how depletion of cholesterol affects BASP1 driven differentiation of K562 cells. (50% of the data presented in Figure 5.5 and all data presented in Figure 5.6 was generated by Samantha Carrera).

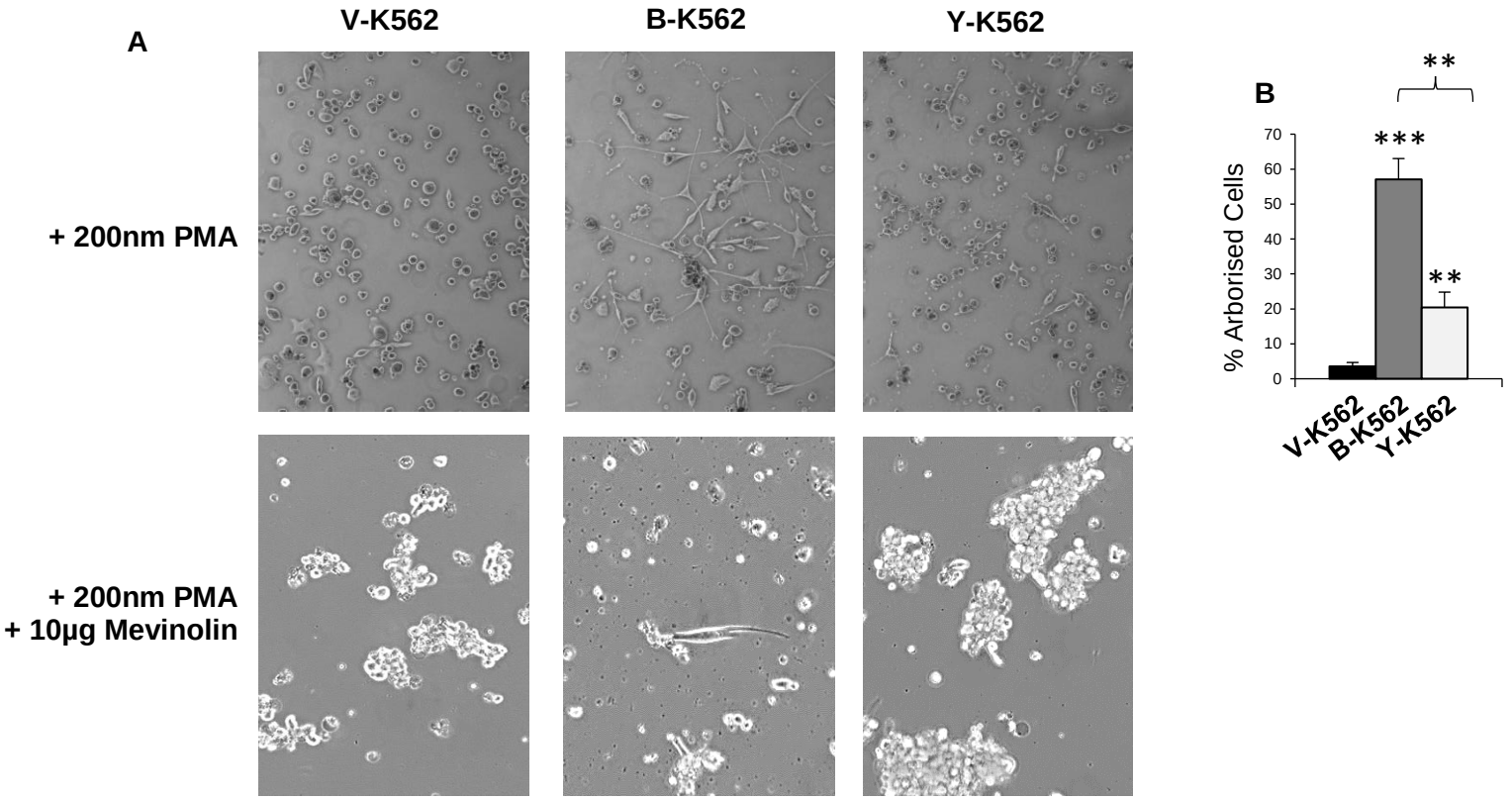

Figure 5.5. Y12L-BASP1 is Partially Functional in Differentiation. A, Top Panel: V-K562, B-K562 and Y-K562 cells were treated with 200nm PMA for 72 hours in 6 well plates and examined for the presence of differentiating cells. Lower Panel: V-K562, B-K562 and Y-K562 cells were pre-treated with 10µg mevinolin for 12 hours, and then treated with 200nm PMA for 72 hours, and examined for the presence of differentiating cells. **B**, Quantification of arborised cells following PMA treatment. Error bars representative of the standard deviation across 3 independent experiments. **p<0.005, ***p<0.0005 by Student's t test comparing B-K562 and Y-K562 with V-K562 cells. p value following Student's t test comparing B-K562 with Y-K562 also shown above brace. ***Work partially carried out by Samantha Carrera***

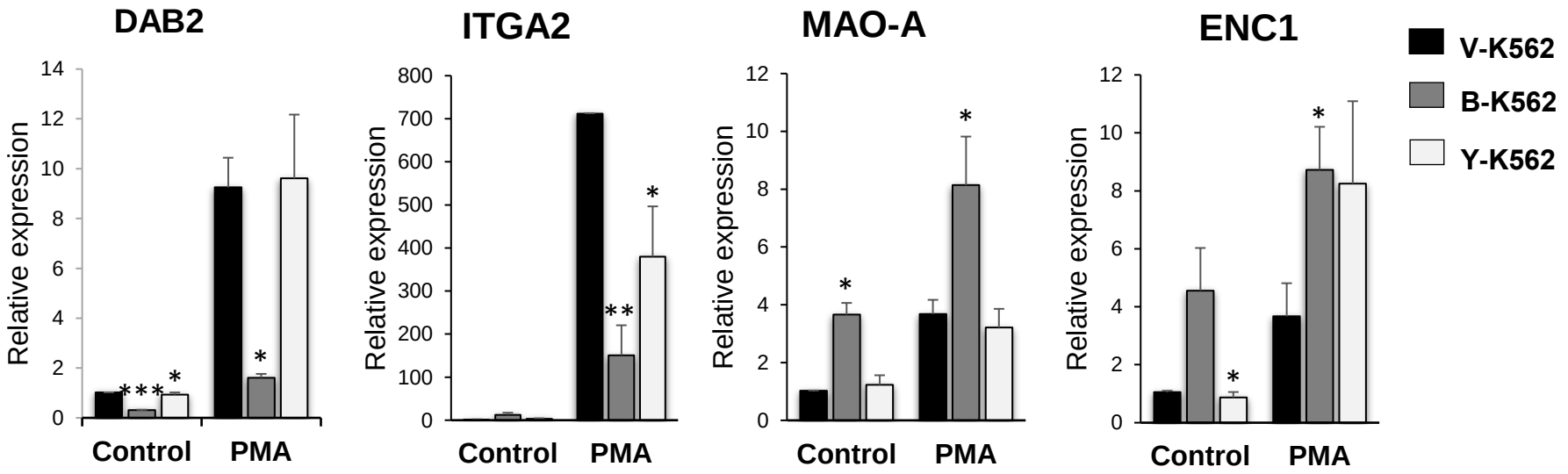

Figure 5.6. Y12L-BASP1 Upregulates Expression of Megakaryocyte Markers and Neuronal Genes During K562 Differentiation. The relative expression of megakaryocyte markers (DAB2, ITGA2) and neuronal markers (MAO-A, ENC1) in V-K562, B-K562 and Y-K562 cell lines was analysed, compared to control gene GAPDH following either vehicle control treatment, or 72 hour 100nm PMA treatment. Error bars representative of the standard deviation across 5 independent experiments. *p<0.05, **p<0.005, ***p<0.0005 by Student's t test comparing B-K562 or Y-K562 with V-K562 cells within control or PMA treated condition. ***Work carried out by Samantha Carrera.***

5.6 The Role of Cholesterol in Chromatin Modification at WT1 Target Gene Promoters

The data presented so far in this chapter has shown that the cholesterol binding mutant, Y12L-BASP1, is selectively defective at gene repression. This mutant is also defective at inducing the neuron-like differentiation of K562 cells. To further examine how the interaction of BASP1 with cholesterol may be important for the mechanism of WT1/BASP1 mediated gene repression, a series of ChIP and click-ChIP experiments were conducted.

5.6.1 Chromatin Immunoprecipitation of BASP1 and WT1 at WT1 Target Gene Promoters in V-K562, B-K562 and Y-K562 Cells

Detection of BASP1 and WT1 at the promoters of WT1 target genes in V-K562, B-K562 and Y-K562 cells was performed (Figure 5.7). Both wtBASP1 and Y12L-BASP1 were found to localise at the AREG, ETS-1, REN, VDR and JUNB promoters. The fold enrichment of BASP1 signal at these gene promoters was significantly greater in B-K562 and Y-K562 cells than in V-K562 cells (with the exception of Y12L-BASP1 at the VDR promoter) as determined using a student's t test (Figure 5.7A). The enrichment of BASP1 at these sites was also statistically significantly higher than background from the IgG control. These findings show that Y12L-BASP1 is equally capable of binding to WT1 target gene promoters as wtBASP1.

WT1 was also found to be bound at the AREG, ETS-1, REN, VDR and JUNB promoters, and binding was statistically significantly greater than the level of background signal (IgG) in all three cell lines, indicating that WT1 was bound to its target gene promoters regardless of wtBASP1 or Y12L-BASP1 expression (Figure 5.7B). There was no statistically significant difference in the binding of WT1 at these promoters between V-K562, B-K562 and Y-K562 cells, as determined using a student's t test, showing that WT1 is equally capable of binding to its target genes in all K562 derivative cell lines.

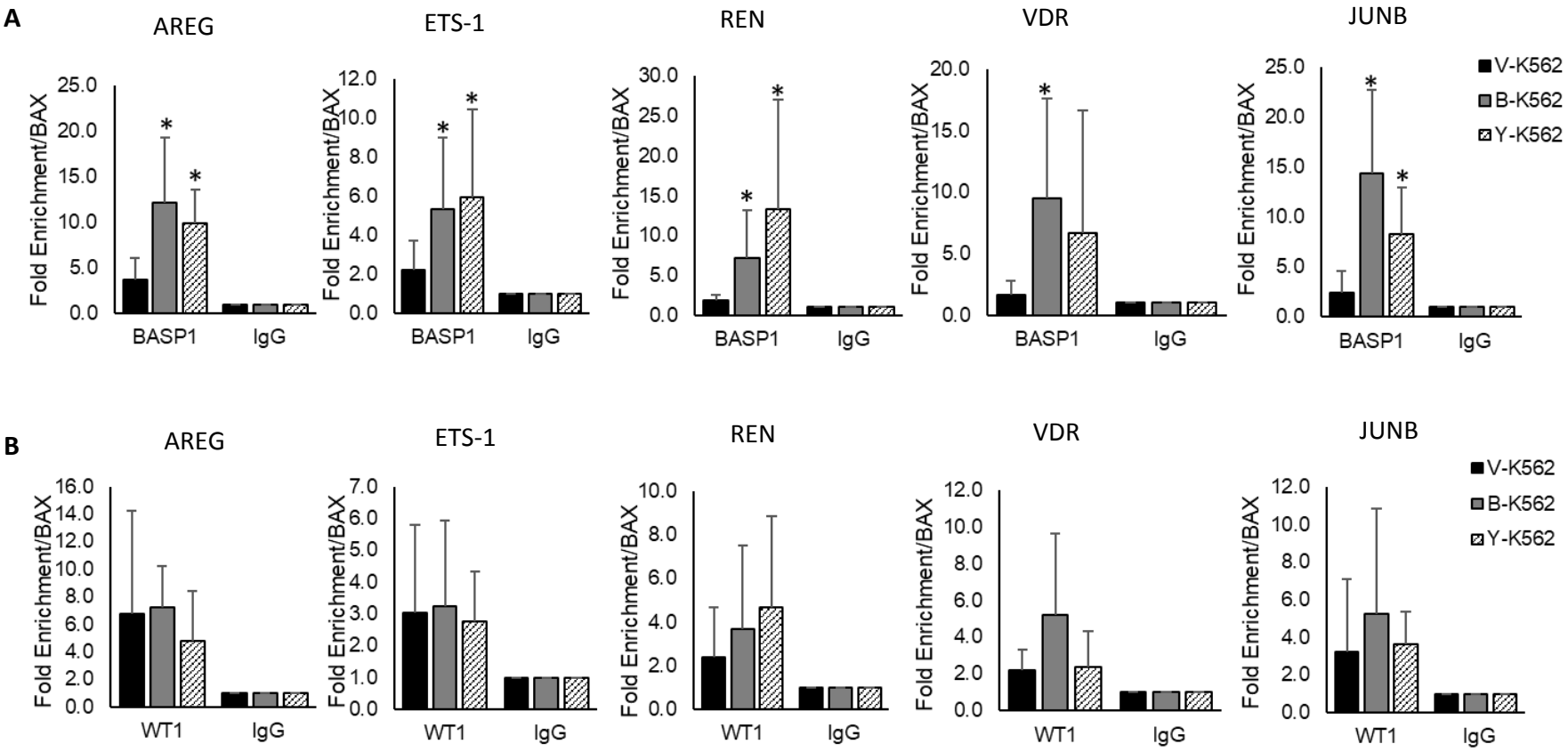

Figure 5.7. Recruitment of BASP1 and WT1 to AREG, ETS-1, REN, VDR and JUNB Promoters in K562 Cells. The presence of BASP1 (**A**) and WT1 (**B**) at the promoters of AREG, ETS-1, REN, VDR and JUNB was examined using chromatin immunoprecipitation in V-K562, B-K562 and Y-K562 cells. Error bars representative of the standard deviation of the mean, A) n=8, B) n=7. *p<0.05 by Student's t test comparing B-K562 or Y-K562 with control line V-K562.

5.6.2 Click Chemistry Chromatin Immunoprecipitation of Cholesterol at WT1 Target Gene Promoters

Following successful detection of wtBASP1, Y12L-BASP1 and WT1 bound to target gene promoters by ChIP, the presence of cholesterol itself at these promoters was next examined. A click-ChIP technique was developed in the previous chapter. Using this same technique with alkyne-cholesterol enabled detection of cholesterol binding at target genes in V-K562, B-K562 and Y-K562 cells (Figure 5.8). For this method, following incubation with alkyne-cholesterol cells were fixed in 4% formaldehyde for 4 hours, subjected to click reaction, then fixed again in 4% formaldehyde for 15 mins before cell pellets were lysed, chromatin sheared via sonication and lysates incubated with streptavidin beads to capture cholesterol (refer to Materials and Methods for full protocol). Fold enrichment was calculated as enrichment of cholesterol above signal from the alkyne-free negative control ChIP from each cell line. Fold enrichment of cholesterol was then compared to a control gene region (18S).

Cholesterol was enriched at multiple target gene promoters, coinciding with wtBASP1 recruitment, and not Y12L-BASP1 recruitment (Figure 5.8). When compared with the V-K562 cells BASP1-dependent recruitment of cholesterol only occurred to a statistically significant level at the VDR promoter. Although not to a significant level, cholesterol enrichment is raised in B-K562 compared to V-K562 and Y-K562 cells at all the remaining gene promoters, except REN. This indicates that cholesterol may be recruited by wtBASP1 to a subset of WT1 target genes.

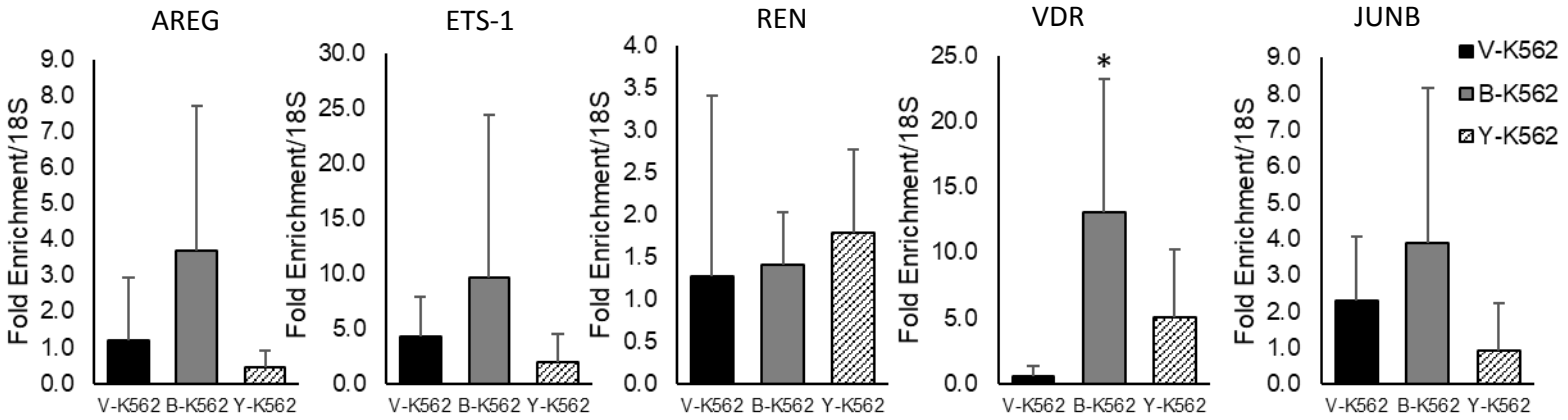

Figure 5.8. Cholesterol Detection at the Promoters of WT1 Target Genes in wtBASP1 Expressing K562 Cells. V-K562, B-K562 and Y-K562 cells were incubated with either ethanol (alkyne-free control) or 10ug/ml alkyne-Cholesterol, followed by a click chemistry reaction and sonication of the DNA. ChIP experiments were performed using a streptavidin-biotin pull down of azide-alkyne-cholesterol bound DNA regions. Fold enrichment of alkyne-Cholesterol at the AREG, ETS-1, REN, JUNB and VDR promoters in V-K562, B-K562 and Y-K562 cells compared to the alkyne-free control pull down, and control region 18S is shown. Error bars representative of the standard deviation of the mean, n=9. *$p<0.05$, by Student's t test comparing B-K562 or Y-K562 with control cell line V-K562.

5.6.3 Chromatin Immunoprecipitation of Active Chromatin Marks and RNA Polymerase II at WT1 Target Gene Promoters in V-K562, B-K562 and Y-K562 Cells

As previously described, our lab has demonstrated a decrease in activating H3K9Ac marks at BASP1 bound sites in a PIP_2-dependent manner [3]. Work completed in results chapter 1 of this study revealed that BASP1 causes the removal of several other activating histone marks including H3K4me^3 and affects RNA polymerase II recruitment and phosphorylation in a myristoyl-dependent manner. Here, following the detection of Y12L-BASP1 at WT1 target gene promoters, and the detection of cholesterol at multiple wtBASP1 bound promoters, the potential contribution of cholesterol to the removal of active marks at WT1/BASP1 target genes was assessed through ChIP. ChIP was conducted in V-K562, B-K562 and Y-K562 cells using antibodies targeting H3K9Ac, H3K4me^3 and total RNA polymerase II (Figure 5.9). Two genes were selected for examination, one gene that appears regulated by cholesterol in our analysis thus far (AREG) and one gene that does not appear to be regulated by cholesterol (REN).

In agreement with previous findings H3K9Ac marks were significantly reduced by wtBASP1 at both the AREG and REN promoters [3]. At the AREG promoter Y12L-BASP1 did not lead to a decrease in H3K9Ac marks. Similarly, a decrease in H3K4me^3 was observed in B-K562 cells compared to V-K562 cells, but Y-K562 cells do not show diminished H3K4me^3 marks at the AREG promoter. Total RNA polymerase II recruitment was also specifically reduced in B-K562 cells and not V-K562 or Y-K562 cells. This demonstrates that the Y12 residue is critical for BASP1 mediated removal of both H3K9Ac and H3K4me^3 marks and blocking RNA polymerase II recruitment at the AREG promoter.

At the REN promoter in Y-K562 cells H3K9Ac marks appear at an intermediate level between that of V-K562 and B-K562 cells (Figure 5.9). Furthermore, no difference in H3K4me^3 was seen at the REN promoter in Y-K562 compared to V-K562 cells, again suggesting Y12L-BASP1 has no capacity to remove H3K4me^3 marks at this site. It is important to note that although a decrease in H3K4me^3 marks was observed in B-K562 compared to V-K562 cells the abundance of H3K4me^3 at this promoter in all cell lines is substantially lower than at AREG (or any of the other genes) when compared to H3K9Ac and control IgG. A fold enrichment/control of only 1.10 in V-K562 cells suggests that H3K4me^3 does not play a significant role in the regulation of the REN gene. Similarly, total RNA polymerase II levels are only

marginally reduced at the REN promoter when either wtBASP1 or Y12L-BASP1 are present. This suggests that RNA polymerase II recruitment is not significantly regulated by BASP1 at this gene. These data again indicate that BASP1 elicits distinct effects at the AREG and REN promoters and further highlights that the role of cholesterol in transcription regulation is promoter specific. All data presented in Figure 5.9 was generated by Samantha Carrera.

As mentioned in results chapter 2, our laboratory has undertaken a number of approaches to analyse BASP1 interactors, including TMT/multiplexing of BASP1 immunoprecipitates to identify differences in wtBASP1 and G2A-BASP1 interactomes (Figure 4.2). The same approach was also used to examine Y12L-BASP1 interactors and revealed that BASP1-PIP_2 and BASP1-cholesterol interact with both distinct and overlapping protein complexes. BASP1 interactions with HDAC1, BRG1 and emerin are known to require PIP_2 but not cholesterol, whereas prohibitin requires both lipids [3, 54, 96]. Conversely, a BASP1-Lysine demethylase 2B (KDM2B) interaction was identified and appears to be solely reliant on cholesterol. H3K4me^3 is the major substrate of KDM2B suggesting that the BASP1-cholesterol interaction may function to remove H3K4me^3 activation marks through this enzyme [330]. Furthermore, given that Y12L-BASP1 interacts with HDAC1 but fails to support deacetylation of H3K9Ac it can be speculated that the removal of H3K4me^3 marks by wtBASP1 may be a prerequisite for inducing the activity of HDAC1.

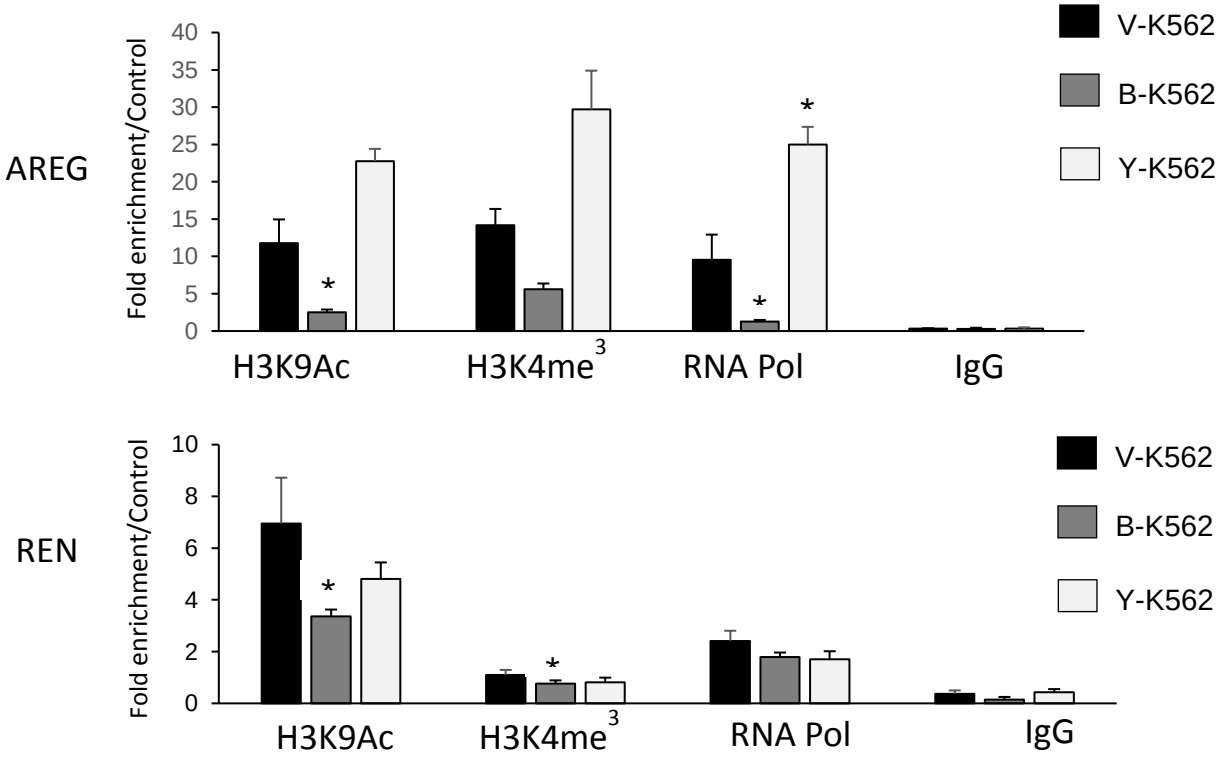

Figure 5.9. Y12L-BASP1 is Selectively Defective in Histone Modification at WT1 Target Genes. The presence of H3K9Ac, H3K4me^3 and RNA polymerase II (total) at the promoters of the WT1 target genes AREG and REN was examined using chromatin immunoprecipitation in V-K562, B-K562 and Y-K562 cells. Error bars representative of the standard deviation of the mean, n=4. *p<0.05, by Student's t test comparing B-K562 or Y-K562 with control cell line V-K562. ***Work carried out by Samantha Carrera.***

5.7 Discussion of Chapter 3 Results

5.7.1 Validation of Y12L-BASP1 Cholesterol Binding Mutant

The work presented in this chapter builds upon our previous studies identifying the role of PIP_2 in WT1/BASP1 mediated gene repression. Having previously characterised PIP_2-dependent transcriptional regulation by BASP1, here the previously unexplored contribution of cholesterol to WT1/BASP1 mediated gene repression was investigated. Firstly, a K562 cell line was generated to stably express a cholesterol binding mutant BASP1 protein via Y12L mutation to disrupt the critical tyrosine residue in the CRAC domain. Others have previously reported disruption of cholesterol interaction through mutation of the central tyrosine within a CRAC domain [331] and this has also previously been reported for BASP1 [88]. Confirmation of the lack of cholesterol binding by Y12L-BASP1 was achieved through an *in vitro* cholesterol binding assay and cholesterol click-ChIP. This analysis confirms that cholesterol cannot interact with BASP1 through any other means.

5.7.2 Imaging Intranuclear BASP1 and Cholesterol

Previously, the study of nuclear cholesterol has been limited by lack of tools to reliably distinguish membrane cholesterol from intranuclear cholesterol [332]. Application of the click chemistry imaging technique developed earlier in this study has provided a reliable method to examine the localisation and abundance of BASP1 and cholesterol in the K562 cell lines. Images collected here support biochemical evidence in the literature that cholesterol is present throughout the nucleus; in the membrane, in intranuclear pools and within the nucleolus (Figure 5.3). This data also provides further quantitative evidence of reduced cholesterol binding by Y12L-BASP1 compared to wtBASP1.

Here cholesterol was observed throughout the nucleus, often within puncta in the nucleoplasm. This fits with the evidence that nuclear cholesterol forms complexes with sphingomyelin and nuclear proteins that are not just restricted to the nuclear membrane [333]. Other intranuclear cholesterol complexes containing sphingomyelin and phosphatidylcholine have functional roles in transcription, including the stabilisation of newly transcribed RNA and the activation of signalling pathways such as STAT3 during cell proliferation [122, 334, 335]. It would be interesting to assess in more detail whether cholesterol interacts with the WT1/BASP1 repression complex within these nuclear speckles. This would improve

our knowledge of the subnuclear localisation of the cholesterol that contributes to gene regulation. This is important as cholesterol-sphingomyelin-phosphatidylcholine complexes are known to interact with chromatin and have been shown to associate with lamin B, suggesting these complexes could also potentially contribute to the linking of chromatin and the inner nuclear membrane [334]. Throughout results chapter 2 it was hypothesised that PIP_2 binding is important for WT1/BASP1 complex localisation to the nuclear periphery to induce gene repression; it would be interesting to establish whether cholesterol is also important for localisation of the complex to the nuclear periphery, and what effect this has on the repression of WT1 target genes.

It is interesting that expression of BASP1 coincides with increased cholesterol signal within the nucleus in both MCF7 and K562 cells. This implies that BASP1 may stabilise cholesterol levels and/or intranuclear cholesterol complexes. WT1 is already known to regulate the SREBP genes and can therefore affect the cholesterol/fatty acid synthesis pathway, plus cholesterol itself is involved in a feedback loop for its own synthesis and uptake [336, 337]. It is possible that, as a cofactor of WT1, BASP1 binding could alter cholesterol regulation.

Alternatively, the lower levels of cholesterol detected in shB-MCF7 and V-K562 could also be reflective of the increased tumourigenicity of these cells [89]. The role of cholesterol in cancer is complex and it is not yet known if changes in cholesterol regulation are a consequence of, or actually contribute to, cellular transformation. However, cholesterol is increasingly thought to actively alter the progression and severity of multiple cancer types, with both hypocholesterolaemia and hypercholesterolaemia implicated in tumour progression [166-168]. Interestingly, hypocholesterolaemia has been proposed as a biomarker for severe leukaemia, where cells with lower cholesterol levels express higher levels of cell proliferation genes including RNA polymerase II, STAT3, PKCz and Cyclin D1, and consequently a greater rate of growth [167]. It would be interesting to assess whether the tumour suppressor function of BASP1 extends to modulating these cell proliferation genes through cholesterol regulation.

5.7.3 The Role of Cholesterol in the Mechanism of BASP1/WT1 Mediated Gene Regulation

Further experiments presented in this chapter looked at whether the BASP1-cholesterol interaction could be important for the role of BASP1 in differentiation. We have previously established that the WT1/BASP1 complex redirects the

differentiation pathway of K562 cells away from a megakaryocytic lineage towards a neuron-like lineage [2]. Here Y12L-BASP1 expressing cells differentiated into an intermediate cell-type, expressing markers of both megakaryocytes and neurons (DAB2, ITGA2, ENC1), implicating cholesterol binding as important for the regulation of a selection of WT1/BASP1 targets through differentiation. The mixed gene expression profile likely explains the intermediate arborisation and morphology phenotype of these cells. Mevinolin treatment appeared to block the differentiation of all K562 derivatives, indicative of a vital requirement for cholesterol during differentiation of this cell line. In many cell types cholesterol depletion activates signalling proteins such as extracellular signal-regulated kinase (ERK), human epidermal growth factor receptor 2 (HER2) or epidermal growth factor receptor (EGFR) which are known to affect differentiation [338, 339]. Cholesterol depletion is also known to activate the Wnt/beta-catenin pathway to enhance myogenic differentiation and activate p38α/β which alters gene expression of the keratinocyte differentiation marker involucrin during the early stages of keratinocyte differentiation [338, 340].

The molecular basis of the observed inhibition of differentiation following mevinolin treatment in this study was not investigated. More thorough study through gene expression analysis may provide greater insight into the role of cholesterol during K562 differentiation. It must also be acknowledged that depletion of total cholesterol in this manner could diminish overall cellular health thus the observed block of differentiation in K562 following cholesterol depletion could be an artefact of poor cell viability. Different doses of mevinolin, treatment with other statins (atorvastatin), or use of siRNA targeting HMG-CoA reductase should be trialled to optimise the cholesterol depletion. Subsequent protein and gene expression analysis would provide thorough assessment of the effect of cholesterol depletion on K562 differentiation.

The mechanism by which cholesterol contributes to WT1/BASP1 mediated transcriptional repression was next investigated. Firstly, the binding of Y12L-BASP1 to WT1 target genes was confirmed via ChIP assays with V-K562, B-K562 and Y-K562 cells. This demonstrated that the BASP1-cholesterol interaction is not required for BASP1 to bind promoters. Following this, using the click-ChIP technique previously developed in this study, cholesterol was detected at select wtBASP1 bound promoters. Unlike other WT1 targets, the REN promoter does not undergo BASP1-mediated cholesterol recruitment. This is interesting as the gene expression

analysis conducted earlier in this chapter indicated that the repression of REN by BASP1 occurs through a cholesterol-independent mechanism. This click-ChIP data forms the first evidence for the direct recruitment of cholesterol to gene promoters and raises the possibility that cholesterol plays a role in BASP1 mediated repression at selected WT1 target genes.

It should be noted that there was large variability in cholesterol signal detected in the click-ChIP assay, particularly when compared to the myristoyl-click-ChIP and signal gained from standard ChIP assays in this study. This is likely due to the difficulty in cross linking cholesterol. As cholesterol lacks formaldehyde targeted structures such as primary amines or tyrosine rings the crosslinking of cholesterol is reliant upon its capture within protein complexes. Further optimisation of the crosslinking and fixing stages would be beneficial to conduct further repeats of the click-ChIP assay and validate these findings.

Combined with the gene expression data showing that Y12L-BASP1 is defective at inducing gene repression at the same select target genes, the click-ChIP data provides powerful evidence for the role of cholesterol in gene repression by BASP1. Previously cholesterol has only been shown to directly interact with nucleosomes, binding to multiple key histone amino acids in the H4 tail and the docking domain between the histone clusters H3-H4 and H2A-H2B [139]. Cholesterol's interaction with nucleosomes is thought to contribute to chromatin compaction by promoting the formation of 10nm and 30nm chromatin fibres [139]. Data presented here provides evidence that cholesterol also contributes to gene repression through binding transcriptional complexes on DNA at specific sites.

Others have shown that cholesterol-sphingomyelin-protein complexes interact with chromatin and dynamically change in composition during the transcription process, such as during liver regeneration [122, 133]. As BASP1 has an established role in mediating changes to chromatin modifications, work presented towards the end of this chapter examined how cholesterol interaction may contribute to BASP1 mediated removal of activating histone marks and the recruitment of RNA polymerase II. Through the examination of H3K9Ac, H3K4me^3 and total RNA polymerase II at WT1 target genes via ChIP it was revealed here for the first time that BASP1 mediated reduction in H3K9Ac and H3K4me^3 and reduction of RNA polymerase II recruitment is dependent upon a functional CRAC domain in BASP1. These data implicate cholesterol as an important player in the regulation of

chromatin modifications and the initiation of transcription at a subset of BASP1 regulated WT1 targets.

Identification of KDM2B as a candidate BASP1-cholesterol interactor provides a potential mechanism through which BASP1 and cholesterol mediate changes in chromatin marks at targeted genes. The KDM2B enzyme predominantly targets H3K4me^3 for demethylation, but also shows activity towards H3K36me^3, a mark shown in results chapter 1 of this study to be down regulated in a BASP1-myristoyl dependent manner (Figure 3.9A) [330, 341]. Validation of a BASP1-KDM2B interaction, and the recruitment of KDM2B to WT1 target genes is required to confirm whether this mechanism may account for the observed downregulation of H3K4me^3 in this study. Interestingly, KDM2B is known to upregulate EZH2 expression and subsequently contribute to the progression of ovarian cancer *in vitro* and *in vivo* [341]. Furthermore, the KDM2B-EZH2 interaction has been shown to promote demethylation of H3K36me^2 and H3K4me^3 at the *Ink4a*/*Arf* locus in mouse embryonic fibroblasts [342]. Demethylation of these marks at the *Ink4a*/*Arf* locus then interferes with RNA polymerase II binding, leading to transcriptional silencing [342]. This KDM2B-EZH2 based gene silencing mechanism is similar to the observations at BASP1-bound sites described in this study. It would therefore be of great interest to examine whether a BASP1-KDM2B-EZH2 interaction at WT1 target genes may contribute to the removal of H3K4me^3 and H3K36me^2, upregulation of H3K27me^3 and H3K9me^3, and decrease in RNA polymerase II recruitment and activation, as demonstrated in results chapter 1 (Figures 3.10-3.12). Validation that the BASP1-KDM2B interaction is cholesterol-dependent would solidify a role for cholesterol in the molecular mechanism of gene silencing by the BASP1 repression complex.

Interestingly, although repression of the AREG gene has been shown to be dependent on the BASP1-cholesterol interaction, H3K9Ac is not deacetylated at the AREG promoter when Y12L-BASP1 is present. Our BASP1-interactome proteomic analysis showed that Y12L-BASP1 can still interact with HDAC1, and it therefore could be recruited with Y12L-BASP1 to the AREG promoter. ChIP analysis to examine HDAC1 recruitment in V-K562, B-K562 and Y-K562 cells could confirm this. If indeed HDAC1 is recruited, this raises the possibility that H3K4me^3 demethylation is a prerequisite for HDAC1 to deacetylate H3K9. Interestingly, the HDAC Rpd3L has recently been shown to be targeted to active promoters marked by H3K4 methylation in order to induce histone deacetylation and transcriptional

repression in yeast [343]. A functional link between H3 acetylation and H3K4me^3 has further been reported whereby the inhibition of HDACs leads to the upregulation of H3K4 methylation, resulting in transcriptional activation of genes including *KLF4* and *E-cadherin* in prostate cancer cells [344, 345]. The exact nature of the functional connection between H3 acetylation and H3K4 methylation remains to be explored but it would be interesting to investigate whether a specific sequence of chromatin modifications is required at BASP1 regulated target genes.

The gene specific requirement for cholesterol in the WT1/BASP1 repression mechanism has consistently been identified throughout this chapter. REN, a gene repressed in both B-K562 and Y-K562 cells, did not show cholesterol recruitment at the promoter via click-ChIP, displayed endogenously low levels of H3K4me^3 and shows no determinable difference in RNA polymerase II recruitment. Conversely, AREG, a gene repressed only in B-K562 cells and not Y-K562 cells recruited cholesterol to the promoter via click-ChIP, displayed clear removal of active histone marks H3K9Ac and H3K4me^3 and showed reduced RNA polymerase II recruitment. Together these findings suggest that cholesterol is selectively required for WT1/BASP1 mediated gene repression and is important for the mechanism of BASP1 mediated gene silencing. The low abundance of H3K4me^3 marks at the REN promoter even in V-K562 cells may explain why a BASP1-cholesterol based repression mechanism is not apparent at this gene, as there is limited scope for further demethylation and therefore limited scope to alter the chromatin environment through removal of this mark. Evidence from results chapter 1 showed that at the REN promoter RNA polymerase II Ser5 phosphorylation and CDK7 recruitment was reduced by wtBASP1. The observed repression of REN by Y12L-BASP1 signifies that these BASP1 functions are cholesterol independent. It would be interesting to assess RNA polymerase II Ser5 phosphorylation and CDK7 recruitment in Y-K562 cells via ChIP to test this. One further explanation as to why the repression mechanism of REN may differ to that of other genes could be that the WT1 binding site for REN is located within an enhancer sequence, rather than within the proximal promoter region like the majority of WT1 targets [346-349]. WT1 binds within the human renin conserved region (hRENc), part of a highly conserved enhancer sequence approximately 11kb upstream of the promoter [346, 350]. BASP1 may therefore require a different mechanism of repression to influence chromatin dynamics 11kb from the promoter.

5.7.4 Summary of Results Chapter 3

A summary of the data presented in this final chapter is shown in Figure 5.10. The schematic illustrates the hypothesis that, like PIP_2, cholesterol is an important component of the WT1/BASP1 repression complex but is recruited to selected target gene promoters. The figure demonstrates that cholesterol is present and is important for the recruitment of further chromatin modifying components, which ultimately reduce active histone marks H3K9Ac and $H3K4me^3$ and contribute to reduced RNA polymerase II recruitment and repression of transcription. The histone lysine demethylase enzyme KDM2B is shown as a candidate for mediating the removal of $H3K4me^3$ marks. Ultimately, these cholesterol-dependent changes at select WT1 target genes have been shown to lead to altered gene expression profiles and an altered differentiation pathway in K562 cells.

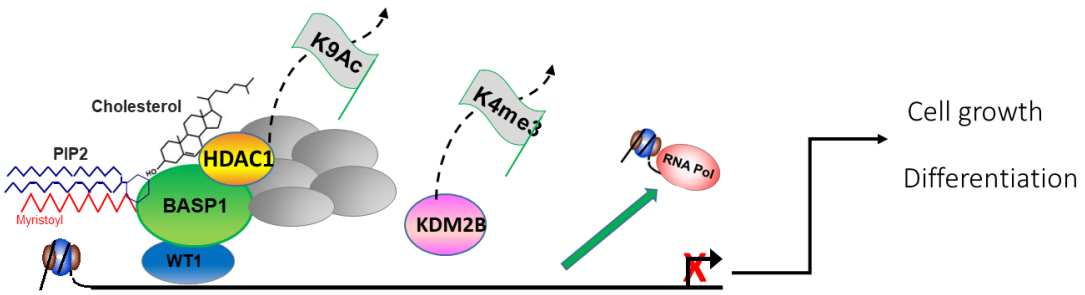

Figure 5.10. Chapter 3 Summary: A Role for Cholesterol in Selective Transcriptional Repression by BASP1.
Representation of WT1 target gene promoters in wtBASP1 expressing cells, with bound cholesterol. Cholesterol is shown as part of the WT1/BASP1 repression complex. Dashed black arrows represent HDAC1 removal of H3K9Ac, an established mechanism of gene repression for this complex. Dashed black arrow also indicates removal of $H3K4me^3$ marks by KDM2B, the hypothesised cholesterol-dependent activity. Subsequently, RNA polymerase II is displaced from DNA (indicated by green arrow), and transcription is downregulated (red cross). This cholesterol-dependent activity ultimately leads to changes in expression of genes that control cell growth and differentiation.

6 Final Discussion

6.1 The Role of BASP1 Lipidation in WT1/BASP1 Mediated Gene Regulation

This study has generated several new findings about the activity of BASP1 and provided molecular evidence that demonstrates the importance of lipid interactions for BASP1 transcription regulation function. This includes evidence that myristoylation of BASP1 is important for the removal of the histone methylation marks H3K36me^3 an H3K4me^3. This is in addition to previous evidence demonstrating BASP1-mediated removal of H3K9Ac [3]. Together, this now shows that the WT1/BASP1/PIP_2 complex mediates the removal of multiple histone modifications associated with transcription activation in order to facilitate gene repression. Further, it was demonstrated that BASP1 recruits EZH2 to target gene promoters, which correlated with an increase in H3K27 and H3K9 trimethylation. This implicates BASP1 as a mediator of repressive histone modifications for the first time, possibly through recruitment of the PRC2 complex. Gene repression by the WT1/BASP1/PIP_2 complex was also accompanied by reduced CDK7 recruitment and reduced RNA pol II phosphorylation suggesting BASP1 can additionally contribute to gene repression through the inhibition of transcription initiation. These findings expand our understanding of the mechanism of action of the WT1/BASP1/PIP_2 complex in modifying the chromatin environment at its target genes and inhibiting transcription initiation.

Additional findings in this study demonstrated for the first time that the mechanism of action of the BASP1 transcription repression complex is also dependent on an interaction with cholesterol at select target genes. Cholesterol was shown to be directly recruited to BASP1 bound gene promoters and binding of BASP1 to cholesterol was required for the removal of H3K9Ac and H3K4me^3. The importance of the cholesterol interaction for BASP1 function in transcription and cell response was further demonstrated through the defective differentiation of Y12L-BASP1 expressing cells. This work shows a direct role for cholesterol in BASP1-mediated gene regulation for the first time and implicates cholesterol as an important regulator of chromatin modifications at select target genes.

Work in this thesis demonstrates that myristoylation of BASP1 affects its interactions with multiple proteins of the inner nuclear membrane (INM), its association with the nuclear matrix as well as its subnuclear localisation. This further implicates a critical role for lipids in controlling the subnuclear localisation of the WT1/BASP1 complex. A key question remains whether the WT1/BASP1/PIP_2

complex carries out its regulation of WT1 target genes at the nuclear periphery, associated with the nuclear membrane, or within chromatin bodies in the nuclear matrix. Results from this study show that emerin, BAF and LAP2α can all bind to BASP1 bound promoters in a myristoyl-dependent manner and suggest that emerin may contribute to the mechanism of gene repression. Fluorescence Recovery After Photobleaching (FRAP) and Fluorescence Loss In Photobleaching (FLIP) analysis has demonstrated that emerin is present at the nuclear membrane and is relatively immobile [351]. Similarly, transmission electron microscopy and fluorescence microscopy have also provided evidence that emerin is restricted to the nuclear membrane [352, 353]. Emerin has been observed in the nuclear space, bound to BAF, but only for a very restricted period during the two minutes immediately following mitosis, after which time both proteins promptly recolocalise at the nuclear periphery [353]. Furthermore, Fluorescence Resonance Energy Transfer (FRET) results using fluorescent tagged proteins have shown that BAF associates directly with emerin at the INM of living cells [351]. It is possible that the established bridging activity of BAF also applies to BASP1 regulated genes, such that BAF contributes to the linking of BASP1 regulated chromatin and the nuclear lamina [184, 187, 188]. Such evidence supports the proposal that emerin and BAF binding to WT1/BASP1 bound promoters could facilitate localisation of the WT1/BASP1/PIP_2 complex and target genes at the nuclear periphery. This proposal aligns with the body of evidence that suggests the nuclear periphery is frequently a site of gene repression.

However, in stark contrast to other INM components (such as emerin, LAP2β and MAN1), FRAP and FLIP analysis of BAF showed that whilst it is present at the nuclear membrane it also diffuses rapidly throughout the nuclear space [351]. This raises the question of whether BAF binds chromatin at the nuclear lamina, in the nuclear interior, or both. For some genomic regions, even including many genes within lamina associated domains (LADs), detachment from the nuclear membrane does not always lead to strong transcriptional activation [227]. Like BAF, lamin A is located at the INM and partially within the nucleoplasm [351]. Binding of lamin A to gene promoters has an established association with gene repression, and downregulation of lamin A results in an increase in the active histone mark $H3K4me^3$ [354, 355]. Furthermore, LAP2α also resides in the nuclear lamina and throughout the nucleoplasm and has an established role in the structural organisation of the nucleus and gene regulation in the nuclear matrix [311, 356]. It is possible that the association of nucleoplasmic proteins such as BAF, lamin A, and

LAP2α could facilitate the maintenance of a repressive state of WT1/BASP1 targeted promoters in the nucleoplasm. BASP1, WT1, PIP_2 are after all also known to reside in nuclear speckles [3, 222].

If the WT1/BASP1 transcription repression complex does function in the nuclear space the complex must somehow facilitate the binding of lipids in a biochemically feasible manner. The assembly of large protein complexes that shield PIP_2 and cholesterol is one possible mechanism. A large number of BASP1 repression complex components including prohibitin, BRG1, HDAC1 in addition to those implicated in this study, emerin, LAP2α and BAF, EZH2, KDM2B and components of nuclear actin complexes β-actin, Myosin 1C, nucleophosmin, gelsolin and flightless, are already known suggesting that BASP1 can indeed participate in large complexes [3, 89, 96]. Previous gel filtration analysis has also evidenced that BASP1 is contained within high-molecular-weight complexes of ~700 kDa [85]. Furthermore, given the evidence that BASP1 forms oligomeric structures, it is reasonable to speculate that multimers of BASP1 could also potentially shield hydrophobic lipid tails and stabilise intranuclear lipid complexes [123, 124]. The contribution of lipids to the functional segregation of membrane proteins and interactors is well established, perhaps it is also possible that lipids act as a molecular glue to facilitate the organisation and formation of different nuclear bodies and complexes, including the BASP1 repression complex.

Although debated for some time, it has now been shown using confocal and electron microscopy that nuclear lipid droplets are localised within the nucleoplasm of a range of human and mammalian cell lines [127]. Interestingly, nuclear lipid droplets were found to be closely associated with protrusions of the inner nuclear envelope and with PML bodies [357]. PML-II, one PML protein isoform found in PML bodies, appears to be closely linked to the formation of nuclear lipid droplets. PML-II correlated with the presence of nuclear lipid droplets and overexpression of mutant PML-II, which does not distribute along the nuclear envelope, failed to increase the number of nuclear lipid droplets seen after overexpression of the wild type protein [357]. This suggests that the binding of PML-II to the nuclear membrane may be involved in the formation of nuclear lipid droplets. Interestingly, BASP1 has already been identified in the proteome of cholesterol rich nuclear lipid droplets [358]. It is possible that BASP1, as a lipid binding protein which is also found in both PML bodies and the nuclear membrane, could also contribute to the formation of nuclear lipid droplets [85].

Nuclear lipid droplets contribute to the newly accepted phase separation of nuclear content. The emulsion of phase separated droplets of DNA and protein that forms the basis of the nucleoplasm is thought to aid the compartmentalisation of chromosomes, the assembly of nuclear bodies, and the regulation of gene expression [247, 250, 251]. The importance of phase separation for gene regulation has so far predominantly focused on its effect on gene activation, where it has been linked to the clustering of coactivated genes and enhancers [359]. More recent evidence, however, has shown that phase separation could also be important for heterochromatin formation as HP1α was shown to induce the formation of liquid droplets containing known components of heterochromatin, including nucleosomes [249, 253]. Studying the structure and function of nuclear lipid droplets is a means to better understand how phase separation of nuclear content controls nuclear structure and function including the activation and repression of gene expression. It is possible that BASP1, as a lipid binding protein that associates with the nuclear membrane and PML bodies could also contribute to the formation nuclear lipid droplets. Further, the formation of nuclear lipid droplets could be a further means by which BASP1 interfaces the INM with chromatin modification and gene regulation.

In conclusion, data presented in this study shows that $PI(4,5)P_2$ and cholesterol play critical roles in the mechanism of transcriptional repression by the WT1/BASP1 complex. Myristoylation of BASP1 and the BASP1-cholesterol interaction are now known to be important for the recruitment of repression complex components, in mediating changes to the chromatin environment at WT1/BASP1 target gene promoters and in regulating the subnuclear localisation of BASP1. This evidence supports a model whereby an interaction between BASP1 and INM proteins is important for mediating transcriptional repression, and implicate $PI(4,5)P_2$ as a linker between BASP1 and INM proteins. These findings provide insight into the molecular mechanisms through which nuclear lipids contribute to transcriptional regulation. Further study of BASP1 and nuclear lipid complexes could give important insights into the nature of nuclear protein-lipid complexes, their regulation of gene expression and their contribution to nuclear domain organisation.

6.2 Future Directions

6.2.1 BASP1 Recruitment of EZH2/PRC2 Complex

It was demonstrated here for the first time that BASP1 exhibits myristoyl-independent addition of repressive chromatin marks to WT1 target genes. It is now important to establish whether the observed increase in H3K27me^3 and H3K9me^3 is indeed performed by EZH2 as part of the PRC2 complex, and whether repression of WT1 target genes is dependent upon this activity. Firstly, validation of the BASP1-EZH2 interaction should be completed through BASP1 immunoprecipitation (wtBASP1 and G2A-BASP1) and immunoblotting for EZH2, as well as other PRC2 components (Suz12, Eed and RbAp48). The dependence on EZH2 for BASP1 mediated repression should be assessed through siRNA depletion of EZH2 followed by gene expression analysis of WT1 target genes in the K562 cell lines. ChIP should also be conducted to assess changes in chromatin marks at these sites following siRNA depletion of EZH2. It is predicted that EZH2 depletion will affect the placement of H3K27me^3 and H3K9me^3 marks at promoters in both B-K562 and G-K562 cells. As a consequence, it is predicted that repression of WT1 target genes would be relieved in the B-K562 cell line. Gene expression analysis of WT1 targets and ChIP of chromatin marks following PRC2 inhibitor treatment inhibitor would further support the above proposed experiments. These experiments will establish EZH2 as an essential cofactor for myristoyl independent function of BASP1. Furthermore, completion of these proposed experiments also in Y12L-BASP1 expressing cells would allow assessment of whether cholesterol is required for these BASP1 functions at select WT1 targets.

6.2.2 WT1/BASP1 Mediated Gene Repression at the Nuclear Periphery

Data presented in results chapter 2 suggest that BASP1 regulates chromatin dynamics and represses transcription through myristoyl-dependent interactions with INM proteins. To experimentally examine this proposal high resolution Stimulated Emission Depletion (STED) imaging and cryogenic electron microscopy should now be conducted followed by colocalisation analysis to study the subnuclear localisation of wtBASP1, G2A-BASP, emerin, BAF and lap2α. High resolution imaging and colocalisation of BASP1 and PRC2 components would also complement findings from results chapter 1 and further implicate PRC2 as a partner in BASP1 mediated repression. Imaging studies should be complemented by in depth biochemical fractionation of nuclei to study the subnuclear localisation of

wtBASP1, G2A-BASP, emerin, BAF and lap2α. Isolation of the nuclear membrane domains, including lipid microdomains, and internal nuclear compartments can be achieved following sucrose gradient fractionation and centrifugation [122, 360]. Immunoblotting of BASP1 repression complex components, chromatin remodelling interactors and INM proteins could then determine their subnuclear localisation and enable understanding of how BASP1 localisation and repression function is controlled by its interaction with lipids.

Additionally, RNA analysis experiments utilising siRNA targeting emerin should be repeated and extended to include RNA analysis following siRNA depletion of BAF and lap2α. Expression levels of multiple WT1 target genes (AREG, ETS-1, JUNB, VDR, REN) should be examined in V-K562, B-K562 and G-K562 to determine the roles of INM proteins in transcriptional repression and the myristoyl-dependence of this activity. Greater insight into the role of INM proteins in BASP1 mediated gene repression could also be gained from ChIP analysis of histone marks present at WT1 target genes in V-K562, B-K562 and G-K562 cells following siRNA depletion of emerin, BAF and lap2α.

Ultimately the gold-standard to determine the localisation of BASP1 bound promoters would be to perform Fluorescence in Situ Hybridisation (FISH) to localise specific promoters of WT1 target genes in V-K562, B-K562 and G-K562 (plus other stably expressing CML cell lines). Using this approach would enable direct visualisation of WT1 target genes in wtBASP1 and G2A-BASP1 expressing cells to determine if BASP1 (and its myristoylation) causes the relocalisation of gene promoters to the nuclear periphery. The proposed experiments would also identify the subnuclear location of components of the BASP1 repressor complex and determine how the myristoyl-dependent repressor function of BASP1 is related to target gene localisation. These results would provide new insights into the organisation of repressed genes in the nucleus and how this is regulated by protein-lipid interactions.

6.2.3 Role of Cholesterol in WT1/BASP1 Mechanism of Gene Regulation

Proteomic analysis of wtBASP1 and Y12L-BASP1 immunoprecipitates revealed KDM2B as a candidate cholesterol-dependent BASP1 interactor. Validation of this interaction via wtBASP1 and Y12L-BASP1 immunoprecipitation followed by western blotting and probing for KDM2B is now required. Recruitment of KDM2B to BASP1 regulated WT1 target genes should be assessed via ChIP in V-K562, B-K562 and

Y-K562. In addition, siRNA depletion of KDM2B followed by gene expression analysis of WT1 targets would assess the requirement for KDM2B in the WT1/BASP1 repression mechanism. Further ChIP to examine the presence of histone modifications at WT1 target genes following siRNA depletion of KDM2B would reveal whether removal of H3K4me^3 marks is a mechanism by which BASP1 and cholesterol mediate gene repression. These experiments could also be conducted following depletion of cholesterol via statin treatment (Mevinolin, Atorvastatin), or blocking of cholesterol synthesis via siRNA targeting HMG-CoA reductase to further assess the contribution of cholesterol to BASP1 mediated gene repression.

It would also be interesting to complete the proposed experiments examining WT1/BASP1 mediated gene repression at the nuclear periphery in Y12L-BASP1 expressing cells to assess the contribution of cholesterol to the localisation of the BASP1 repression complex, interaction with INM proteins, and the regulation of WT1 target gene expression by INM proteins.

7 Bibliography

1. Chodaparambil, J.V., et al., *A charged and contoured surface on the nucleosome regulates chromatin compaction.* Nat Struct Mol Biol, 2007. **14**(11): p. 1105-7.
2. Goodfellow, S.J., et al., *WT1 and its transcriptional cofactor BASP1 redirect the differentiation pathway of an established blood cell line.* Biochem J, 2011. **435**(1): p. 113-25.
3. Toska, E., et al., *Repression of transcription by WT1-BASP1 requires the myristoylation of BASP1 and the PIP2-dependent recruitment of histone deacetylase.* Cell Rep, 2012. **2**(3): p. 462-9.
4. Henry, S.A., S.D. Kohlwein, and G.M. Carman, *Metabolism and regulation of glycerolipids in the yeast Saccharomyces cerevisiae.* Genetics, 2012. **190**(2): p. 317-49.
5. Study.com. *Saturated Fatty Acid: Structure, Formula & Example*. Human Anatomy & Physiology 2018 [cited 2018 21.12.18]; Available from: https://study.com/academy/lesson/saturated-fatty-acid-structure-formula-example.html.
6. Wikibooks. *Structural Biochemistry/Lipids/Cholesterol*. Structural Biochemistry 2018 [cited 21 2018.12.18] ; Available from : https://en.wikibooks.org/wiki/Structural_Biochemistry/Lipids/Cholesterol.
7. Wikipedia. *Ganglioside*. 2018 [cited 2018 21.12.18]; Available from: https://en.wikipedia.org/wiki/Ganglioside#/media/File:GM1_ganglioside.png.
8. Wikipedia. *Sphingolipid*. 2018 [cited 2018 21.12.18]; Available from: https://en.wikipedia.org/wiki/Sphingolipid#/media/File:Sphingolipids_general_structures.png.
9. McGinty, R.K. and S. Tan, *Nucleosome structure and function.* Chem Rev, 2015. **115**(6): p. 2255-73.
10. Mao, Y.S., B. Zhang, and D.L. Spector, *Biogenesis and function of nuclear bodies.* Trends Genet, 2011. **27**(8): p. 295-306.
11. Layman, W.S. and J. Zuo, *Epigenetic regulation in the inner ear and its potential roles in development, protection, and regeneration.* Front Cell Neurosci, 2014. **8**: p. 446.
12. Epigenetics, W.I. *Histone Modifications*. 2018 [cited 2018 23.11.18]; Available from: https://www.whatisepigenetics.com/histone-modifications/.
13. Alberts B, J.A., Lewis J, et al, *An Overview of Gene Control*, in *Molecular Biology of the Cell*. 2002, Garland Science: New York.
14. International Human Genome Sequencing, C., *Finishing the euchromatic sequence of the human genome.* Nature, 2004. **431**(7011): p. 931-45.
15. Alberts B, J.A., Lewis J, et al, *From DNA to RNA*, in *Molecular Biology of the Cell*. 2002, Garland Science: New York.
16. Alberts B, J.A., Lewis J, et al, *From RNA to Protein*, in *Molecular Biology of the Cell*. 2002, Garland Science: New York.
17. Lander, E.S., et al., *Initial sequencing and analysis of the human genome.* Nature, 2001. **409**(6822): p. 860-921.
18. Venter, J.C., et al., *The sequence of the human genome.* Science, 2001. **291**(5507): p. 1304-51.
19. Lodish H, B.A., Zipursky SL, et al., *The Three Roles of RNA in Protein Synthesis*, in *Molecular Cell Biology*. 2000, W.H. Freeman: New York.

20. Giza, D.E., C. Vasilescu, and G.A. Calin, *Key principles of miRNA involvement in human diseases.* Discoveries (Craiova), 2014. **2**(4): p. e34.
21. Lodish H, B.A., Zipursky SL, et al., *Molecular Mechanisms of Eukaryotic Transcriptional Control*, in *Molecular Cell Biology*. 2000, W. H. Freeman: New York.
22. Lodish H, B.A., Zipursky SL, et al., *Eukaryotic Gene Control: Purposes and General Priniciples*, in *Molecular Cell Biology*. 2000, W. H. Freeman: New York.
23. Hanahan, D. and R.A. Weinberg, *Hallmarks of cancer: the next generation.* Cell, 2011. **144**(5): p. 646-74.
24. Hahn, S., *Structure and mechanism of the RNA polymerase II transcription machinery.* Nat Struct Mol Biol, 2004. **11**(5): p. 394-403.
25. Ebright, R.H., *RNA polymerase: structural similarities between bacterial RNA polymerase and eukaryotic RNA polymerase II.* J Mol Biol, 2000. **304**(5): p. 687-98.
26. Lodish H, B.A., Zipursky SL, et al., *RNA Polymerase II Transcription-Initiation Complex*, in *Molecular Cell Biology*. 2000, Freeman: New York.
27. Kuehner, J.N., E.L. Pearson, and C. Moore, *Unravelling the means to an end: RNA polymerase II transcription termination.* Nat Rev Mol Cell Biol, 2011. **12**(5): p. 283-94.
28. Kornberg, R.D., *The molecular basis of eukaryotic transcription.* Proc Natl Acad Sci U S A, 2007. **104**(32): p. 12955-61.
29. Sainsbury, S., C. Bernecky, and P. Cramer, *Structural basis of transcription initiation by RNA polymerase II.* Nat Rev Mol Cell Biol, 2015. **16**(3): p. 129-43.
30. Lodish H, B.A., Zipursky SL, et al., *Eukaryotic Transcription Activators and Repressors*, in *Molecular Cell Biology*. 2000, Freeman: New York.
31. Li, W., D. Notani, and M.G. Rosenfeld, *Enhancers as non-coding RNA transcription units: recent insights and future perspectives.* Nat Rev Genet, 2016. **17**(4): p. 207-23.
32. Shlyueva, D., G. Stampfel, and A. Stark, *Transcriptional enhancers: from properties to genome-wide predictions.* Nat Rev Genet, 2014. **15**(4): p. 272-86.
33. Kornberg, R.D., *Chromatin structure: a repeating unit of histones and DNA.* Science, 1974. **184**(4139): p. 868-71.
34. Ettig, R., et al., *Dissecting DNA-histone interactions in the nucleosome by molecular dynamics simulations of DNA unwrapping.* Biophys J, 2011. **101**(8): p. 1999-2008.
35. Alberts B, J.A., Lewis J, et al, *Chromosomal DNA and Its Packaging in the Chromatin Fiber*, in *Molecular Biology of the Cell*. 2002, Garland Science: New York.
36. Ou, H.D., et al., *ChromEMT: Visualizing 3D chromatin structure and compaction in interphase and mitotic cells.* Science, 2017. **357**(6349).
37. Biswas, S. and C.M. Rao, *Epigenetic tools (The Writers, The Readers and The Erasers) and their implications in cancer therapy.* Eur J Pharmacol, 2018. **837**: p. 8-24.
38. Lee, B.M. and L.C. Mahadevan, *Stability of histone modifications across mammalian genomes: implications for 'epigenetic' marking.* J Cell Biochem, 2009. **108**(1): p. 22-34.
39. Wang, X. and J.J. Hayes, *Physical methods used to study core histone tail structures and interactions in solution.* Biochem Cell Biol, 2006. **84**(4): p. 578-88.

40. Bowman, G.D., *Mechanisms of ATP-dependent nucleosome sliding.* Curr Opin Struct Biol, 2010. **20**(1): p. 73-81.
41. Allis, C.D. and T. Jenuwein, *The molecular hallmarks of epigenetic control.* Nat Rev Genet, 2016. **17**(8): p. 487-500.
42. Wilm, B. and R. Munoz-Chapuli, *The Role of WT1 in Embryonic Development and Normal Organ Homeostasis.* Methods Mol Biol, 2016. **1467**: p. 23-39.
43. Wagner, K.D., et al., *The Wilms' tumor gene Wt1 is required for normal development of the retina.* EMBO J, 2002. **21**(6): p. 1398-405.
44. Wagner, N., et al., *A splice variant of the Wilms' tumour suppressor Wt1 is required for normal development of the olfactory system.* Development, 2005. **132**(6): p. 1327-36.
45. McHaffie, S. and Y.Y. Chau, *Isolation and Colony Formation of Murine Bone and Bone Marrow Cells.* Methods Mol Biol, 2016. **1467**: p. 73-80.
46. Pelletier, J., et al., *Germline mutations in the Wilms' tumor suppressor gene are associated with abnormal urogenital development in Denys-Drash syndrome.* Cell, 1991. **67**(2): p. 437-47.
47. Rose, E.A., et al., *Complete physical map of the WAGR region of 11p13 localizes a candidate Wilms' tumor gene.* Cell, 1990. **60**(3): p. 495-508.
48. Miller-Hodges, E. and P. Hohenstein, *WT1 in disease: shifting the epithelial-mesenchymal balance.* J Pathol, 2012. **226**(2): p. 229-40.
49. Carpenter, B., et al., *BASP1 is a transcriptional cosuppressor for the Wilms' tumor suppressor protein WT1.* Mol Cell Biol, 2004. **24**(2): p. 537-49.
50. Montano, G., et al., *WT1-mediated repression of the proapoptotic transcription factor ZNF224 is triggered by the BCR-ABL oncogene.* Oncotarget, 2015. **6**(29): p. 28223-37.
51. Hsu, S.Y., et al., *Wilms' tumor protein WT1 as an ovarian transcription factor: decreases in expression during follicle development and repression of inhibin-alpha gene promoter.* Mol Endocrinol, 1995. **9**(10): p. 1356-66.
52. Mrowka, C. and A. Schedl, *Wilms' tumor suppressor gene WT1: from structure to renal pathophysiologic features.* J Am Soc Nephrol, 2000. **11 Suppl 16**: p. S106-15.
53. Haber, D.A., et al., *Alternative splicing and genomic structure of the Wilms tumor gene WT1.* Proc Natl Acad Sci U S A, 1991. **88**(21): p. 9618-22.
54. Toska, E. and S.G. Roberts, *Mechanisms of transcriptional regulation by WT1 (Wilms' tumour 1).* Biochem J, 2014. **461**(1): p. 15-32.
55. Roberts, S.G., *Transcriptional regulation by WT1 in development.* Curr Opin Genet Dev, 2005. **15**(5): p. 542-7.
56. Hammes, A., et al., *Two splice variants of the Wilms' tumor 1 gene have distinct functions during sex determination and nephron formation.* Cell, 2001. **106**(3): p. 319-29.
57. Sharma, P.M., et al., *RNA editing in the Wilms' tumor susceptibility gene, WT1.* Genes Dev, 1994. **8**(6): p. 720-31.
58. Scharnhorst, V., et al., *Internal translation initiation generates novel WT1 protein isoforms with distinct biological properties.* J Biol Chem, 1999. **274**(33): p. 23456-62.
59. Bruening, W. and J. Pelletier, *A non-AUG translational initiation event generates novel WT1 isoforms.* J Biol Chem, 1996. **271**(15): p. 8646-54.

60. Wang, Z.Y., et al., *A second transcriptionally active DNA-binding site for the Wilms tumor gene product, WT1.* Proc Natl Acad Sci U S A, 1993. **90**(19): p. 8896-900.
61. Madden, S.L., D.M. Cook, and F.J. Rauscher, 3rd, *A structure-function analysis of transcriptional repression mediated by the WT1, Wilms' tumor suppressor protein.* Oncogene, 1993. **8**(7): p. 1713-20.
62. Holmes, G., et al., *Two N-terminal self-association domains are required for the dominant negative transcriptional activity of WT1 Denys-Drash mutant proteins.* Biochem Biophys Res Commun, 1997. **233**(3): p. 723-8.
63. Sakamoto, Y., et al., *Inhibition of the DNA-binding and transcriptional repression activity of the Wilms' tumor gene product, WT1, by cAMP-dependent protein kinase-mediated phosphorylation of Ser-365 and Ser-393 in the zinc finger domain.* Oncogene, 1997. **15**(17): p. 2001-12.
64. Ye, Y., et al., *Regulation of WT1 by phosphorylation: inhibition of DNA binding, alteration of transcriptional activity and cellular translocation.* EMBO J, 1996. **15**(20): p. 5606-15.
65. Wang, Z.Y., et al., *Molecular cloning of the cDNA and chromosome localization of the gene for human ubiquitin-conjugating enzyme 9.* J Biol Chem, 1996. **271**(40): p. 24811-6.
66. McKay, L.M., B. Carpenter, and S.G. Roberts, *Regulation of the Wilms' tumour suppressor protein transcriptional activation domain.* Oncogene, 1999. **18**(47): p. 6546-54.
67. Roberts, S.G., *In Vitro Transcription to Study WT1 Function.* Methods Mol Biol, 2016. **1467**: p. 137-54.
68. Wang, W., et al., *A functional interaction with CBP contributes to transcriptional activation by the Wilms tumor suppressor WT1.* J Biol Chem, 2001. **276**(20): p. 16810-6.
69. Essafi, A., et al., *A wt1-controlled chromatin switching mechanism underpins tissue-specific wnt4 activation and repression.* Dev Cell, 2011. **21**(3): p. 559-74.
70. Xu, B., et al., *Tumor suppressor menin represses paired box gene 2 expression via Wilms tumor suppressor protein-polycomb group complex.* J Biol Chem, 2011. **286**(16): p. 13937-44.
71. Maheswaran, S., et al., *Physical and functional interaction between WT1 and p53 proteins.* Proc Natl Acad Sci U S A, 1993. **90**(11): p. 5100-4.
72. Hastie, N., *The Wilms' Tumor (WT1) Gene, Methods and Protocols*. 1 ed, ed. J.M. Walker. 2016: Humana Press.
73. Kreidberg, J.A., et al., *WT-1 is required for early kidney development.* Cell, 1993. **74**(4): p. 679-91.
74. Hu, Q., et al., *Wt1 ablation and Igf2 upregulation in mice result in Wilms tumors with elevated ERK1/2 phosphorylation.* J Clin Invest, 2011. **121**(1): p. 174-83.
75. Kaneko, Y., et al., *A high incidence of WT1 abnormality in bilateral Wilms tumours in Japan, and the penetrance rates in children with WT1 germline mutation.* Br J Cancer, 2015. **112**(6): p. 1121-33.
76. Rivera, M.N., et al., *The tumor suppressor WTX shuttles to the nucleus and modulates WT1 activity.* Proc Natl Acad Sci U S A, 2009. **106**(20): p. 8338-43.
77. Zhang, X., G. Xing, and G.F. Saunders, *Proto-oncogene N-myc promoter is down regulated by the Wilms' tumor suppressor gene WT1.* Anticancer Res, 1999. **19**(3A): p. 1641-8.

78. Huff, V., *Wilms' tumours: about tumour suppressor genes, an oncogene and a chameleon gene.* Nat Rev Cancer, 2011. **11**(2): p. 111-21.
79. Inoue, K., et al., *Aberrant overexpression of the Wilms tumor gene (WT1) in human leukemia.* Blood, 1997. **89**(4): p. 1405-12.
80. Mosevitsky, M.I., et al., *The BASP1 family of myristoylated proteins abundant in axonal termini. Primary structure analysis and physico-chemical properties.* Biochimie, 1997. **79**(6): p. 373-84.
81. Korshunova, I., et al., *Characterization of BASP1-mediated neurite outgrowth.* J Neurosci Res, 2008. **86**(10): p. 2201-13.
82. Epand, R.M., et al., *Cholesterol-dependent partitioning of PtdIns(4,5)P2 into membrane domains by the N-terminal fragment of NAP-22 (neuronal axonal myristoylated membrane protein of 22 kDa).* Biochem J, 2004. **379**(Pt 3): p. 527-32.
83. Maekawa, S., et al., *Cholesterol-dependent localization of NAP-22 on a neuronal membrane microdomain (raft).* J Biol Chem, 1999. **274**(30): p. 21369-74.
84. Aigner, L., et al., *Overexpression of the neural growth-associated protein GAP-43 induces nerve sprouting in the adult nervous system of transgenic mice.* Cell, 1995. **83**(2): p. 269-78.
85. Green, L.M., et al., *Dynamic interaction between WT1 and BASP1 in transcriptional regulation during differentiation.* Nucleic Acids Res, 2009. **37**(2): p. 431-40.
86. Kropotova, E., B. Klementiev, and M. Mosevitsky, *BASP1 and its N-end fragments (BNEMFs) dynamics in rat brain during development.* Neurochem Res, 2013. **38**(6): p. 1278-84.
87. Peitzsch, R.M. and S. McLaughlin, *Binding of acylated peptides and fatty acids to phospholipid vesicles: pertinence to myristoylated proteins.* Biochemistry, 1993. **32**(39): p. 10436-43.
88. Epand, R.F., B.G. Sayer, and R.M. Epand, *Induction of raft-like domains by a myristoylated NAP-22 peptide and its Tyr mutant.* FEBS J, 2005. **272**(7): p. 1792-803.
89. Marsh, L.A., et al., *BASP1 interacts with oestrogen receptor alpha and modifies the tamoxifen response.* Cell Death Dis, 2017. **8**(5): p. e2771.
90. Blanchard, J.W., et al., *Replacing reprogramming factors with antibodies selected from combinatorial antibody libraries.* Nat Biotechnol, 2017. **35**(10): p. 960-968.
91. Hartl, M., et al., *Inhibition of Myc-induced cell transformation by brain acid-soluble protein 1 (BASP1).* Proc Natl Acad Sci U S A, 2009. **106**(14): p. 5604-9.
92. Ransohoff, K.J., et al., *Two-stage genome-wide association study identifies a novel susceptibility locus associated with melanoma.* Oncotarget, 2017.
93. Guo, R.S., et al., *Restoration of Brain Acid Soluble Protein 1 Inhibits Proliferation and Migration of Thyroid Cancer Cells.* Chin Med J (Engl), 2016. **129**(12): p. 1439-1446.
94. Bhayat, F., et al., *The incidence of and mortality from leukaemias in the UK: a general population-based study.* BMC Cancer, 2009. **9**: p. 252.
95. Tang, H., et al., *High brain acid soluble protein 1(BASP1) is a poor prognostic factor for cervical cancer and promotes tumor growth.* Cancer Cell Int, 2017. **17**: p. 97.
96. Toska, E., et al., *Prohibitin is required for transcriptional repression by the WT1-BASP1 complex.* Oncogene, 2014. **33**(43): p. 5100-8.

97. Tsiftsoglou, A.S., I.S. Pappas, and I.S. Vizirianakis, *Mechanisms involved in the induced differentiation of leukemia cells.* Pharmacol Ther, 2003. **100**(3): p. 257-90.
98. Muro, E., G.E. Atilla-Gokcumen, and U.S. Eggert, *Lipids in cell biology: how can we understand them better?* Mol Biol Cell, 2014. **25**(12): p. 1819-23.
99. Welte, M.A., *Expanding roles for lipid droplets.* Curr Biol, 2015. **25**(11): p. R470-81.
100. van Meer, G., D.R. Voelker, and G.W. Feigenson, *Membrane lipids: where they are and how they behave.* Nat Rev Mol Cell Biol, 2008. **9**(2): p. 112-24.
101. Albi, E. and M.P. Viola Magni, *The role of intranuclear lipids.* Biol Cell, 2004. **96**(8): p. 657-67.
102. Hamann, B.L. and R.D. Blind, *Nuclear phosphoinositide regulation of chromatin.* J Cell Physiol, 2018. **233**(1): p. 107-123.
103. Cocco, L., et al., *Rapid changes in phospholipid metabolism in the nuclei of Swiss 3T3 cells induced by treatment of the cells with insulin-like growth factor I.* Biochem Biophys Res Commun, 1988. **154**(3): p. 1266-72.
104. Divecha, N., H. Banfic, and R.F. Irvine, *The polyphosphoinositide cycle exists in the nuclei of Swiss 3T3 cells under the control of a receptor (for IGF-I) in the plasma membrane, and stimulation of the cycle increases nuclear diacylglycerol and apparently induces translocation of protein kinase C to the nucleus.* EMBO J, 1991. **10**(11): p. 3207-14.
105. Rose, H.G. and J.H. Frenster, *Composition and metabolism of lipids within repressed and active chromatin of interphase lymphocytes.* Biochim Biophys Acta, 1965. **106**(3): p. 577-91.
106. Watt, S.A., et al., *Subcellular localization of phosphatidylinositol 4,5-bisphosphate using the pleckstrin homology domain of phospholipase C delta1.* Biochem J, 2002. **363**(Pt 3): p. 657-66.
107. Osborne, S.L., et al., *Nuclear PtdIns(4,5)P2 assembles in a mitotically regulated particle involved in pre-mRNA splicing.* J Cell Sci, 2001. **114**(Pt 13): p. 2501-11.
108. Albi, E., *Role of intranuclear lipids in health and disease.* Clinical Lipidology, 2011. **6**(1): p. 59-69.
109. Alberts B, J.A., Lewis J, et al., *The Lipid Bilayer*, in *Molecular Biology of the Cell*. 2002, Garland Science: New York.
110. Lindsay, Y., et al., *Localization of agonist-sensitive PtdIns(3,4,5)P3 reveals a nuclear pool that is insensitive to PTEN expression.* J Cell Sci, 2006. **119**(Pt 24): p. 5160-8.
111. Hunt, A.N. and A.D. Postle, *Mass spectrometry determination of endonuclear phospholipid composition and dynamics.* Methods, 2006. **39**(2): p. 104-11.
112. Albi, E. and M. Villani, *Nuclear lipid microdomains regulate cell function.* Commun Integr Biol, 2009. **2**(1): p. 23-4.
113. Shah, Z.H., et al., *Nuclear phosphoinositides and their impact on nuclear functions.* FEBS J, 2013. **280**(24): p. 6295-310.
114. Jones, D.R. and N. Divecha, *Linking lipids to chromatin.* Curr Opin Genet Dev, 2004. **14**(2): p. 196-202.
115. Romanauska, A. and A. Kohler, *The Inner Nuclear Membrane Is a Metabolically Active Territory that Generates Nuclear Lipid Droplets.* Cell, 2018. **174**(3): p. 700-715 e18.
116. Lemmon, M.A., *Membrane recognition by phospholipid-binding domains.* Nat Rev Mol Cell Biol, 2008. **9**(2): p. 99-111.

117. Rando, O.J., et al., *Phosphatidylinositol-dependent actin filament binding by the SWI/SNF-like BAF chromatin remodeling complex.* Proc Natl Acad Sci U S A, 2002. **99**(5): p. 2824-9.
118. Zhao, K., et al., *Rapid and phosphoinositol-dependent binding of the SWI/SNF-like BAF complex to chromatin after T lymphocyte receptor signaling.* Cell, 1998. **95**(5): p. 625-36.
119. Ulicna, L., et al., *Phospholipids and inositol phosphates linked to the epigenome.* Histochem Cell Biol, 2018. **150**(3): p. 245-253.
120. Blind, R.D., *Disentangling biological signaling networks by dynamic coupling of signaling lipids to modifying enzymes.* Adv Biol Regul, 2014. **54**: p. 25-38.
121. Rohrbach, T.D., et al., *The Effector Domain of MARCKS Is a Nuclear Localization Signal that Regulates Cellular PIP2 Levels and Nuclear PIP2 Localization.* PLoS One, 2015. **10**(10): p. e0140870.
122. Cascianelli, G., et al., *Lipid microdomains in cell nucleus.* Mol Biol Cell, 2008. **19**(12): p. 5289-95.
123. Zakharov, V.V. and M.I. Mosevitsky, *Oligomeric structure of brain abundant proteins GAP-43 and BASP1.* Journal of Structural Biology, 2010. **170**(3): p. 470-483.
124. Forsova, O.S. and V.V. Zakharov, *High-order oligomers of intrinsically disordered brain proteins BASP1 and GAP-43 preserve the structural disorder.* FEBS J, 2016. **283**(8): p. 1550-69.
125. Sever, R. and C.K. Glass, *Signaling by nuclear receptors.* Cold Spring Harb Perspect Biol, 2013. **5**(3): p. a016709.
126. Blind, R.D., et al., *The signaling phospholipid PIP3 creates a new interaction surface on the nuclear receptor SF-1.* Proc Natl Acad Sci U S A, 2014. **111**(42): p. 15054-9.
127. Ohsaki, Y., et al., *PML isoform II plays a critical role in nuclear lipid droplet formation.* J Cell Biol, 2016. **212**(1): p. 29-38.
128. Boronenkov, I.V., et al., *Phosphoinositide signaling pathways in nuclei are associated with nuclear speckles containing pre-mRNA processing factors.* Mol Biol Cell, 1998. **9**(12): p. 3547-60.
129. Heessen, S. and M. Fornerod, *The inner nuclear envelope as a transcription factor resting place.* EMBO Rep, 2007. **8**(10): p. 914-9.
130. Thinon, E., et al., *Global profiling of co- and post-translationally N-myristoylated proteomes in human cells.* Nat Commun, 2014. **5**: p. 4919.
131. Linde, N. and R. Stick, *Intranuclear membranes induced by lipidated proteins are derived from the nuclear envelope.* Nucleus, 2010. **1**(4): p. 343-53.
132. Viola Magni, M.P., et al., *Chromatin phospholipids and DNA synthesis in hepatic cells.* Basic Appl Histochem, 1985. **29**(3): p. 253-9.
133. Albi, E. and M.V. Magni, *The presence and the role of chromatin cholesterol in rat liver regeneration.* J Hepatol, 2002. **36**(3): p. 395-400.
134. Halstead, J.R., K. Jalink, and N. Divecha, *An emerging role for PtdIns(4,5)P2-mediated signalling in human disease.* Trends Pharmacol Sci, 2005. **26**(12): p. 654-60.
135. Fernandes, V., et al., *Fat nucleosome: Role of lipids on chromatin.* Prog Lipid Res, 2018. **70**: p. 29-34.
136. Itoh, T., et al., *Structural basis for the activation of PPARgamma by oxidized fatty acids.* Nat Struct Mol Biol, 2008. **15**(9): p. 924-31.

137. Gonzalez, F.J., et al., *Intestinal Farnesoid X Receptor Signaling Modulates Metabolic Disease.* Dig Dis, 2017. **35**(3): p. 178-184.
138. Carroll, J.S., et al., *Genome-wide analysis of estrogen receptor binding sites.* Nat Genet, 2006. **38**(11): p. 1289-97.
139. Silva, I.T.G., et al., *Biophysical studies of cholesterol effects on chromatin.* J Lipid Res, 2017. **58**(5): p. 934-940.
140. Ferrero, G.O., et al., *c-Fos-activated synthesis of nuclear phosphatidylinositol 4,5-bisphosphate [PtdIns(4,5)P(2)] promotes global transcriptional changes.* Biochem J, 2014. **461**(3): p. 521-30.
141. Yu, H., et al., *Phosphatidylinositol 4,5-bisphosphate reverses the inhibition of RNA transcription caused by histone H1.* Eur J Biochem, 1998. **251**(1-2): p. 281-7.
142. Gozani, O., et al., *The PHD finger of the chromatin-associated protein ING2 functions as a nuclear phosphoinositide receptor.* Cell, 2003. **114**(1): p. 99-111.
143. Shi, X., et al., *ING2 PHD domain links histone H3 lysine 4 methylation to active gene repression.* Nature, 2006. **442**(7098): p. 96-9.
144. Bua, D.J., et al., *Nuclear phosphatidylinositol-5-phosphate regulates ING2 stability at discrete chromatin targets in response to DNA damage.* Sci Rep, 2013. **3**: p. 2137.
145. Watson, P.J., et al., *Insights into the activation mechanism of class I HDAC complexes by inositol phosphates.* Nat Commun, 2016. **7**: p. 11262.
146. Millard, C.J., et al., *Class I HDACs share a common mechanism of regulation by inositol phosphates.* Mol Cell, 2013. **51**(1): p. 57-67.
147. Kutateladze, T.G., *Histone deacetylation: IP4 is an epigenetic coregulator.* Nat Chem Biol, 2012. **8**(3): p. 230-1.
148. Spiegel, S. and S. Milstien, *Functions of the multifaceted family of sphingosine kinases and some close relatives.* J Biol Chem, 2007. **282**(4): p. 2125-9.
149. Hait, N.C., et al., *Regulation of histone acetylation in the nucleus by sphingosine-1-phosphate.* Science, 2009. **325**(5945): p. 1254-7.
150. Ulicna, L., et al., *PIP2 epigenetically represses rRNA genes transcription interacting with PHF8.* Biochim Biophys Acta Mol Cell Biol Lipids, 2018. **1863**(3): p. 266-275.
151. Yildirim, S., et al., *Involvement of phosphatidylinositol 4,5-bisphosphate in RNA polymerase I transcription.* J Cell Sci, 2013. **126**(Pt 12): p. 2730-9.
152. Jungmichel, S., et al., *Specificity and commonality of the phosphoinositide-binding proteome analyzed by quantitative mass spectrometry.* Cell Rep, 2014. **6**(3): p. 578-91.
153. Lewis, A.E., et al., *Identification of nuclear phosphatidylinositol 4,5-bisphosphate-interacting proteins by neomycin extraction.* Mol Cell Proteomics, 2011. **10**(2): p. M110 003376.
154. Gelato, K.A., et al., *Accessibility of different histone H3-binding domains of UHRF1 is allosterically regulated by phosphatidylinositol 5-phosphate.* Mol Cell, 2014. **54**(6): p. 905-19.
155. Burton, A., et al., *Inositol pyrophosphates regulate JMJD2C-dependent histone demethylation.* Proc Natl Acad Sci U S A, 2013. **110**(47): p. 18970-5.
156. Hanahan, D. and R.A. Weinberg, *The hallmarks of cancer.* Cell, 2000. **100**(1): p. 57-70.

157. Krahmer, N., R.V. Farese, Jr., and T.C. Walther, *Balancing the fat: lipid droplets and human disease.* EMBO Mol Med, 2013. **5**(7): p. 973–83.
158. Baenke, F., et al., *Hooked on fat: the role of lipid synthesis in cancer metabolism and tumour development.* Dis Model Mech, 2013. **6**(6): p. 1353–63.
159. Santos, C.R. and A. Schulze, *Lipid metabolism in cancer.* FEBS J, 2012. **279**(15): p. 2610–23.
160. Xiao, W., et al., *Tumor suppression by phospholipase C-beta3 via SHP-1-mediated dephosphorylation of Stat5.* Cancer Cell, 2009. **16**(2): p. 161–71.
161. Leung, D.W., et al., *Phospholipase C delta-4 overexpression upregulates ErbB1/2 expression, Erk signaling pathway, and proliferation in MCF-7 cells.* Mol Cancer, 2004. **3**: p. 15.
162. Albi, E., et al., *Involvement of nuclear phosphatidylinositol-dependent phospholipases C in cell cycle progression during rat liver regeneration.* J Cell Physiol, 2003. **197**(2): p. 181–8.
163. Baum, B. and M. Georgiou, *Dynamics of adherens junctions in epithelial establishment, maintenance, and remodeling.* J Cell Biol, 2011. **192**(6): p. 907–17.
164. Struchkov, V.A., N.B. Strazhevskaya, and R.I. Zhdanov, *DNA-bound lipids of normal and tumor cells: retrospective and outlooks for functional genomics.* Bioelectrochemistry, 2002. **58**(1): p. 23–30.
165. Martelli, A.M., et al., *Intranuclear 3'-phosphoinositide metabolism and Akt signaling: new mechanisms for tumorigenesis and protection against apoptosis?* Cell Signal, 2006. **18**(8): p. 1101–7.
166. Llaverias, G., et al., *Role of cholesterol in the development and progression of breast cancer.* Am J Pathol, 2011. **178**(1): p. 402–12.
167. Pugliese, L., et al., *Severe hypocholesterolaemia is often neglected in haematological malignancies.* Eur J Cancer, 2010. **46**(9): p. 1735–43.
168. Tatidis, L., et al., *Cholesterol catabolism in patients with acute myelogenous leukemia and hypocholesterolemia: suppressed levels of a circulating marker for bile acid synthesis.* Cancer Lett, 2001. **170**(2): p. 169–75.
169. Freed-Pastor, W.A., et al., *Mutant p53 disrupts mammary tissue architecture via the mevalonate pathway.* Cell, 2012. **148**(1-2): p. 244–58.
170. Dobrzynska, A., et al., *The nuclear lamina in health and disease.* Nucleus, 2016. **7**(3): p. 233–48.
171. Muller, I., et al., *Stable morphology, but dynamic internal reorganisation, of interphase human chromosomes in living cells.* PLoS One, 2010. **5**(7): p. e11560.
172. Lemaitre, C. and W.A. Bickmore, *Chromatin at the nuclear periphery and the regulation of genome functions.* Histochem Cell Biol, 2015. **144**(2): p. 111–22.
173. Bickmore, W.A. and B. van Steensel, *Genome architecture: domain organization of interphase chromosomes.* Cell, 2013. **152**(6): p. 1270–84.
174. Peric-Hupkes, D., et al., *Molecular maps of the reorganization of genome-nuclear lamina interactions during differentiation.* Mol Cell, 2010. **38**(4): p. 603–13.
175. Therizols, P., et al., *Chromatin decondensation is sufficient to alter nuclear organization in embryonic stem cells.* Science, 2014. **346**(6214): p. 1238–42.
176. Reddy, K.L., et al., *Transcriptional repression mediated by repositioning of genes to the nuclear lamina.* Nature, 2008. **452**(7184): p. 243–7.
177. Finlan, L.E., et al., *Recruitment to the nuclear periphery can alter expression of genes in human cells.* PLoS Genet, 2008. **4**(3): p. e1000039.

178. Kumaran, R.I. and D.L. Spector, *A genetic locus targeted to the nuclear periphery in living cells maintains its transcriptional competence.* J Cell Biol, 2008. **180**(1): p. 51-65.
179. Hetzer, M.W., *The nuclear envelope.* Cold Spring Harb Perspect Biol, 2010. **2**(3): p. a000539.
180. Watson, M.L., *The nuclear envelope; its structure and relation to cytoplasmic membranes.* J Biophys Biochem Cytol, 1955. **1**(3): p. 257-70.
181. Beck, M., et al., *Nuclear pore complex structure and dynamics revealed by cryoelectron tomography.* Science, 2004. **306**(5700): p. 1387-90.
182. Fridkin, A., et al., *SUN-domain and KASH-domain proteins during development, meiosis and disease.* Cell Mol Life Sci, 2009. **66**(9): p. 1518-33.
183. Fenelon, K.D. and S. Hopyan, *Structural components of nuclear integrity with gene regulatory potential.* Curr Opin Cell Biol, 2017. **48**: p. 63-71.
184. Kind, J. and B. van Steensel, *Stochastic genome-nuclear lamina interactions: modulating roles of Lamin A and BAF.* Nucleus, 2014. **5**(2): p. 124-30.
185. Coutinho, H.D., et al., *Molecular ageing in progeroid syndromes: Hutchinson-Gilford progeria syndrome as a model.* Immun Ageing, 2009. **6**: p. 4.
186. van Steensel, B. and A.S. Belmont, *Lamina-Associated Domains: Links with Chromosome Architecture, Heterochromatin, and Gene Repression.* Cell, 2017. **169**(5): p. 780-791.
187. Jamin, A. and M.S. Wiebe, *Barrier to Autointegration Factor (BANF1): interwoven roles in nuclear structure, genome integrity, innate immunity, stress responses and progeria.* Curr Opin Cell Biol, 2015. **34**: p. 61-8.
188. Mamada, H., N. Takahashi, and M. Taira, *Involvement of an inner nuclear membrane protein, Nemp1, in Xenopus neural development through an interaction with the chromatin protein BAF.* Dev Biol, 2009. **327**(2): p. 497-507.
189. Demmerle, J., A.J. Koch, and J.M. Holaska, *The nuclear envelope protein emerin binds directly to histone deacetylase 3 (HDAC3) and activates HDAC3 activity.* J Biol Chem, 2012. **287**(26): p. 22080-8.
190. Nili, E., et al., *Nuclear membrane protein LAP2beta mediates transcriptional repression alone and together with its binding partner GCL (germ-cell-less).* J Cell Sci, 2001. **114**(Pt 18): p. 3297-307.
191. Cesarini, E., et al., *Lamin A/C sustains PcG protein architecture, maintaining transcriptional repression at target genes.* J Cell Biol, 2015. **211**(3): p. 533-51.
192. Worman, H.J. and G. Bonne, *"Laminopathies": a wide spectrum of human diseases.* Exp Cell Res, 2007. **313**(10): p. 2121-33.
193. Razin, S.V., et al., *Nuclear matrix and structural and functional compartmentalization of the eucaryotic cell nucleus.* Biochemistry (Mosc), 2014. **79**(7): p. 608-18.
194. Adam, S.A., *The Nucleoskeleton.* Cold Spring Harb Perspect Biol, 2017. **9**(2).
195. Albi, E., et al., *Nuclear lipid microdomain as place of interaction between sphingomyelin and DNA during liver regeneration.* Int J Mol Sci, 2013. **14**(4): p. 6529-41.
196. Coelho, M.B., et al., *Matrin3: connecting gene expression with the nuclear matrix.* Wiley Interdiscip Rev RNA, 2016. **7**(3): p. 303-15.
197. Linnemann, A.K., A.E. Platts, and S.A. Krawetz, *Differential nuclear scaffold/matrix attachment marks expressed genes.* Hum Mol Genet, 2009. **18**(4): p. 645-54.

198. Martins, R.P., G.C. Ostermeier, and S.A. Krawetz, *Nuclear matrix interactions at the human protamine domain: a working model of potentiation.* J Biol Chem, 2004. **279**(50): p. 51862-8.
199. Mortillaro, M.J., et al., *A hyperphosphorylated form of the large subunit of RNA polymerase II is associated with splicing complexes and the nuclear matrix.* Proc Natl Acad Sci U S A, 1996. **93**(16): p. 8253-7.
200. Nakayasu, H. and R. Berezney, *Nuclear matrins: identification of the major nuclear matrix proteins.* Proc Natl Acad Sci U S A, 1991. **88**(22): p. 10312-6.
201. Depreux, F.F., et al., *Disruption of the lamin A and matrin-3 interaction by myopathic LMNA mutations.* Hum Mol Genet, 2015. **24**(15): p. 4284-95.
202. Marangi, G., et al., *Matrin 3 variants are frequent in Italian ALS patients.* Neurobiol Aging, 2017. **49**: p. 218 e1-218 e7.
203. Muller, T.J., et al., *Phenotype of matrin-3-related distal myopathy in 16 German patients.* Ann Neurol, 2014. **76**(5): p. 669-80.
204. Senderek, J., et al., *Autosomal-dominant distal myopathy associated with a recurrent missense mutation in the gene encoding the nuclear matrix protein, matrin 3.* Am J Hum Genet, 2009. **84**(4): p. 511-8.
205. Harborth, J., et al., *Self assembly of NuMA: multiarm oligomers as structural units of a nuclear lattice.* EMBO J, 1999. **18**(6): p. 1689-700.
206. Gueth-Hallonet, C., et al., *Induction of a regular nuclear lattice by overexpression of NuMA.* Exp Cell Res, 1998. **243**(2): p. 434-52.
207. Sleeman, J.E. and L. Trinkle-Mulcahy, *Nuclear bodies: new insights into assembly/dynamics and disease relevance.* Curr Opin Cell Biol, 2014. **28**: p. 76-83.
208. Dundr, M. and T. Misteli, *Functional architecture in the cell nucleus.* Biochem J, 2001. **356**(Pt 2): p. 297-310.
209. Busch, H., K.S. Narayan, and J. Hamilton, *Isolation of nucleoli in a medium containing spermine and magnesium acetate.* Exp Cell Res, 1967. **47**(1): p. 329-36.
210. Mintz, P.J., et al., *Purification and biochemical characterization of interchromatin granule clusters.* EMBO J, 1999. **18**(15): p. 4308-20.
211. Cooper, G., *The Nucleolus*, in *The Cell: A Molecular Approach.* 2000, Sinauer Associates: Sunderland (MA).
212. Monneron, A. and W. Bernhard, *Fine structural organization of the interphase nucleus in some mammalian cells.* J Ultrastruct Res, 1969. **27**(3): p. 266-88.
213. Gall, J.G., *Cajal bodies: the first 100 years.* Annu Rev Cell Dev Biol, 2000. **16**: p. 273-300.
214. Klingauf, M., D. Stanek, and K.M. Neugebauer, *Enhancement of U4/U6 small nuclear ribonucleoprotein particle association in Cajal bodies predicted by mathematical modeling.* Mol Biol Cell, 2006. **17**(12): p. 4972-81.
215. Wang, Q., et al., *Cajal bodies are linked to genome conformation.* Nat Commun, 2016. **7**: p. 10966.
216. Novotny, I., et al., *In vivo kinetics of U4/U6.U5 tri-snRNP formation in Cajal bodies.* Mol Biol Cell, 2011. **22**(4): p. 513-23.
217. Malatesta, M., et al., *Cytochemical and immunocytochemical characterization of nuclear bodies during hibernation.* Eur J Cell Biol, 1994. **65**(1): p. 82-93.
218. Ochs, R.L., T.W. Stein, Jr., and E.M. Tan, *Coiled bodies in the nucleolus of breast cancer cells.* J Cell Sci, 1994. **107 (Pt 2)**: p. 385-99.

219. Koken, M.H., et al., *The PML growth-suppressor has an altered expression in human oncogenesis.* Oncogene, 1995. **10**(7): p. 1315-24.
220. Lallemand-Breitenbach, V. and H. de The, *PML nuclear bodies.* Cold Spring Harb Perspect Biol, 2010. **2**(5): p. a000661.
221. Reymond, A., et al., *The tripartite motif family identifies cell compartments.* EMBO J, 2001. **20**(9): p. 2140-51.
222. Spector, D.L. and A.I. Lamond, *Nuclear speckles.* Cold Spring Harb Perspect Biol, 2011. **3**(2).
223. Misteli, T., *Cell biology of transcription and pre-mRNA splicing: nuclear architecture meets nuclear function.* J Cell Sci, 2000. **113 (Pt 11)**: p. 1841-9.
224. Rieder, D., Z. Trajanoski, and J.G. McNally, *Transcription factories.* Front Genet, 2012. **3**: p. 221.
225. Melnik, S., et al., *The proteomes of transcription factories containing RNA polymerases I, II or III.* Nat Methods, 2011. **8**(11): p. 963-8.
226. Meuleman, W., et al., *Constitutive nuclear lamina-genome interactions are highly conserved and associated with A/T-rich sequence.* Genome Res, 2013. **23**(2): p. 270-80.
227. Kind, J., et al., *Single-cell dynamics of genome-nuclear lamina interactions.* Cell, 2013. **153**(1): p. 178-92.
228. Towbin, B.D., et al., *Step-wise methylation of histone H3K9 positions heterochromatin at the nuclear periphery.* Cell, 2012. **150**(5): p. 934-47.
229. Bian, Q., et al., *β-Globin cis-elements determine differential nuclear targeting through epigenetic modifications.* J Cell Biol, 2013. **203**(5): p. 767-83.
230. Gonzalez-Sandoval, A., et al., *Perinuclear Anchoring of H3K9-Methylated Chromatin Stabilizes Induced Cell Fate in C. elegans Embryos.* Cell, 2015. **163**(6): p. 1333-47.
231. Wen, B., et al., *Large histone H3 lysine 9 dimethylated chromatin blocks distinguish differentiated from embryonic stem cells.* Nat Genet, 2009. **41**(2): p. 246-50.
232. Harr, J.C., et al., *Directed targeting of chromatin to the nuclear lamina is mediated by chromatin state and A-type lamins.* J Cell Biol, 2015. **208**(1): p. 33-52.
233. Zullo, J.M., et al., *DNA sequence-dependent compartmentalization and silencing of chromatin at the nuclear lamina.* Cell, 2012. **149**(7): p. 1474-87.
234. Olins, A.L., et al., *Lamin B receptor: multi-tasking at the nuclear envelope.* Nucleus, 2010. **1**(1): p. 53-70.
235. Solovei, I., et al., *LBR and lamin A/C sequentially tether peripheral heterochromatin and inversely regulate differentiation.* Cell, 2013. **152**(3): p. 584-98.
236. Ho, C.Y., et al., *Lamin A/C and emerin regulate MKL1-SRF activity by modulating actin dynamics.* Nature, 2013. **497**(7450): p. 507-11.
237. Berk, J.M., K.E. Tifft, and K.L. Wilson, *The nuclear envelope LEM-domain protein emerin.* Nucleus, 2013. **4**(4): p. 298-314.
238. Demmerle, J., A.J. Koch, and J.M. Holaska, *Emerin and histone deacetylase 3 (HDAC3) cooperatively regulate expression and nuclear positions of MyoD, Myf5, and Pax7 genes during myogenesis.* Chromosome Res, 2013. **21**(8): p. 765-79.

239. Zuleger, N., et al., *Specific nuclear envelope transmembrane proteins can promote the location of chromosomes to and from the nuclear periphery.* Genome Biol, 2013. **14**(2): p. R14.
240. Nemeth, A., et al., *Initial genomics of the human nucleolus.* PLoS Genet, 2010. **6**(3): p. e1000889.
241. van Koningsbruggen, S., et al., *High-resolution whole-genome sequencing reveals that specific chromatin domains from most human chromosomes associate with nucleoli.* Mol Biol Cell, 2010. **21**(21): p. 3735-48.
242. Szczerbal, I. and J.M. Bridger, *Association of adipogenic genes with SC-35 domains during porcine adipogenesis.* Chromosome Res, 2010. **18**(8): p. 887-95.
243. Brown, J.M., et al., *Association between active genes occurs at nuclear speckles and is modulated by chromatin environment.* J Cell Biol, 2008. **182**(6): p. 1083-97.
244. Schoenfelder, S., et al., *Preferential associations between co-regulated genes reveal a transcriptional interactome in erythroid cells.* Nat Genet, 2010. **42**(1): p. 53-61.
245. Osborne, C.S., et al., *Myc dynamically and preferentially relocates to a transcription factory occupied by Igh.* PLoS Biol, 2007. **5**(8): p. e192.
246. Skowronska-Krawczyk, D., et al., *Required enhancer-matrin-3 network interactions for a homeodomain transcription program.* Nature, 2014. **514**(7521): p. 257-61.
247. Hyman, A.A., C.A. Weber, and F. Jülicher, *Liquid-liquid phase separation in biology.* Annu Rev Cell Dev Biol, 2014. **30**: p. 39-58.
248. Brangwynne, C.P., T.J. Mitchison, and A.A. Hyman, *Active liquid-like behavior of nucleoli determines their size and shape in Xenopus laevis oocytes.* Proc Natl Acad Sci U S A, 2011. **108**(11): p. 4334-9.
249. Larson, A.G., et al., *Liquid droplet formation by HP1α suggests a role for phase separation in heterochromatin.* Nature, 2017. **547**(7662): p. 236-240.
250. Erdel, F. and K. Rippe, *Formation of Chromatin Subcompartments by Phase Separation.* Biophys J, 2018. **114**(10): p. 2262-2270.
251. Cho, W.K., et al., *Mediator and RNA polymerase II clusters associate in transcription-dependent condensates.* Science, 2018. **361**(6400): p. 412-415.
252. Sabari, B.R., et al., *Coactivator condensation at super-enhancers links phase separation and gene control.* Science, 2018. **361**(6400).
253. Strom, A.R., et al., *Phase separation drives heterochromatin domain formation.* Nature, 2017. **547**(7662): p. 241-245.
254. Takasaki, A., et al., *Identification of the calmodulin-binding domain of neuron-specific protein kinase C substrate protein CAP-22/NAP-22. Direct involvement of protein myristoylation in calmodulin-target protein interaction.* J Biol Chem, 1999. **274**(17): p. 11848-53.
255. Terashita, A., et al., *Lipid binding activity of a neuron-specific protein NAP-22 studied in vivo and in vitro.* J Neurosci Res, 2002. **70**(2): p. 172-9.
256. Kang, C.D., et al., *Signaling mechanism of PMA-induced differentiation of K562 cells.* Biochem Biophys Res Commun, 1996. **221**(1): p. 95-100.
257. Kang, C.D., et al., *Activation of NF-kappaB mediates the PMA-induced differentiation of K562 cells.* Cancer Lett, 1998. **132**(1-2): p. 99-106.
258. Borowicz, S., et al., *The soft agar colony formation assay.* J Vis Exp, 2014(92): p. e51998.

259. Pene-Dumitrescu, T. and T.E. Smithgall, *Expression of a Src family kinase in chronic myelogenous leukemia cells induces resistance to imatinib in a kinase-dependent manner.* J Biol Chem, 2010. **285**(28): p. 21446-57.
260. Zeng, P.Y., et al., *In vivo dual cross-linking for identification of indirect DNA-associated proteins by chromatin immunoprecipitation.* Biotechniques, 2006. **41**(6): p. 694, 696, 698.
261. Nowak, D.E., B. Tian, and A.R. Brasier, *Two-step cross-linking method for identification of NF-kappaB gene network by chromatin immunoprecipitation.* Biotechniques, 2005. **39**(5): p. 715-25.
262. Margueron, R. and D. Reinberg, *The Polycomb complex PRC2 and its mark in life.* Nature, 2011. **469**(7330): p. 343-9.
263. Hansen, K.H., et al., *A model for transmission of the H3K27me3 epigenetic mark.* Nat Cell Biol, 2008. **10**(11): p. 1291-300.
264. Cho, Y., et al., *EZH2, the moderator in the discussion between methyltransferases at histone H3?* J Cell Commun Signal, 2015. **9**(1): p. 77-9.
265. Li, Z., et al., *EZH2 regulates neuroblastoma cell differentiation via NTRK1 promoter epigenetic modifications.* Oncogene, 2018.
266. Wang, C., et al., *EZH2 Mediates epigenetic silencing of neuroblastoma suppressor genes CASZ1, CLU, RUNX3, and NGFR.* Cancer Res, 2012. **72**(1): p. 315-24.
267. Li, J., et al., *EZH2-mediated H3K27 trimethylation mediates neurodegeneration in ataxia-telangiectasia.* Nat Neurosci, 2013. **16**(12): p. 1745-53.
268. Boros, J., et al., *Polycomb repressive complex 2 and H3K27me3 cooperate with H3K9 methylation to maintain heterochromatin protein 1alpha at chromatin.* Mol Cell Biol, 2014. **34**(19): p. 3662-74.
269. Coward, W.R., et al., *A central role for G9a and EZH2 in the epigenetic silencing of cyclooxygenase-2 in idiopathic pulmonary fibrosis.* FASEB J, 2014. **28**(7): p. 3183-96.
270. Zawel, L., K.P. Kumar, and D. Reinberg, *Recycling of the general transcription factors during RNA polymerase II transcription.* Genes Dev, 1995. **9**(12): p. 1479-90.
271. Komarnitsky, P., E.J. Cho, and S. Buratowski, *Different phosphorylated forms of RNA polymerase II and associated mRNA processing factors during transcription.* Genes Dev, 2000. **14**(19): p. 2452-60.
272. Ahn, S.H., M. Kim, and S. Buratowski, *Phosphorylation of serine 2 within the RNA polymerase II C-terminal domain couples transcription and 3' end processing.* Mol Cell, 2004. **13**(1): p. 67-76.
273. Bernstein, B.E., et al., *A bivalent chromatin structure marks key developmental genes in embryonic stem cells.* Cell, 2006. **125**(2): p. 315-26.
274. Hastie, N.D., *Wilms' tumour 1 (WT1) in development, homeostasis and disease.* Development, 2017. **144**(16): p. 2862-2872.
275. Roberts, S.G. and M.R. Green, *Transcription. Dichotomous regulators.* Nature, 1995. **375**(6527): p. 105-6.
276. Karmodiya, K., et al., *H3K9 and H3K14 acetylation co-occur at many gene regulatory elements, while H3K14ac marks a subset of inactive inducible promoters in mouse embryonic stem cells.* BMC Genomics, 2012. **13**: p. 424.
277. Bernhart, S.H., et al., *Changes of bivalent chromatin coincide with increased expression of developmental genes in cancer.* Sci Rep, 2016. **6**: p. 37393.

278. Boyer, L.A., et al., *Polycomb complexes repress developmental regulators in murine embryonic stem cells.* Nature, 2006. **441**(7091): p. 349–53.
279. Das, P.P., et al., *PRC2 Is Required to Maintain Expression of the Maternal Gtl2–Rian–Mirg Locus by Preventing De Novo DNA Methylation in Mouse Embryonic Stem Cells.* Cell Rep, 2015. **12**(9): p. 1456–70.
280. Sobol, M., et al., *UBF complexes with phosphatidylinositol 4,5–bisphosphate in nucleolar organizer regions regardless of ongoing RNA polymerase I activity.* Nucleus, 2013. **4**(6): p. 478–86.
281. Sobol, M., et al., *Nuclear phosphatidylinositol 4,5–bisphosphate islets contribute to efficient RNA polymerase II–dependent transcription.* J Cell Sci, 2018. **131**(8).
282. Mosevitsky, M.I., *Nerve ending "signal" proteins GAP–43, MARCKS, and BASP1.* Int Rev Cytol, 2005. **245**: p. 245–325.
283. Ladomery, M., et al., *Expression in Xenopus oocytes shows that WT1 binds transcripts in vivo, with a central role for zinc finger one.* Journal of Cell Science, 2003. **116**(8): p. 1539–1549.
284. Dutton, J.R., D. Lahiri, and A. Ward, *Different isoforms of the Wilms' tumour protein WT1 have distinct patterns of distribution and trafficking within the nucleus.* Cell Prolif, 2006. **39**(6): p. 519–35.
285. Laity, J.H., H.J. Dyson, and P.E. Wright, *Molecular basis for modulation of biological function by alternate splicing of the Wilms' tumor suppressor protein.* Proc Natl Acad Sci U S A, 2000. **97**(22): p. 11932–5.
286. Caricasole, A., et al., *RNA binding by the Wilms tumor suppressor zinc finger proteins.* Proc Natl Acad Sci U S A, 1996. **93**(15): p. 7562–6.
287. Davies, R.C., et al., *WT1 interacts with the splicing factor U2AF65 in an isoform–dependent manner and can be incorporated into spliceosomes.* Genes Dev, 1998. **12**(20): p. 3217–25.
288. Wang, S., et al., *Prohibitin co–localizes with Rb in the nucleus and recruits N–CoR and HDAC1 for transcriptional repression.* Oncogene, 2002. **21**(55): p. 8388–96.
289. Sun, J.M., et al., *Purification and characterization of chicken erythrocyte histone deacetylase 1.* Biochemistry, 1999. **38**(18): p. 5939–47.
290. Fairley, E.A., et al., *The cell cycle dependent mislocalisation of emerin may contribute to the Emery–Dreifuss muscular dystrophy phenotype.* J Cell Sci, 2002. **115**(Pt 2): p. 341–54.
291. Tifft, K.E., K.A. Bradbury, and K.L. Wilson, *Tyrosine phosphorylation of nuclear–membrane protein emerin by Src, Abl and other kinases.* J Cell Sci, 2009. **122**(Pt 20): p. 3780–90.
292. Mortier, E., et al., *Nuclear speckles and nucleoli targeting by PIP2–PDZ domain interactions.* EMBO J, 2005. **24**(14): p. 2556–65.
293. Dunn, K.W., M.M. Kamocka, and J.H. McDonald, *A practical guide to evaluating colocalization in biological microscopy.* Am J Physiol Cell Physiol, 2011. **300**(4): p. C723–42.
294. Lin, C.Y., et al., *ARL4, an ARF–like protein that is developmentally regulated and localized to nuclei and nucleoli.* J Biol Chem, 2000. **275**(48): p. 37815–23.
295. Michaut, M.A., C.J. Williams, and R.M. Schultz, *Phosphorylated MARCKS: a novel centrosome component that also defines a peripheral subdomain of the cortical actin cap in mouse eggs.* Dev Biol, 2005. **280**(1): p. 26–37.

296. Maurer-Stroh, S., et al., *MYRbase: analysis of genome-wide glycine myristoylation enlarges the functional spectrum of eukaryotic myristoylated proteins.* Genome Biol, 2004. **5**(3): p. R21.
297. Hantschel, O., et al., *A myristoyl/phosphotyrosine switch regulates c-Abl.* Cell, 2003. **112**(6): p. 845-57.
298. Markiewicz, E., et al., *The inner nuclear membrane protein emerin regulates beta-catenin activity by restricting its accumulation in the nucleus.* EMBO J, 2006. **25**(14): p. 3275-85.
299. Wozniak, M.A., et al., *The emerin-binding transcription factor Lmo7 is regulated by association with p130Cas at focal adhesions.* PeerJ, 2013. **1**: p. e134.
300. Holaska, J.M. and K.L. Wilson, *An emerin "proteome": purification of distinct emerin-containing complexes from HeLa cells suggests molecular basis for diverse roles including gene regulation, mRNA splicing, signaling, mechanosensing, and nuclear architecture.* Biochemistry, 2007. **46**(30): p. 8897-908.
301. Lee, B., T.H. Lee, and J. Shim, *Emerin suppresses Notch signaling by restricting the Notch intracellular domain to the nuclear membrane.* Biochim Biophys Acta Mol Cell Res, 2017. **1864**(2): p. 303-313.
302. Holaska, J.M., et al., *Transcriptional repressor germ cell-less (GCL) and barrier to autointegration factor (BAF) compete for binding to emerin in vitro.* J Biol Chem, 2003. **278**(9): p. 6969-75.
303. Wang, X., et al., *Barrier to autointegration factor interacts with the cone-rod homeobox and represses its transactivation function.* J Biol Chem, 2002. **277**(45): p. 43288-300.
304. Margalit, A., et al., *Barrier-to-autointegration factor is required to segregate and enclose chromosomes within the nuclear envelope and assemble the nuclear lamina.* Proc Natl Acad Sci U S A, 2005. **102**(9): p. 3290-5.
305. Loi, M., et al., *Barrier-to-autointegration factor (BAF) involvement in prelamin A-related chromatin organization changes.* Oncotarget, 2016. **7**(13): p. 15662-77.
306. Oh, H.S., P. Traktman, and D.M. Knipe, *Barrier-to-Autointegration Factor 1 (BAF/BANF1) Promotes Association of the SETD1A Histone Methyltransferase with Herpes Simplex Virus Immediate-Early Gene Promoters.* MBio, 2015. **6**(3): p. e00345-15.
307. Montes de Oca, R., K.K. Lee, and K.L. Wilson, *Binding of barrier to autointegration factor (BAF) to histone H3 and selected linker histones including H1.1.* J Biol Chem, 2005. **280**(51): p. 42252-62.
308. Margalit, A., et al., *Barrier-to-autointegration factor--a BAFfling little protein.* Trends Cell Biol, 2007. **17**(4): p. 202-8.
309. Shumaker, D.K., et al., *LAP2 binds to BAF.DNA complexes: requirement for the LEM domain and modulation by variable regions.* EMBO J, 2001. **20**(7): p. 1754-64.
310. Dorner, D., J. Gotzmann, and R. Foisner, *Nucleoplasmic lamins and their interaction partners, LAP2alpha, Rb, and BAF, in transcriptional regulation.* FEBS J, 2007. **274**(6): p. 1362-73.
311. Dechat, T., et al., *Detergent-salt resistance of LAP2alpha in interphase nuclei and phosphorylation-dependent association with chromosomes early in nuclear assembly implies functions in nuclear structure dynamics.* EMBO J, 1998. **17**(16): p. 4887-902.

312. Alsheimer, M., E. Fecher, and R. Benavente, *Nuclear envelope remodelling during rat spermiogenesis: distribution and expression pattern of LAP2/thymopoietins.* J Cell Sci, 1998. **111 (Pt 15)**: p. 2227-34.
313. Furukawa, K., C.E. Fritze, and L. Gerace, *The major nuclear envelope targeting domain of LAP2 coincides with its lamin binding region but is distinct from its chromatin interaction domain.* J Biol Chem, 1998. **273**(7): p. 4213-9.
314. Ozawa, R., et al., *Emerin-lacking mice show minimal motor and cardiac dysfunctions with nuclear-associated vacuoles.* Am J Pathol, 2006. **168**(3): p. 907-17.
315. Bione, S., et al., *Identification of a novel X-linked gene responsible for Emery-Dreifuss muscular dystrophy.* Nat Genet, 1994. **8**(4): p. 323-7.
316. Nagano, A., et al., *Emerin deficiency at the nuclear membrane in patients with Emery-Dreifuss muscular dystrophy.* Nat Genet, 1996. **12**(3): p. 254-9.
317. Manilal, S., et al., *Distribution of emerin and lamins in the heart and implications for Emery-Dreifuss muscular dystrophy.* Hum Mol Genet, 1999. **8**(2): p. 353-9.
318. Reis-Sobreiro, M., et al., *Emerin deregulation links nuclear shape instability to metastatic potential.* Cancer Res, 2018.
319. Collins, C.M., J.A. Ellis, and J.M. Holaska, *MAPK signaling pathways and HDAC3 activity are disrupted during differentiation of emerin-null myogenic progenitor cells.* Dis Model Mech, 2017. **10**(4): p. 385-397.
320. Frock, R.L., et al., *Lamin A/C and emerin are critical for skeletal muscle satellite cell differentiation.* Genes Dev, 2006. **20**(4): p. 486-500.
321. Wang, J., et al., *The Msx1 Homeoprotein Recruits Polycomb to the Nuclear Periphery during Development.* Dev Cell, 2011. **21**(3): p. 575-88.
322. Zheng, B., et al., *Nuclear actin and actin-binding proteins in the regulation of transcription and gene expression.* FEBS J, 2009. **276**(10): p. 2669-85.
323. Visa, N. and P. Percipalle, *Nuclear functions of actin.* Cold Spring Harb Perspect Biol, 2010. **2**(4): p. a000620.
324. Hofmann, W.A., et al., *Actin is part of pre-initiation complexes and is necessary for transcription by RNA polymerase II.* Nat Cell Biol, 2004. **6**(11): p. 1094-101.
325. Philimonenko, V.V., et al., *Nuclear actin and myosin I are required for RNA polymerase I transcription.* Nat Cell Biol, 2004. **6**(12): p. 1165-72.
326. Chuang, C.H., et al., *Long-range directional movement of an interphase chromosome site.* Curr Biol, 2006. **16**(8): p. 825-31.
327. Dundr, M., et al., *Actin-dependent intranuclear repositioning of an active gene locus in vivo.* J Cell Biol, 2007. **179**(6): p. 1095-103.
328. Khan, T.K., et al., *Binding of NAP-22, a calmodulin-binding neuronal protein, to raft-like domains in model membranes.* Biochemistry, 2003. **42**(17): p. 4780-6.
329. Alberts, A.W., et al., *Mevinolin: a highly potent competitive inhibitor of hydroxymethylglutaryl-coenzyme A reductase and a cholesterol-lowering agent.* Proc Natl Acad Sci U S A, 1980. **77**(7): p. 3957-61.
330. Janzer, A., et al., *The H3K4me3 histone demethylase Fbxl10 is a regulator of chemokine expression, cellular morphology, and the metabolome of fibroblasts.* J Biol Chem, 2012. **287**(37): p. 30984-92.
331. Gal, Z., et al., *Mutations of the central tyrosines of putative cholesterol recognition amino acid consensus (CRAC) sequences modify folding, activity, and sterol-sensing of the human ABCG2 multidrug transporter.* Biochim Biophys Acta, 2015. **1848**(2): p. 477-87.

332. Zhdanov, R., et al., *Lipids contribute to epigenetic control via chromatin structure and functions.* ScienceOpen Research, 2015. **0**(0): p. 1–12.
333. Tyrrell, L.W. and D. Richter, *The lipids of cell nuclei isolated from human brain cortex.* Biochem J, 1951. **49**(4): p. li–lii.
334. Rossi, G., M.V. Magni, and E. Albi, *Sphingomyelin–cholesterol and double stranded RNA relationship in the intranuclear complex.* Arch Biochem Biophys, 2007. **459**(1): p. 27–32.
335. Rossi, G., M. Viola Magni, and E. Albi, *Signal transducer and activator of transcription 3 and sphingomyelin metabolism in intranuclear complex during cell proliferation.* Arch Biochem Biophys, 2007. **464**(1): p. 138–43.
336. Rae, F.K., et al., *Anlaysis of complementary expression profiles following WT1 induction versus repression reveals the cholesterol/fatty acid synthetic pathways as a possible major target of WT1.* Oncogene, 2004. **23**(17): p. 3067–79.
337. Gong, Y., et al., *Sterol-regulated ubiquitination and degradation of Insig-1 creates a convergent mechanism for feedback control of cholesterol synthesis and uptake.* Cell Metab, 2006. **3**(1): p. 15–24.
338. Jans, R., et al., *Cholesterol depletion upregulates involucrin expression in epidermal keratinocytes through activation of p38.* J Invest Dermatol, 2004. **123**(3): p. 564–73.
339. Sanchez-Martin, C.C., et al., *Cholesterol starvation induces differentiation of human leukemia HL-60 cells.* Cancer Res, 2007. **67**(7): p. 3379–86.
340. Portilho, D.M., et al., *A soluble and active form of Wnt-3a protein is involved in myogenic differentiation after cholesterol depletion.* FEBS Lett, 2007. **581**(30): p. 5787–95.
341. Kuang, Y., et al., *Histone demethylase KDM2B upregulates histone methyltransferase EZH2 expression and contributes to the progression of ovarian cancer in vitro and in vivo.* Onco Targets Ther, 2017. **10**: p. 3131–3144.
342. Tzatsos, A., et al., *Ndy1/KDM2B immortalizes mouse embryonic fibroblasts by repressing the Ink4a/Arf locus.* Proc Natl Acad Sci U S A, 2009. **106**(8): p. 2641–6.
343. Lee, B.B., et al., *Rpd3L HDAC links H3K4me3 to transcriptional repression memory.* Nucleic Acids Res, 2018. **46**(16): p. 8261–8274.
344. Nightingale, K.P., et al., *Cross-talk between histone modifications in response to histone deacetylase inhibitors: MLL4 links histone H3 acetylation and histone H3K4 methylation.* J Biol Chem, 2007. **282**(7): p. 4408–16.
345. Huang, P.H., et al., *Histone deacetylase inhibitors stimulate histone H3 lysine 4 methylation in part via transcriptional repression of histone H3 lysine 4 demethylases.* Mol Pharmacol, 2011. **79**(1): p. 197–206.
346. Steege, A., et al., *Wilms' tumor protein (-KTS) modulates renin gene transcription.* Kidney Int, 2008. **74**(4): p. 458–66.
347. Lee, S.B., et al., *The Wilms tumor suppressor WT1 encodes a transcriptional activator of amphiregulin.* Cell, 1999. **98**(5): p. 663–73.
348. Lee, T.H. and J. Pelletier, *Functional characterization of WT1 binding sites within the human vitamin D receptor gene promoter.* Physiol Genomics, 2001. **7**(2): p. 187–200.
349. Wagner, N., et al., *The Wilms' tumour suppressor WT1 is involved in endothelial cell proliferation and migration: expression in tumour vessels in vivo.* Oncogene, 2008. **27**(26): p. 3662–72.

350. Adams, D.J., et al., *Renin enhancer is critical for control of renin gene expression and cardiovascular function.* J Biol Chem, 2006. **281**(42): p. 31753-61.
351. Shimi, T., et al., *Dynamic interaction between BAF and emerin revealed by FRAP, FLIP, and FRET analyses in living HeLa cells.* J Struct Biol, 2004. **147**(1): p. 31-41.
352. Cohen, M., et al., *Transmission electron microscope studies of the nuclear envelope in Caenorhabditis elegans embryos.* J Struct Biol, 2002. **140**(1-3): p. 232-40.
353. Lee, K.K., et al., *Distinct functional domains in emerin bind lamin A and DNA-bridging protein BAF.* J Cell Sci, 2001. **114**(Pt 24): p. 4567-73.
354. Lee, D.C., et al., *A-type nuclear lamins act as transcriptional repressors when targeted to promoters.* Exp Cell Res, 2009. **315**(6): p. 996-1007.
355. Lund, E., et al., *Lamin A/C-promoter interactions specify chromatin state-dependent transcription outcomes.* Genome Res, 2013. **23**(10): p. 1580-9.
356. Markiewicz, E., et al., *Lamin A/C binding protein LAP2alpha is required for nuclear anchorage of retinoblastoma protein.* Mol Biol Cell, 2002. **13**(12): p. 4401-13.
357. Farese, R.V., Jr. and T.C. Walther, *Lipid droplets go nuclear.* J Cell Biol, 2016. **212**(1): p. 7-8.
358. Khor, V.K., et al., *The proteome of cholesteryl-ester-enriched versus triacylglycerol-enriched lipid droplets.* PLoS One, 2014. **9**(8): p. e105047.
359. Hnisz, D., et al., *A Phase Separation Model for Transcriptional Control.* Cell, 2017. **169**(1): p. 13-23.
360. Macdonald, J.L. and L.J. Pike, *A simplified method for the preparation of detergent-free lipid rafts.* J Lipid Res, 2005. **46**(5): p. 1061-7.

8. Appendix

Table 1. V-K562, B-K562, G-K562 Interactome as Identified by TMT Mass Spectrometry. Triplicates of BASP1 immunoprecipitates from V-K562, B-K562 and G-K562 were labelled using TMT isobaric mass tags and pooled together prior to high performance liquid chromatography (HPLC) separation. Peptides were analysed using SEQUEST to generate a score for each protein. The dataset was filtered to include only proteins identified with >95% confidence, as assessed via false discovery rate (FDR) estimation following comparison to the human reverse decoy database. The relative abundance of each identified protein in the replicates of V-K562, B-K562 and G-K562 compared to replicate 1 of B-K562 was calculated. The average relative abundance for V-K562, B-K562 and G-K562 was then calculated. The dataset was filtered to include only proteins with relatively greater abundance in the B-K562 replicates compared to V-K562 (negative control).

Accession	Description	Score	Coverage	# Unique Peptides	Average Relative Abundance		
					B-K562	G-K562	V-K562
P78527	DNA-dependent protein kinase catalytic subunit	1291.72	61.89	233	0.894	1.280	0.714
P09874	Poly [ADP-ribose] polymerase	355.32	64.00	68	0.848	1.228	0.700
Q15149	Plectin	339.00	27.75	108	1.499	1.160	0.910
P35580	Myosin-10	336.57	43.78	64	1.265	0.750	0.174
P13010	X-ray repair cross-complementing protein 5	314.50	70.63	44	0.786	1.221	0.587
P11388	DNA topoisomerase 2-alpha	313.34	48.01	59	0.984	1.727	0.559
P35579	Myosin-9	309.42	39.95	58	0.971	1.210	0.268
P12956	X-ray repair cross-complementing protein 6	248.72	61.41	42	0.811	1.241	0.547
A2VCL5	FLOT1 protein (Fragment)	7.50	9.70	2	2.546	1.422	0.542
Q5JQC4	Cancer/testis antigen 47A	4.64	8.33	2	0.827	0.305	0.178
P19338	Nucleolin	226.77	54.51	43	0.700	1.402	0.350
H6VRF8	Keratin 1	224.27	64.29	34	0.517	0.135	0.106
Q6NTA2	HNRNPL protein (Fragment)	199.77	67.48	25	0.668	0.748	0.534
O14980	Exportin-1	194.54	43.32	37	0.922	1.116	0.817
P35527	Keratin, type I cytoskeletal	185.58	68.54	28	0.392	0.056	0.083
P11233	Ras-related protein Ral-A	5.43	8.74	2	1.438	0.552	0.362

Accession	Description	Score	Coverage	# Unique Peptides	Average Relative Abundance		
					B-K562	G-K562	V-K562
Q02880	DNA topoisomerase 2-beta	183.43	30.87	32	0.897	1.174	0.595
I3L192	Basigin (Fragment)	4.24	9.32	2	1.703	0.757	0.452
Q8WVW5	Putative uncharacterized protein (Fragment)	174.10	61.71	5	1.035	0.736	0.587
Q8N5A0	Eukaryotic translation initiation factor 5B	171.54	36.80	41	0.771	1.094	0.483
P09496	Clathrin light chain A	7.46	9.27	3	0.886	0.523	0.274
P08670	Vimentin	169.05	73.18	32	2.031	1.776	0.799
Q9P258	Protein RCC2	166.96	73.75	32	0.695	0.747	0.353
Q00610	Clathrin heavy chain 1	165.68	28.78	39	0.801	0.431	0.264
P80723	Brain acid soluble protein 1	157.32	89.43	17	2.255	1.352	0.123
C9J3L8	Translocon-associated protein subunit alpha	5.07	7.17	2	1.163	0.687	0.419
Q99543	DnaJ homolog subfamily C member 2	4.77	4.67	2	0.996	0.985	0.377
Q9UQ80	Proliferation-associated protein 2G4	132.10	62.18	21	1.238	2.202	0.414
A8K7S5	Katanin p60 ATPase-containing subunit A1	3.74	3.87	2	1.418	2.483	0.558
P05771	Protein kinase C beta type	10.26	4.32	3	0.976	0.607	0.386
Q8NE71	ATP-binding cassette sub-family F member 1	123.84	40.83	30	0.791	1.149	0.525
A0A024R3R7	HEAT repeat containing 1, isoform CRA_b	122.75	19.74	30	1.215	1.184	0.772
P55060	Exportin-2	122.37	36.35	28	0.958	1.383	0.860
H0UID5	AP complex subunit beta	121.44	38.44	15	0.595	0.679	0.368
P36578	60S ribosomal protein L4	115.09	59.48	30	0.764	1.193	0.669
Q9H0A0	RNA cytidine acetyltransferase	111.41	33.95	8	1.129	1.278	0.499
P39023	60S ribosomal protein L3	108.72	61.54	6	0.786	1.232	0.664
P07900	Heat shock protein HSP 90-alpha	105.84	36.34	12	0.835	1.284	0.650
A9Z1X7	Serine/arginine repetitive matrix protein 1	102.31	33.95	24	0.805	0.710	0.703
P05198	Eukaryotic translation initiation factor 2 subunit 1	96.40	65.08	17	0.796	1.554	0.469
Q6P2E9	Enhancer of mRNA-decapping protein 4	96.31	24.41	23	0.785	1.126	0.601
B2R5W2	Heterogeneous nuclear ribonucleoproteins C1/C2	96.22	57.24	21	0.561	0.485	0.493
P62424	60S ribosomal protein L7a	92.45	56.02	17	0.798	1.166	0.594

Accession	Description	Score	Coverage	# Unique Peptides	Average Relative Abundance		
					B-K562	G-K562	V-K562
O95782	AP-2 complex subunit alpha-1	89.23	33.67	18	0.598	0.649	0.456
Q14008	Cytoskeleton-associated protein 5	89.04	17.47	27	0.679	0.910	0.430
A8K4Z4	60S acidic ribosomal protein P0	88.97	61.83	17	0.796	1.247	0.577
B2R7F8	Plasminogen	11.38	2.96	2	1.073	1.833	0.495
Q9P2P1	Protein NYNRIN	1.85	1.32	2	0.914	1.834	0.433
P63241	Eukaryotic translation initiation factor 5A-1	88.25	51.95	6	1.195	3.091	0.658
Q14258	E3 ubiquitin/ISG15 ligase TRIM25	87.31	41.11	20	0.564	0.767	0.450
Q9Y2X3	Nucleolar protein 58	86.75	43.86	19	0.904	1.045	0.755
Q5JSL3	Dedicator of cytokinesis protein 11	85.63	14.76	27	0.644	0.737	0.372
O75330	Hyaluronan mediated motility receptor	85.13	39.23	6	0.575	1.023	0.517
P62906	60S ribosomal protein L10a	82.96	63.13	16	0.774	1.152	0.595
P05387	60S acidic ribosomal protein P2	81.72	92.17	7	0.898	1.551	0.654
Q9Y608	Leucine-rich repeat flightless-interacting protein 2	19.01	9.15	5	0.771	0.876	0.403
P19474	E3 ubiquitin-protein ligase TRIM21	7.50	6.95	3	1.097	0.849	0.577
O76021	Ribosomal L1 domain-containing protein 1	78.52	36.73	21	0.698	0.847	0.609
O43776	Asparagine--tRNA ligase, cytoplasmic	9.98	7.48	3	0.648	0.620	0.348
P46777	60S ribosomal protein L5	77.62	67.34	19	0.817	1.250	0.658
Q9NZI8	Insulin-like growth factor 2 mRNA-binding protein 1	76.16	41.25	20	0.695	0.901	0.555
O60832	H/ACA ribonucleoprotein complex subunit 4	74.19	42.02	20	0.853	1.003	0.680
P41091	Eukaryotic translation initiation factor 2 subunit 3	73.55	54.66	19	0.785	1.347	0.378
A0A024R2V0	Microtubule-associated protein	73.53	48.14	7	1.232	1.700	0.802
P16403	Histone H1.2	72.93	42.72	5	0.739	1.299	0.469
D3DRH1	Dedicator of cytokinesis 8, isoform CRA_a	7.89	2.22	2	0.573	0.669	0.320
Q9NX58	Cell growth-regulating nucleolar protein	71.22	51.19	2	0.866	1.034	0.517
Q9P016	Thymocyte nuclear protein 1	1.95	9.33	2	0.938	1.492	0.529
P48668	Keratin, type II cytoskeletal 6C	70.69	37.23	8	0.581	0.227	0.209
P30050	60S ribosomal protein L12	70.67	70.91	11	0.781	1.138	0.526

Accession	Description	Score	Coverage	# Unique Peptides	Average Relative Abundance		
					B-K562	G-K562	V-K562
P08779	Keratin, type I cytoskeletal 16	69.85	42.28	8	0.652	0.378	0.324
P62917	60S ribosomal protein L8	69.05	59.14	16	0.784	1.197	0.672
Q5F1R6	DnaJ homolog subfamily C member 21	11.97	7.16	2	0.723	0.662	0.420
Q5VYK3	Proteasome-associated protein ECM29 homolog	68.99	12.09	16	0.775	0.767	0.675
P18124	60S ribosomal protein L7	65.71	47.98	15	0.784	1.185	0.592
Q96BS4	FBL protein (Fragment)	65.70	69.23	15	0.965	1.094	0.863
Q9UHB9	Signal recognition particle subunit SRP68	64.48	33.81	16	0.982	1.324	0.853
E9PFH4	Transportin-3	63.26	28.24	17	0.866	0.917	0.770
P32969	60S ribosomal protein L9	63.02	61.46	12	0.816	1.146	0.645
M0R0Y2	Alpha-soluble NSF attachment protein	6.35	8.98	2	1.480	1.370	0.878
M0R3D6	60S ribosomal protein L18a (Fragment)	62.92	55.32	9	0.797	1.133	0.603
A0A0D9SFL2	Bifunctional polynucleotide phosphatase/kinase	14.38	8.25	3	1.127	3.763	0.672
P13647	Keratin, type II cytoskeletal 5	61.94	29.49	7	0.761	0.377	0.312
A0A0C4DGS1	Dolichyl-diphosphooligosaccharide--protein glycosyltransferase 48 kDa subunit	11.83	9.11	3	1.506	1.233	0.900
Q6FG43	FLOT2 protein	8.54	9.50	3	1.272	1.073	0.760
F1JVV5	EWSR1/ATF1 fusion protein type 1	11.51	8.94	3	0.870	2.376	0.523
A0A0A0MS07	Ig gamma-1 chain C region (Fragment)	6.37	5.08	2	1.039	0.873	0.630
B2R7C5	DNA helicase	60.02	22.28	14	0.765	1.072	0.681
P43487	Ran-specific GTPase-activating protein	6.88	9.95	2	0.994	0.753	0.606
A0A0D9SFK2	Unconventional myosin-XVIIIa	58.81	12.32	16	0.933	1.064	0.599
Q14554	Protein disulfide-isomerase A5	7.85	5.59	2	0.778	1.197	0.484
H0Y465	Neurofibromin (Fragment)	22.30	4.28	6	1.046	1.510	0.653
B2RAM6	Kinesin-like protein	58.77	18.75	15	0.727	1.105	0.638
O76094	Signal recognition particle subunit SRP72	58.20	31.30	19	0.850	1.129	0.698
Q7Z3Z9	L1 cell adhesion molecule (Fragment)	2.50	1.67	2	0.732	0.582	0.459
H3BPZ1	Very-long-chain (3R)-3-hydroxyacyl-CoA dehydratase 3	2.19	5.64	2	1.176	1.041	0.737
Q03111	Protein ENL	13.19	6.62	3	0.788	0.719	0.494

Accession	Description	Score	Coverage	# Unique Peptides	Average Relative Abundance		
					B-K562	G-K562	V-K562
A0A087WXM6	60S ribosomal protein L17 (Fragment)	56.22	59.17	10	0.950	1.468	0.726
Q02878	60S ribosomal protein L6	56.00	52.43	20	0.770	1.115	0.607
O75475	PC4 and SFRS1-interacting protein	55.69	28.49	14	0.714	0.930	0.325
Q7Z3N6	Putative uncharacterized protein DKFZp686A01173 (Fragment)	16.64	3.82	4	1.104	1.835	0.699
A0A087WY71	AP-2 complex subunit mu	55.01	43.09	15	0.611	0.725	0.469
O00567	Nucleolar protein 56	54.46	32.83	19	0.973	1.007	0.690
P16402	Histone H1.3	53.18	33.03	2	0.716	1.824	0.635
A0A024RC67	Protein regulator of cytokinesis 1, isoform CRA_e	53.03	24.68	16	0.772	1.093	0.626
O60814	Histone H2B type 1-K	52.32	62.70	2	0.976	2.193	0.624
Q8WYA6	Beta-catenin-like protein 1	51.57	28.95	14	0.756	0.884	0.679
Q5SWX3	Calcium/calmodulin-dependent protein kinase (CaM kinase) II gamma, isoform CRA_n	10.34	5.81	3	0.600	0.693	0.386
P06899	Histone H2B type 1-J	51.50	62.70	2	0.976	2.187	0.560
P62805	Histone H4	49.22	58.25	7	1.226	3.821	0.714
O43684	Mitotic checkpoint protein BUB3	48.50	43.60	12	0.596	0.750	0.505
P62888	60S ribosomal protein L30	48.04	77.39	9	0.825	1.179	0.538
Q9NSY1	BMP-2-inducible protein kinase	22.43	9.22	5	0.643	0.672	0.421
P62753	40S ribosomal protein S6	46.87	33.33	11	0.797	1.267	0.706
G3V1D0	Echinoderm microtubule associated protein like 3, isoform CRA_f	12.88	7.76	4	0.763	0.948	0.502
Q9BSQ6	RPL13A protein (Fragment)	45.85	49.75	15	0.799	1.184	0.610
Q99848	Probable rRNA-processing protein EBP2	45.56	42.48	11	0.771	0.902	0.570
G3V203	60S ribosomal protein L18	45.33	43.90	8	0.820	1.217	0.593
Q08ES8	Cell growth-inhibiting protein 34	45.21	37.85	8	0.788	1.190	0.641
Q04695	Keratin, type I cytoskeletal 17	45.12	29.17	4	0.712	0.175	0.142
P46781	40S ribosomal protein S9	44.48	51.03	15	0.806	1.286	0.709
Q12771	P37 AUF1	43.51	34.97	9	0.758	1.233	0.618
P20042	Eukaryotic translation initiation factor 2 subunit 2	43.22	43.84	13	0.795	1.520	0.356
P11021	78 kDa glucose-regulated protein	42.74	20.80	9	1.650	1.849	1.038

Accession	Description	Score	Coverage	# Unique Peptides	Average Relative Abundance		
					B-K562	G-K562	V-K562
O94973	AP-2 complex subunit alpha-2	42.20	14.27	3	0.559	0.613	0.355
P62081	40S ribosomal protein S7	41.74	48.45	9	0.979	1.457	0.854
Q9Y490	Talin-1	30.62	4.92	6	1.089	2.079	0.758
P26373	60S ribosomal protein L13	41.67	48.82	13	0.791	1.105	0.586
A0RZB8	Diaphanous-1	40.99	13.79	11	0.943	1.373	0.833
Q8IU60	m7GpppN-mRNA hydrolase	7.83	7.14	3	0.737	1.373	0.516
P61011	Signal recognition particle 54 kDa protein	40.89	32.94	12	0.860	1.084	0.719
A0A0A0MR02	Voltage-dependent anion-selective channel protein 2 (Fragment)	40.87	41.13	8	1.043	0.488	0.262
Q15717	ELAV-like protein 1	40.57	32.52	8	0.656	0.759	0.577
O75934	Pre-mRNA-splicing factor SPF27	40.46	44.44	9	0.794	0.927	0.713
Q15019	Septin-2	39.55	37.12	9	0.555	0.947	0.465
Q96HI4	Glycylpeptide N-tetradecanoyltransferase (Fragment)	39.11	21.46	8	1.146	0.872	0.243
P62750	60S ribosomal protein L23a	39.07	55.13	11	0.895	1.413	0.637
Q9UHB7	AF4/FMR2 family member 4	5.66	2.58	3	0.782	0.684	0.558
E7EXA6	Chromosome transmission fidelity protein 18 homolog	7.18	3.38	2	0.904	1.259	0.650
Q15061	WD repeat-containing protein 43	5.27	5.17	3	0.775	0.986	0.559
P18754	Regulator of chromosome condensation	39.06	37.53	9	0.693	0.885	0.402
Q96SB8	Structural maintenance of chromosomes protein 6	20.29	8.62	8	0.929	1.190	0.672
A8K9K1	Calcium-transporting ATPase	8.99	3.61	3	0.856	1.075	0.620
B5BUB5	Autoantigen La (Fragment)	38.51	33.33	13	0.761	1.338	0.630
P46778	60S ribosomal protein L21	37.96	49.38	11	0.794	1.211	0.622
A6NHN7	Zinc finger MYM-type protein 3	37.67	10.39	11	0.952	1.075	0.800
P60891	Ribose-phosphate pyrophosphokinase 1	37.41	31.45	5	0.409	0.307	0.110
P02008	Hemoglobin subunit zeta	36.54	76.76	9	0.814	1.031	0.704
E4W6B6	RPL27/NME2 fusion protein (Fragment)	35.75	57.14	8	0.796	1.150	0.561
O43670	BUB3-interacting and GLEBS motif-containing protein ZNF207	17.13	8.16	4	0.620	0.802	0.456
A6NK02	Putative tripartite motif-containing protein 75	2.86	6.84	2	0.715	1.023	0.528

Accession	Description	Score	Coverage	# Unique Peptides	Average Relative Abundance		
					B-K562	G-K562	V-K562
Q8N9V7	Testis- and ovary-specific PAZ domain-containing protein 1	3.49	0.95	2	0.762	0.694	0.563
Q96P70	Importin-9	20.39	9.13	4	0.866	1.161	0.641
D6R9P3	Heterogeneous nuclear ribonucleoprotein A/B	34.86	37.50	8	0.687	0.832	0.574
Q5SSJ5	Heterochromatin protein 1-binding protein 3	34.54	22.78	12	0.770	0.819	0.667
Q8TED0	U3 small nucleolar RNA-associated protein 15 homolog	34.42	16.41	8	0.928	0.926	0.687
P16104	Histone H2AX	34.00	64.34	4	0.925	1.622	0.592
Q9BW19	Kinesin-like protein KIFC1	33.74	21.25	11	0.816	1.246	0.644
Q8TDN6	Ribosome biogenesis protein BRX1 homolog	33.53	28.90	11	0.743	0.878	0.503
D3YTB1	60S ribosomal protein L32 (Fragment)	33.18	56.39	10	0.815	1.278	0.613
A0A0J9YWM9	U3 small nucleolar RNA-associated protein 4 homolog (Fragment)	14.46	9.20	4	1.100	1.202	0.825
Q9UG63	ATP-binding cassette sub-family F member 2	32.91	19.10	11	0.936	1.373	0.795
Q9NW13	RNA-binding protein 28	32.79	16.60	10	0.734	1.308	0.643
P31942	Heterogeneous nuclear ribonucleoprotein H3	31.65	25.72	7	0.645	0.572	0.433
J3QR09	Ribosomal protein L19	30.38	44.56	11	0.783	1.123	0.679
Q9Y6M1	Insulin-like growth factor 2 mRNA-binding protein 2	30.11	17.53	6	0.697	1.033	0.592
P15924	Desmoplakin	2.80	0.84	2	0.653	0.822	0.499
P27824	Calnexin	29.97	16.39	9	2.007	0.869	0.720
B7Z7P8	Eukaryotic peptide chain release factor subunit 1	29.79	22.22	8	0.784	1.375	0.671
Q96F86	Enhancer of mRNA-decapping protein 3	29.65	22.83	8	0.724	0.877	0.510
Q16777	Histone H2A type 2-C	29.58	55.04	2	0.769	2.297	0.571
Q9UKD2	mRNA turnover protein 4 homolog	29.55	36.82	9	0.871	1.248	0.709
H3BN98	Uncharacterized protein (Fragment)	29.33	26.58	2	1.178	1.078	0.762
Q96PK6	RNA-binding protein 14	28.25	16.59	9	0.677	0.817	0.601
A0A024RDA1	Exocyst complex component 1, isoform CRA_a	28.04	11.83	7	0.643	0.832	0.572
E7EQV9	Ribosomal protein L15 (Fragment)	27.97	56.32	11	0.803	1.231	0.614
C9J0I9	Nuclear-interacting partner of ALK	27.86	17.65	5	0.794	0.727	0.712
P15104	Glutamine synthetase	2.44	4.02	2	0.980	1.455	0.765

Accession	Description	Score	Coverage	# Unique Peptides	Average Relative Abundance		
					B-K562	G-K562	V-K562
P46779	60S ribosomal protein L28	27.79	48.91	8	0.829	1.210	0.577
B4DUD5	cDNA FLJ58787	26.62	15.01	5	0.616	0.839	0.528
P50914	60S ribosomal protein L14	26.34	43.72	12	0.757	1.141	0.552
P53999	Activated RNA polymerase II transcriptional coactivator p15	26.27	68.50	8	1.135	0.783	0.183
B2R860	cDNA, FLJ93752	25.94	23.58	4	0.465	0.510	0.277
P46063	ATP-dependent DNA helicase Q1	25.66	16.49	9	0.637	1.393	0.399
E7EU96	Casein kinase II subunit alpha	25.49	19.74	5	1.099	1.443	0.951
Q9UES0	SNARE protein Ykt6 (Fragment)	25.38	37.70	7	0.900	0.804	0.631
P63173	60S ribosomal protein L38	25.19	50.00	4	1.098	1.559	0.913
O75531	Barrier-to-autointegration factor	24.98	73.03	6	1.351	2.093	0.795
P46087	Probable 28S rRNA (cytosine(4447)-C(5))-methyltransferase	24.57	13.18	7	0.947	1.565	0.662
Q9H8H0	Nucleolar protein 11	24.57	11.40	9	0.859	0.972	0.659
O75569	Interferon-inducible double-stranded RNA-dependent protein kinase activator A	24.08	29.07	7	0.658	1.086	0.578
P18077	60S ribosomal protein L35a	23.96	58.18	8	0.766	1.117	0.556
Q5QPL9	RNA-binding protein Raly (Fragment)	23.77	44.30	10	0.607	0.611	0.517
Q9NQT5	Exosome complex component RRP40	23.66	30.91	6	0.782	0.832	0.690
P61513	60S ribosomal protein L37a	23.42	45.65	5	0.809	1.195	0.624
F8VZJ2	Nascent polypeptide-associated complex subunit alpha	23.27	51.47	5	1.645	2.749	0.757
P61254	60S ribosomal protein L26	23.13	40.00	10	0.880	1.331	0.703
A0A024QYZ6	Exocyst complex component 3, isoform CRA_a	22.92	13.56	7	0.762	0.947	0.672
Q6FI30	Nuclear factor 1	7.63	6.81	2	0.639	0.896	0.519
Q96HX3	Dolichyl-diphosphooligosaccharide-protein glycosyltransferase subunit 1	22.72	16.20	8	1.371	0.954	0.563
F5H018	GTP-binding nuclear protein Ran (Fragment)	22.58	28.14	5	0.713	0.993	0.581
Q8WXA9	Splicing regulatory glutamine/lysine-rich protein 1	22.43	17.13	2	0.803	1.079	0.694
P62854	40S ribosomal protein S26	22.10	49.57	5	0.853	1.251	0.747
Q92608	Dedicator of cytokinesis protein 2	32.20	6.23	9	0.750	0.362	0.611
E5KBQ3	TRAF2	22.05	14.17	8	0.622	0.749	0.485

Accession	Description	Score	Coverage	# Unique Peptides	Average Relative Abundance		
					B-K562	G-K562	V-K562
F8VQE1	LIM domain and actin-binding protein 1	21.83	12.21	6	0.974	0.726	0.639
Q0EFC6	HSR1 protein	4.32	2.94	2	0.901	1.060	0.738
P51692	Signal transducer and activator of transcription 5B	21.41	12.07	8	0.719	1.150	0.639
Q92522	Histone H1x	21.16	37.09	9	0.737	1.031	0.511
J3QSY4	H/ACA ribonucleoprotein complex subunit 2	21.04	42.22	3	1.004	1.302	0.756
P08240	Signal recognition particle receptor subunit alpha	6.25	5.96	2	1.000	0.995	0.824
P62306	Small nuclear ribonucleoprotein F	21.02	24.42	3	0.759	1.120	0.665
Q8IW76	EIF2AK2 protein (Fragment)	11.17	7.41	2	1.160	2.309	0.957
M0QXD6	General transcription factor IIF subunit 1 (Fragment)	20.52	22.40	6	0.672	0.738	0.421
P37108	Signal recognition particle 14 kDa protein	20.17	36.03	7	0.698	1.063	0.596
Q00688	Peptidyl-prolyl cis-trans isomerase FKBP3	19.46	37.05	9	1.156	2.171	0.490
H0Y4R1	Inosine-5'-monophosphate dehydrogenase 2 (Fragment)	19.37	16.38	5	0.450	0.202	0.132
Q9UID3	Vacuolar protein sorting-associated protein 51 homolog	6.23	4.35	2	0.743	1.701	0.617
B4DVE4	cDNA FLJ56793	19.15	16.30	6	0.828	1.126	0.719
Q16643	Drebrin	18.93	13.56	7	1.182	0.769	0.611
Q92979	Ribosomal RNA small subunit methyltransferase NEP1	18.70	29.51	6	0.693	0.588	0.532
Q8IY33	MICAL-like protein 2	21.37	8.63	7	0.642	0.726	0.535
A8K4B4	cDNA FLJ78441	9.81	8.62	3	0.620	0.928	0.517
Q4VB87	EPB41 protein	18.64	12.36	4	1.599	0.589	0.387
P21796	Voltage-dependent anion-selective channel protein 1	18.32	24.03	5	1.011	0.614	0.457
P46776	60S ribosomal protein L27a	18.07	36.49	7	0.810	1.281	0.724
Q7L576	Cytoplasmic FMR1-interacting protein 1	24.10	6.38	7	0.764	1.044	0.639
Q9Y266	Nuclear migration protein nudC	17.68	25.08	8	1.160	2.506	1.017
Q7Z524	HUMEEP	17.46	12.80	4	0.995	1.638	0.663
P41223	Protein BUD31 homolog	17.19	41.67	5	0.818	1.332	0.680
F8VYY9	5'-AMP-activated protein kinase subunit gamma-1	17.02	13.21	3	0.750	0.822	0.555
Q96AG4	Leucine-rich repeat-containing protein 59	16.84	17.26	5	1.255	0.738	0.551

Accession	Description	Score	Coverage	# Unique Peptides	Average Relative Abundance		
					B-K562	G-K562	V-K562
P14618	Pyruvate kinase PKM	16.48	16.57	5	0.884	0.937	0.795
A0A024RAC0	Leucine zipper protein 1, isoform CRA_a	13.92	6.04	5	0.818	1.005	0.691
P61221	ATP-binding cassette sub-family E member 1	16.10	12.69	6	0.833	0.936	0.713
P0C0S5	Histone H2A.Z	16.09	53.91	3	0.979	1.565	0.440
P49207	60S ribosomal protein L34	15.88	41.88	6	0.783	1.201	0.587
P61927	60S ribosomal protein L37	15.49	41.24	7	0.849	1.295	0.700
P60953	Cell division control protein 42 homolog	15.49	26.18	3	0.896	0.653	0.486
A0A0S2Z5K3	DCP1 decapping enzyme-like protein A isoform 3 (Fragment)	15.02	11.72	5	0.828	1.231	0.602
Q8WV22	Non-structural maintenance of chromosomes element 1 homolog	14.99	27.44	5	0.834	0.987	0.668
B3KSJ3	cDNA FLJ36409	6.14	4.89	2	0.723	1.125	0.615
E9PL38	26S proteasome non-ATPase regulatory subunit 13 (Fragment)	8.14	9.51	2	0.713	0.504	0.606
Q8IVI9	Nostrin	14.96	12.65	4	0.782	1.018	0.338
P39880	Homeobox protein cut-like 1	28.06	7.44	10	0.665	1.058	0.566
Q9NPQ8	Synembryn-A	14.70	12.24	5	0.854	0.842	0.718
I3L1K6	Myosin light chain 4 (Fragment)	14.56	30.81	5	0.975	1.128	0.763
A0A0S2Z476	Proteasome 26S subunit non-ATPase 12 isoform 2	14.13	10.13	3	0.803	0.693	0.706
P55010	Eukaryotic translation initiation factor 5	13.64	12.53	4	1.299	2.133	0.617
P53680	AP-2 complex subunit sigma	13.25	28.17	5	0.608	0.784	0.524
H3BQN4	Fructose-bisphosphate aldolase	13.10	16.62	5	1.063	1.641	0.713
P49458	Signal recognition particle 9 kDa protein	12.95	40.70	4	0.778	1.262	0.536
Q9BRZ2	E3 ubiquitin-protein ligase TRIM56	17.92	8.34	5	0.673	0.831	0.578
Q13131	5'-AMP-activated protein kinase catalytic subunit alpha-1	6.51	9.66	4	0.718	0.846	0.619
P07355	Annexin A2	12.49	13.57	4	0.850	1.003	0.745
O60732	Melanoma-associated antigen C1	8.68	4.03	4	0.687	1.330	0.593
Q96GW1	Endoplasmin	11.95	13.65	3	1.292	1.168	0.878
Q0VDF9	Heat shock 70 kDa protein 14	11.56	10.02	5	0.752	1.210	0.606
Q9ULW0	Targeting protein for Xklp2	10.46	7.90	5	0.637	0.871	0.551

Accession	Description	Score	Coverage	# Unique Peptides	Average Relative Abundance		
					B-K562	G-K562	V-K562
C9J9W2	LIM and SH3 domain protein 1 (Fragment)	10.91	22.29	4	0.450	0.425	0.362
A0A024R326	Ribosomal protein L29, isoform CRA_a	10.76	31.21	6	0.806	1.433	0.655
Q5U071	High-mobility group box 2	10.28	12.50	2	1.706	2.773	0.386
Q9Y3U8	60S ribosomal protein L36	10.15	40.95	4	0.785	1.216	0.671
Q4LE74	MYO9B variant protein (Fragment)	14.05	1.97	3	0.602	0.851	0.523
P0DMU6	Cancer/testis antigen family 45 member A4	9.94	21.69	4	0.602	0.848	0.352
P61224	Ras-related protein Rap-1b	9.59	17.93	3	1.675	0.882	0.708
A0A024R5H8	RAB6A, member RAS oncogene family, isoform CRA_b	9.44	16.35	2	1.206	0.925	0.761
P09429	High mobility group protein B1	9.06	32.09	6	1.522	3.261	0.665
Q5T6U8	High mobility group AT-hook 1	8.89	41.67	5	0.975	1.575	0.405
Q86TJ2	Transcriptional adapter 2-beta	10.98	8.81	3	0.927	1.632	0.810
Q5HYL6	Putative uncharacterized protein DKFZp686E1899	8.63	14.49	3	0.806	1.174	0.670
P35244	Replication protein A 14 kDa subunit	8.39	25.62	2	0.810	1.251	0.569
P13984	General transcription factor IIF subunit 2	8.16	14.86	3	0.749	0.862	0.635
H3BMH2	Ras-related protein Rab-11A (Fragment)	7.84	20.65	3	0.898	0.911	0.734
A0A075BPP5	Methyl CpG binding protein 2 (Fragment)	7.66	11.74	3	0.853	1.908	0.662
Q9H444	Charged multivesicular body protein 4b	7.51	11.61	2	1.837	1.479	0.969
Q5HY57	Emerin	7.45	12.33	2	1.143	0.802	0.476
F2Z2Y6	U6 snRNA-associated Sm-like protein LSm8	7.34	38.81	2	0.763	1.287	0.685
B3GQE6	DEAD box polypeptide 27	12.53	6.67	5	0.802	1.142	0.704
A4UCT1	Glyceraldehyde 3-phosphate dehydrogenase (Fragment)	7.29	16.27	2	0.794	0.970	0.431
A0A024RAC6	Transcription elongation factor B	13.38	6.87	3	0.800	1.222	0.704
K7EJ44	Profilin 1, isoform CRA_b	7.19	21.15	2	1.069	1.057	0.526
F8VPF3	Myosin light polypeptide 6 (Fragment)	7.02	25.38	3	0.821	1.368	0.673
A0A024R5L7	Phosphatidylinositol binding clathrin assembly protein, isoform CRA_c	10.05	4.10	2	1.013	1.588	0.891
P31151	Protein S100-A7	7.00	31.68	2	2.913	6.875	1.885
Q9BRL5	CALM3 protein	6.79	17.69	2	0.817	1.522	0.665

Accession	Description	Score	Coverage	# Unique Peptides	Average Relative Abundance		
					B-K562	G-K562	V-K562
E9PI77	Baculoviral IAP repeat-containing protein 2 (Fragment)	6.72	20.14	2	0.573	0.620	0.478
D3DU05	Tousled-like kinase 2, isoform CRA_a	25.16	7.33	2	0.673	0.883	0.595
P62820	Ras-related protein Rab-1A	6.58	18.05	2	1.694	1.534	0.996
P51571	Translocon-associated protein subunit delta	6.11	13.87	2	1.078	1.003	0.586
C9IZZ0	Ras-related protein Rab-7a (Fragment)	5.98	20.69	2	1.117	1.391	0.860
P12318	Low affinity immunoglobulin gamma Fc region receptor II-a	5.81	11.99	3	1.663	0.711	1.325
Q5G0E1	2-5-3p (Fragment)	5.71	11.20	3	0.892	1.318	0.758
Q32NB1	RRBP1 protein (Fragment)	5.57	22.84	2	0.730	0.970	0.630
J3KND1	Protein SAAL1	8.87	8.03	3	1.050	1.288	0.934
P43362	Melanoma-associated antigen 9	5.41	13.65	2	0.658	0.708	0.561
Q96MX6	WD repeat-containing protein 92	6.58	8.12	2	0.759	0.980	0.677
B1AKQ8	Guanine nucleotide-binding protein G(I)/G(S)/G(T) subunit beta-1 (Fragment)	5.36	19.44	2	1.476	0.807	0.618
P19105	Myosin regulatory light chain 12A	5.33	17.54	3	0.858	0.707	0.301
B7Z4K8	cDNA FLJ52869	11.70	9.41	3	0.898	1.421	0.803
Q6R327	Rapamycin-insensitive companion of mTOR	14.14	3.69	5	0.669	0.976	0.600
Q01469	Fatty acid-binding protein, epidermal	4.83	21.48	3	0.616	0.722	0.508
B4DWF4	cDNA FLJ55404	4.70	12.50	2	0.590	0.692	0.490
Q06210	Glutamine--fructose-6-phosphate aminotransferase [isomerizing] 1	16.61	6.29	3	0.803	1.200	0.721
A0A0A0MRQ5	Peroxiredoxin-1	4.69	18.56	2	0.819	0.735	0.597
B2R5H5	cDNA, FLJ92476	4.36	19.61	2	0.904	1.406	0.755
P62273	40S ribosomal protein S29	3.49	35.71	3	0.932	1.298	0.792
B4DJK4	cDNA FLJ54005, highly similar to Transcription elongation factor SPT5	2.19	2.84	2	0.811	0.945	0.729
F5H1S8	Malectin (Fragment)	2.14	13.70	2	1.075	1.086	0.761
Q15084	Protein disulfide-isomerase A6	5.53	6.14	2	0.936	1.186	0.843
Q9NTA6	Putative uncharacterized protein DKFZp761I2124 (Fragment)	9.05	4.87	3	0.717	0.856	0.646
Q7Z5Y0	EIF4B protein (Fragment)	5.91	7.45	2	1.231	1.819	1.114
F2Z2E2	Ras GTPase-activating-like protein IQGAP3	19.42	4.60	5	0.750	0.842	0.680

Accession	Description	Score	Coverage	# Unique Peptides	Average Relative Abundance		
					B-K562	G-K562	V-K562
D6W5C0	Spectrin, beta, non-erythrocytic 1, isoform CRA_b	13.15	2.33	3	0.844	1.562	0.769
B4DVN5	cDNA FLJ55372	13.88	9.56	5	0.742	1.067	0.678
Q96IB4	DIP2B protein (Fragment)	8.83	4.59	3	0.632	0.916	0.577
Q0MQR4	Poly (ADP-ribose) glycohydrolase	12.73	4.71	4	0.751	1.332	0.687
Q96MG7	Non-structural maintenance of chromosomes element 3 homolog	8.28	8.88	3	0.857	1.186	0.785
O43747	AP-1 complex subunit gamma-1	10.16	4.50	4	0.834	1.268	0.764
A8K8N3	cDNA FLJ78740	15.20	5.70	5	0.769	1.187	0.705
A0A024R1Y2	ATP-citrate synthase	6.40	2.84	3	0.668	0.989	0.615
A8K4P8	cDNA FLJ75337	6.75	1.84	2	0.893	1.011	0.824
Q9UPU5	Ubiquitin carboxyl-terminal hydrolase 24	5.91	2.75	4	0.793	1.306	0.733
O75529	TAF5-like RNA polymerase II p300/CBP-associated factor- 65 kDa subunit 5L	9.88	7.30	3	0.972	1.387	0.898
B7ZKN7	BLM protein	6.14	2.78	3	0.933	1.135	0.865
B9ZVT1	RNA-binding protein 12B	4.76	2.16	2	0.669	0.653	0.621
O94874	E3 UFM1-protein ligase 1	5.52	2.90	2	0.910	1.036	0.848
Q14566	DNA replication licensing factor MCM6	16.18	8.40	5	0.948	0.834	0.885
Q5TIG5	Afadin	6.82	2.64	4	0.705	0.910	0.658
Q8IYI6	Exocyst complex component 8	4.17	2.21	2	0.663	0.802	0.621
Q05DA9	SFRS17A protein (Fragment)	4.75	6.16	2	0.886	1.045	0.831
Q13595	Transformer-2 protein homolog alpha	4.72	8.16	2	0.666	0.951	0.627
Q9H4H8	Protein FAM83D	10.14	8.89	3	0.678	0.825	0.638
O75177	Calcium-responsive transactivator	7.96	9.60	2	0.802	0.882	0.760
A4QPB0	IQ motif containing GTPase activating protein 1	32.49	6.88	9	0.830	1.402	0.787
Q92888	Rho guanine nucleotide exchange factor 1	18.65	7.24	4	0.798	1.046	0.757
A8K9S3	Coronin OS=Homo sapiens PE=2 SV=1 - [A8K9S3_HUMAN]	3.98	3.43	2	1.129	1.194	1.072
O14578	Citron Rho-interacting kinase	35.18	7.10	13	0.699	0.869	0.664
Q92973	Transportin-1	18.65	8.80	3	1.038	1.587	0.990
Q9Y2X0	Mediator of RNA polymerase II transcription subunit 16	17.49	7.87	4	0.911	1.118	0.872

Accession	Description	Score	Coverage	# Unique Peptides	Average Relative Abundance		
					B-K562	G-K562	V-K562
Q9H2G2	STE20-like serine/threonine-protein kinase	5.68	1.54	2	0.773	1.137	0.741
A0A024DAK3	RNA-specific adenosine deaminase	23.87	7.67	9	0.648	0.729	0.622
Q53H75	Chromosome 14 open reading frame 133 variant (Fragment)	5.23	4.67	3	0.772	2.665	0.741
Q14692	Ribosome biogenesis protein BMS1 homolog	8.84	3.35	4	0.688	0.832	0.665
O60673	DNA polymerase zeta catalytic subunit	2.52	0.61	2	0.686	1.059	0.664
Q9H2K8	Serine/threonine-protein kinase TAO3	19.38	8.91	7	0.745	1.107	0.721
Q99856	AT-rich interactive domain-containing protein 3A	12.17	5.40	3	0.881	1.747	0.856
E9PBF6	Lamin-B1	8.38	8.01	2	0.813	1.722	0.791
Q96BN2	Transcriptional adapter 1	5.04	6.27	2	0.932	1.146	0.907
Q8IWQ7	Non-specific serine/threonine protein kinase	5.30	1.34	2	0.792	1.015	0.772
A0A0C4DFL8	Lysine-specific demethylase 4B	3.00	4.01	2	0.675	1.089	0.660
Q15042	Rab3 GTPase-activating protein catalytic subunit	6.74	4.28	3	1.031	1.613	1.013
P26038	Moesin	9.48	6.24	2	0.869	1.317	0.854
Q15050	Ribosome biogenesis regulatory protein homolog	9.15	9.04	3	0.586	0.687	0.578
P85037	Forkhead box protein K1	5.11	3.55	3	0.635	1.151	0.628
P57772	Selenocysteine-specific elongation factor	7.24	3.69	3	0.665	1.448	0.659
Q15058	Kinesin-like protein KIF14	41.70	9.04	14	0.808	1.037	0.802
Q14677	Clathrin interactor 1	11.69	7.52	4	0.898	1.108	0.894
Q15555	Microtubule-associated protein RP/EB family member 2	8.79	9.48	2	0.718	1.049	0.716
Q9H5Z1	Probable ATP-dependent RNA helicase DHX35	10.72	5.83	3	0.786	1.078	0.785
E7EQZ4	Survival motor neuron protein	6.14	6.46	2	0.617	0.654	0.616